HYPERINSULINEMIA AND INSULIN RECEPTOR SIGNALING IN PANCREATIC CANCER DEVELOPMENT

by

Anni Zhang

B.Sc., The University of British Columbia, 2016

A THESIS SUBMITTED IN PARTIAL FULFILLMENT OF

THE REQUIREMENTS FOR THE DEGREE OF

DOCTOR OF PHILOSOPHY

in

THE FACULTY OF GRADUATE AND POSTDOCTORAL STUDIES

(Genome Science and Technology)

THE UNIVERSITY OF BRITISH COLUMBIA

(Vancouver)

April 2022

The following individuals certify that they have read, and recommend to the Faculty of Graduate and Postdoctoral Studies for acceptance, the dissertation entitled:

Hyperinsulinemia and Insulin Receptor Signaling in Pancreatic Cancer Development

submitted by Anni Zhang in partial fulfillment of the requirements for

the degree of Doctor of Philosophy

in Genome Science and Technology

Examining Committee:

Dr. James D. Johnson, Cellular and Physiological Sciences, UBC
Co-supervisor

Dr. Janel L. Kopp, Cellular and Physiological Sciences, UBC
Co-supervisor

Dr. Francis Lynn, Cellular and Physiological Sciences, UBC
Supervisory Committee Member

Dr. Kenneth W. Harder, Microbiology and Immunology, UBC
University Examiner

Dr. William Lockwood, Pathology and Laboratory Medicine, UBC
University Examiner

Additional Supervisory Committee Members:

Dr. Daniel J. Renouf, Medical Oncology, UBC
Supervisory Committee Member

Abstract

Pancreatic ductal adenocarcinoma (PDAC) is the 3rd leading cause of cancer death in Canada and its incidence is increasing, largely driven by the expanding epidemics of PDAC risk factors including obesity and type 2 diabetes (T2D). Hyperinsulinemia is a cardinal feature of obesity and T2D, and is associated with increased PDAC incidence and mortality. Despite epidemiological data linking hyperinsulinemia to PDAC, there was no direct *in vivo* evidence of a causal role for endogenous insulin in any cancer type before this work. We studied how reduced insulin production or local insulin action affected the development of pancreatic intraepithelial neoplasia (PanIN) precursor lesions in *Ptf1a*^{CreER};*Kras*$^{LSL\text{-}G12D}$ mice. We first generated *Ptf1a*^{CreER};*Kras*$^{LSL\text{-}G12D}$;*Ins1*$^{+/+}$;*Ins2*$^{-/-}$ control and *Ptf1a*^{CreER};*Kras*$^{LSL\text{-}G12D}$;*Ins1*$^{+/-}$;*Ins2*$^{-/-}$ experimental mice. We found high fat diet (HFD)-induced hyperinsulinemia was modestly reduced in experimental mice without affecting glucose homeostasis. Genetically reduced insulin production resulted in ~50% suppression of PanIN. However, in this study, only female mice remained normoglycemic and only the gene dosage of rodent-specific *Ins1* alleles was tested. Therefore, we then generated *Ptf1a*^{CreER};*Kras*$^{LSL\text{-}G12D}$;*Ins1*$^{-/-}$;*Ins2*$^{+/+}$ control and *Ptf1a*^{CreER};*Kras*$^{LSL\text{-}G12D}$;*Ins1*$^{-/-}$;*Ins2*$^{+/-}$ experimental mice. Mice with reduced insulin production tended to develop fewer PanIN and acinar-to-ductal metaplasia (ADM) lesions. Using single-cell transcriptomics, we found hyperinsulinemia modulated pathways associated with protein translation, MAPK/ERK signaling and PI3K/AKT/mTOR signaling, which were changed in epithelial cells and subsets of immune cells. Finally, we examined whether hyperinsulinemia contributed to PDAC development directly through insulin receptor (INSR) signaling in *Kras*^{G12D} carrying pancreatic acinar cells. We generated *Ptf1a*^{CreER};LSL-*Kras*^{G12D};nTnG mice with an *Insr*$^{wt/wt}$, *Insr*$^{wt/f}$, or *Insr*$^{f/f}$ genotype to reduce insulin receptor mRNA by 0%, 50%, or

100% in acinar cells. Loss of insulin receptors from acinar cells did not significantly influence body weight, fasting glucose, or insulin levels. Compared to mice with wild-type INSR expression in acinar cells, mice lacking INSR had a 2.7-fold and 5.3-fold significant reduction in PanIN plus tumor area in males and females, respectively. Collectively, these results indicate that hyperinsulinemia and INSR signaling in acinar cells are important for the early stages of pancreatic cancer. Insulin-lowering interventions such as lifestyle management and therapies targeting insulin receptor signaling may be beneficial in preventing and/or treating pancreatic cancer.

Lay Summary

Pancreatic cancer is one of the most lethal cancers and 90% of those diagnosed with pancreatic cancer will die from it. In 2020, 6000 Canadians were diagnosed with this disease. It is therefore urgent for us to find new methods to treat this deadly cancer. High levels of circulating insulin are associated with an increased risk of getting and dying from cancer, but it was not clear whether this was cause or effect. To study how insulin affects pancreatic cancer development, we made mice with less insulin and found that early-stage cancer was reduced compared with mice with more insulin. This tells us high insulin can contribute to pancreatic cancer development. When we prevented cancer cells from receiving the insulin signal, we also found reduced early cancer. This work improves our understanding of insulin's effects on pancreatic cancer and may point to new ways to prevent and treat the disease.

Preface

All studies presented in this dissertation were conceived, designed, performed, and analyzed by the author AMY Zhang, with assistance as outlined below. This thesis was written by myself with editing provided by JD Johnson, JL Kopp, F Lynn and D Renouf.

A version of Chapter 3 has been published. AMY Zhang, J Magrill, TJJ de Winter, X Hu, S Skovsø, DF Schaeffer, J L Kopp, and JD Johnson. (2019) Endogenous Hyperinsulinemia Contributes to Pancreatic Cancer Development. *Cell Metabolism*. Sep 3;30(3):403-404. This manuscript was also published as a pre-print on the Biorxiv server (https://www.biorxiv.org/content/10.1101/530097v1). I designed, managed the study, acquired, analyzed, and interpreted all data unless otherwise noted. J Magrill acquired the CK19, Ki67 and Alcian blue staining data (Figure 3.2B-C & Figure 3.4A). TJJ de Winter acquired and analyzed the male mice hematoxylin and eosin staining (Figure 3.3D-F). X Hu managed the mouse colony and performed husbandry. S Skovsø provided expert advice on breeding and study design. DF Schaeffer provided expert advice on pancreatic cancer pathology and study design. J L Kopp, and JD Johnson designed, analyzed, and interpreted experiments and supervised the study.

A version of Chapter 4 has been submitted with requested revisions. AMY Zhang, KH Chu, BF Daly, T Ruiter, Y Dou, JCC Yang, TJJ de Winter, J Chhuor, S Wang, S Flibotte, YB Zhao, X Hu, H Li, EJ Rideout, DF Schaeffer, JD Johnson, and JL Kopp. (2021) Effects of hyperinsulinemia on pancreatic cancer development and the immune microenvironment revealed through single-cell transcriptomics. This manuscript was also published as a pre-print on the Biorxiv server (https://www.biorxiv.org/content/10.1101/2021.03.10.434504v1). I designed, managed, and conducted the project including acquiring, analyzing, and interpreting all data (*in vivo* animal experiments, genotyping, histology, and single cell RNA-sequencing (scRNA-seq)).

KH Chu performed immunohistochemical (IHC) staining of Cd20, F4/80 (Figure 4.8A & Figure 4.8D). BF Daly performed IHC staining of ERK (Figure 4.10A), T Ruiter performed IHC staining of Cd8 (Figure 4.8G), and JCC Yang performed IHC staining of Foxp3 (Figure 4.8F). Y Dou quantified the percent F4/80 area (Figure 4.8E). TJJ de Winter performed *in vivo* animal experiments and genotyping. J Chhuor helped on optimizing the IHC staining. EJ Rideout helped with interpretation of the data in a sex-specific manner and edited the manuscript. S Flibotte, YB Zhao, and S Wang provided advice on scRNA-seq analysis. X Hu and H Li provided help with *in vivo* animal experiments. DF Schaeffer provided histopathology analysis and expertise. JD J Johnson, and JL Kopp supervised the project, interpreted the data, and edited the manuscript.

Data from chapter 5 of this thesis will be submitted for publication in a peer-reviewed journal and also posted on Biorxiv. I designed, managed the study, acquired, analyzed, and interpreted all data unless otherwise notes. KH Chu, BF Daly, JCC Yang, and J Chhuor helped with sectioning slides, Alcian blue staining (Figure 5.6A&C), hematoxylin and eosin staining (Figure 5.8A&C and Figure 5.9A&E), and performing IHC staining of GFP (Figure 5.4 & Figure 5.5) and CK19 (Figure 5.7A&C). JCC Yang and T Ruiter helped with mouse dissection. T Ruiter and J Lin helped with mouse genotyping.

Animal protocols were approved by the University of British Columbia Animal Care Committee (certificate # A16–0022, # A19-0267, and # A21-0135), consistent with national and international guidelines.

Table of Contents

List of Tables

List of Figures

List of Abbreviations

ADM - acinar to ductal metaplasia

AGEs - advanced glycation end products

ATP - adenosine triphosphate

BAD - BCL2 associated agonist of cell death f

BIM - Bcl-2-like protein 11

BMI - body mass index

CCK - cholecystokinin

CD - control diet

CK19 - cytokeratin 19

DAB - 3,3’-diaminobenzidine

ECM - extracellular matrix

FGF2 - fibroblast growth factor-2

FOXO - forkhead family box O

GDP - guanosine diphosphate

GEF - guanosine exchange factor

GLUT4 - glucose transporter type 4

GRB2 - growth factor receptor-bound protein 2

GSK3β - glycogen synthase kinase 3β

GTP - guanosine triphosphate

H&E - hematoxylin and eosin

HbA1c - glycated haemoglobin A1c

HFD - high-fat diet

HMGA1 - high mobility group protein A1

IAPP - islet amyloid polypeptide

IGF-1 - Insulin-like growth factor 1

IGF1R - insulin-like growth factor 1 receptor

IGFBP - insulin-like growth factor binding proteins

IHC - immunohistochemical

IL-6 - interleukin 6

Insr - insulin receptor

IPMN - intraductal papillary mucinous neoplasm

IRS - insulin receptor substrate

LDL - low-density lipoprotein

LSL - Lox-Stop-Lox

MAPK - mitogen-activated protein kinase

MCN - mucinous cystic neoplasm

MCP-1 - monocyte chemoattractant protein-1

MODY - maturity onset diabetes of the young

ncRNA - non-coding RNA

NDS - normal donkey serum

nTnG - nuclear TdTomato-to-nuclear EGFP

OGTT - oral glucose tolerance test

PanIN - pancreatic intraepithelial neoplasia

PDAC - pancreatic ductal adenocarcinoma

PDGF - platelet-derived growth factor

PDK - phosphoinositide-dependent kinase

PD-L1 - programmed death-ligand 1

PFKFB2 - phosphofructokinase fructose bisphosphatase-2

PI3K - phosphatidylinositol 3-kinase

Pik3ca - Phosphatidylinositol-4,5-Bisphosphate 3-Kinase Catalytic Subunit Alpha

PIP2 - phosphatidylinositol 4,5-bisphosphate

PIP3 - phosphatidylinositol (3,4,5)-triphosphate

PK - $Ptfa1^{CreER};Kras^{LSL\text{-}G12D}$

PTP1B - protein tyrosine phosphatase 1B

RR - relative risk

scRNA-seq - single cell RNA-sequencing

SHBG - sex-hormone-binding globulin

SOS - Son of Sevenless

T1D - type 1 diabetes

T2D - type 2 diabetes

TBC1D4 - rabGAP TBC1 domain family member 4

TGF-β1 - transforming growth factor beta-1

TM - tamoxifen

TNF-α - tumor necrosis factor alpha

UMAP - uniform manifold approximation and projection

VEGF - vascular endothelial growth factor

Acknowledgements

First and foremost, I offer my enduring gratitude to my supervisors: Dr. James Johnson and Dr. Janel Kopp for offering me endless support and guidance over the past 5 years, and for teaching me experimental design, scientific presentation, scientific writing, and critical thinking which all will surely play an important role in my future endeavors. I would like to thank them for creating such a supportive and collaborative laboratory working environment that I feel I am part of a big and warm family. I am also forever grateful for them always being professional, helpful, and considerate for both my study and life.

Second, I would like to thank my supervisory committee, Dr. Francis Lynn, and Dr. Dan Renouf for their invaluable advice and support. I would also like to thank Dr. David Schaeffer for his assistance with matters related to pathology.

I would like to thank previous and present members of the Johnson lab and Kopp lab including Jenny Yang, Ken Chu, Shilpa Patil, Jamie Magrill, Twan de Winter, Titine Ruiter, Jeffrey Lin, Brian Daly, Alice Wang, Justin Chhuor, Leanne Beet, Alex Lee, Grace Li, Betty Hu, Dr. Søs Skovsø, Dr. Evgeniy Panzhinskiy, Dr. Jelena Kolic, Dr. Howard Cen, Peter Overby, Jamie Chu, Stella Baehring, Aurora Mattison, Mikky Atser, Andy Wang, Angela Dou, Wesley Hunt, and Grace Dong for always being eager to help and support me. Your friendships are invaluable.

Finally, I want to thank my parents for their endless love and for supporting me to overcome all the difficulties in my life. I want to thank all my friends for supporting my career goals and for sharing in my happiness and sadness.

To my mother and father for their endless support and love.

Chapter 1: Introduction

1.1 Pancreatic ductal adenocarcinoma

In 2021, pancreatic cancer is expected to become the 3rd leading cause of cancer death in Canada and even though it only accounts for about ~3% of new cancer cases, it contributes to ~7% of cancer death (1). Pancreatic cancer is projected to become the 2nd leading cause of cancer death by 2030 (2). Due to a lack of specific symptoms and difficulties in early tumor detection, patients are often diagnosed with pancreatic cancer at advanced stages making curative surgical tumor removal impossible (3). Moreover, pancreatic cancer is resistant to most anti-cancer therapies, including radiotherapy, immunotherapy, and chemotherapy. As a result, the 5-year survival rate of pancreatic cancer is only 10% (1,3,4).

Pancreas is an elongated and tapered organ which is located at the back of the abdomen behind the stomach. Anatomically, pancreas can be divided into head, neck, body, and tail. The head of pancreas lies within the curvature of the duodenum, the neck of pancreas separates the head and body, the body of the pancreas mostly lies behind the stomach, and the tail of pancreas is adjacent to the spleen (5). The main pancreatic duct, which joins the pancreas to the common bile duct, runs through the body of the pancreas and collects pancreatic juice. Pancreas has both exocrine functions required for good digestion and endocrine functions regulating glucose homeostasis. The exocrine pancreas, comprising ~99% of the pancreas, is comprised of digestive enzyme-secreting acinar cells and bicarbonate-secreting ductal cells (5). The endocrine pancreas, only ~1% of the mass, consists of pancreatic islets cells, including insulin-secreting β-cells, glucagon-secreting α-cells, and somatostatin-secreting δ-cells (5). The pancreas also contains sympathetic and parasympathetic nerves, rich vasculature, and resident immune cells. More than 95% of pancreatic cancers originate from the exocrine pancreas while the remaining ~5% of

cases are classified as neuroendocrine tumors (3,4). The most common type of exocrine pancreatic cancer is pancreatic ductal adenocarcinoma. Other less common types of exocrine pancreatic cancers include acinar cell carcinomas, squamous cell carcinoma, adenosquamous carcinoma, and colloid carcinoma (6). Regardless of the types of pancreatic cancer, early detection and treatment of non-invasive pancreatic cancer would significantly improve the survival rates; especially if we can target this disease at the precursor stage.

1.1.1 The PDAC precursor lesions

The most common precursor lesion of PDAC is PanIN, which is defined as a microscopic noninvasive epithelial neoplasm with varying amounts of mucin and varying degrees of cytologic and architectural atypia (7). Low-grade PanINs can progress into increasingly dysplastic high-grade PanINs and can finally become PDAC (Figure 1.1). Although the majority of PDAC is thought to arise from PanIN, the size of PanIN (usually <5 mm) is often below the detection limits of current clinical imaging techniques (8). Other common precursor lesions of PDAC include intraductal papillary mucinous neoplasm (IPMN) and mucinous cystic neoplasm (MCN) which are macroscopic and can be detected by imaging techniques like CT scanning (7). IPMN arises in the main pancreatic duct or branch ducts, and it is papillary noninvasive mucin-producing epithelial neoplasm (Figure 1.2) (7). MCN is defined as a mucin-producing epithelial neoplasm with ovarian-type stroma (Figure 1.2) (7). Currently, the determinants of precursor lesion type are not well known but likely originate from the combined effects of cancer cell of origin and cancer driver mutations (9,10).

1.1.2 Mutational landscape of PDAC

PDAC is a relatively genetically homogeneous cancer. Four genes account for the mutations in >50% of PDAC patients: *KRAS, TP53, SMAD4,* and *CDKN2A* (3,4,8). Genes mutated at a lower prevalence (5-10%) include those involved in nucleosome remodeling (*ARID1A* and *ARID1B*), histone methylation (*MLL3*, *MLL2*, and *KDM6A*), and DNA damage response (*ATM, BRCA1,* and *BRCA2*) (3,8). *KRAS* mutations can be found in >90% of PDAC cases and are thought to be the early driver mutation because they can be detected in the earliest precancerous lesions. KRAS is a small G protein which transduces upstream activating signals from receptor tyrosine kinases, including the insulin receptor (INSR), to various signaling cascades such as the mitogen-activated protein kinase (MAPK)/ERK pathway (Figure 1.3) (11,12). Components of MAPK/ERK signaling pathway are frequently mutated in cancers, and this pathway regulates cell proliferation and survival. KRAS can exist in two states: the inactive guanosine diphosphate (GDP)-bound state and the active guanosine triphosphate (GTP)-bound state. Upon activation, the guanosine exchange factor (GEF) exchanges the GDP from the nucleotide binding site with a GTP and then the GTP-bound KRAS activates its downstream effector proteins and signaling cascade (Figure 1.3) (11,12). KRAS returns to its inactive state when the bound GTP is hydrolyzed to a GDP (12). The G12D mutation (glycine to aspartate substitution) is the most common KRAS mutation, and it impairs GTP hydrolysis, so KRAS is in its active GTP-bound state (12). This increases MAPK/ERK signaling, driving uncontrolled cellular proliferation and eventually cancer (11,12). However, some studies have suggested that RAS activity in $Kras^{G12D}$ mice was not as high as expected and lower than RAS activity seen in other cancer cells (13). This suggests that MAPK/ERK signaling pathway is not fully

constitutive activated by KRAS mutations and external stimuli could further enhance Ras activity, including inflammation (13) and growth factor signalling.

Loss of function mutations in *TP53* (50-70%), *SMAD4* (30-40%), and *CDKN2A* (40-60%) tumor suppressor genes are detected at less frequency, and they are thought to be acquired after *KRAS* mutations as they are more prevalent in the higher grade of precancerous lesions (3,8). The acinar cells or ductal cells carrying *KRAS* mutations can give rise to PanIN or IPMN lesions and the subsequent mutations in *TP53, SMAD4* and *CDKN2A* make the precursors eventually become tumors (4). Studies of the PDAC mutational landscape have deepened our understanding of PDAC pathophysiology.

1.1.3 The tumor microenvironment in PDAC

PDAC microenvironment is characterized by a dense desmoplastic stroma, which can account for up to 50-80% of the tumor volume (14-17). PDAC is very resistant to radiotherapy and chemotherapy because of the dense desmoplasia in which fibroblasts and dense extracellular matrix (ECM) are the main constituents (14,15). During PDAC tumorigenesis, cancer cells can secrete transforming growth factor beta-1 (TGF-β1), sonic hedgehog, platelet-derived growth factor (PDGF), and fibroblast growth factor-2 (FGF2) to stimulate the activation, proliferation, and ECM deposition of fibroblasts (14,18).

At PanIN initiation, fibroblast accumulation can already be detected, and conflicting reports suggest that fibroblasts can be both tumor-promoting and tumor-restraining (18). For instance, mice orthotopically injected with primary fibroblasts and PDAC cells developed larger tumors and had more metastasis compared to mice only injected with cancer cells (19). This suggests that fibroblasts support PDAC development. Moreover, fibroblasts can promote tumor

progression by providing cancer cells with amino acids and lipids to support their rapid proliferation (18). They can also activate the mitogenic signaling pathways (insulin-like growth factor 1 (IGF-1) and AKT) in cancer cells through paracrine signaling and secrete cytokines (CXCL12 and interleukin 6 (IL-6)) to promote immune suppression (18). However, several studies showed that fibroblasts could be tumor-suppressive (16,20,21). For example, Rhim *et al*. demonstrated that when sonic hedgehog-dependent fibroblasts were deleted in a pancreatic cancer mouse model, the mice without fibroblasts died from tumors earlier and had more metastasis in compared to the controls (20). This suggests that at least a subpopulation of fibroblasts may restrain PDAC growth, and fibroblast heterogeneity is increasingly recognized.

During pancreatic tumorigenesis, the pancreas is significantly infiltrated with immune cells, but these cells are generally immunosuppressive in nature (22,23). Pancreatic cancer cells can employ various methods to escape immune elimination including recruiting regulatory immune cells, secreting immunosuppressive cytokines (IL-6, TGF-β1, IL10, and TGF-β1), and expressing checkpoint inhibitor molecules (programmed death-ligand 1 (PD-L1)) (22). Additionally, different types of immune cells also play their specific roles during PDAC progression. For instance, macrophages, which are the most dominant immune cell population in PDAC, are correlated with poor PDAC prognosis and mediate immunosuppression, as well as promoting tumor progression and metastasis (24-27). In contrast, natural killer (NK) cells are anti-tumor, and the number of NK cells was positively correlated with PDAC survival rate (23,28). Consistently, NK cells exhibit a low PDAC localization which impairs their tumor elimination function (23,29). T cells are another type of immune cell that is highly abundant in PDAC microenvironment. $CD4^+$ T cells are tumor-promoting and can stimulate PDAC cell proliferation and enhance the MAPK and AKT pathways (30), while $CD8^+$ T cells are cytotoxic

and increased $CD8^+$ T cells accumulation in the tumor was associated with a better PDAC survival (31,32). T regulatory cells (Treg) are considered tumor-promoting and low numbers of Tregs were associated with better PDAC prognosis (23,33). A study showed that genetic ablation of Tregs after the onset of tumors in mice could delay tumor development and prolong survival (23,34). However, Zhang *et al*. showed that Treg depletion during the onset and progression of PDAC caused an accelerated tumor progression via losing the tumor-restraining fibroblast population and recruiting myeloid cells (35). Thus, Tregs may play different roles dependent on the PDAC tumor stage. More detailed reviews on inflammation and cancer relationships, especially pancreatic cancer can be found elsewhere (23,36-40).

1.1.4 Mouse models of PDAC

To have a better understanding of PDAC biology, PDAC mouse models have been developed which are generally based on the *Kras*^{G12D} driver mutation with or without additional mutations on *Trp53*, *Cdkn2a*, *Smad4,* or *Tgfb1*. For these PDAC mouse models, one of the *Kras* alleles is modified by insertion of a Lox-Stop-Lox (LSL) construct upstream of an exon 1 that contains a G12D mutation. In the presence of Cre recombinases, the LSL sequence is removed and a mutated form of *Kras* is expressed (41) (Figure 1.4). *Pdx1*-Cre;LSL-*Kras*^{G12D} and *Ptf1a*^{Cre}; LSL-*Kras*^{G12D} mice are the two most commonly used PDAC mouse models and they were generated by Hingorani *et al*. in 2003 (42). Nonetheless, in these mouse models, the *Kras*^{G12D} mutation is induced in all pancreas cell types as the Cre recombinase is expressed in the pancreas either under a *Pdx1* promoter-driven transgene or by Cre knockin at the *Ptf1a* locus (Figure 1.4). During embryonic development, both *Pdx1* and *Ptf1a* genes are expressed in pancreatic

precursor cells, but in adult mice, the *Pdx1* is expressed exclusively in pancreatic islet beta- and delta-cells, while *Ptf1a* is restricted to acinar cells (41).

PDAC can arise from either acinar cells or ductal cells (10,43). Therefore, to have pancreatic cell type-specific expression of oncogenic *Kras,* tamoxifen-inducible mouse models were developed using promoters of cell marker genes, like *Ptf1a* and *Sox9*. Lee *et al*. showed in mouse models that acinar cell-driven PDAC and ductal cell-driven PDAC have differences in disease progression, tumor phenotype, and precursor lesion initiation (10). In these models, the Cre is fused to a mutated hormone-binding domain of the estrogen receptor (CreER), so that CreER recombinase is translocated from cytoplasm to nucleus in the presence of tamoxifen (44). For the *Ptf1a*^{CreER};*Kras*$^{LSL\text{-}G12D}$ (PK) mouse model, tamoxifen is injected into the mice after weaning so the expression of *Kras*^{G12D} is restricted to acinar cells; these mice usually begin to develop low-grade PanINs around 3-months of age (9,10). As the mice age, high-grade PanIN lesions are observed more frequently, and acinar parenchyma is replaced by PanINs, desmoplastic fibroblasts, and infiltrating immune cells (10,41,43). At a low frequency, some of these mice will eventually develop tumors when they are 8- to 12-month-old.

Because of the long tumor latency and low tumor frequency in *Kras*^{G12D} mouse models, researchers have also generated pancreatic cancer mouse models carrying loss of function mutations in tumor suppressor genes. For example, the *Pdx1*-Cre;*Kras*$^{LSL\text{-}G12D}$; *Trp53*$^{LSL\text{-}R172H}$ and *Pdx1*-Cre;*Kras*$^{LSL\text{-}G12D}$; *Smad4*$^{flox/flox}$ mouse models, which have both KRAS and TP53 (or SMAD4) mutations expressed in pancreatic cells (45). Compared to the PK mouse model, these triple mutant mice can start to develop tumors at 2 to 3-month-old and die from tumors around 5-6 months (41). In addition, PanIN and PDAC progression in PDAC mouse models can also be accelerated by inducing pancreatitis through injecting caerulein, which is an analog to the

intestinal hormone, cholecystokinin (CCK), which stimulates digestive enzyme release from acinar cells (43). As early as 1 month following caerulein injections, numerous high-grade PanINs can already be detected in the pancreas.

1.1.5 PDAC risk factors

The main risk factors for PDAC are chronic pancreatitis, family history, smoking, obesity, and diabetes. Several studies suggest that diet, alcohol consumption, non-O blood type, and *Helicobacter pylori* infections are also risk factors for PDAC (46,47). Epidemiology studies show that pancreatitis and smoking are positively associated with PDAC risk. For instance, a meta-analysis of 6 cohort studies showed that chronic pancreatitis is associated with a 13.3-fold increased risk of getting PDAC (48). Smoking is associated with a ~2-fold excess risk of PDAC (46,49). Although pancreatitis and family history have a stronger association with PDAC risk, obesity and diabetes as risk factors are beginning to attract more attention from investigators because of the rapid increase in the number of people with these metabolic disorders (see statistics below in section 1.2). Pooled analysis of 14 cohort studies showed that compared to normal-weight individuals, pancreatic cancer risk was 47% higher in obese individuals with another study showing that obesity is associated with 1.72-fold excess PDAC risk (50,51). Meanwhile, diabetes is associated with ~1.5- to 3-fold increased risk of PDAC; however, the risk is higher in individuals with new-onset type 2 diabetes (≤2 years) (46,52), which is incidentally the phase of the disease where endogenous insulin levels are highest (53). The association with early diabetes has also led to speculation that pancreatic cancer is causing diabetes, and not necessarily the other way around (46,52,54). However, individuals having long-term diabetes also have a ~2-fold excess risk of getting PDAC, which suggests that diabetes itself is a risk

factor for PDAC (46,52). Since people noticed obesity and diabetes are positively associated with increased risk of PDAC (and many other types of cancers), more studies have been performed to investigate the potential factors linking obesity and diabetes to PDAC. However, few of these studies have been able to identify causal links using definitive loss-of-function studies.

1.2 Diabetes, obesity, and pancreatic cancer risk

1.2.1 Diabetes

In 2019, diabetes was estimated to affect 463 million people globally. This number is projected to grow to 578 million people by 2030 (55). Every year, 1.5 million deaths can be directly attributed to diabetes worldwide, and in Canada, 7.8% of males and 6.5% of females live with diabetes (56). Diabetes, which is defined as a chronic metabolic disorder with elevated blood glucose or hyperglycemia, is caused by insufficient insulin production or impaired response to insulin (56,57). In Canada, diabetes can be diagnosed by a fasting plasma glucose (at least 8 hours fasting) of ≥ 7 mmol/L, 2-hour plasma glucose of ≥ 11.1 mmol/L during a 75 g oral glucose tolerance test (OGTT), and/or glycated haemoglobin A1c (HbA1c) $\geq 6.5\%$ (57). Long-term unmanaged diabetes can cause severe complications such as retinopathy, nephropathy, or neuropathy, as well as cardiovascular diseases (56).

There are 3 main types of diabetes: type 1 diabetes (T1D), type 2 diabetes (T2D), and gestational diabetes (57). Type 1 diabetes is caused by autoimmune destruction of insulin-producing pancreatic β cells with consequent insulin deficiency and is usually diagnosed in children and young adults. Type 2 diabetes is the most common type of diabetes and is also the type of diabetes that correlates with increased cancer risk (discussed in more detail below).

Gestational diabetes develops during pregnancy and women who experience gestational diabetes have an increased chance to develop T2D later compared to those never having gestational diabetes. Maturity onset diabetes of the young (MODY) is a rare type of diabetes caused by impaired insulin production resulting from a single gene mutation. Diabetes can also be caused by other genetic syndromes, drugs, and pancreatic disorders (including PDAC).

1.2.1.1 Increased cancer incidence and mortality in type 2 diabetes

Type 2 diabetes accounts for ~90% of diabetes cases and its incidence continues to rise. Type 2 diabetes is caused by both genetic and environmental factors. The common genetic risk for type 2 diabetes manifests mostly at the level of the pancreatic beta-cell. Risk factors for type 2 diabetes include family history, being overweight or obese, sedentary lifestyles, unhealthy dietary factors, and smoking (58). Type 2 diabetes is caused by a combination of impaired insulin secretion in β cells, and insulin resistance in the liver, muscle, and adipocytes (58). Investigators have suggested several molecular mechanisms of β cell death and insulin resistance such as ER stress, free radical overload, inflammation, glucotoxicity, and lipotoxicity (59). Today, the first-line treatment for type 2 diabetes is a lifestyle, but many drugs can treat the symptoms of the disease including sulfonylureas, glucagon-like peptide 1 agonists and dipeptidyl-peptidase 4 inhibitors, sodium-glucose transport protein 2 inhibitors, which improve insulin secretion (58), or metformin or thiolazinediones that improve insulin sensitivity (58). However, many patients with type 2 diabetes ultimately are prescribed exogenous insulin injections. A better understanding of the molecular mechanisms underlying type 2 diabetes pathophysiology can help us develop better antidiabetic strategies.

The association between diabetes and increased cancer risk has been widely reported; especially for T2D (60-63). Meta-analyses indicated that T2D was associated with a 10% increased risk of developing cancers (60). For specific cancer types, the relative risk (RR) for type 2 diabetic patients were: 2.3 for liver cancer, 1.95 for pancreatic cancer, 1.2 for breast cancer, 1.17 for ovarian cancer, 1.38 for kidney cancer, 1.35 for bladder, and 1.28 for non-Hodgkin's lymphoma (60). Pancreatic and liver cancer have the strongest association with T2D. T2D has also been linked to increased cancer mortality. For example, one study showed that in the presence of T2D, overall cancer mortality was increased 16%, while in another study T2D was associated with 1.9-fold and 1.73-fold excess cancer mortality in women and men, respectively (60,64). Specifically, the presence of T2D was associated with 2.43-fold, 1.4-fold, 1.24-fold, 1.16-fold, 1.44-fold increased risk of deaths from liver cancer, pancreatic cancer, breast cancer, kidney cancer, and colon cancer (60,63). Thus, understanding the mechanisms that connect diabetes and cancer risk may provide us with novel strategies to treat or even prevent some types of cancer.

1.2.2 Obesity

Obesity is defined as excessive fat accumulation that may cause a risk to health. A person is considered clinically obese when their body mass index (BMI) is over 30 kg/m^2 (65). Since 1975, obesity has nearly tripled around the globe. In 2016, over 650 million people were obese (65). Obesity is a risk factor for most chronic diseases, including cardiovascular diseases and T2D. Over 2.8 million people's deaths can be attributed to overweight or obesity every year (65).

Obesity is also associated with increased cancer incidence and mortality. The presence of obesity leads to a relative risk (RR) of: 7.1 for endometrial cancer, 4.8 for oesophagus cancer,

1.8 for gastric cancer, 1.8 for renal cancer, 1.8 for liver cancer, 1.5 for pancreatic cancer, and 1.5 for multiple myeloma (37). Obesity is associated with 52% and 62% increased risk of death from any cancer in men and women, respectively (66). Specifically, obesity (BMI 35.0-39.9 kg/m^2) was associated with increased mortality from esophageal cancer (RR 1.63), stomach cancer (RR 1.08-1.94), colorectal cancer (RR 1.46-1.84), liver cancer (RR 1.68-4.52), pancreatic cancer (RR 1.41-1.49), kidney cancer (RR 1.7), and breast cancer (RR 1.7) (66). Overall in this study, 14% and 20% of all deaths from cancer can be attributed to obesity in men and women, respectively (66). The fundamental cause of obesity is energy imbalance resulting from increased intake of high fat and high sugar as well as reduced physical activity (65). Therefore, the best way to reduce obesity is lifestyle changes, with studies showing reduced BMI in obese individuals was associated with decreased cancer incidence and mortality (63,67-69).

1.2.2.1 A high fat diet accelerates PanIN and PDAC development

The obesity associated PDAC risk has been validated with *in vivo* PDAC mouse models subjected to unhealthy diets. Several studies used high fat diets to induce obesity and as expected, the mice fed with HFD had significantly higher body weight than the mice consuming control diet (CD). As early as 3- month-old, the HFD-fed mice started to develop more PanIN lesions than CD-fed mice and they also had more high-grade PanINs, which suggested HFD could accelerate PanIN initiation (70-72). HFD promoted PDAC formation as well, because, at 3-month-old, there were already tumors detected in mice fed with HFD, while in mice fed with CD, none of the mice developed tumors until 9 months of age (72). Meanwhile, using a leptin deficient obese mouse model (*ob*/*ob* mice), researchers showed obese *Pdx1*-Cre;LSL-*Kras*^{G12D} mice had more PanINs and more mice developed tumors compared to lean *Pdx1*-Cre;LSL-

Kras^{G12D} mice (73). In both obesity PDAC mouse models, there was more tumor burden (tumor weight or area) and metastasis in mice with higher body weight which suggested obesity accelerated the progression of PDAC (70,72,73). Researchers have suggested multiple mechanisms for HFD-accelerated PDAC initiation and development including increased inflammation, desmoplasia, hyperinsulinemia, and elevated CCK expression (70-74).

1.2.3 Putative mechanisms linking obesity, type 2 diabetes, and pancreatic cancer

One study estimated that about 5.7% of cancers were attributable to the combined effects of diabetes and obesity (BMI $\geq$ 25 kg/m^2), but they did not differentiate between T1D and T2D (75). Broken down by cancer type, the combined effects of diabetes and obesity account for 16.5%-18.8% of liver cancer, 13.1% of pancreatic cancer, 7.2% of breast cancer, 31.3% of endometrial cancer, 28.7%-29.5% of esophagus, and 18%-21.3% kidney cancer incidences (75). Additionally, between 1980 and 2002, the percentage of cancer incidence that could be attributed to obesity and diabetes increased 20% and 30%, respectively (75). Therefore, it is important and urgent for us to find the potential factors linking obesity and T2D to increased cancer risk and mortality.

T2D and obesity share some cardinal features including hyperinsulinemia, hyperglycemia, dyslipidemia, increased inflammation and increased adipokine levels, which are proposed to be the potential factors linking T2D and obesity to cancer risks (Figure 1.5) (63,76,77). The roles hyperinsulinemia plays in cancer development and the possible mechanisms are introduced in more detail below.

Compared to noncancerous cells, many types of cancer cells are thought to preferentially use aerobic glycolysis over oxidative phosphorylation to generate energy, which is known as the

Warburg effect (78). Although aerobic glycolysis is inefficient in energy production, it can support the high proliferation rate of cancer cells by generating precursors necessary for nucleotide, amino acid, and lipid synthesis (79). Therefore, investigators have suggested that hyperglycemia may provide tumor cells with more glucose to use and therefore, promote and support a tumor's high proliferation rate. Moreover, hyperglycemia increases the formation of advanced glycation end products (AGEs), which are formed when glucose is nonenzymatically added to the free amino group on protein, lipids, or nucleic acids (63,80). It has been reported that the interaction of AGEs with their receptors leads to an increase in inflammation and oxidative stress, which promotes tumor growth and angiogenesis. To examine effects of hyperglycemia on cancer growth *in vivo*, investigators generated hyperglycemia mouse models using streptozotocin, which kills β cells and results in a loss of insulin secretion (81-83). However, in those models, streptozotocin-induced hyperglycemia inhibited pancreatic and breast cancer growth (81-83), and potentially implicated insulin as a causal factor. Therefore, more *in vivo* studies should be designed to clearly demonstrate if hyperglycemia itself promotes cancer development.

Dyslipidemia, especially dysregulation of cholesterol levels, is common in obesity and T2D. Cholesterol may promote tumor growth through increasing phosphatidylinositol 3-kinase (PI3K)/AKT/mTOR signaling and increasing cell proliferation (84,85). Moreover, cholesterol is a precursor for androgen, estrogen, and progesterone synthesis so it may especially promote hormone sensitive tumors like prostate and breast cancers through providing extra androgens or estrogens (86,87). Studies showed that low-density lipoprotein (LDL) cholesterol increases breast and prostate cancer cell proliferation *in vitro* and using high-cholesterol diets, researchers demonstrated that hyperlipidemia could promote growth of ERα-positive breast and prostate

cancer *in vivo* (88-90). Epidemiological studies also showed that high intake of cholesterol and serum cholesterol levels increased the risk of pancreatic cancer and cholesterol pathway inhibition can promote epithelial-mesenchymal transition in pancreatic cancer (91,92). Therefore, the high cholesterol levels associated with T2D, and obesity could be the factor linking them to sex hormone associated cancers, such as breast and prostate cancers, as well as non-hormone associated cancers, like pancreatic cancer.

T2D and obesity are associated with chronic low-grade inflammation and adipose tissue and the pancreas are infiltrated with immune cells (63). Moreover, obesity is a risk factor for acute pancreatitis and can worsen its severity (93,94). It is well-known that inflammation plays significant, but complex roles in cancer initiation, progression, and metastasis (36). For instance, IL-6 and tumor necrosis factor alpha (TNF-α), which are expressed at higher levels in obesity, can induce cancer cell proliferation, survival, and invasion (63). Inflammation is also the key mediator of pancreatic cancer initiation and development as introduced above.

Obesity is commonly associated with dysregulated levels of adipokines which are the factors secreted by adipocytes (63,77). Leptin is one of the adipokines produced by adipocytes and it regulates appetite. When leptin binds to its receptor, it can stimulate multiple intracellular signaling cascades including MAPK/ERK, PI3K/AKT/mTOR, and JAK/STAT pathways which all promote tumor growth (63,77). Leptin promotes cell proliferation and increases glucose uptake of human pancreatic cancer cells *in vitro* via PI3K/AKT pathway and leptin receptor deletion reduced tumor growth in an *in vivo* orthotopic pancreatic cancer mouse model (95,96). The leptin receptor is also expressed in human breast and gastrointestinal cancers and high expression of the leptin receptor is associated with a poor prognosis in breast cancer (63). Another adipokine, adiponectin, is detected at lower levels in obese individuals, and its effects

are anti-inflammatory (63,97). Adiponectin knockout mice had increased liver and colon tumor formation but decreased mammary tumors (97). In pancreatic cancer, a study showed that adiponectin treatment inhibited pancreatic cancer cell growth while another study demonstrated that adiponectin promoted pancreatic cancer progression through inhibiting cancer cell apoptosis (98,99). Therefore, more studies are needed to demonstrate the role adiponectin plays in PDAC. Resistin is another adipokine proposed to play a role in tumorigenesis and it is proinflammatory (100). An *in vitro* study showed that resistin stimulated prostate cancer cell proliferation through activating PI3K/AKT/mTOR pathway and another study showed that silencing resistin's cognitive receptors could reduce pancreatic cancer cell proliferation and migration (101,102). However, based on current studies, adipokine effects on tumorigenesis remain controversial and further studies should be performed to have a better understanding of their roles in cancer.

1.3 Insulin, hyperinsulinemia, and pancreatic cancer

1.3.1 Insulin

Insulin is a 5.8kDa peptide hormone that acts as a major regulator of metabolism (103). In pancreatic β cells, insulin is first produced as a precursor called preproinsulin and at the rough endoplasmic reticulum, preproinsulin is cleaved into proinsulin and a signal peptide (103). The folded proinsulin is then transported to the Golgi apparatus to be cleaved into insulin and C-peptide (103). Glucose is the main stimulator for the release of insulin from β cells; however, other nutrients like amino acids and fatty acids can also stimulate insulin secretion (103). In addition to insulin and C-peptide, β cells produce other hormones including islet amyloid polypeptide (IAPP). IAPP has been reported to cause *p53*-deficient tumor regression (104), although these findings have not been independently reproduced.

Three main organs respond to insulin signaling to regulate glucose homeostasis: liver, adipose tissue, and muscle. When insulin binds to the insulin receptor in muscle cells and adipocytes, it activates adipocytes and muscle cells to transport more glucose transporter type 4 (GLUT4) to the cell membrane which increases the glucose uptake (105,106). Insulin signaling also increases protein synthesis in muscle cells and reduces lipolysis in adipocytes (105,106). When insulin binds to the insulin receptors in hepatocytes, the signaling reduces glucose production but increases glycogen and protein synthesis in the liver (105,106). Therefore, liver, muscle, and fat work together to increase the utilization and storage of glucose, which leads to a reduction in plasma glucose levels. Insulin also regulates other cell types in the body. For instance, amylase enzyme production was reduced in rats where β-cells were killed by streptozotocin and its synthesis was restored when insulin was injected (107). In addition, when the insulin signaling cascade is activated in the brain it increases physical activity and reduces food intake and the activation of insulin signaling in endothelial cells reduces inflammation (105,106). Recently, an increasing number of studies have been proposed and conducted to understand insulin's effects on various cell types.

1.3.1.1 Insulin gene in mouse and hyperinsulinemia

Unlike humans, who have only one insulin gene (*INS*), rodents have two insulin genes, *Ins1* and *Ins2*. Deletion of *Ins1* or *Ins2* does not cause hyperglycemia in mice which illustrates redundancy and genetic compensation; however, it is lethal for mice to lose both *Ins1* and *Ins2* (108-110). *Ins2* is the ancestral gene which resembles the human *INS* gene, and it contributes to 2/3 of the insulin mRNA in islets (111,112). A trace amount of *Ins2* can also be detected in the thymus and brain (112). The rodent-specific *Ins1* likely arose from a reverse-transcribed,

partially processed *Ins2* mRNA transposition and its expression is restricted to β cells (113). Compared to *Ins2*, *Ins1* lacks one of the two introns, and they reside on different chromosomes (111). Although *Ins1* and *Ins2* share high homology, their promoter elements, imprinting status, temporal expression pattern, translation and processing rates are different which may explain why evolutionarily, both are retained (112,114-117).

Although elevated circulating insulin, or hyperinsulinemia, is a well-known characteristic of obesity and T2D, there is no agreed upon clinical or research definition of this feature. Fasting insulin of >12.2mU/L has been suggested as a cutoff to define hyperinsulinemia but conceptually, we can define hyperinsulinemia as excess insulin relative to what is required to maintain a normal glucose level (118,119). Hyperinsulinemia can arise from insulin hypersecretion or reduced systemic insulin clearance, or a combination of both. Many studies have demonstrated that hyperinsulinemia is associated with metabolic disorders (like obesity and insulin resistance) and cancer (introduced in more detail below).

By manipulating the gene dosages of *Ins1* and *Ins2*, the Johnson group has developed mouse models that can be used to examine the causal roles of HFD-induced hyperinsulinemia in many conditions, including obesity, insulin resistance, fatty liver, and longevity (112,120-124). In a *Ins2*-null ($Ins2^{-/-}$) genetic background, mice having only one allele of *Ins1* gene ($Ins1^{+/-}$) exhibit a significant reduction in fasting insulin and are protected from HFD-induced obesity compared to control mice having two alleles of *Ins1* gene ($Ins1^{+/+}$) (112). In addition, they showed that in a *Ins1*-null ($Ins1^{-/-}$) genetic background, $Ins2^{+/-}$ ($Ins1^{-/-}$;$Ins2^{+/-}$) mice have significantly lower fasting insulin levels, body weight, as well as an extended lifespan compared to $Ins1^{-/-}$;$Ins2^{+/+}$ mice (120-122). Those studies showed the causal role of hyperinsulinemia in

obesity and these models can be used to study hyperinsulinemia's causal effects on various pathophysiological parameters.

1.3.2 Hyperinsulinemia and cancers

Many epidemiology studies showed that hyperinsulinemia is associated with an increased risk of cancer. Through comparing the individuals with the highest quartile and lowest quartile of C-peptide level or insulin level, researchers found hyperinsulinemia increased the risk of getting pancreatic, breast, colorectal, liver, endometrial, gastric, and ovarian cancers (125-132). Moreover, genetic predisposition to hyperinsulinemia was associated with an elevated risk of pancreatic, lung, and endometrial cancer (76,133). Interestingly, a study showed that even for healthy-weight women, they were at higher risk of breast cancer if their fasting insulin level was at the highest quartile. In contrast, overweight women did not have excess breast cancer risk if their fasting insulin level was in the lowest quartile (134). Hyperinsulinemia is also associated with cancer mortality (135). For instance, studies showed hyperinsulinemia was associated with a 1.35-fold, 1.5-fold, and 2.72-fold increased risk of death from breast, colorectal, liver cancer, respectively (136-138). Even for non-obese individuals, hyperinsulinemia was associated with increased cancer mortality (139). Therefore, these studies suggested that hyperinsulinemia can be an independent risk factor for cancer incidence and mortality.

Hyperinsulinemia may promote tumorigenesis through several mechanisms. Hyperinsulinemia can promote tumor growth through classical insulin signaling. When insulin binds to its receptor, it will stimulate multiple downstream signaling cascades such as PI3K/AKT/mTOR pathway and MAPK/ERK pathway, which both are highly mutated in many

types of cancer. The insulin receptor and its downstream signaling pathway will be discussed in more detail below.

Hyperinsulinemia may promote tumor growth through regulating the farnesylation of Ras (140,141). The activation of Ras can only occur if Ras is anchored at the cell membrane and a farnesyl moiety is needed to be attached to Ras before it is translocated to the cell membrane, which is known as farnesylation (141). Insulin signaling can phosphorylate and activate farnesyltransferase which is the enzyme that facilitates farnesylation (141). Therefore, hyperinsulinemia may augment the amount of farnesylated Ras available for GTP loading and as a result, the MAPK/ERK signaling is overactivated and mitogenesis is enhanced (141).

Additionally, hyperinsulinemia may indirectly affect tumorigenesis by regulating the levels of IGF-1 and sex-hormone-binding globulin (SHBG) (Figure 1.5) (80,140). IGF-1 signaling can increase cell proliferation and survival, thus acting as a mitogen for cancer cells (142-144). In the liver, IGF-1 release is dependent on growth hormone signaling and insulin can upregulate growth hormone receptors in hepatocytes which consequently increase IGF-1 levels (145,146). Meanwhile, insulin-like growth factor binding proteins (IGFBP), especially IGFBP-3 can bind IGF-1 and IGF-2 and reduce their bioavailability (80). Moreover, IGFBP-3 can directly regulate the interaction between IGF-1 and its receptor which inhibits cell proliferation and increases apoptosis (80). Same as IGF-1, IGFBP-3 is also produced by hepatocytes and is suppressed by insulin (80,147,148). As a result, hyperinsulinemia may indirectly promote tumor growth through enhancing the IGF-1 signaling cascade. Insulin also inhibits the hepatic synthesis of SHBGs, which bind to testosterone and estradiol (63,80). Therefore, the bioavailability of sex hormones is increased under hyperinsulinemia status, which may lead to the greater risk of estrogen-dependent breast and endometrial cancer.

Hyperinsulinemia may contribute to tumorigenesis through inducing excess reactive oxygen species which can cause genetic damage (149). An *in vitro* study showed that 5 nM insulin can induce significant DNA damage in human colon adenocarcinoma and peripheral lymphocyte cells (150). Moreover, using a hyperinsulinemic-euglycemic clamp, chronic hyperinsulinemia caused elevated reactive oxygen species production and genomic stress in rat kidney cells (151). Reactive oxygen species was not only shown to lead to the development of acute pancreatitis but also shown to drive the formation and progression of pancreatic precancerous lesions (152-154). This suggests that hyperinsulinemia may accelerate tumor progression through supporting tumor cells gaining additional mutations.

Studies have also suggested hyperinsulinemia is associated with increased inflammation (119). For example, a study showed that modest hyperinsulinemia is sufficient to cause adipose tissue inflammation in experimental animals (155). Additionally, in human serum and adipose tissue, insulin infusion increased IL-6, TNF-α, and monocyte chemoattractant protein-1 (MCP-1) levels during a hyperinsulinemic-euglycemic clamp (156-158). Insulin signaling in immune cells is also important for their function. Studies found knocking out the insulin receptor (*Insr)* gene in T cells diminished cytotoxicity and reduced the production of IL-10 and IL-4 (159,160). Insulin signaling is also required to maximize T cell proliferation and differentiation (159,161). Therefore, hyperinsulinemia may promote tumorigenesis indirectly through affecting immune cells in the microenvironment.

1.3.3 Hyperinsulinemia in PDAC

As introduced above, epidemiological studies demonstrated how PDAC is cancer with one of the strongest associations with hyperinsulinemia. For instance, a study comparing male

Finnish smokers with insulin concentration in the highest quartile to those with insulin in the lowest quartile had a 2.01-fold increased risk of PDAC, with associations being stronger when the follow-up was longer than 10 years (RR 2.9) (162). A meta-analysis demonstrated that hyperinsulinemia was associated with a 70% higher risk of PDAC (163). Hyperinsulinemia and insulin resistance were also associated with increased aggressiveness and mortality of PDAC. Dugnani *et al*. showed the median overall survival rate was significantly lower in PDAC patients with insulin resistance (164). Moreover, when examining the use of antidiabetic agents and PDAC risk, researchers found that usage of insulin or insulin secretagogues was associated with ~2-fold higher risk of PDAC (165,166). Therefore, these epidemiological studies support the insulin-cancer hypothesis in PDAC.

The exocrine pancreas is anatomically unique due to its proximity to the insulin-producing β cells. The local pancreatic insulin concertation is approximately 10 times higher than the circulating insulin concentration after post-hepatic circulation because over 50% of secreted insulin is absorbed in liver (167-169). Interestingly, researchers found there were more mitoses in acinar cells proximal to islets compared to distant acinar cells, and in T1D patients, there was a smaller number of acinar cells (107,170,171). At levels that do not cause hypoglycemia, hyperinsulinemia alone can promote hepatic neoplasia in pre-clinical islet transplant experiments (172,173). Therefore, it is important to investigate if hyperinsulinemia will promote PDAC using an *in vivo* mouse model.

1.4 Insulin receptor signaling and pancreatic cancer

1.4.1 Insulin receptor signaling

It is commonly accepted that insulin executes its metabolic roles through PI3K/AKT/mTOR pathway and executes its mitogenic role through MAPK/ERK pathway, although the former pathway can also drive proliferation (Figure 1.6). When insulin binds to insulin receptor, INSR, this receptor tyrosine kinase is autophosphorylated and insulin receptor substrate (IRS) is then recruited to the phosphorylated INSR through its phosphotyrosine binding domain (105,140). IRS is also phosphorylated by INSR tyrosine kinase and phosphorylated IRS interacts with the p85 regulatory subunit of PI3K which activates the PI3K p110 catalytic subunit (105,140). PI3K then phosphorylates membrane attached phosphatidylinositol 4,5-bisphosphate (PIP2) to phosphatidylinositol (3,4,5)-triphosphate (PIP3) which recruits phosphoinositide-dependent kinase (PDK) to directly phosphorylate serine/threonine protein kinase AKT (105,140). Activated AKT can phosphorylate and consequently inhibit or activate a broad range of proteins like the transcription factor forkhead family box O (FOXO), mTOR, ribosomal protein S6 (S6K), glycogen synthase kinase 3β (GSK3β), and the RabGAP TBC1 domain family member 4 (TBC1D4) (105). These effector proteins then regulate glucose production, uptake, and storage, as well as glycogen, lipid, and protein synthesis. The mitogenic aspects of the PI3K/AKT/mTOR signaling cascade will be discussed in more detail below. Additionally, insulin signaling cascade has negative feedback loops that converge on IRS proteins. For instance, phosphatases like protein tyrosine phosphatase 1B (PTP1B) can dephosphorylate tyrosine residue on IRS while S6K and mTOR can carry out inhibitory phosphorylation of IRS proteins (105). These antagonistic signaling events can desensitize insulin signaling and are suggested to contribute to insulin resistance in T2D.

For the MAPK/ERK arm, a SH2 domain containing growth factor receptor-bound protein 2 (GRB2) can bind to the phosphorylated INSR, as well as to the guanine nucleotide exchange factor Son of Sevenless (SOS) (140). SOS then activates Ras by stimulating the exchange of bound GDP for GTP. Ras can then activate the downstream Raf/Mek/Erk signaling cascade (140). Moreover, GTP bound Ras can directly interact and activate PI3K p110 catalytic subunit independently of p85 and studies showed that Ras-PI3K interaction was important for Ras-driven tumorigenesis (174). The MAPK/ERK pathway regulates cell cycle entry and cell survival, and it is highly mutated during tumorigenesis (introduced in more detail below).

1.4.2 Insulin receptor signaling in cancer

Although insulin mainly utilizes the PI3K/AKT/mTOR axis to conduct its metabolic role, this pathway is also an important regulator of cell proliferation, and proteins that activate or suppress this pathway are frequently mutated in tumor cells. For instance, phosphatidylinositol-4,5-Bisphosphate 3-Kinase Catalytic Subunit Alpha (*PIK3CA*), which is the gene encoding the catalytic p110α subunit of PI3K, is frequently mutated in many human cancers including breast, gastric, prostate, lung, cervical, and colon (175-178). The mutations commonly occur at two hotspots: H1047R and E545K, which will increase PI3K interaction with the lipid membrane and reduce inhibition by the regulatory subunit p85, respectively (179). Studies also showed that non-coding RNA (ncRNA) can activate or inhibit PI3K/AKT/mTOR signaling during tumorigenesis. For example, the ncRNA GRNDE can promote cell proliferation through activating PI3K signaling and is upregulated in non-small cell lung cancer, colorectal cancer, gastric cancer, and hepatocellular carcinoma (180-185). Moreover, GAS5, which is another ncRNA that inhibits PI3K activity, is downregulated in tumor cells (178,186-188). Furthermore,

the phosphatase PTEN, which is a negative regulator of PI3K/AKT/mTOR pathway, is a well-known tumor suppressor and its loss of function mutations are frequently detected in many cancers including brain, breast, and prostate cancers (178,189-191).

The active PI3K/AKT/mTOR signaling cascade can provide tumor cells with growth advantages through several mechanisms. AKT can indirectly arrest the cell-cycle and reduce apoptosis through inhibiting FOXO, which induces apoptosis by upregulating Bcl-2-like protein 11 (BIM) and Fas ligand expression (192). MDM2 is a proto-oncogene that inhibits TP53, and it can be phosphorylated and activated by AKT (193). As a consequence, tumor cells can escape TP53-induced cell-cycle arrest. Moreover, insulin can increase protein synthesis through activating mTOR and its downstream targets, like S6K, supporting the rapid proliferation of cancer cells (105). Thus, insulin can also execute its mitogenic function through PI3K/AKT/mTOR arm.

The MAPK/ERK pathway is highly mutated in tumorigenesis. RAS proteins are mutated in ~30% of human cancers and for certain types of cancers, RAS is mutated at a higher frequency. For example, 90% in pancreatic cancer, 40% in colorectal cancer, and 27-36% in ovarian cancer (194,195). B-RAF has been reported to be mutated in ~7% of all cancers and it is especially mutated in melanomas (27-70%), colorectal (5-22%), ovarian (30%), and thyroid cancers (36-53%) (194-196). The most common *B-Raf* mutation is V600E which can account for >90% of *B-Raf* mutations found in melanomas and thyroid cancers (194,196). The V600E mutation in BRAF is also found in ~3% of pancreatic cancer cases (197). ERK can also be found mutated in 67-90% of melanomas, which demonstrates how important the MAPK/ERK pathway is for tumor growth (195).

MAPK/ERK signaling can regulate diverse processes that are important for tumor progression and metastasis such as proliferation, survival, migration, angiogenesis, and extracellular degradation. As an example, Ras can alter the expression of p16, p15, and p21 which can regulate cell cycle, while the presence of ERK in the nucleus is essential for G1 to S phase transition (194,198,199). Also, when ERK is translocated into the nucleus, ERK can activate various transcription factors like the proto-oncogenes c-Fos, c-Jun, and c-Myc (195). ERK can also phosphorylate myosin light chain kinase, paxillin, focal adhesion kinase, and matrix metalloproteinases which can promote tumor migration and invasion, as well as induce vascular endothelial growth factor (VEGF) expression to promote angiogenesis (194,200,201). Similar to AKT, ERK can phosphorylate BAD, BIM, and caspase 9 to inhibit apoptosis and increase cancer cell survival (194). Consequently, hyperinsulinemia could enhance tumor progression through stimulating either the PI3K/AKT/mTOR or MAPK/ERK signaling cascades.

1.4.2.1 The insulin receptor isoforms in cancer

Insr mRNA can undergo a differential splicing pattern which generates two INSR isoforms: INSR-A and INSR-B, which are expressed in different relative abundance in various tissues (149,202). INSR-B contains exon 11, while INSR-A does not, and it is well established that INSR-A carries more of the mitogenic and anti-apoptotic effects of insulin while INSR-B mediates metabolic effects (149,202). INSR-A/INSR-A homodimer and INSR-B/INSR-B homodimer can bind to insulin at similar affinities, while INSR-A/INSR-A binds to IGF-2 at a much higher affinity compared to INSR-B/INSR-B (EC_{50} 3.3 nM vs 36 nM) (149,203). INSR-A and INSR-B can also form heterodimers with insulin-like growth factor 1 receptor (IGF1R) as

INSR-A/IGF1R and INSR-B/IGF1R. Insulin, IGF-1, and IGF-2 can all bind to these heterodimers (149,202,204).

INSR level is upregulated in cancers and in certain types of cancers, INSR may play a more significant role than the IGF1R. INSR-A is believed to be the isoform predominantly overexpressed during tumorigenesis and either INSR-A or the ratio of INSR-A to INSR-B has been found to increase in breast cancer, prostate cancer, lung cancer, endometrial cancer, and liver cancer, but the expression of INSR-A and INSR-A to INSR-B ratio in pancreatic cancer is not very clear (149,202,205-207). Specifically, INSR-A to INSR-B ratio seems to significantly increase in all breast cancer stages and INSR is associated with poor breast cancer patient survival (149,205,207). Interestingly, hormone-resistant ER positive tumors had an increased INSR expression but a reduced IGF1R expression (206), and similarly, in colorectal carcinoma, IGF1R was expressed at lower levels than INSR (208).

The mechanism of increased INSR expression in cancer cells is still poorly studied; however, some studies suggested that *Insr* gene transcription may be dysregulated by oncogene or tumor suppressor genes. For instance, the frequently mutated TP53 is a negative regulator for *Insr* (209). In addition, high mobility group protein A1 (HMGA1) and specificity protein 1 were shown to be upregulated in some cancers and they positively affected *Insr* expression (149,210-213). Investigators also found that some microRNAs (miRNAs) can regulate INSR abundance. For example, miR-195 can post-transcriptionally suppress INSR expression and miR103/107 can destabilize INSR at the membrane by targeting caveolin-1 (149,214,215). Moreover, some studies suggested that the increased ratio of INSR-A to INSR-B in cancer was because of changes in splicing factor expression (149). For instance, SRP20/SRSF3, which are splicing

factors that retain exon 11 and promote INSR-B isoform formation, were decreased in human hepatocellular carcinoma (149).

Hyperinsulinemia can cause INSR internalization (124), which can reduce the number of INSR proteins available on the membrane for insulin ligand binding. Nevertheless, researchers demonstrated that breast cancer cells are insensitive to hyperinsulinemia-induced INSR downregulation (216,217). Interestingly, insulin may induce SPR20/SRSF3 degradation which may then lead to increased INSR-A levels, and consistent with this an elevated INSR-A to INSR-B ratio is positively correlated with hyperinsulinemia (149,218,219). Therefore, cancer cells may have many methods to escape the desensitization of INSR.

1.4.2.2 Insulin receptor signaling in PDAC

Not many studies have investigated whether insulin and/or insulin receptors play a specific role in acinar cells during normal physiology. Bruce *et al*. showed that when insulin bound to INSR on acinar cells, AKT was activated, which then phosphorylated and activated the key glycolytic enzyme, phosphofructokinase fructose bisphosphatase-2 (PFKFB2) (220). PFKFB2 catalyzed the synthesis of fructose 2,6-bisphosphate which then drove glycolytic adenosine triphosphate (ATP) production, and this could provide acinar cells with sufficient ATP and protect them during acute pancreatitis (220). This study suggests the importance of insulin receptor signaling in supporting energy production in normal acinar cells, but more studies are needed to characterize other aspects of INSR function in acinar cells.

In contrast, multiple studies have examined the importance of factors involved downstream of INSR signaling during pancreatic tumorigenesis, since mutations in both MAPK/ERK and PI3K/AKT/mTOR pathways can induce PDAC. As mentioned above, KRAS

mutations are detected in ~90% of PDAC and most PDAC mouse models are designed based on a *Kras*^{G12D} mutation (41). *PIK3CA* mutations can also be detected in 3-5% of PDAC patients (221-223). Additionally, when a constitutively activated PI3K was expressed in pancreatic cells (*Pdx-1*-Cre), PanIN lesions and tumors developed in these mice (224). The precursors lesions could be detected as early as 10 days of age and at 20-days old, PDAC was already be detected in some mice (224). Moreover, Sivaram *et al* found PI3K/AKT/mTOR signaling limits T cell recognition and tumor cell clearance in PDAC because when *Pik3ca* was silenced in *Pdx1*-Cre;*Kras*$^{LSL\text{-}G12D}$;*Trp53*$^{LSL\text{-}R172H}$ mice, it induced T cells infiltration, tumor repression, and increased the survival of the mice (225). Strategies developed to inhibit PI3K/AKT/mTOR signaling have also inhibited PDAC development (224,226). Furthermore, when the PI3K inhibitor PTEN is disrupted specifically in ductal cells, Kopp *et al* found the *Pten*$^{\Delta Duct/\Delta Duct}$ mice developed IPMN lesions and 31.5% of the lesions were invasive (9). In summary, the signaling cascades downstream of insulin action: the PI3K/AKT/mTOR and MAPK/ERK pathways, are both important for and dysregulated in PDAC as shown by *in vivo* mouse models.

1.5 Thesis overview

Although a correlative link between hyperinsulinemia in cancer has been proposed previously, there have been no published *in vivo* loss-of-function studies published that could directly demonstrate that hyperinsulinemia and insulin signaling can contribute causally to cancer development. Pancreatic cancer is one of the cancers that showed the strongest association with hyperinsulinemia. Therefore, we wanted to reduce endogenous insulin production or inhibit insulin signaling in a well-established PDAC mouse model to investigate if

and how hyperinsulinemia and insulin signaling affects HFD-promoted PDAC initiation and progression.

The first aim of my doctoral project was to determine whether the increase in insulin is necessary for HFD-mediated PDAC progression in *Ins2* null mice. I generated *Ptf1a*^{CreER};*Kras*$^{LSL\text{-}G12D}$;*Ins1*$^{+/+}$;*Ins2*$^{-/-}$ control mice in which HFD can induce high circulating insulin levels, and *Ptf1a*^{CreER};*Kras*$^{LSL\text{-}G12D}$;*Ins1*$^{+/-}$;*Ins2*$^{-/-}$ experimental mice which are protected from HFD-induced hyperinsulinemia. I first checked if there was a difference in glucose homeostasis between the two genotypes and then compared the pancreatic area occupied by PanIN lesions in each mice group to examine if endogenous hyperinsulinemia affects PDAC development.

The second aim was to determine whether the increase in insulin is necessary for HFD-mediated PDAC progression in *Ins1* null mice. To examine if PanIN development would also be affected by reducing *Ins2* gene dosage in an *Ins1*-null background, I generated *Ptf1a*^{CreER};*Kras*$^{LSL\text{-}G12D}$;*Ins1*$^{-/-}$;*Ins2*$^{+/+}$ control mice and *Ptf1a*^{CreER};*Kras*$^{LSL\text{-}G12D}$;*Ins1*$^{-/-}$;*Ins2*$^{+/-}$ experimental mice. I investigated if the reduction in insulin production affected glucose homeostasis. Also, I measured the percent pancreatic area occupied by PanIN, acinar to ductal metaplasia, or adipocytes to assess the difference in histopathology between the two genotypes. Finally, we used single-cell RNA sequencing to investigate the potential molecular mechanisms by which hyperinsulinemia promotes PanIN development.

The third aim was to determine whether insulin signaling in *Kras*^{G12D} expressing pancreatic acinar cells is necessary for HFD-mediated promotion of PanIN and PDAC initiation and progression. To accomplish this aim, I combined a conditional knockout allele for the *Insr* gene with the PDAC mouse model to generate *Ptf1a*^{CreER}*Kras*$^{LSL\text{-}G12D}$;*Insr*$^{w/w}$;nTnG,

Ptf1a^{CreER};*Kras*$^{LSL\text{-}G12D}$;*Insr*$^{w/f}$;nTnG, and *Ptf1a*^{CreER};*Kras*$^{LSL\text{-}G12D}$;*Insr*$^{f/f}$;nTnG mice. I first determined if loss of *Insr* in acinar cells affected glucose metabolism and then measured the Alcian blue^{+} area, CK19^{+} area, acinar cell area, PanIN area, and PanIN plus tumor area in each genotype to understand whether and how insulin signaling affects PanIN and PDAC initiation and development.

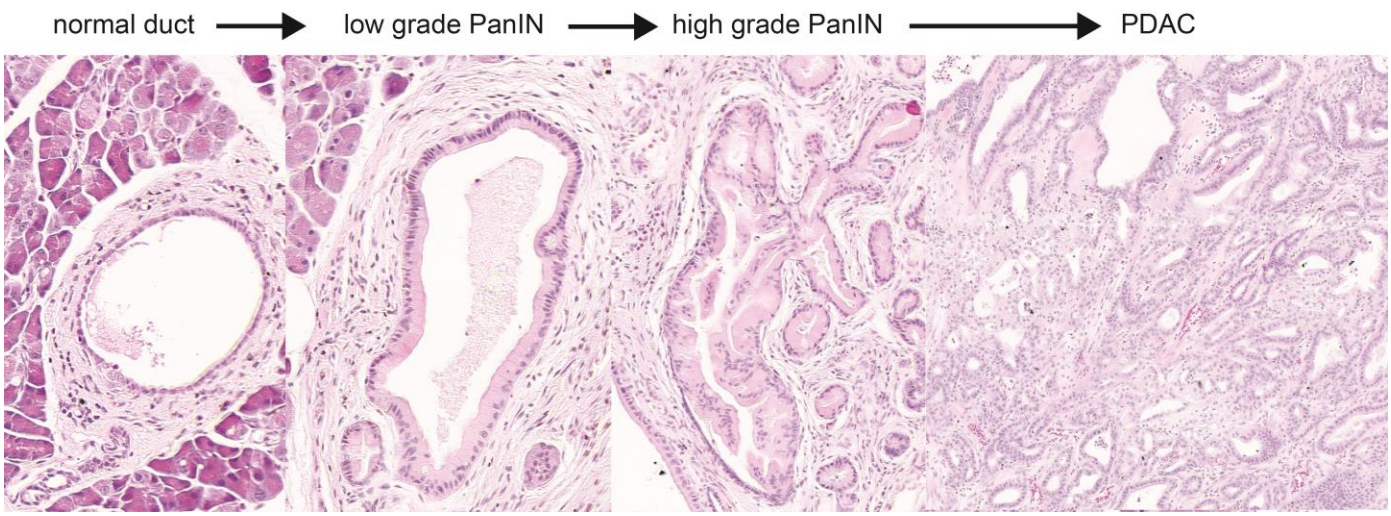

Figure 1.1. Progression of normal pancreatic duct to low grade PanIN to high-grade PanIN to PDAC.

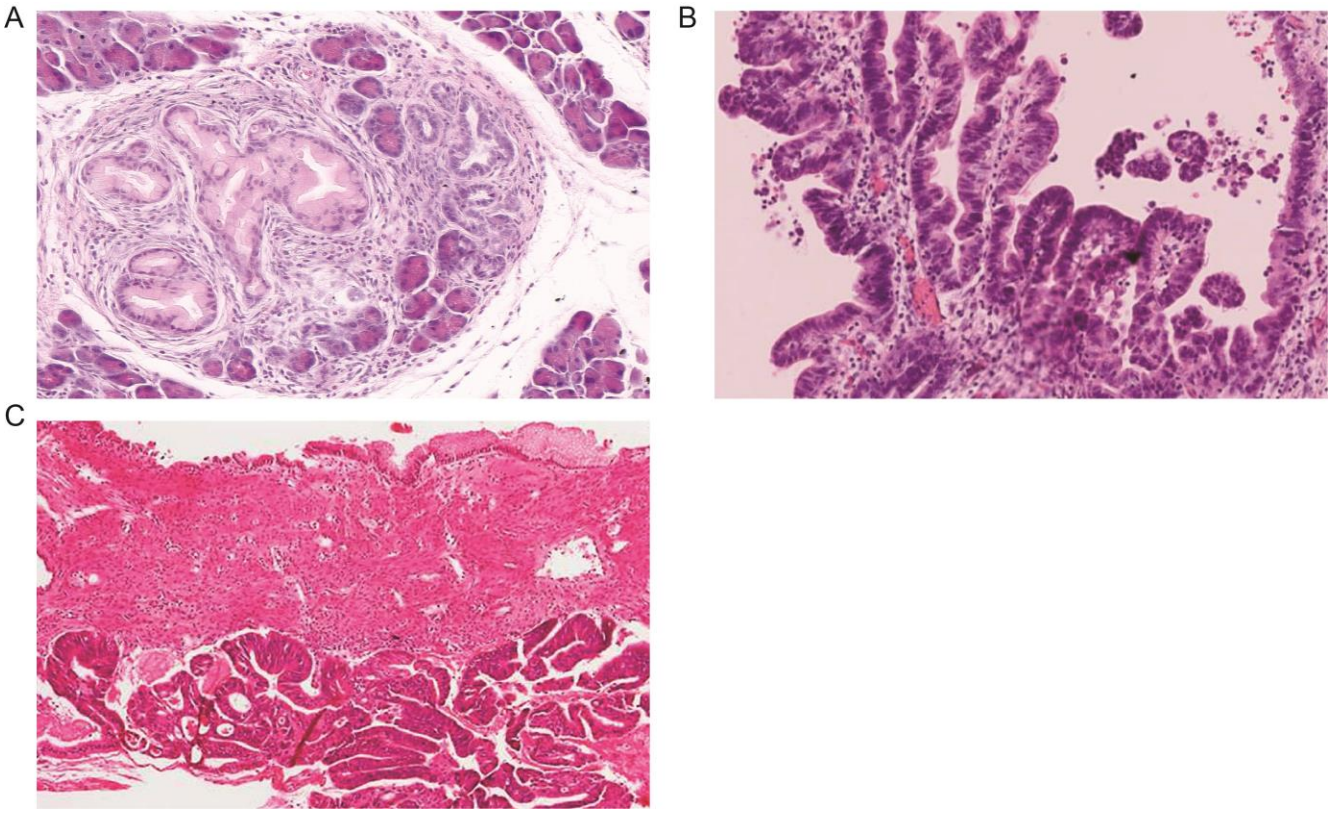

Figure 1.2. The representative pancreatic precancerous lesions.
A, PanIN, **B,** IPMN and **C,** MCN. Figure 1.1A and Figure 1.1B adapted from (227,228) with permission.

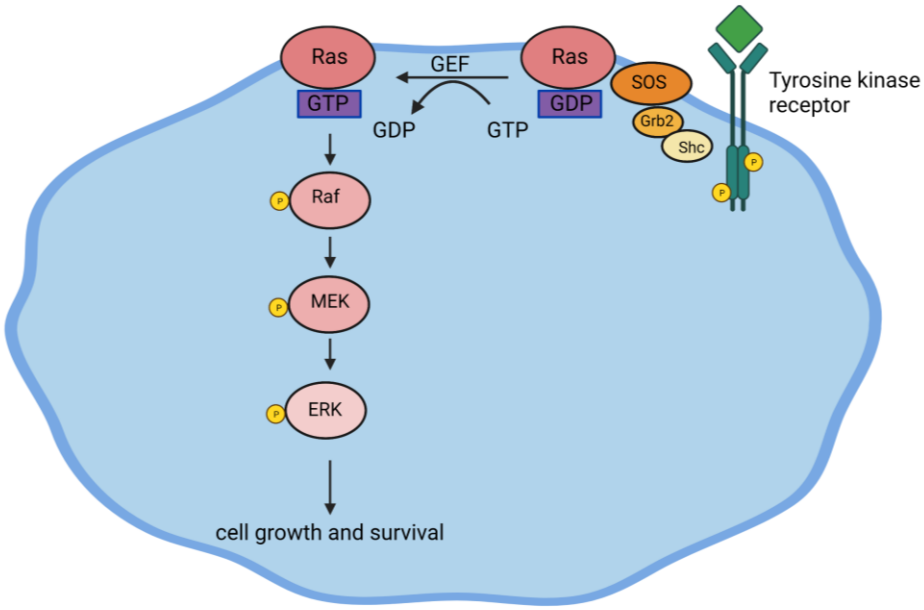

Figure 1.3. The MAPK/ERK signaling pathway.

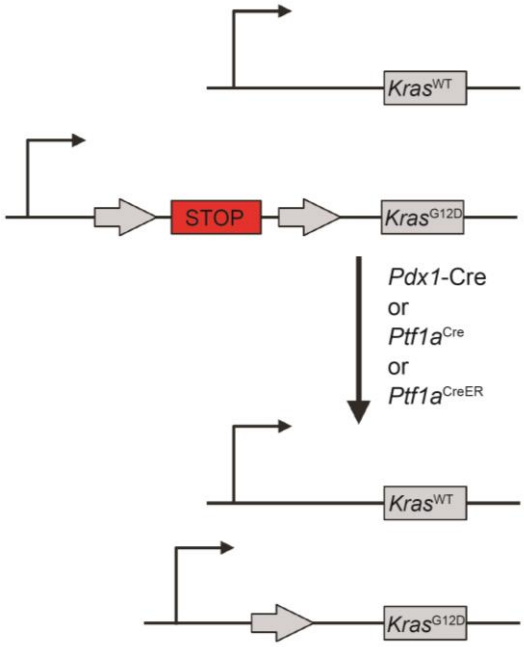

Figure 1.4. The schematic of *Kras* alleles in PDAC mouse models.
Cre recombinase expression is regulated by *Pdx1* or *Ptf1a* promoter and in the cells that Cre recombinases are expressed, the lox-stop-lox construct is removed and *Kras*^{G12D} mutation is induced in these pancreatic cells.

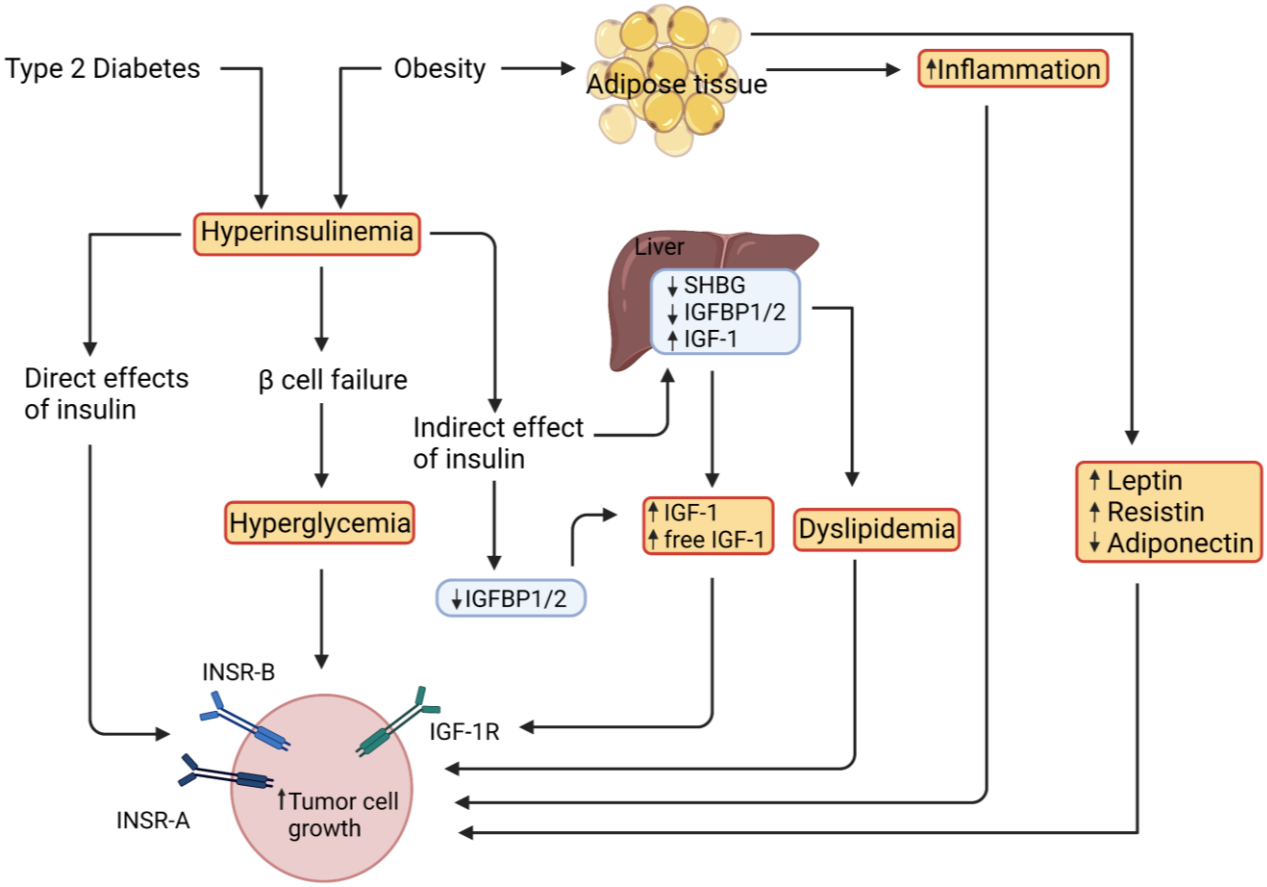

Figure 1.5. The proposed mechanisms linking T2D, obesity to cancer.
Adapted from Gallagher *et al* 2015 (63).

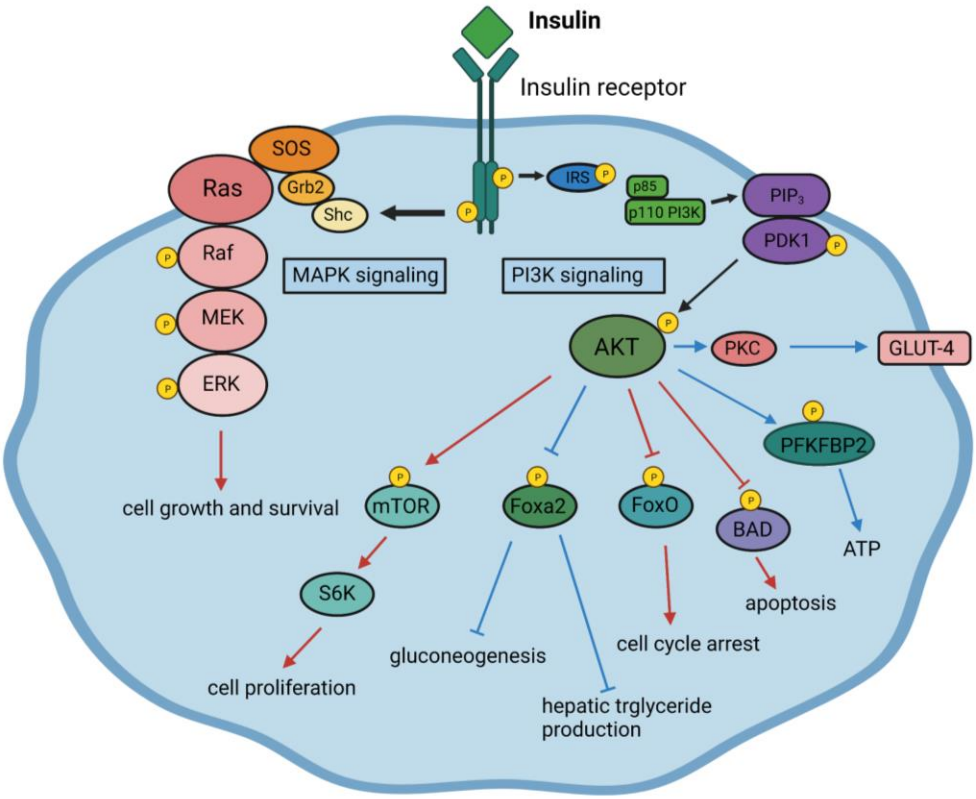

Figure 1.6. Signaling pathways activated by the insulin receptor.
The blue arrows indicate the pathways that are important in normal acinar cells and the red arrows indicate the pathways that are important in PanIN and tumor cells. Adapted from Godsland *et al* 2010 (140).

Chapter 2: Methods and Materials

2.1 Mice

All described animal experiments were conducted at the University of British Columbia with approval of the University of British Columbia Animal Care Committee in accordance with Canadian Council for Animal Care guidelines. *Kras*$^{LSL\text{-}G12D}$ mice (C57BL/6) were purchased from Jackson Labs (Bar Harbour, USA), *Ptf1a*^{CreER} mice (C57BL/6) were a gift from Chris Wright (Vanderbilt, USA), *Ins1*$^{-/-}$ and *Ins2*$^{-/-}$ mice (C57BL/6) were a gift from Jacques Jami (INSERM, France), *Insr*$^{f/f}$ mice, and nTnG mice were purchased from Jackson Labs (#006955 and #023035, respectively). Mice were maintained on C57BL/6 genetic background and housed at the University of British Columbia Modified Barrier Facility. They were kept in temperature-controlled specific pathogen-free conditions on a 12:12 hr light: dark cycle with food and drinking water *ad libitum*. The knock-in knock out *Ptf1a*$^{CreER/w}$ and *Kras*$^{LSL\text{-}G12D/w}$ genes and, *Ins1*$^{-/-}$, *Ins2*$^{-/-}$, *Insr*$^{w/f}$, *Insr*$^{f/f}$ and nuclear TdTomato-to-nuclear EGFP (nTnG) alleles have been previously described (112,120-122,229-233). To generate background-matched *Ptf1a*$^{CreER/w}$;*Kras*$^{LSL\text{-}G12D/w}$;*Ins1*$^{+/+}$;*Ins2*$^{-/-}$ control mice and *Ptf1a*$^{CreER/w}$;*Kras*$^{LSL\text{-}G12D/w}$;*Ins1*$^{+/-}$;*Ins2*$^{-/-}$ experimental mice, *Ptf1a*$^{CreER/w}$;*Kras*$^{LSL\text{-}G12D/w}$;*Ins1*$^{+/+}$;*Ins2*$^{-/-}$ males mice were bred with *Ins1*$^{+/-}$;*Ins2*$^{-/-}$ females mice, so the mice in control and experimental groups were from the same parental sets. The resulting litters were fed with a high-fat diet of 60% fat (Research Diets D12492; Research Diets) at weaning (3 weeks) and recombination was induced by four consecutive intraperitoneal injections of tamoxifen (Sigma-Aldrich) in corn oil (10 mg/mL) at 0.075 g tamoxifen/g body mass when the mice were 5-9 weeks old. The mice were euthanized at 57 weeks of age for histopathology analyses. To generate background-matched *Ptf1a*$^{CreER/w}$;*Kras*$^{LSL\text{-}G12D/w}$;*Ins1*$^{-/-}$;*Ins2*$^{+/+}$ control mice and *Ptf1a*$^{CreER/w}$;*Kras*$^{LSL\text{-}G12D/w}$;*Ins1*$^{-/-}$

;*Ins2*$^{+/-}$ experimental mice, *Ptf1a*$^{CreER/w}$;*Kras*$^{LSL\text{-}G12D/w}$;*Ins1*$^{-/-}$;*Ins2*$^{+/+}$ males mice were bred with *Ins1*$^{-/-}$;*Ins2*$^{+/-}$ females mice. The resulting litters were fed with an HFD at weaning and at 4 weeks of age, recombination was induced by three consecutive subcutaneous injections of tamoxifen in corn oil (20 mg/mL) at 5mg tamoxifen/40g body mass. The mice were euthanized at 57 weeks of age for histopathology analyses and single-cell transcriptomic analysis. To generate background-matched *Ptf1a*$^{CreER/w}$;*Kras*$^{LSL\text{-}G12D/w}$;*Insr*$^{w/w}$;nTnG, *Ptf1a*$^{CreER/w}$;*Kras*$^{LSL\text{-}G12D/w}$;*Insr*$^{w/f}$;nTnG, and *Ptf1a*$^{CreER/w}$;*Kras*$^{LSL\text{-}G12D/w}$;*Insr*$^{f/f}$;nTnG mice, *Ptf1a*$^{CreER/w}$;*Kras*$^{LSL\text{-}G12D/w}$;*Insr*$^{w/f}$;nTnG mice were bred with *Insr*$^{w/f}$ mice. After weaning, the resulting litters were fed with HFD and at 4 weeks of age, recombination was induced by three consecutive subcutaneous injections of tamoxifen in corn oil (20 mg/mL) at 5mg tamoxifen/40g body mass. One cohort of mice was euthanized at 10 months of age for histopathology analyses. Another cohort of mice was euthanized at 12 weeks of age. During dissection, the extracted pancreata were cut into three pieces roughly based on pancreas anatomical structure: pancreas head, pancreas body, and pancreas tail. For each mouse, the pancreas head was sent for phosphoproteomics analysis, the pancreas body was kept for histopathology analyses and the pancreas tail was used for single nucleus RNA sequencing and bulk RNA sequencing. The primers used for mouse genotyping were shown in Table 2.1.

2.2 Assessment of glucose homeostasis and plasma amylase levels

Mouse body weight and fasting blood glucose levels were measured every 4 or 5 weeks and the fasting insulin and amylase levels were measured every 3 months. Before the measurements, mice were fasted for 4 hours in clean and fresh cages during the light period. One drop of blood was collected from each mouse's leg and a Lifescan OneTouch Ultra Mini glucometer was used to measure the fasting blood glucose levels. About 30 µl of blood was

collected with heparinized microhematocrit capillary tube (fisher scientific, 22-362566, Waltham, MA, USA) for measuring fasting insulin levels and about 20 µl of blood was collected with a non-heparinized microhematocrit capillary tube (fisher scientific, 22-362574, Waltham, MA, USA) for measuring fasting amylase levels. The collected blood was centrifuged at 10,000 rpm for 10 minutes to collect the blood serum. Then the blood serum was used to measure the fasting insulin levels using insulin ELISA (80-INSMSU-E10; ALPCO Diagnostics, Salem, NH), and fasting amylase levels were measured with amylase activity assay kits (MAK009-1KT, MilliporeSigma, MA, USA).

The glucose-stimulated insulin secretion, intraperitoneal glucose tolerance, and insulin tolerance tests were conducted according to previously described protocols (112,120,122). Briefly, for glucose-stimulated insulin secretion, mice were fasted for 4 hours and 30 µl of blood was collected with a heparinized microhematocrit capillary tube before glucose injections. Then glucose was injected intraperitoneally (2 g/kg), and 30 µl of blood was collected 15 minutes and 30 minutes after injections. Then blood serum was used to measure the fasting insulin levels as described above. For intraperitoneal glucose tolerance test and insulin tolerance test, mice were fasted for 4 hours, and the fasting blood glucose levels were measured with the Lifescan OneTouch Ultra Mini glucometer before glucose injections or insulin injections. Then glucose (2 g/kg) or insulin (0.75 U/kg, Eli Lilly, USA) was injected intraperitoneally, and fasting glucose levels were measured 30 minutes, 60 minutes, 90 minutes, and 120 minutes after the injections.

2.3 Histopathological and morphological analyses

Ptf1a$^{CreER/w}$;*Kras*$^{LSL\text{-}G12D/w}$;*Ins1*$^{+/+}$;*Ins2*$^{-/-}$ and *Ptf1a*$^{CreER/w}$;*Kras*$^{LSL\text{-}G12D/w}$;*Ins1*$^{+/-}$;*Ins2*$^{-/-}$ mice pancreata were fixed for 24 hours using Z-FIX (Anatech Ltd.) followed by 48 hours with

4% paraformaldehyde. These were then embedded in paraffin for histopathology analyses. *Ptf1a*$^{CreER/w}$;*Kras*$^{LSL\text{-}G12D/w}$;*Ins1*$^{-/-}$;*Ins2*$^{+/+}$, *Ptf1a*$^{CreER/w}$;*Kras*$^{LSL\text{-}G12D/w}$;*Ins1*$^{-/-}$;*Ins2*$^{+/-}$, *Ptf1a*$^{CreER/w}$;*Kras*$^{LSL\text{-}G12D/w}$;*Insr*$^{w/w}$;nTnG, *Ptf1a*$^{CreER/w}$;*Kras*$^{LSL\text{-}G12D/w}$;*Insr*$^{w/f}$;nTnG, and *Ptf1a*$^{CreER/w}$;*Kras*$^{LSL\text{-}G12D/w}$;*Insr*$^{f/f}$;nTnG mice pancreta were fixed in 4% paraformaldehyde for 24 hours followed by paraffin embedding. Mouse pancreata were sectioned and stained with hematoxylin and eosin (H&E), Alcian blue, which stains the highly acidic mucin content, and Sirius red as previously described (74,234,235). The stained slides were scanned with a 20x objective using a 3DHISTECH Panoramic MIDI (Quorum Technologies Inc. Guelph, Canada) slide scanner.

Histopathological analyses were conducted by Anni Zhang in a de-identified manner and verified by Janel Kopp and David Schaeffer. All histopathological analyses were performed on one of the stained sections that displayed the maximal pancreatic cross-sectional area unless otherwise stated. For *Ptf1a*$^{CreER/w}$;*Kras*$^{LSL\text{-}G12D/w}$;*Ins1*$^{-/-}$;*Ins2*$^{+/+}$ and *Ptf1a*$^{CreER/w}$;*Kras*$^{LSL\text{-}G12D/w}$;*Ins1*$^{-/-}$;*Ins2*$^{+/-}$ mice, the PanIN plus tumor area, ADM area, and adipocytes area were analyzed on 3 H&E-stained sections, which were 140 μm away from each other. Every gland with a lumen was categorized as normal, ADM, PanIN, or neoplasia, and glands representing more than one of these categories were scored based on their highest-grade feature. The total pancreatic area, PanIN plus tumor area, PanIN area, fibrosis area, ADM area, adipocytes area, and, normal acinar cell area were measured as previously described (74). Briefly, the total pancreatic area, PanIN plus tumor area, PanIN area, normal acinar cell area was determined by masking all pancreatic tissue, selective masking of the PanIN plus tumor area, selective masking of the only PanIN area, and selective masking of the normal acinar cell area by Adobe Photoshop, respectively. The pixels for the total pancreatic area or each histological feature were

measured by ImageJ and this was used to calculate the percentage area occupied by each histological feature. The fibrotic area was determined by selective masking of the Sirius red stained area by Adobe Photoshop CC and the percentage area occupied by fibrosis per pancreas was calculated based on pixel numbers. The adipocyte area was selected by Adobe Photoshop 2020 magic wand tool and the whole pancreas area was selected by using magnetic lasso tool and magic wand tool. Then the selected adipocyte area and whole pancreas area were measured using Adobe Photoshop 2020 measurement log function. For Alcian blue positive area, Adobe Photoshop 2020 Black & White function was used to highlight the blue area (red filter). The total pixels for pancreas or Alcian blue positive area were counted by ImageJ and this was used to calculate the percent of Alcian blue positive area per pancreatic section.

2.4 Immunohistochemistry

The IHC staining was performed according to previously published standard protocols (234). Briefly, the pancreatic sections were deparaffinized and rehydrated in xylene, 100% ethanol, 95% ethanol, 70% ethanol, 50% ethanol, and water twice for 2 minutes. Antigens were unmasked using citrate buffer (10mM, pH 6) and antigen retrieval was done using a pressure cooker for 1 hour. After antigen retrieval, the slides were cooled below 62 degrees before removing and were rinsed with 0.1% Tween-20 in 1xPBS 3 times for 5 minutes. The slides were immersed in 2% H_2O_2 for 15 minutes to quench endogenous peroxidases and washed 3 times as described above. Then the slides were blocked and permeabilized with blocking solution (5% normal donkey serum (NDS), 0.1% Triton-X in 1x PBS, pH 7.4) for 30-60 minutes at room temperature. Primary antibodies were diluted with blocking solution and sections were incubated with primary antibodies overnight at 4°C. After washing 3 times in 0.1% Tween-20 in 1xPBS,

the slides were incubated with secondary antibodies, which were diluted in blocking buffer, at room temperature for 1-2 hours. After 3 washes, the slides were incubated with VECTASTAIN Elite Avidin-biotin complex (ABC, Vector Labs), which was prepared based on manufacturer's instruction, at room temperature for 2-5 hours. After 3 washes, 500 µl 3,3'-diaminobenzidine (DAB) solution, which was prepared based on the manufacturer's instruction, was added to each slide and the color change was observed under the scope to monitor the reaction. The reaction was stopped by adding water. After 3 washes with 1XPBS, the slides were counter stained with Mayer's hematoxylin (Thermo Fisher Scientific, 22-050-262) and mounted with Cytoseal (Sigma-Aldrich, MHS16). The primary and secondary antibodies used for IHC staining are listed in Table 2.2 and Table 2.3, respectively. All IHC slides were scanned with a 20x objective using a 3DHISTECH Panoramic MIDI slide scanner.

For Ki67 analysis, five 400 x 400 µm squares were randomly distributed in one pancreatic section for each mouse. We selected and analyzed 6 of the *Ptf1a*^{CreER};LSL-*Kras*^{G12D};*Ins1*$^{+/+}$;*Ins2*$^{-/-}$ mice and 5 of the *Ptf1a*^{CreER};LSL-*Kras*^{G12D};*Ins1*$^{+/-}$;*Ins2*$^{-/-}$ mice for Ki67 analysis. The total number of cells within each square was counted and the cells were assigned into one of the following cell types: acinar cells, PanIN cells, ductal cells, stromal cells, undetermined, reactive ductal cells/ ADM, or cancer cells. For each specific cell type, the ratio of Ki67^{+} cells to the total number of cells was calculated.

For CD20, phospho-ERK, and CK19 positive area measurements, Adobe Photoshop 2020 Black & White function was used to filter and highlight the brown area (blue filter). The percent of CD20^{+}, phospho-ERK^{+}, and CK19^{+} area per pancreatic section was calculated based on the ratio of pixels. Macrophage infiltration was quantified using the positive pixel count tool in Aperio ImageScope software (Leica Biosystems). In short, after IHC staining of F4/80.

pancreatic pathology areas were assigned into one of the following categories: ADM, PanIN, and PDAC. The infiltration density (%) of F4/80^{+} macrophages in each pathology category was expressed as the pixel area occupied by the DAB staining (F4/80^{+}) normalized to the pixel area occupied by the DAB staining plus the hematoxylin staining (all nuclei). The average infiltration density for each specific type of pathology for the entire pancreatic section per mouse was calculated.

2.5 Pancreas tissue dissociation and single-cell sorting

Single-cell RNA-sequencing was performed for *Ptf1a*$^{Cre\text{ER}}$;*Kras*$^{\text{LSL-G12D}}$;*Ins1*$^{-/-}$;*Ins2*$^{+/+}$ and *Ptf1a*$^{Cre\text{ER}}$;*Kras*$^{\text{LSL-G12D}}$;*Ins1*$^{-/-}$;*Ins2*$^{+/-}$ mice. Six *Ptf1a*$^{Cre\text{ER}}$;*Kras*$^{\text{LSL-G12D}}$;*Ins1*$^{-/-}$;*Ins2*$^{+/+}$ and six *Ptf1a*$^{Cre\text{ER}}$;*Kras*$^{\text{LSL-G12D}}$;*Ins1*$^{-/-}$;*Ins2*$^{+/-}$ mice pancreata were dissociated into single cells for scRNA-seq as previously described (evenly divided by sex) (235). Briefly, freshly dissected pancreata were minced into ~1mm pieces using sharp dissection scissors in HBSS and the pancreas pieces were collected into 15 ml conical tubes to be centrifuged at 720g for 2 minutes. After discarding the supernatant, tissues were resuspended in 5 ml of ice-cold HBSS containing 0.4 mg/ml collagenase P (Roche, #11213857001) and 10 mg/ml DNase I (Roche, #11284932001), and the tissues were transferred into 50 ml conical tubes. Several marbles were transferred into the tissue-containing tubes, which were then incubated in a water bath (37ºC) for 10-18 minutes with gentle shaking by hand. After the incubation, 10 ml HBSS + 5% FBS (ThermoFisher Scientific, #A3160701) was added to samples, and samples were centrifuged at 720g for 2 minutes. After washing 3 times with 10 ml HBSS + 5% FBS, tissues were filtered through a 100 μM cell strainer, and the strainer was washed with another 10ml HBSS + 5% FBS. Then the samples were centrifuged at 180g for 2 minutes to collect the dissociated cells. The

resuspended samples were stained with 0.05 μg/ml Hoechst 33342 (Invitrogen, #H3570) and 0.5 μg/ml propidium iodide (Sigma, #P4864) and were sorted for live cells using BD LSR II Flow Cytometer.

2.6 Processing, quality control, and analysis of single-cell transcriptomic data

The single-cell libraries were prepared with the Chromium Single Cell 3' Reagent Kits V3 (10X genomics, Pleasanton, CA, USA) according to the manufacturer's instructions and sequenced on a NextSeq500 (Illumina). The Cell Ranger pipeline (10X genomics, CA, USA) was used to perform the demultiplexing (cellranger mkfastq, 10X genomics) and alignment (cellranger count, 10X genomics). The R package SoupX was used to remove ambient RNA contamination (https://github.com/constantAmateur/SoupX). The cleaned gene-cell matrices were then loaded into R package Seurat 3.2.1 and filtered to remove cells with unique feature counts over 6000 or less than 200. The cells that had >20% mitochondrial gene counts or genes that were expressed by fewer than 3 cells were also removed. Using Seurat 3.2.1 (236,237), the filtered gene-cell matrices were integrated and clustered in uniform manifold approximation and projection (UMAP) space using default settings with resolution of 0.1. The cell identity for each cluster was assigned based on the expression of the typical marker genes (like *Prss2*, *Krt19*, and *Col1a1*) that are commonly used for pancreas scRNA-seq analysis (238-240). When the cluster identity could not be determined, Seurat 3.2.1 FindConservedMarkers function was used to find the top 50 genes that are conserved between mice. This gene list was then uploaded to Enrichr (https://maayanlab.cloud/Enrichr/) and I used similarities to the enriched gene expression profiles of different cell types identified by Enrichr to determine the cellular identities for the latter clusters (241).

2.7 Differential gene expression, pathway enrichment, and visualization

Single-cell transcriptomics analysis was performed for *Ptf1a*$^{Cre\text{ER}}$;*Kras*$^{\text{LSL-G12D}}$;*Ins1*$^{-/-}$;*Ins2*$^{+/+}$ and *Ptf1a*$^{Cre\text{ER}}$;*Kras*$^{\text{LSL-G12D}}$;*Ins1*$^{-/-}$;*Ins2*$^{+/-}$ mice. Seurat 3.2.1 FindMarkers function with default settings was applied to the integrated and normalized dataset to find the genes that were differentially expressed between *Ptf1a*$^{Cre\text{ER}}$; *Kras*$^{\text{LSL-G12D}}$;*Ins1*$^{-/-}$;*Ins2*$^{+/+}$ control and *Ptf1a*$^{Cre\text{ER}}$;*Kras*$^{\text{LSL-G12D}}$;*Ins1*$^{-/-}$;*Ins2*$^{+/-}$ experimental mice (236,237). Then the pathway enrichment analyses were performed by g:profiler (https://biit.cs.ut.ee/gprofiler/) using the Reactome database (http://www.reactome.org) based on the Reimand *et al*. published protocol (242). R package pheatmap 1.0.12 was used to visualize the pathways that were up-regulated and down-regulated in *Ptf1a*$^{Cre\text{ER}}$;*Kras*$^{\text{LSL-G12D}}$;*Ins1*$^{-/-}$;*Ins2*$^{+/-}$ experimental mice. Seurat 3.2.1 DoHeatmap function was used to visualize the single-cell expression of selected immune checkpoint receptors and ligands genes (236,237). Violin plots were used to visualize single-cell expression distributions for markers of macrophage subtypes and fibroblast subtypes.

2.8 Statistical analyses

Animals were excluded from the analysis if they were found dead or nTnG recombination efficiency, which was the percentage of acinar cells or PanIN cells labeled with GFP, was lower than 20% (for *Ptf1a*$^{\text{CreER/w}}$;*Kras*$^{\text{LSL-G12D/w}}$;*Insr*$^{\text{w/w}}$;nTnG, *Ptf1a*$^{\text{CreER/w}}$;*Kras*$^{\text{LSL-G12D/w}}$;*Insr*$^{\text{w/f}}$;nTnG, and *Ptf1a*$^{\text{CreER/w}}$;*Kras*$^{\text{LSL-G12D/w}}$;*Insr*$^{\text{f/f}}$;nTnG mice only). Statistical parameters include the exact value of sample size n (animal number), precision measures and dispersion (mean ± SEM), and statistical significance levels are reported in the figures and figure legends. For chapter 3, statistical analyses were conducted with GraphPad Prism 7.04 or the statistical programming language R (version 3.31). Shapiro-Wilk tests were run to test the

normality of the data and unless otherwise stated, a two-tailed student's t-test was run for normally distributed data. When the data failed the normality test, the Mann-Whitney test was performed, and Welch's t-test was conducted when the two samples have unequal variances, which was assessed by F test. The two-way ANOVA was run when comparing mice body weight and fasting glucose level.

For chapter 4, statistical analyses were conducted with GraphPad Prism 9.0.0. Shapiro-Wilk tests were run to test the normality of the data and a two-tailed student's t-test was run for normally distributed data unless otherwise stated while the Mann-Whitney test was performed for non-normally distributed data. Mixed-effects analyses were conducted for IPGTT, ITT, and GSIS experiments. During the correlation investigations, GraphPad Prism 9.0.0 was used to generate and assess the linear regressions. Nonparametric Spearman correlation was run for data of non-normal distribution while Pearson correlation coefficients were computed for data of normal distribution. Non-parametric Wilcoxon rank sum test was run for differential gene expression analysis in scRNA-seq analysis.

In chapter 5, statistical analyses were conducted with GraphPad Prism 9.3.0. Shapiro-Wilk tests were run to test the normality of the data and one-way ANOVA was performed unless otherwise stated. Mixed-effect analyses were run for glucose homeostasis data (mouse body weight, fasting glucose level, and fasting insulin level). When comparing the histopathological measurements between male and female mice from the same genotype, a two-tailed student's t-test was run for normally distributed data and a Mann-Whitney test was performed for non-normally distributed data. A p-value <0.05 was considered as significant and in figures, asterisks denote statistical significance level as following: *$p<0.05$, **$p<0.01$, ***$p<0.001$, and ****$p<0.0001$.

Table 2.1. PCR Primers used for mice genotyping.

Mouse allele	**Primer Name**	**Sequence (5' – 3')**
Ptf1a^{CreER}	*Ptf1a*^{CreER}-CO	TCCAGCAAGCGGGTACTATC
	Ptf1a^{CreER}-WT	AGGCGCTTTTCGTAGGGTAG
	Ptf1a^{CreER}-MU	TAAGCAATCCCCAGAAATGC
Kras$^{LSL-G12D}$	*Kras*^{G12D}-CO	CGCAGACTGTAGAGCAGCG
	Kras^{G12D}-MU	CCATGGCTTGAGTAAGTCTGC
	Kras^{G12D}-WT	GTCGACAAGCTCATGCGGG
Ins1	*Ins1*-1	CCAGATACTTGAATTATTCCTGGTGTTTTATCAC
	Ins1-2	GCTGCACCAGCATCTGCTCCCTCTACC
	Ins1-3	TTCTCGGCAGGAGCAAGGTGAGATGAC
Ins2	g16-*Ins2*-S	TGCTCAGCTACTCCTGACTG
	g17-*Ins2*-AS	GTGCAGCACTGATCTACAAT
	g19-LacZ-L	ACGGCACGCTGATTGAAGCA
	g20-LacZ-R	CCAGCGACCAGATGATCACA
Insr	4F_InsR	GAT GTG CAC CCC ATG TCT G
	4R_InsR	CTG AAT AGC TGA GAC CAC AG
nTnG	3a_nTnG	CCA GGC GGG CCA TTT ACC GTA AG
	3b_nTnG	AAA GTC GCT CTG AGT TGT TAT
	3c_nTnG	GGA GCG GGA GAA ATG GAT ATG

Table 2.2. Primary antibodies used for IHC staining.

Antigen	Source	Catalog	Dilution	Species	Antigen retrieval
CK19	abcam	ab133496	1:1000	Rabbit	Low pH buffer 200mL 10mM citrate buffer at pH 6
Ki67	Thermo Fisher	MA5-14520	1:200	Rabbit	Low pH buffer 200mL 10mM citrate buffer at pH 6
Cd20	Cell Signaling Technology	70168T	1:500.	Rabbit	Low pH buffer 200mL 10mM citrate buffer at pH 6
F4/80	Invitrogen eBioscience Thermo Fisher	14-4801-82	1:100.	Rat	No antigen retrieval was performed
Foxp3	Invitrogen	14-5773-82	1:200.	Rat	Low pH buffer 200mL 10mM citrate buffer at pH 6
Cd8	Invitrogen eBioscience Thermo Fisher	14-0808-82	1:1000.	Rat	Low pH buffer 200mL 10mM citrate buffer at pH 6
p-Erk	Cell Signaling Technology	4370S	1:500.	Rabbit	Low pH buffer 200mL 10mM citrate buffer at pH 6
GFP	Abcam	ab6673	1:200	Goat	Low pH buffer 200mL 10mM citrate buffer at pH 6

Table 2.3. The secondary antibody was used for IHC staining.

Antigen	Source	Catalog	Dilution	Species
Rat	Vector Laboratories	MP-7404	1:2.	Goat
Rabbit	Jackson ImmunoResearch laboratories, Inc.	711-065-152	1:500.	Donkey
Rat	Jackson ImmunoResearch laboratories, Inc.	712-065-150	1:500.	Donkey

Chapter 3: Endogenous hyperinsulinemia contributes to PDAC initiation in the context of high fat diet

3.1 Introduction

In 2021, pancreatic cancer became the 3rd leading cause of cancer death in Canada and the 5-year survival rate of PDAC was only 10% (1). Chronic pancreatitis, family history, smoking, obesity, and T2D are risk factors for pancreatic cancer (46,47). In 2012, a study showed that the combined effects of high BMI and diabetes were responsible for approximately 13.1% of pancreatic cancers and as the obese and diabetic populations are increasing, they are becoming even more ominous risk factors for PDAC (75). Therefore, efforts to understand the roles of diet and lifestyle in cancer risk and prevention strategies are expanding, as are efforts to determine the underlying pathophysiological mechanisms that mediate obesity and T2D-driven risk. Obesity and T2D are usually accompanied by metabolic disorders like hyperinsulinemia, hyperglycemia, dyslipidemia, and increased inflammation, which are proposed as candidate factors that may contribute to the associated increase of cancer morbidity and mortality (63,76,77).

Primary hyperinsulinemia can be defined as circulating insulin levels more than what is required to maintain glucose homeostasis and it is demonstrated to be associated with increased cancer risk and mortality independent of obesity (134,139). A meta-analysis showed that hyperinsulinemia increases the risk of PDAC 1.7-fold (163) and studies also showed that hyperinsulinemia and insulin resistance were associated with elevated PDAC aggressiveness and mortality (164,243). Nevertheless, even though these epidemiological and clinical studies have reported the association between hyperinsulinemia and PDAC, the cause-and-effect relationship between hyperinsulinemia and cancer remains to be determined directly.

Caloric restriction, fasting, and low-carbohydrate diets have been proposed for prevention or as an adjunct to cancer therapy based, in part, on what has come to be known as insulin-cancer hypothesis. Insulin has mitogenic effects on pancreatic cancer cell lines (244,245), but there is no direct evidence that a reduction in insulin production can decrease PDAC initiation or progression. KRAS mutations are found in 90% of PDAC and reliably induce preneoplastic PanIN precursor lesions when expressed in murine pancreatic acinar cells using an inducible *Ptf1a*$^{\mathrm{CreER}}$ allele. To reduce circulating insulin in *Ptf1a*$^{Cre\mathrm{ER}}$;*Kras*$^{\mathrm{LSL\text{-}G12D}}$ mice, we took advantage of a previously described mouse model system where mice with only one allele of the *Ins1* (*Ins1*$^{+/-}$) gene are compared to mice with two alleles of the *Ins1* (*Ins1*$^{+/+}$) gene in a *Ins2*-null genetic background (*Ins2*$^{-/-}$) to examine the effect of having a sustained reduction in fasting insulin levels when fed high-fat diet (112).

Thus, in this study, we directly compared the PanIN formation between mice with varying fasting insulin levels through generating *Ptf1a*$^{Cre\mathrm{ER}}$;*Kras*$^{\mathrm{LSL\text{-}G12D}}$ with the *Ins1*$^{+/+}$;*Ins2*$^{-/-}$ or *Ins1*$^{+/-}$;*Ins2*$^{-/-}$ genotypes. We also assessed if hyperinsulinemia promoted PanIN development by regulating cell proliferation and/or fibrogenesis.

3.2 Results

3.2.1 Effects of reduced *Ins1* gene dosage on obesity and glucose homeostasis

To address the causal contribution of hyperinsulinemia to PDAC development, we crossed *Ptf1a*$^{Cre\mathrm{ER/w}}$;*Kras*$^{\mathrm{LSL\text{-}G12D/w}}$;*Ins1*$^{+/+}$;*Ins2*$^{-/-}$ mice with *Ptf1a*$^{\mathrm{w/w}}$;*Ins1*$^{+/-}$;*Ins2*$^{-/-}$ mice to activate mutant *Kras*$^{\mathrm{G12D}}$ expression in adult acinar cells and modulate insulin dosage. By this breeding strategy, we generated *Ptf1a*$^{\mathrm{CreER}}$;*Kras*$^{\mathrm{LSL\text{-}G12D}}$;*Ins1*$^{+/+}$;*Ins2*$^{-/-}$ (PK-*Ins1*$^{+/+}$;*Ins2*$^{-/-}$) control mice and *Ptf1a*$^{\mathrm{CreER}}$;*Kras*$^{\mathrm{LSL\text{-}G12D}}$;*Ins1*$^{+/-}$;*Ins2*$^{-/-}$ (PK-*Ins1*$^{+/-}$;*Ins2*$^{-/-}$) experimental mice (Figure

3.1A). To stimulate hyperinsulinemia, the mice were fed with HFD after weaning (3-weeks-old) and at week 5-9, the mice were injected with tamoxifen to induce expression of *Kras*^{G12D} in acinar cells (Figure 3.1B). On the *Ptf1a*^{CreER};*Kras*$^{LSL\text{-}G12D}$ background, there was the expected modest reduction in fasting insulin and body weight in mice with reduced *Ins1* compared to controls (Figure 3.1C-E) (112). Moreover, consistent with our previous findings (112,120,122), fasting insulin levels were positively correlated with body weight (Figure 3.1F). Importantly, this reduction in insulin in PK-*Ins1*$^{+/-}$;*Ins2*$^{-/-}$ mice did not affect fasting glucose levels in females over one year of age (Figure 3.1G). In male mice from the same litters, we observed impaired fasting glucose, and in some cases frank diabetes (Figure 3.1H), consistent with known sex differences in insulin sensitivity. Therefore, comparing female PK-*Ins1*$^{+/-}$;*Ins2*$^{-/-}$ experimental mice to PK-*Ins1*$^{+/+}$;*Ins2*$^{-/-}$ control mice offered us the unique opportunity to test the role of insulin in pancreatic cancer development, in the absence of changes in fasting glucose.

3.2.2 Mice with reduced insulin production have less PanIN formation

To test our primary hypothesis that decreasing endogenous insulin production would affect the initiation of *Kras*^{G12D}-driven PDAC, we measured the percent of total pancreatic area occupied by PanINs and tumor. At 57 weeks of age, abundant ductal lesions with histologic and molecular characteristics of low-grade PanINs, including highly acidic mucin content indicated by Alcian blue staining, were found in both groups (Figure 3.2A-B). Only one mouse from each genotype developed PDAC tumor, which expressed the ductal marker CK19 (Figure 3.2C&E). Remarkably, PK-*Ins1*$^{+/-}$;*Ins2*$^{-/-}$ experimental mice had approximately half the area covered by PanINs or tumor (12.7±3.4%) compared with PK-*Ins1*$^{+/+}$;*Ins2*$^{-/-}$ control mice (25.4±3.8%) (Figure 3.1C). Without including tumor area, experimental mice still had approximately half the

area covered by PanIN lesions (12.3±3.1%) compared to controls (24.7±3.3%) (Figure 3.2F). Mice with reduced insulin also had significantly fewer high-grade PanIN per section or per whole pancreas area (Figure 3.2G). There was no significant difference between the genotypes when the number of high-grade PanIN was normalized to the total PanIN area. At 1 year of age, PanIN plus tumor area correlated with fasting insulin, but not with glucose levels, arguing against a prominent role for glycemia in PanIN formation in our model (Figure 3.3A-C). Although we were unable to follow them 1-year, male mice with reduced *Ins1* also had fewer PanIN lesions, but the difference was not statistically significant (Figure 3.3D-F). Together, our data implicate elevated endogenous insulin, but not elevated glucose, in HFD-mediated promotion of PanIN development leading to pancreatic cancer.

3.2.3 The desmoplastic reaction is reduced in mice with reduced insulin production

We investigated possible underlying mechanisms associated with insulin-driven PanIN formation, starting with the mitogenic effects of insulin. Many studies have shown that insulin can promote cell proliferation and reduce apoptosis through activating either PI3K/AKT/mTOR or MAPK/ERK signaling cascades (105,140). We were unable to measure statistically significant differences in proliferation rate in any cell types, although variation was high between mice within the same genotype (Figure 3.4A-B). PDAC is characterized by an intense desmoplastic reaction, and the increased inflammation associated with PanIN formation could drive the desmoplasia. Studies have suggested that the resulting cancer-associated stroma could support tumor survival and growth (246). Insulin has also been shown to enhance the proliferation of pancreatic stellate cells and augment their production of extracellular matrix through PI3K (247). By staining the collagen with Sirius red, we found that mice with reduced insulin had

significantly less collagen deposition than controls (20.1±4.3% vs 41.3± 5.1%) (Figure 3.4C-D). This result is consistent with the idea that hyperinsulinemia promotes PanIN development in part by contributing to the fibrogenesis associated with PanIN.

3.3 Discussion

Despite the strong epidemiological link between hyperinsulinemia and pancreatic cancer, the specific reduction of insulin is required to formally validate the hypothesis that insulin plays a causal role. Our study demonstrates that the formation of PanIN lesions is significantly reduced in mice with reduced insulin production, and it is the first to separate the causal role of hyperinsulinemia from hyperglycemia and directly test the insulin-cancer hypothesis *in vivo*. However, we were only able to include female mice for histopathological analyses in this study because PK-*Ins1*$^{+/-}$;*Ins2*$^{-/-}$ male mice started to show hyperglycemia as early as 5 weeks of age and many of them died because of overt diabetes. One copy of the *Ins1* gene, which contributes to only about 1/3 of secreted insulin, was not sufficient for the male mice to maintain their glucose homeostasis. This was previously observed in studies of non-cancer models. Therefore, future studies should investigate if this hyperinsulinemia-promoted PanIN progression can be observed in male mice as well.

Many investigators have proposed that hyperglycemia is a key factor linking obesity and T2D to PDAC, as extra glucose could theoretically support aerobic glycolysis of cancer cells and provide the building blocks for rapid growth. However, in this study, we demonstrated that hyperinsulinemia alone positively correlates with PanIN plus tumor area and that reducing hyperinsulinemia directly protects mice from pancreatic cancer development (Figure 3.3A&C). This suggests that hyperinsulinemia is an important component of PDAC development in the

context of metabolic disease-associated risk. In addition, we evaluated the PanIN plus tumor area in the pancreas at a late time point (57 weeks), which shows the cumulative influence of hyperinsulinemia on PanIN development. However, we were unable to determine whether there were more PanINs because hyperinsulinemia increased the survival and proliferation of existing PanIN cells or hyperinsulinemia supported more *Kras*^{G12D} expressing acinar cells transitioning into PanIN cells. Consequently, it will be interesting to assess this mouse model at an earlier time point (e.g. 12 weeks) when the PanINs start to initiate, so one can assess if hyperinsulinemia also contributes to PanIN initiation.

Some *in vitro* studies showed that increasing the insulin concentration in cell culture media could stimulate pancreatic cancer cell proliferation (244,245), but we did not detect a difference in the number of Ki67^{+} cells between PK-*Ins1*$^{+/-}$;*Ins2*$^{-/-}$ and PK-*Ins1*$^{+/+}$;*Ins2*$^{-/-}$ mice in the cell types we assessed. However, our data cannot exclude the possibility that insulin provided a mitogenic signal to cells expressing oncogenic *Kras*^{G12D} prior to the time points we studied. Therefore, future studies should measure the proliferation rate of PanIN and stromal cells when the mice are 12-weeks-old. Moreover, we do know whether hyperinsulinemia enhances PanIN development through reducing apoptosis and IHC staining for the apoptosis markers (like caspase-3) at earlier ages should be performed.

The desmoplastic reaction is a prominent characteristic of PDAC and the dense layers of stromal cells around cancer cells are hypothesized to be one of the reasons that PDAC is highly resistant to various anti-cancer therapies (248). Several studies have demonstrated that the fibroblasts in the microenvironment support pancreatic cancer cell survival and proliferation, meanwhile pancreatic cancer cells stimulate the fibrogenesis process (238). In our mouse model, we observed significantly less collagen deposition in mice with reduced insulin production, so it

is possible that hyperinsulinemia indirectly accelerates PanIN development through augmenting the fibrogenic process. Nevertheless, the increased fibrosis in PK-*Ins1*$^{+/+}$;*Ins2*$^{-/-}$ control mice could also occur because there were greater numbers of PanIN lesions in these mice than in experimental mice. Thus, future studies like scRNA-seq should be conducted to see how hyperinsulinemia alters the cells in the PanIN microenvironment, especially fibroblasts, or we could knock out the *Insr* in fibroblasts to see how this affects PanIN development.

Our findings are consistent with our previous studies demonstrating that a reduction of fasting insulin, so mild that it did not significantly increase fasting glucose, was sufficient to significantly extend the mean and maximum lifespan of mice (121). Therefore, insulin-lowering interventions, such as exercise and diet, warrant further investigation as strategies to prevent pancreatic cancer or limit its progression.

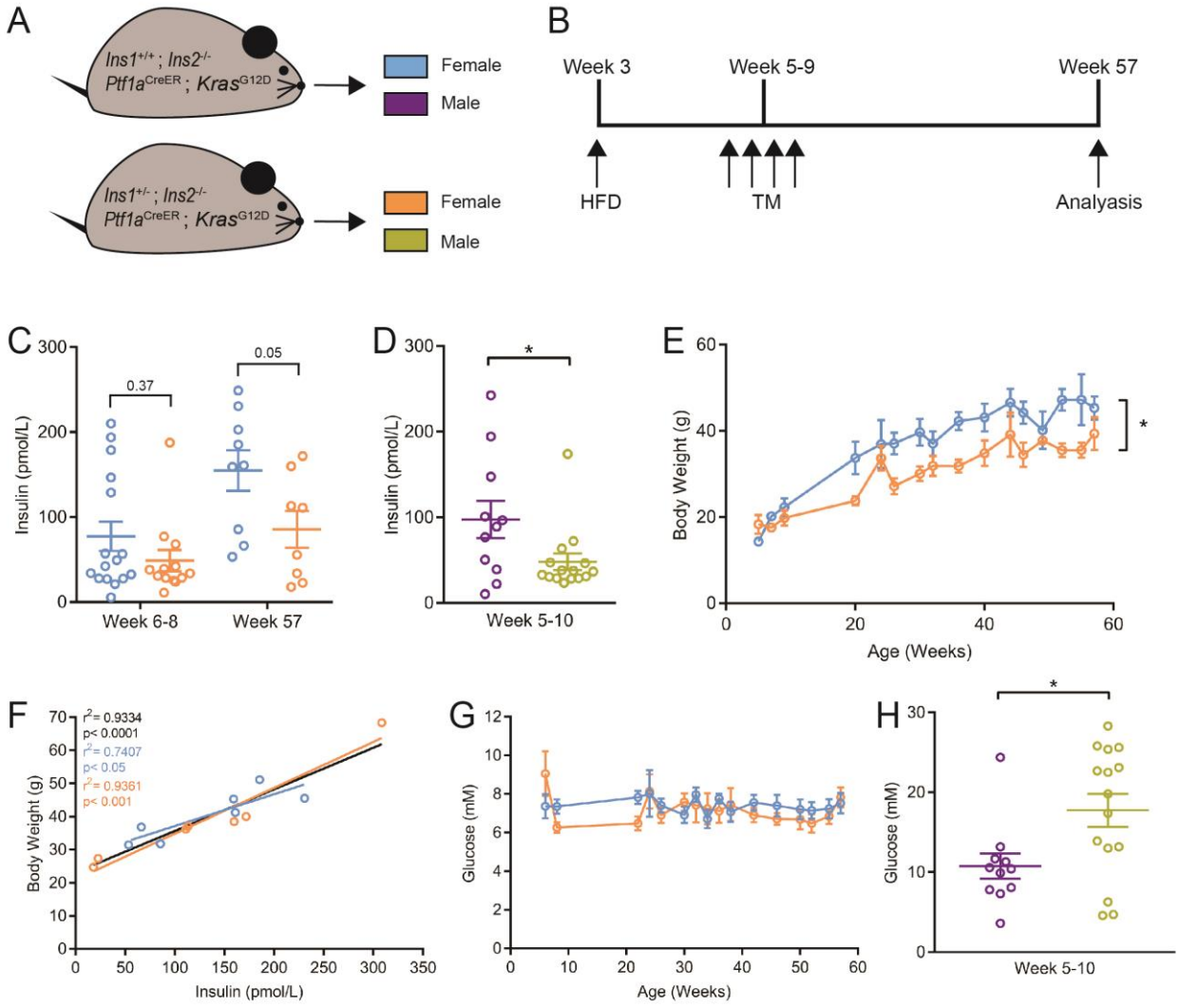

Figure 3.1. ***Ins2*-null background mice with reduced *Ins1* gene dosage have reduced fasting insulin levels and body weight.**

A, Schematic describing the mouse model. On the background of *Ptf1a*^{CreER}-induced *Kras*^{G12D} pancreatic cancer model (PK), we compared experimental mice with 1 null allele of *Ins1* (*Ins1*$^{+/-}$), and control mice with 2 full alleles of *Ins1* (*Ins1*$^{+/+}$), all in the absence of *Ins2* (*Ins2*$^{-/-}$) to prevent compensation. **B**, Mice were weaned to an HFD at 3-week-old and were injected with tamoxifen (TM) for 4 consecutive days at 5-9 weeks. Mice were euthanized at 57 weeks of age for histopathology analyses. **C**-**D**, Fasting circulating insulin levels of female (**C**) and male (**D**) mice (n= 8-16). **E**, Body weights were measured over 1 year for female mice (n= 13-16). **F**, The correlation between body weight and insulin at 1 year of age for female mice (n= 7). The black trend line represents the linear regression of pooled fasting insulin levels and body weight data points from both genotypes. **G**, The fasting blood glucose for female mice (n= 13-16). **H**, The fasting glucose of male mice at week 5-10 (n= 11-15). *p<0.05.

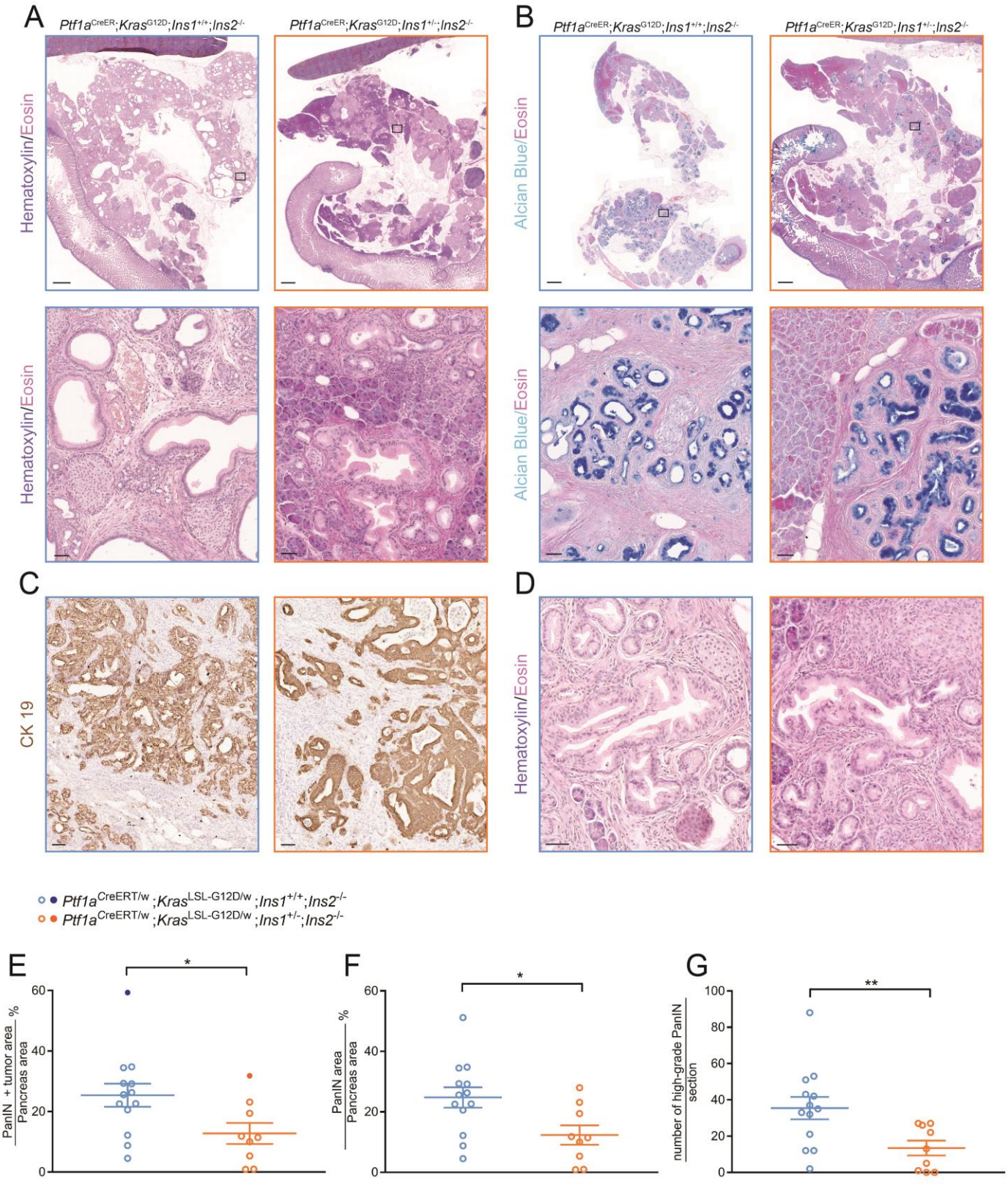
A
Ptf1a^CreER;Kras^G12D;Ins1^+/+;Ins2^-/-
Ptf1a^CreER;Kras^G12D;Ins1^+/-;Ins2^-/-
Hematoxylin/Eosin
B
Alcian Blue/Eosin
C
CK 19
D
Ptf1a^CreERT/w;Kras^LSL-G12D/w;Ins1^+/+;Ins2^-/-
Ptf1a^CreERT/w;Kras^LSL-G12D/w;Ins1^+/-;Ins2^-/-
E
PanIN + tumor area / Pancreas area %
F
PanIN area / Pancreas area %
G
number of high-grade PanIN / section
*
**

Figure 3.2. PanIN lesions were reduced in mice with reduced insulin production.
A-B, Representative whole-section (top) and high-magnification (bottom) H&E (**A**) and Alcian blue (**B**) stained pancreatic slides of *Ptf1a*^{CreER};LSL-*Kras*^{G12D};*Ins1*$^{+/+}$;*Ins2*$^{-/-}$ and *Ptf1a*^{CreER};LSL-*Kras*^{G12D};*Ins1*$^{+/-}$;*Ins2*$^{-/-}$ mice. **C**, CK19 IHC staining in the one PDAC presented in each genotype. **D**, Representative high-grade PanIN lesions formed in *Ptf1a*^{CreER};LSL-*Kras*^{G12D};*Ins1*$^{+/+}$;*Ins2*$^{-/-}$ and *Ptf1a*^{CreER};LSL-*Kras*^{G12D};*Ins1*$^{+/-}$;*Ins2*$^{-/-}$ mice pancreata. **E**, Quantification of percent of total pancreatic area occupied by PanIN plus tumor in *Ptf1a*^{CreER};LSL-*Kras*^{G12D};*Ins1*$^{+/+}$;*Ins2*$^{-/-}$ and *Ptf1a*^{CreER};LSL-*Kras*^{G12D};*Ins1*$^{+/-}$;*Ins2*$^{-/-}$ female (dark blue and dark orange dots denote mice that developed tumours) (n= 9-13). **F**, Quantification of percent of total pancreatic area occupied by only PanIN lesions in female mice of each genotype (n= 9-13). **G**, Number of high-grade PanIN lesions per section for female mice of each genotype (n= 9-13). Scale bars: 1 mm (**A-B,** top) and 50 µm (**A-B**, bottom; **C-D**). Values are shown as mean ± SEM. *$p<0.05$ and **$p<0.01$.

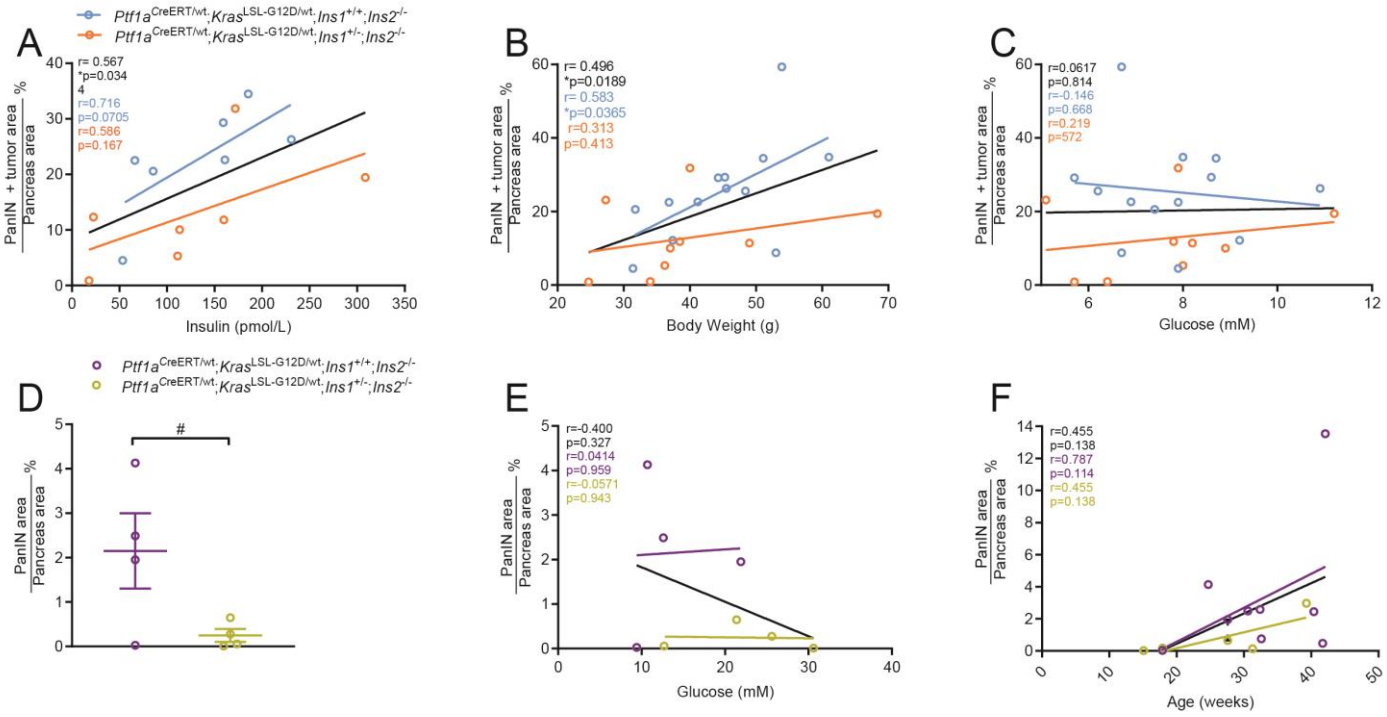

Figure 3.3. Fasting insulin levels are correlated with PanIN plus tumor area.
A, The relationship between PanIN plus tumour area and fasting insulin at 1 year of age for female mice. (n= 7). **B**, The relationship between PanIN plus tumour area and body weight at 1 year of age for female mice (n= 9-13). **C**, No correlation between PanIN plus tumour area and fasting blood glucose level at 57 weeks of age for female mice (n= 9-13). **D**, The percent of total pancreatic area occupied by PanIN in male mice of each genotype at 15-30 weeks (n= 4). **E**, The relationship between PanIN plus tumour area and body weight at 15-30 weeks for male mice (n= 4). **F**, Relationship between PanIN area and euthanasia age for male mice (n= 6-9). For **A-F**, The black trend line represents the linear regression of pooled data from both genotypes. Values are shown as mean ± SEM. #p<0.05 for F-test to compare variances.

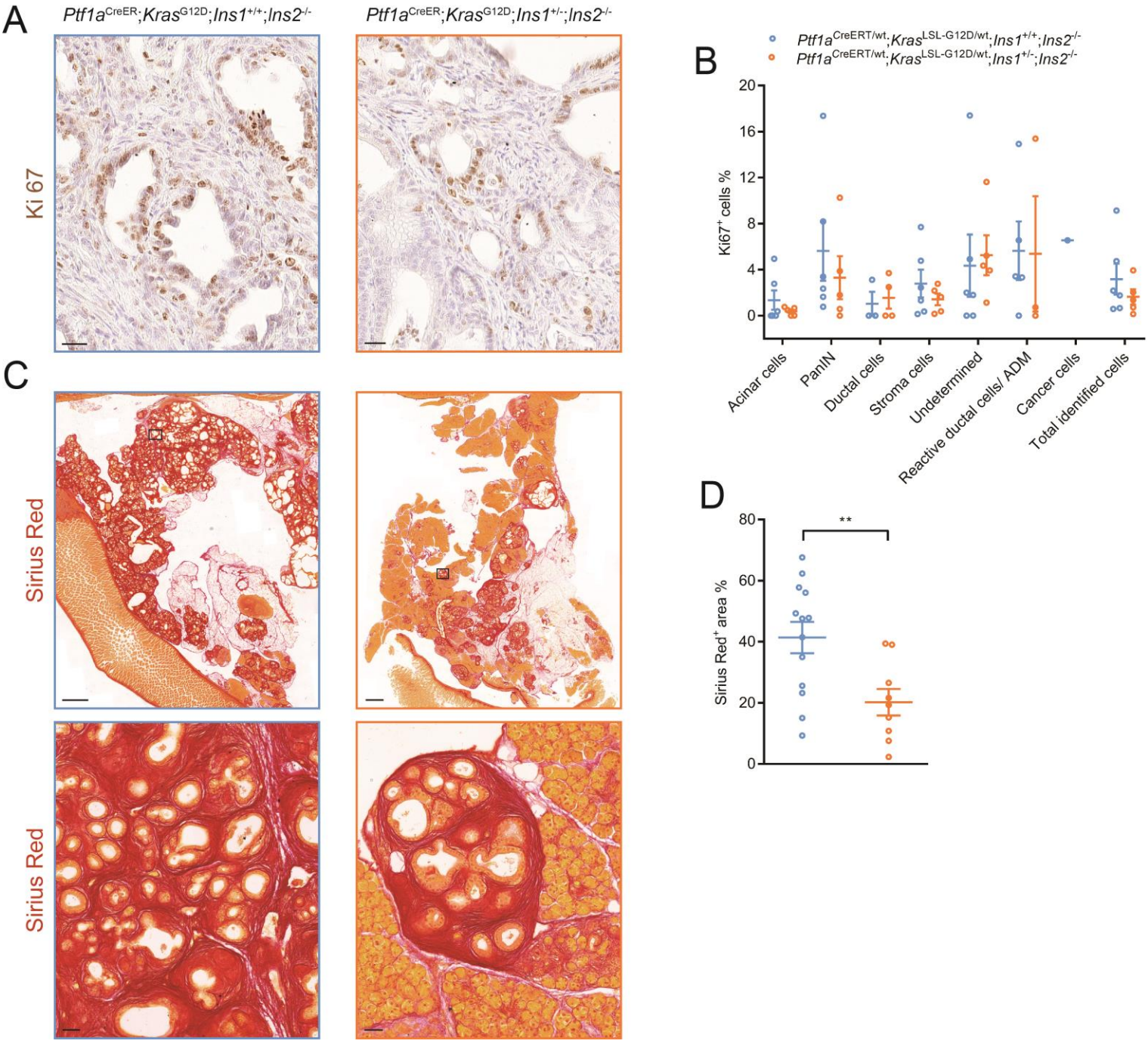

Figure 3.4. Fibrogenesis is reduced in mice with reduced insulin production.
A, IHC staining of Ki67 for female mice from both genotypes. **B,** Quantification of the percent of Ki67$^+$ cells for each cell type (n= 5-6). **C,** Representative whole-section (top) and high-magnification (bottom) Sirius red stained pancreatic slides for female mice both genotypes. **D,** Quantification of percent Sirius Red$^+$ area for each genotype. Values are shown as mean ± SEM. **p<0.01. Scale bars: 1 mm (**C**, top) and 50 μm (**A**; **C**, bottom).

Chapter 4: Molecular mechanisms associated with the contribution of endogenous hyperinsulinemia to PDAC initiation in high fat diet-fed *Ins1* null mice.

4.1 Introduction

Multiple epidemiological studies have shown that hyperinsulinemia is associated with increased cancer morbidity and mortality and pancreatic cancer is one of the cancers with the strongest association with hyperinsulinemia (51,126-129,131,132,134,135,139). Complementing these epidemiological studies, our *in vivo* animal studies showed for the first time that hyperinsulinemia plays a causal role in PDAC initiation in the context of a known hyperinsulinemia-promoting high fat diet (74) (Chapter 3). Specifically, we found that *Ptf1a*$^{Cre\text{ER}}$;*Kras*$^{\text{LSL-G12D}}$ female mice, a commonly used PDAC mouse model, with ~50% reduction in fasting insulin (*Ins1*$^{+/-}$;*Ins2*$^{-/-}$ compared to *Ins1*$^{+/+}$;*Ins2*$^{-/-}$) but no difference in glucose homeostasis, had a ~50% reduction in PanIN lesions and fibrogenesis. While we were unable to assess the effects of reduced insulin gene dose in males using this model, as *Ptf1a*$^{Cre\text{ER}}$;*Kras*$^{\text{LSL-G12D}}$;*Ins1*$^{+/-}$;*Ins2*$^{-/-}$ males developed hyperglycemia, these studies were the first to directly demonstrate that endogenous hyperinsulinemia contributes to the development of any cancer (74).

The parental imprinting, gene structure, and tissue distribution of the murine *Ins2* gene are similar to human *INS* gene (112-114,116). It is, therefore, crucial to determine if PanIN initiation would also be affected by reducing *Ins2* gene dosage in *Ptf1a*$^{Cre\text{ER}}$;*Kras*$^{\text{LSL-G12D}}$ mice. Moreover, *Ins1* contributes to only ~1/3 of secreted insulin; this means that *Ins1*$^{+/-}$;*Ins2*$^{-/-}$ mice have the lowest amount of insulin compatible with survival, with only female mice remaining consistently normoglycemic in modern mouse housing facilities (112,120-122). In the current study, we

addressed the effects of hyperinsulinemia on PDAC development in both sexes by generating *Ptf1a*$^{Cre\text{ER}}$;*Kras*$^{\text{LSL-G12D}}$ mice with the *Ins1*$^{-/-}$;*Ins2*$^{+/+}$ or *Ins1*$^{-/-}$;*Ins2*$^{+/-}$ genotypes. Comparing *Ins1*$^{-/-}$;*Ins2*$^{+/-}$ experimental mice to *Ins1*$^{-/-}$;*Ins2*$^{+/+}$ controls allowed us to compare males and females side-by-side. Beyond validating our previous results with a milder insulin reduction, the current study also provided an opportunity to examine pancreatic single-cell transcriptomics and gain insights into the molecular mechanisms involved in the complex cellular landscape of PDAC initiation under hyperinsulinemic conditions.

4.2 Results

4.2.1 Effects of reduced *Ins2* gene dosage on hyperinsulinemia, obesity, and glucose homeostasis in the context of PDAC development

We examined the effects of reduced *Ins2* gene dosage on PDAC development by crossing *Ptf1a*$^{Cre\text{ER/w}}$;*Kras*$^{\text{LSL-G12D/w}}$;*Ins1*$^{-/-}$;*Ins2*$^{+/+}$ mice with *Ptf1a*$^{\text{w/w}}$;*Ins1*$^{-/-}$;*Ins2*$^{+/-}$ mice to activate mutant Kras expression in adult acinar cells and modulate insulin dosage (10,43). By this breeding, we generated both *Ptf1a*$^{Cre\text{ER}}$;*Kras*$^{\text{LSL-G12D}}$;*Ins1*$^{-/-}$;*Ins2*$^{+/+}$ (PK-*Ins1*$^{-/-}$;*Ins2*$^{+/+}$) control mice and *Ptf1a*$^{Cre\text{ER}}$;*Kras*$^{\text{LSL-G12D}}$;*Ins1*$^{-/-}$;*Ins2*$^{+/-}$ (PK-*Ins1*$^{-/-}$;*Ins2*$^{+/-}$) experimental mice (Figure 4.1A). Recombination and expression of the *Kras*$^{\text{LSL-G12D}}$ allele were induced by injecting mice with tamoxifen at 4 weeks of age. To stimulate hyperinsulinemia, including both high insulin production and secretion, the mice were fed an HFD after weaning (Figure 4.1B).

In contrast to our previous study, which had more limited physiological data, especially in males (74), body weight and fasting glucose levels were monitored every 4 weeks, and fasting insulin levels were measured every 3 months until euthanasia in both male and female mice (Figure 4.1B). As expected from our previous studies using mice with reduced insulin gene

dosage (120-122,249), PK-*Ins1*$^{-/-}$;*Ins2*$^{+/-}$ mice had lower fasting insulin levels than PK-*Ins1*$^{-/-}$;*Ins2*$^{+/+}$ mice (Figure 4.2A&D). This effect was observed continuously after 12 weeks of age for male mice (Figure 4.2A), and was transiently present between 12 and 50 weeks of age for females (Figure 4.2D), as previously reported (122). Mice with reduced fasting insulin levels exhibited reduced weight gain in the context of HFD, without consistently affecting glucose homeostasis (Figure 4.2B-C & Figure 4.2E-F), consistent with our previous reports (112,120-122). When mice were 52 weeks old, glucose-stimulated insulin secretion tests, insulin tolerance tests, and glucose tolerance tests were conducted to examine glucose homeostasis more closely (Figure 4.2G-L). At this age, PK-*Ins1*$^{-/-}$;*Ins2*$^{+/+}$ and PK-*Ins1*$^{-/-}$;*Ins2*$^{+/-}$ male mice secreted similar levels of insulin in response to intraperitoneal delivery of glucose, in females we noted a clear trend in PK-*Ins1*$^{-/-}$;*Ins2*$^{+/-}$ mice towards reduced glucose-stimulated insulin secretion (Figure 4.2G&J). There were no significant differences in insulin sensitivity between the PK-*Ins1*$^{-/-}$;*Ins2*$^{+/+}$ and PK-*Ins1*$^{-/-}$;*Ins2*$^{+/-}$ genotypes in either male or female mice despite males with reduced insulin production appearing slightly more insulin sensitive (Figure 4.2H&K). Consistent with previous studies (120,122), we found that male mice of both genotypes had a weaker response to insulin challenge than females (Figure 4.2H&K). Glucose tolerance was generally similar between the genotypes with male PK-*Ins1*$^{-/-}$;*Ins2*$^{+/-}$ mice were more hyperglycemic than *Ins2*$^{+/+}$ littermate controls (Figure 4.2I&L). As previous studies suggested insulin might stimulate acinar cells to produce amylase (107), we examined if exocrine physiology was affected by reduced insulin production by monitoring serum amylase levels (250), but we found no differences between the genotypes (Figure 4.2M-N).

In sum, the limited systemic physiological differences between the experimental PK-*Ins1*$^{-/-}$;*Ins2*$^{+/-}$ and control PK-*Ins1*$^{-/-}$;*Ins2*$^{+/+}$ mice offered an opportunity to examine the effects of

reduced insulin production on PanIN formation in the absence of major changes in glucose homeostasis in both sexes.

4.2.2 Effects of modestly reduced insulin on PanIN initiation

Mice were euthanized at 57 weeks of age for histopathological analyses of the percent of total pancreatic area occupied by PanIN and tumor or for scRNA-seq analysis (see below). Similar to our previous study, we detected ductal lesions with histologic characteristics of low-grade PanIN (Figure 4.3A-B) and only one male and one female mouse developed PDAC and both of them were from PK-*Ins1*$^{-/-}$;*Ins2*$^{+/+}$ genotype. Similar to our previous study, the pancreatic area covered by PanIN and tumor in the PK-*Ins1*$^{-/-}$;*Ins2*$^{+/+}$ control mice was approximately twice that of the PK-*Ins1*$^{-/-}$;*Ins2*$^{+/-}$ experimental mice with reduced insulin levels (Figure 4.3C&G, filled circles indicated mice with PDAC). In males, the pancreatic area covered by PanIN and tumor in PK-*Ins1*$^{-/-}$;*Ins2*$^{+/+}$ mice was 1.34 ± 0.88% compared with 0.36 ± 0.088% in the PK-*Ins1*$^{-/-}$;*Ins2*$^{+/-}$ mice. In females, control PK-*Ins1*$^{-/-}$;*Ins2*$^{+/+}$ mice had 3.54 ± 1.75% of the pancreas covered by PanIN and tumor compared with 1.58 ± 0.70% in the PK-*Ins1*$^{-/-}$;*Ins2*$^{+/-}$ mice. While not statistically significant, we observed a trend toward a higher percent PanIN plus tumor area or PanIN area in females compared with males from the control genotype, with a similar trend occurring in the PK-*Ins1*$^{-/-}$;*Ins2*$^{+/-}$ genotype (Figure 4.3K-M). While these results broadly support our previous findings in a mouse model that varied alleles of *Ins1* in an *Ins2*-null background (74); there were far fewer PanIN lesions in both genotypes (~20% of the pancreatic area in previous the study (74) vs <4% in the current study for females) and the reduction in PanIN area was not statistically significant. The low lesion number in our current study may be related to the

overall reduction in non-fat pancreatic area in the *Ins1*-null compared to the *Ins2*-null background (see below).

Next, we examined the correlations between PanIN plus tumor area and fasting insulin levels, glucose levels, and body weight in individual mice measured at 57 weeks of age, by pooled measurements (black) or within each group (colored) (Figure 4.3D-F & Figure 4.3H-J). We found that the relatively modest positive correlations between fasting insulin levels and PanIN plus tumor area were significant in female mice (Figure 4.3H), but not in males (Figure 4.3D). There was also a significant correlation between body weight and PanIN plus tumor area (Figure 4.3J) in females, but not in males (Figure 4.3F). There was no positive correlation between fasting glucose and PanIN plus tumor area in either sex (Figure 4.3E&I), consistent with our previous findings (74). Together, these data add support to our previous observations suggesting that hyperinsulinemia promotes PanIN development in females (74). In males, the effects of hyperinsulinemia on PanIN development are less clear: despite a trend toward lower PanIN plus tumor area in the pancreata of males with reduced *Ins2* gene dose, PanIN plus tumor area did not correlate with insulin levels. While the reasons for this discrepancy between the sexes remains unclear, the relative insulin resistance we observed in both PK-*Ins1*$^{-/-}$;*Ins2*$^{+/+}$ and PK-*Ins1*$^{-/-}$;*Ins2*$^{+/-}$ males compared with females (Figure 4.2H&K) may provide one reason for the lack of correlation between circulating insulin and PanIN development in males.

4.2.3 Acinar ductal metaplasia and adipocyte area in the mice with reduced hyperinsulinemia

Next, we measured the percent of the total pancreatic area covered by ADM. ADM is the histological evidence of normal acinar cells changing into ductal-like cells with ductal cell

morphology and it can be induced by pancreatitis and during PanIN development (7). We detected ADM in both male and female mice for each genotype (Figure 4.4A-B). Similar to our PanIN area measurements, PK-*Ins1*$^{-/-}$;*Ins2*$^{+/+}$ mice had twice the amount of ADM area as PK-*Ins1*$^{-/-}$;*Ins2*$^{+/-}$ mice (1.92 ± 0.86% vs 0.96 ± 0.33%, respectively for males and 9.53 ± 2.84% vs 4.45 ± 1.74%, respectively for females), but the difference was not statistically significant (Figure 4.4C-D). Also, consistent with the PanIN area, we found that the ADM area in PK-*Ins1*$^{-/-}$;*Ins2*$^{+/+}$ female mice was significantly higher than ADM area in PK-*Ins1*$^{-/-}$;*Ins2*$^{+/+}$ males (Figure 4.4M). This trend was also present in the PK-*Ins1*$^{-/-}$;*Ins2*$^{+/-}$ genotype (Figure 4.4N). When we next examined the correlations between percent ADM area and PanIN area, fasting insulin, fasting glucose, and body weight in individual mice at 57 weeks of age, for each genotype (orange or blue) or both together (black) (Figure 4.4E-L), we found, as expected, that ADM area strongly correlated with PanIN area in non-tumor bearing females of both genotypes (Figure 4.4F). However, for male mice, there was no significant correlation between percent ADM area and PanIN only area (Figure 4.4E). We also found that despite a trend for the ADM area to correlate with fasting insulin in both sexes, only when the genotypes were combined did the models that percent ADM area correlates with fasting insulin in males (Figure 4.4G) or body weight in females (Figure 4.4L) significantly explain the spread of data points.

One surprising observation from our histopathological analyses was the significant amount of pancreatic area that had been replaced by adipocytes in our PK-*Ins1*$^{-/-}$ mouse model. This is not a phenomenon that we had previously observed in our PK-*Ins2*$^{-/-}$ model (74). As the representative histological figures show (Figure 4.5A-B), we often observed pancreatic lobules with a few residual normal acinar, ductal, or endocrine cells left amongst large numbers of adipocytes. The percent of pancreatic area replaced by adipocytes was not significantly different between PK-

Ins1$^{-/-}$;*Ins2*$^{+/+}$ and PK-*Ins1*$^{-/-}$;*Ins2*$^{+/-}$ mice (Figure 4.5C-D), suggesting this phenotype was possibly associated with loss of *Ins1* gene specifically. The male mice had a slightly higher percent adipocyte area than female mice for both genotypes, but overall, about 30-50% of the pancreatic area was occupied by adipocytes. The fatty replacement affected the overall parenchymal area, as we found compared to PK-*Ins2*$^{-/-}$ female mice, PK-*Ins1*$^{-/-}$ female mice had a significantly less pancreatic area (PK-*Ins2*$^{-/-}$ male mice did not reach a comparable age and were not assessed) (Figure 4.5E). It is possible that this fatty replacement could have affected the overall number of PanIN lesions, because of a relative lack of Ptf1a-positive acinar cells. Moreover, there was a significant correlation between the percent of adipocyte area and fasting insulin for female, but not male mice (Figure 4.5F&I). We observed no correlation between the percent of adipocyte area and fasting glucose levels for either sex (Figure 4.5.G&J). However, as expected (122), the percent adipocyte area did correlate with body weight in both sexes (Figure 4.5H&K). The underlying cause of fatty replacement in the PK-*Ins1*$^{-/-}$ mice is unknown and could be multifactorial, but the forces driving fat accumulation could potentially influence the accumulation of PanIN lesions, especially in females. This is supported by the significant and strong correlation between the percent of pancreatic area occupied by PanIN vs adipocytes in non-tumor bearing in female, but not male, mice (Figure 4.5L-M). We have previously observed this fatty replacement of normal parenchyma in another colony of *Ins1*$^{-/-}$ mice (unpublished observations), therefore, we do not believe this phenomenon is specific to the exposure of mice to tamoxifen or the influence solely of the PK mutant alleles.

4.2.4 Single cell transcriptomics reveals effects of hyperinsulinemia on cell type-specific gene expression

To investigate the molecular effects of hyperinsulinemia in the context of PDAC formation in an unbiased and cell type-specific manner, we undertook scRNA-seq. At 57 weeks of age, we collected pancreata from 6 PK-*Ins1*$^{-/-}$;*Ins2*$^{+/+}$ control mice and 6 PK-*Ins1*$^{-/-}$;*Ins2*$^{+/-}$ experimental mice, which were fasted for 4 hours, dispersed them into single cells, and FACS purified live cells for single-cell RNA sequencing (Figure 4.6A). We performed scRNA-seq analysis separately for each sex. In total, 49,835 single cells passed quality control tests and were clustered into 15 clusters (Figure 4.6B-C). These cell clusters were assigned cellular identities based on the expression of known markers, which were commonly used by other studies (238-240) (Figure 4.6F). We were able to identify acinar cells, ductal cells, and fibroblasts. The majority of cells that survived dispersion and passed transcriptomics quality controls were immune cells including T cells, Treg, B cells, NK cells, macrophages (both M1 and M2 macrophages), monocytes, dendritic cells, and mast cells (Figure 4.6B-C & Figure 4.6F & Figure 4.7B). We also classified a separate cluster of proliferating cells marked by high expression of *Mki67*. This proliferating cell cluster also included multiple immune cell types, such as T cells, B cells, and NK cells, as well as epithelial cells (Figure 4.6D-E & Figure 4.6G). Because there was inconsistent detection of cell populations across genotypes and sex, we chose to combine the sexes before performing comparisons between genotypes. The numbers of cells for each cell type and each mouse were recorded and we compared if there was a difference in the numbers of cells per cluster between the genotypes. With the exception of twice as many NK cells in mice with reduced insulin production, there were no significant differences for other cell types between the genotypes (Figure 4.6C). Analysis of cell type-specific markers showed that cell identities were

generally comparable between genotypes (Figure 4.6F). Consistent with previous human PDAC single transcriptomics analysis (238), we were able to identify 3 different fibroblasts subtypes within the fibroblast cell cluster from pancreata undergoing metaplastic changes, including inflammatory fibroblasts, myofibroblastic fibroblasts, and antigen-presenting fibroblasts (Figure 4.7C). Additionally, consistent with Steele *et al.* findings (239), the PanIN microenvironment in our model displayed evidence of immunosuppression. Specifically, we observed T cells, Treg cells, and NK cells expressed immune checkpoint receptors like *Cd28*, *Ctla4*, *Icos*, *Tnfrsf18*, and *Cd27*, while macrophages expressed checkpoint ligands, including *Sirpa*, *Havcr2*, *Pvr*, and *Lgals9* (Figure 4.7A). However, as our differentially expressed gene list showed (described below), there was no significant difference in expression of these immune checkpoint receptors and ligands between the two genotypes. This suggested that, even at the PanIN formation stage, the three types of fibroblasts and the immunosuppressive microenvironment were present but unaffected by insulin gene dosage. Our scRNA-seq analysis was rich with B cells (Figure 4.6B-C). To confirm the presence of B cells in our mouse pancreata, we performed IHC staining for the B cell marker, Cd20 (encoded by *Ms4a1*). We observed B cells surrounding PanINs and interestingly, we also observed aggregates of B cells associated with the fatty replacement of the parenchyma (Figure 4.8A), which may indicate the importance of B cells for adipocyte accumulation in the pancreas. We did not observe a significant difference in $Cd20^+$ area between the genotypes for male mice (Figure 4.8B); however, there was a significant increase of $Cd20^+$ area in female PK-*Ins1*$^{-/-}$;*Ins2*$^{+/-}$ mice compared to female PK-*Ins1*$^{-/-}$;*Ins2*$^{+/+}$ mice (Figure 4.8C). This was consistent with our scRNA-seq analysis that also showed there were more cells present in the B cluster in female PK-*Ins1*$^{-/-}$;*Ins2*$^{+/-}$ compared to female PK-*Ins1*$^{-/-}$;*Ins2*$^{+/+}$ mice. Using IHC staining, we were also confirmed the presence of other immune cells, including

macrophages (Figure 4.8D), Treg cells (Figure 4.8F), and $Cd8^+$ T cells (Figure 4.8G) in the PanIN microenvironment. There were a large number of macrophages present surrounding ADM and PanIN lesions, but we did not find a significant difference in the infiltration of macrophages around each type of lesion between the genotypes, and only a relatively small number of $Foxp3^+$ and $Cd8^+$ T cells were observed regardless of genotype (Figure 4.8D-G). Overall, our IHC staining supported our single transcriptomics analysis and confirmed the presence of multiple immune cell types in the neoplastic microenvironment of our mouse model.

After confirming the cell identities, we generated a list of genes that were differentially expressed between genotypes for each cell type. To have a more comprehensive understanding of the function of these differentially expressed genes, we performed pathway enrichment analysis using Reactome and found the pathways that were up- (Figure 4.9A) and down-regulated (Figure 4.9B) in PK-*Ins1*$^{-/-}$;*Ins2*$^{+/-}$ experimental mice compared to PK-*Ins1*$^{-/-}$;*Ins2*$^{+/+}$ control mice. B cells-1, B cells-2, epithelial cells, and M1 macrophages were the cell types that had the most altered pathways (Figure 4.9A-B). Specifically, the pathways that were most significantly altered were rRNA processing, nonsense-meditated decay, and translation pathways and they were also the pathways that were consistently altered across multiple cell types (Figure 4.9A-B). Interestingly, these pathways were down-regulated in epithelial cells, fibroblasts, dendritic cells, macrophages, B cells-1, Treg, NK cells, and mast cells of mice with reduced insulin. However, they were up-regulated in B cells-2, proliferating cells, and acinar cells of mice with reduced insulin (Figure 4.9A-B). We also found pathways that were only altered in acinar cells, which initiate the metaplasia in these mice. For instance, antimicrobial peptides and digestion pathways were down-regulated in acinar cells from PK-*Ins1*$^{-/-}$;*Ins2*$^{+/-}$ experimental mice (Figure 4.9A-B). The antimicrobial peptide category highlighted that the *Reg3a*, *Reg3b*, *Reg3d*,

and *Reg3g* genes, which are known to be induced by inflammation and may have anti-microbial roles (251,252), were significantly downregulated in acinar cells from mice with reduced insulin production (Figure 4.10C). This suggests that the inflammation surrounding acinar cells in the histologically normal pancreatic areas due to HFD treatment (71,72) might be reduced in mice with less insulin. Reg proteins are reported to promote pancreatic tumorigenesis (253-255) and future studies may identify a role for these proteins in mediating the effects of hyperinsulinemia in promoting inflammation and conversion of acinar cells into duct-like cells.

Somewhat expectedly, pathways involved in insulin signaling, like "PIP3 activates AKT signaling", "PTEN regulation", and "MAPK family signaling cascades," were downregulated in mice with reduced insulin production. They were downregulated in several cell types, but most clearly in B cells, epithelial cells, and M1 macrophages (Figure 4.9B). There was also downregulation of genes involved in cell cycle pathways in epithelial cells, B cells, macrophages, Treg cells, and NK cells from mice with reduced insulin production (Figure 4.9B). To validate the pathway enrichment analysis, we performed IHC staining of phospho-Erk. As expected, the PanIN cells had dark staining of phospho-Erk signaling. We also observed some non-epithelial cell types and acinar cells had high levels of phospho-Erk (Figure 4.10A). To see whether the latter areas contributed significantly to the overall phospho-Erk activity in the pancreas, we performed correlation analyses with the PanIN area per individual. As expected, there was a significant correlation between the phospho-Erk^{+} area and PanIN plus tumor area for both genotypes (Figure 4.10A-B). However, the slope of PK-*Ins1*$^{-/-}$;*Ins2*$^{+/+}$ mice was bigger than the slope of PK-*Ins1*$^{-/-}$;*Ins2*$^{+/-}$ mice, which suggested there were more non-PanIN cells with phospho-Erk positivity in PK-*Ins1*$^{-/-}$;*Ins2*$^{+/+}$ mice compared to PK-*Ins1*$^{-/-}$;*Ins2*$^{+/-}$ mice (Figure 4.10B). This was consistent with our pathway enrichment analysis that MAPK-ERK signaling

pathway was downregulated in epithelial and non-epithelial cell types of PK-*Ins1*$^{-/-}$;*Ins2*$^{+/-}$ mice. Altogether, the scRNA-seq analysis demonstrated the transcriptomics of epithelial cells and immune cells were significantly altered by hyperinsulinemia. This suggests that hyperinsulinemia might directly and indirectly affect PanIN development through regulating the epithelial and immune cells, respectively, in the PanIN microenvironment.

4.3 Discussion

This study aimed to investigate the effects of reduced *Ins2* gene dosage on HFD-induced hyperinsulinemia, PanIN initiation, and cell type-specific gene expression in the context of acinar-cell-specific expression of mutant Kras. The results of the present study validate and extend our previous findings that implicated hyperinsulinemia as a causal factor in pancreatic cancer initiation (74), and provide the first molecular insights into the cell-specific mechanisms involved.

Despite the strong epidemiological link between hyperinsulinemia and pancreatic cancer, the specific reduction of insulin is required to formally test the hypothesis that insulin plays a causal role. Our previous study directly demonstrated that endogenous hyperinsulinemia could contribute to cancer development using mice with a reduced dosage of *Ins1* in a *Ins2*-null genetic background (74). Unfortunately, in that study, male PK-*Ins1*$^{+/-}$;*Ins2*$^{-/-}$ mice developed hyperglycemia at a very young age because of insufficient endogenous insulin production, which limited our conclusions to female mice (74). In the present study, we were eager to validate our previous work and extend our observations to both sexes. Indeed, we found that male PK-*Ins1*$^{-/-}$;*Ins2*$^{+/-}$ mice were able to maintain glucose homeostasis and be studied long-term. This is consistent with previous studies showing that limiting *Ins2* gene dosage prevented hyperinsulinemia without pronounced effects on glucose homeostasis (120). Our data showed

that reduced *Ins2* gene dosage led to a moderate reduction in fasting insulin levels without broad effects on glucose homeostasis, in both male and female mice. It should be noted that circulating insulin levels in female mice, even with both *Ins2* alleles, are only ~25% of that seen in male mice. We also noted in female mice that insulin levels were not different at 1 year of age between genotypes, mirroring the transient compensation we have previously observed in the *Ins1*-null model (121,122). Collectively, these observations illustrate that a reduction in *Ins2* gene dosage results in a relatively mild manipulation of circulating insulin in the first year of life. Because *Ins2* is the ancestral gene and contributes to ~2/3 of secreted insulin (114,116), fasting insulin levels were still relatively high for our PK-*Ins1*$^{-/-}$ mouse model compared to the previously studied PK-*Ins2*$^{-/-}$ mouse model (Figure 4.2A&D vs Figure 3.1C-D).

Consistent with the previous study (74), in this study, only 2 animals developed PDAC, therefore we focused on quantifying the effects of reduced insulin on PanIN and ADM development, as well as the observed fatty replacement. Interestingly, in the present study only about 1-4% of pancreas was occupied by PanIN lesions for our PK-*Ins1*$^{-/-}$ mouse model, compared with the 15-30% of pancreas that was occupied by PanIN lesions for our previous PK-*Ins2*$^{-/-}$ mouse model (74). Another major histological difference between this study and our previous one was the observation of a significant amount of fatty replacement of the parenchyma in our PK-*Ins1*$^{-/-}$ mouse model. Approximately 30-50% of the pancreas was replaced by adipocytes. Unfortunately, because we did not collect pancreata at earlier time points and the 10x genomics scRNA-seq platform does not efficiently capture adipocytes, our study could not address when the fatty replacement occurred or the potential transcriptional programs altered in adipocytes, which could have provided us with some insight into the cause of fatty replacement. The presence of fat in the parenchyma was previously observed, but not reported, in our previous

Kras^{w};*Ins1*$^{-/-}$;*Ins2*$^{+/+}$ mouse studies (unpublished observations from animal cohorts in (120-122)). This suggests the *Ins1*$^{-/-}$ genetic background may contribute to the replacement of parenchyma with fat and the relative lack of ductal metaplasia; however, future studies are needed to examine this hypothesis. In addition, pancreatitis can also induce acinar cell necrosis or apoptosis, which is subsequently replaced by adipocytes (256,257). HFD-induced obesity can also cause fat accumulation in the exocrine parenchyma (256,258), but we did not observe this extent of fat accumulation with the same diet in our previous mouse model (74). Together it seems that the combined effects of Kras-associated inflammation, HFD, and the *Ins1*$^{-/-}$ genetic background may have resulted in fat displacing ~2/3 of normal pancreatic parenchyma in our PK-*Ins1*$^{-/-}$ mouse model. Therefore, the loss of acinar cells may explain why fewer and more variable numbers of PanIN lesions developed in our PK-*Ins1*$^{-/-}$ mouse model. Nevertheless, circulating insulin was still significantly correlated with PanIN plus tumor area in female mice, confirming our previous report with another insulin gene dosage configuration. Our histopathological analyses also showed that PK-*Ins1*$^{-/-}$;*Ins2*$^{+/-}$ mice had a ~50% reduction in PanIN area compared with PK-*Ins1*$^{-/-}$;*Ins2*$^{+/+}$ mice, which is similar to our previous findings. Although the pairwise comparison between genotypes did not reach statistical significance in the present study (74), our findings still support a role for hyperinsulinemia promoting PanIN initiation from acinar cells sustaining mutations in the oncogene *Kras*.

Although we did not longitudinally track the dynamic levels of insulin across the day, we performed analyses of glucose stimulated insulin secretion, and noted that response to glucose challenge was not significantly different between the female mice but male PK-*Ins1*$^{-/-}$;*Ins2*$^{+/-}$ mice were more hyperglycemia than male PK-*Ins1*$^{-/-}$;*Ins2*$^{+/+}$ mice. However, the change in insulin appeared to differ between female PK-*Ins1*$^{-/-}$;*Ins2*$^{+/-}$ compared to PK-*Ins1*$^{-/-}$;*Ins2*$^{+/+}$

controls. While this difference in genotype effects on glucose stimulated insulin secretion between the sexes was consistent with previous findings (120,122), our current analyses were limited to one time point. Another limitation of our study is that we were not able to rule out contributions of indirect effects of obesity on PanIN development. Other studies have suggested that obesity can promote PanIN development through sustained inflammation, dysregulated metabolism, or aberrant islet β-cell expression of peptide hormone CCK (70,72,73,259). Interestingly, the induction of CCK, a stimulant of acinar cell secretion, in aberrant islets in the leptin-deficient induced obesity model studied by Chuang *et al*. suggests that communication between the islet and acinar cell compartment occurs (73). To examine whether insulin similarly communicates with acinar cells in the local pancreatic neighborhood, future studies should inhibit insulin receptor signaling in the *Kras*^{G12D} expressing acinar cells to determine the direct effects of hyperinsulinemia on PanIN development. Additionally, studies to test the role of obesity in the absence of hyperinsulinemia are necessary to further address the role of each factor in PanIN development.

Pancreatic cancer is one of the most stroma-rich solid tumor types and immune cells in the microenvironment play essential roles at both early and late stages of PDAC development (260-263). In our single-cell transcriptomics analysis, the primary cell types analyzed were immune cells, including T cells, B cells, macrophages, NK cells, and dendritic cells. We observed a significant change in the number of NK cells present in our scRNA-seq analyses and a trend towards fewer macrophages by F4/80 IHC, suggesting changes in the immune microenvironment during PanIN formation in mice with reduced insulin. However, consistent with previous analyses of the immune cells in human PDAC or mouse models of PDAC, immune cells from our analyses also expressed immune checkpoint receptors regardless of genotype suggesting that

the suppressed immune microenvironment is not affected by the reduction of insulin. However, the major signaling pathways downstream of insulin (e.g. MAPK/ERK, PI3K/AKT, cell cycle, and translation pathways) were downregulated in immune cells from mice with reduced insulin production. MAPK/ERK and PI3K/AKT signaling pathways and their downstream signaling cascades are well-established regulators of multiple immune cell types (159,264,265). Therefore, there may still be differences in immune cell activities that were not captured by our transcriptome analyses.

The largest immune cell population identified by our scRNA-seq was B-cells. Different from other immune cell types, B cells are not well studied in the context of PDAC development, especially at the PanIN initiation stage. B cell infiltration around PanIN and PDAC was previously observed in a murine PDAC model and human samples (239,266,267). By IHC, we found that B cells are located, as expected, in the lymph nodes, around metaplastic areas, as well as in the areas of fatty infiltration. The large numbers of B-cells in our dataset could arise as a consequence of selective enrichment of the pancreatic lymph nodes during cellular dissociation. However, the pronounced B cell infiltration at the fatty replacement regions suggests B cells might be associated with the fatty replacement process, although this remains to be studied in detail. Regardless of their spatial origin, the B cells in our analyses had the greatest number of pathways altered significantly by hyperinsulinemia. Our IHC demonstrated that female mice with reduced insulin production had significantly more B cells than control mice and this was consistent with the trend observed in our scRNA-seq analysis. The role of B cells in PDAC appears to be complex according to the few studies in which it has been investigated. Some studies found that B cells secreted interleukin-35 and promoted tumor progression, while Spear *et al*. proposed that B cells were proinflammatory and limited PDAC development. These genes

(*Ptgs2*, *Cxcl2*, *Ill2a*, *Ebi3*) were not expressed by B cells in our scRNA-seq analysis of early pancreatic changes (267-269). Future studies are therefore required to better understand how hyperinsulinemia affects B cells and how B cells contribute to PanIN development under these conditions. Overall, our scRNA-seq analysis suggested hyperinsulinemia might contribute to PanIN development through changes in the immune microenvironment.

A limitation of our single-cell transcriptomics analysis was that relatively few acinar cells survived the pancreas dispersion and were gated as healthy prior to transcriptomic analysis. This was somewhat expected given the fragility of acinar cells and meant that we had less cell-level power to detect differences in gene expression. Nevertheless, within the limited data, we observed a significant downregulation of *Reg3a*, *Reg3b*, *Reg3d*, and *Reg3g* in acinar cells from PK-*Ins1*$^{-/-}$;*Ins2*$^{+/-}$ mice. Reg proteins have been shown to promote pancreatic carcinogenesis, especially inflammation-linked pancreatic carcinogenesis (253-255). Inflammation in pancreas can cause ADM and accelerate PanIN progression (43,270) and therefore, the decrease of *Reg* transcripts in PK-*Ins1*$^{-/-}$;*Ins2*$^{+/-}$ mice is consistent with the reduction of PanINs and inflammation in those mice. Future studies may seek to directly manipulate Reg proteins in the context of hyperinsulinemia and pancreatic cancer.

One unexpected finding from our study was the observation that males and females showed differences in the way that sex affects the induction of metaplasia and neoplasia. For example, the percentage of pancreas replaced by ADM was higher in PK-*Ins1*$^{-/-}$;*Ins2*$^{+/+}$ females than in males (Figure 4.4M), with a similar trend in the PK-*Ins1*$^{-/-}$;*Ins2*$^{+/-}$ genotype (Figure 4.4N). There was also a sex difference in the correlation between PanIN and ADM area (Figure 4.4E-F), where PanIN area showed a significant positive correlation with ADM area in females, but not males, in animals without tumors. While it remains unclear whether the differences we observe

between the sexes are due to methodological (e.g. tamoxifen pharmacology) or biological factors (e.g. frequency of tumor initiation), our findings suggest that future studies should examine and analyze males and females separately in the *Ins1*$^{-/-}$ genetic background, and potentially other genetic backgrounds. This will allow a more comprehensive examination of whether known sex differences in the regulation and physiological action of insulin in the body contribute to tumor development (271-275).

In future studies, it will be critical to characterize the specific downstream changes for each immune cell type at the protein level. It will also be important to manipulate insulin signaling components, including the insulin receptor, in acinar cells, immune cells, and other components of the PanIN microenvironment to determine which cells are predominately being affected by changes in insulin. Our study represents an important first step in understanding the molecular effects of hyperinsulinemia on all the cell types present in the context of early-stage pancreatic cancer.

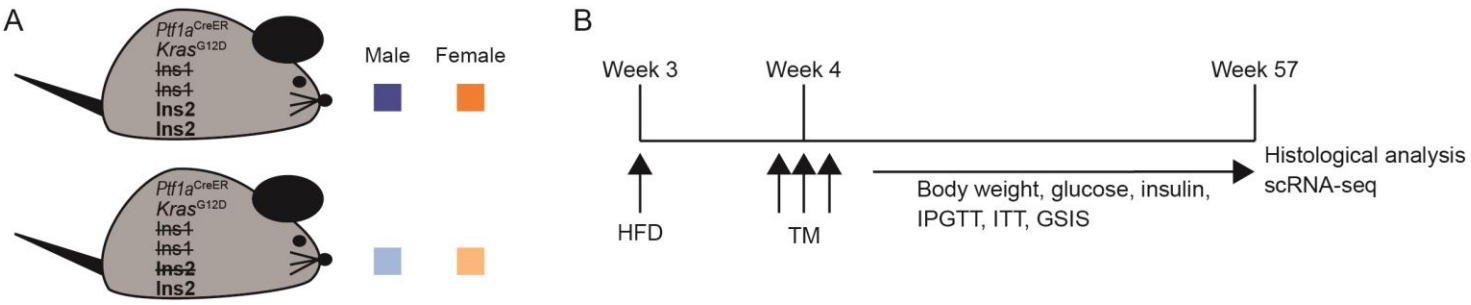

Figure 4.1. The *Ins1*-null mouse model used for testing the role and mechanisms of hyperinsulinemia in pancreatic cancer development.
A, Schematic describing a mouse model designed to test the role of hyperinsulinemia on HFD-accelerated PDAC initiation. On the background of *Ptf1a*^{CreER}-induced *Kras*^{G12D} pancreatic cancer model (PK), we compared experimental mice with 1 null allele of *Ins2* (*Ins2*$^{+/-}$) and control mice with 2 full alleles of *Ins2* (*Ins2*$^{+/+}$), all in the absence of *Ins1* (*Ins1*$^{-/-}$) to prevent compensation. **B,** Three-week-old PK-*Ins1*$^{-/-}$;*Ins2*$^{+/+}$ control and PK-*Ins1*$^{-/-}$;*Ins2*$^{+/-}$ experimental mice were weaned to an HFD and at 4-weeks-old, they were injected with TM for 3 consecutive days. The physiological measures were routinely followed for a year, the mice were then euthanized at 57 weeks of age for histopathological analyses and 12 mice were euthanized for scRNA-seq.

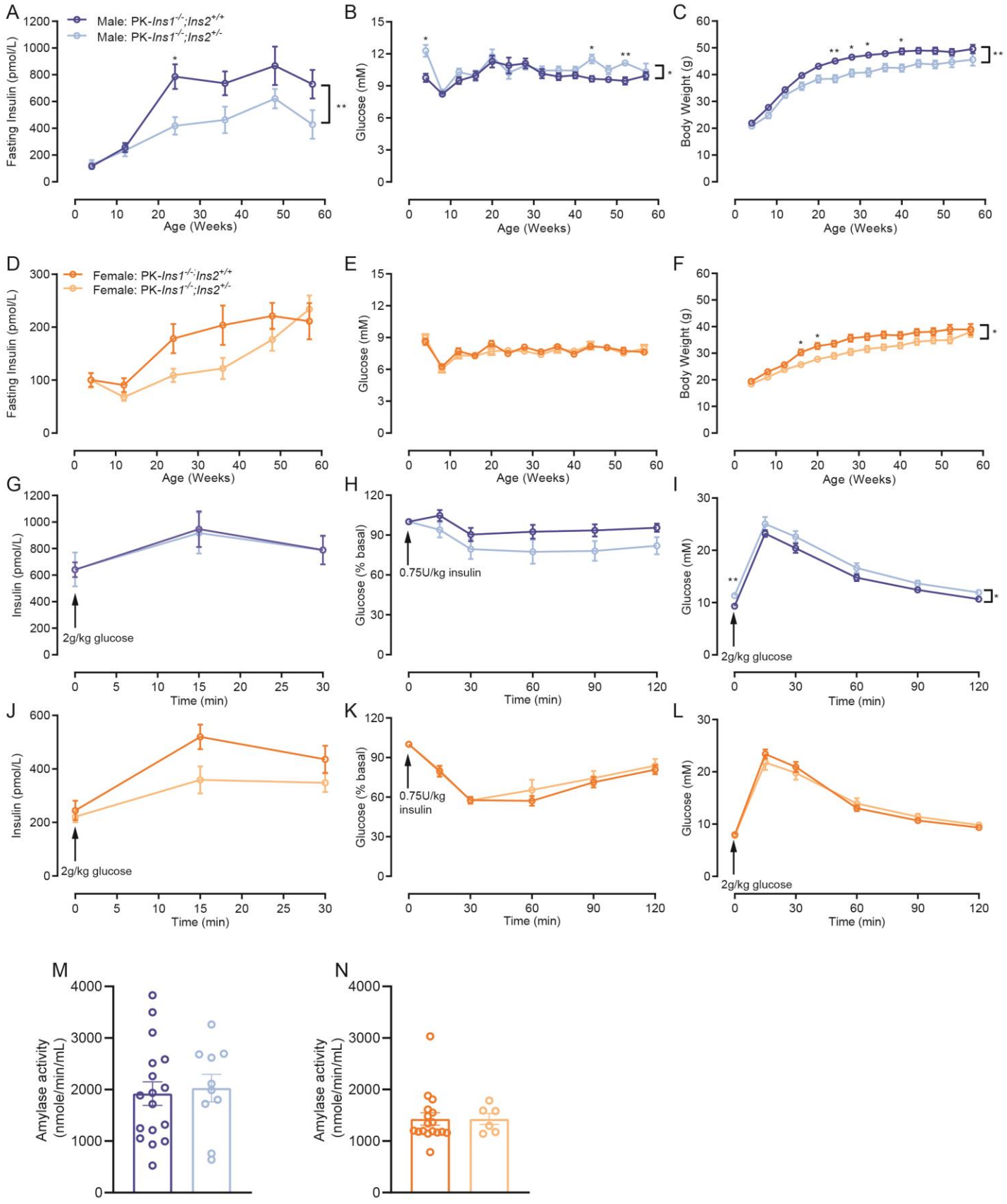
A
Male: PK-Ins1-/-;Ins2+/+
Male: PK-Ins1-/-;Ins2+/-
Fasting Insulin (pmol/L)
Age (Weeks)
B
Glucose (mM)
Age (Weeks)
C
Body Weight (g)
Age (Weeks)
D
Female: PK-Ins1-/-;Ins2+/+
Female: PK-Ins1-/-;Ins2+/-
Fasting Insulin (pmol/L)
Age (Weeks)
E
Glucose (mM)
Age (Weeks)
F
Body Weight (g)
Age (Weeks)
G
Insulin (pmol/L)
2g/kg glucose
Time (min)
H
Glucose (% basal)
0.75U/kg insulin
Time (min)
I
Glucose (mM)
2g/kg glucose
Time (min)
J
Insulin (pmol/L)
2g/kg glucose
Time (min)
K
Glucose (% basal)
0.75U/kg insulin
Time (min)
L
Glucose (mM)
2g/kg glucose
Time (min)
M
Amylase activity (nmole/min/mL)
N
Amylase activity (nmole/min/mL)

Figure 4.2. Mice with reduced insulin gene dosage have reduced fasting insulin levels and body weight.
A-C, The fasting insulin levels (**A**), fasting glucose levels (**B**), and body weight (**C**) in male PK-*Ins1*$^{-/-}$;*Ins2*$^{+/+}$ and PK-*Ins1*$^{-/-}$;*Ins2*$^{+/-}$ mice measured over 1 year (n=18-22). **D-F,** The fasting insulin levels (**D**), fasting glucose levels (**E**), and body weight (**F**) in female PK-*Ins1*$^{-/-}$;*Ins2*$^{+/+}$ and PK-*Ins1*$^{-/-}$;*Ins2*$^{+/-}$ mice measured over 1 year (n=10-29). **G,** Glucose stimulated insulin release in 52-week-old male mice (n= 17-18). **H-I,** Blood glucose response to intraperitoneal delivery of an insulin analog (**H**) or glucose (**I**) in 52-week-old male mice (n= 16-28). **J,** Glucose stimulated insulin release in 52-week-old female mice (n= 17-30). **K-L,** Blood glucose response to intraperitoneal delivery of an insulin analog (**K**) or glucose (**L**) in 52-week-old female mice (n= 19-29). **M-N,** The amylase activity in male (**M**) and female mice (**N**) for PK-*Ins1*$^{-/-}$;*Ins2*$^{+/+}$ and PK-*Ins1*$^{-/-}$;*Ins2*$^{+/-}$ mice. *$p<0.05$ and **$p<0.01$. Values are shown as mean ± SEM.

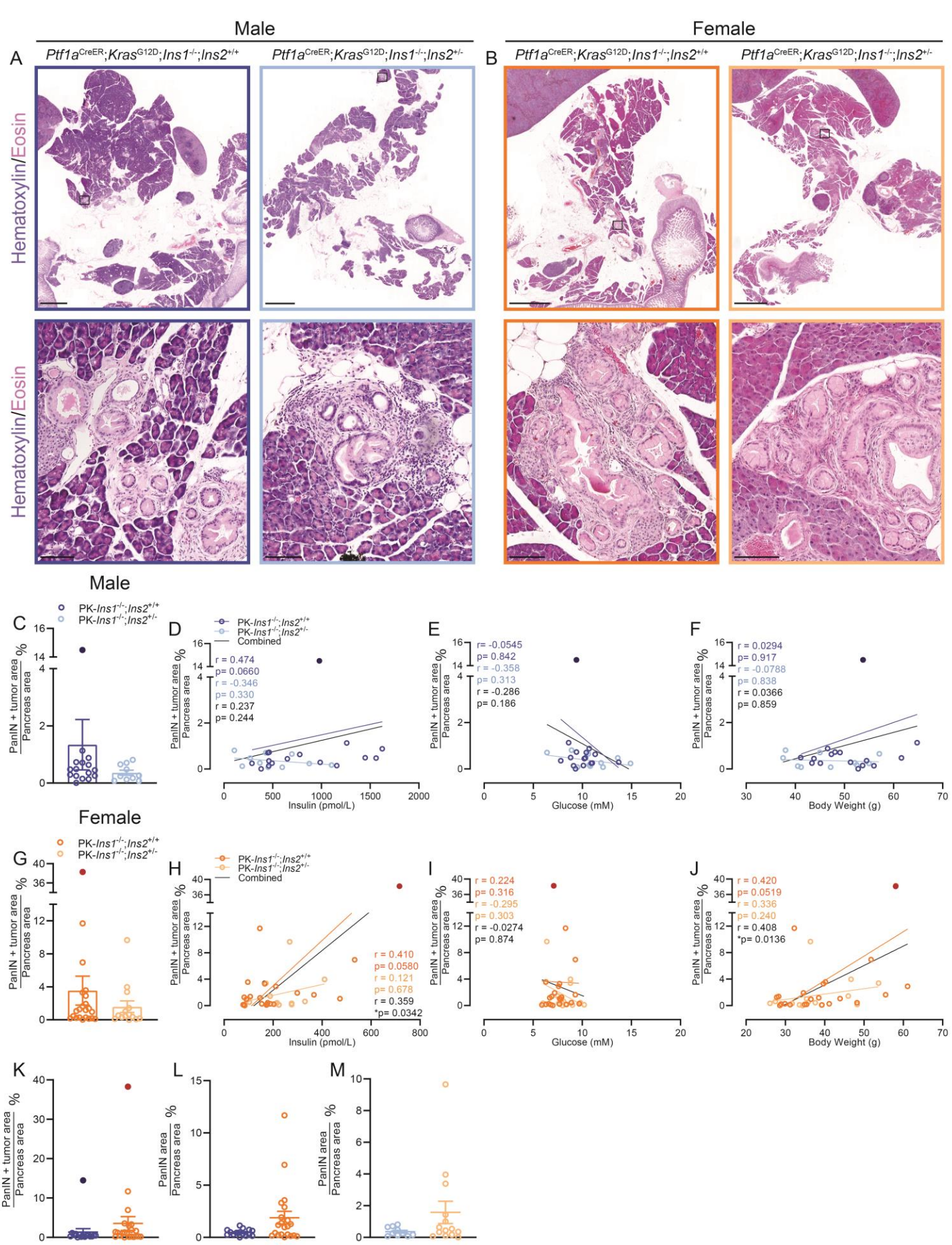
Male
Female
A
B
Ptf1a^CreER;Kras^G12D;Ins1^-/-;Ins2^+/+
Ptf1a^CreER;Kras^G12D;Ins1^-/-;Ins2^+/-
Hematoxylin/Eosin
Male
C
D
E
F
PK-Ins1^-/-;Ins2^+/+
PK-Ins1^-/-;Ins2^+/-
Combined
PanIN + tumor area / Pancreas area %
r = 0.474
p= 0.0660
r = -0.346
p= 0.330
r = 0.237
p= 0.244
Insulin (pmol/L)
r= -0.0545
p= 0.842
r = -0.358
p= 0.313
r = -0.286
p= 0.186
Glucose (mM)
r = 0.0294
p= 0.917
r = -0.0788
p= 0.838
r = 0.0366
p= 0.859
Body Weight (g)
Female
G
H
I
J
r = 0.410
p= 0.0580
r = 0.121
p= 0.678
r = 0.359
*p= 0.0342
r = 0.224
p= 0.316
r = -0.295
p= 0.303
r = -0.0274
p= 0.874
r = 0.420
p= 0.0519
r = 0.336
p= 0.240
r = 0.408
*p= 0.0136
K
L
M
PanIN + tumor area / Pancreas area %
PanIN area / Pancreas area %

Figure 4.3. The effects of reduced hyperinsulinemia on pancreatic cancer initiation. **A-B,** Representative whole section (top) and high-magnification (bottom) H&E stained pancreatic images of PK-*Ins1*$^{-/-}$;*Ins2*$^{+/+}$ and PK-*Ins1*$^{-/-}$;*Ins2*$^{+/-}$ male (**A**) and female (**B**) mice. Scale bars: 2 mm (top) and 0.1mm (bottom). **C,** The percent of total pancreatic area occupied by PanINs and tumor in male mice from each genotype (n= 10-16). Dark blue dot denotes mice that developed tumors. **D-F,** Correlations of composite PanINs plus tumor area with fasting insulin levels (**D**), with fasting glucose levels (**E**), or with body weight (**F**) in male mice (n = 10-16). **G,** Percentage of total pancreatic area occupied by PanINs and tumor in female mice from each genotype (n= 14-22). Dark orange dots denote mice that developed tumors. **H-J,** Correlations of composite PanINs plus tumor area with fasting insulin levels (**H**), with fasting glucose levels (**I**), or with body weight (**J**) in female mice (n = 14-22). **K-L,** Percentage of total pancreatic area occupied by PanINs and tumor (**K**) or only PanINs (excluding tumor bearing mice) (**L**) in PK-*Ins1*$^{-/-}$; *Ins2*$^{+/+}$ mice (n= 15-22). **M,** The percent of total pancreatic area occupied by only PanINs in PK-*Ins1*$^{-/-}$; *Ins2*$^{+/-}$ mice (n= 10-14). Values are shown as mean ± SEM. *$p<0.05$.

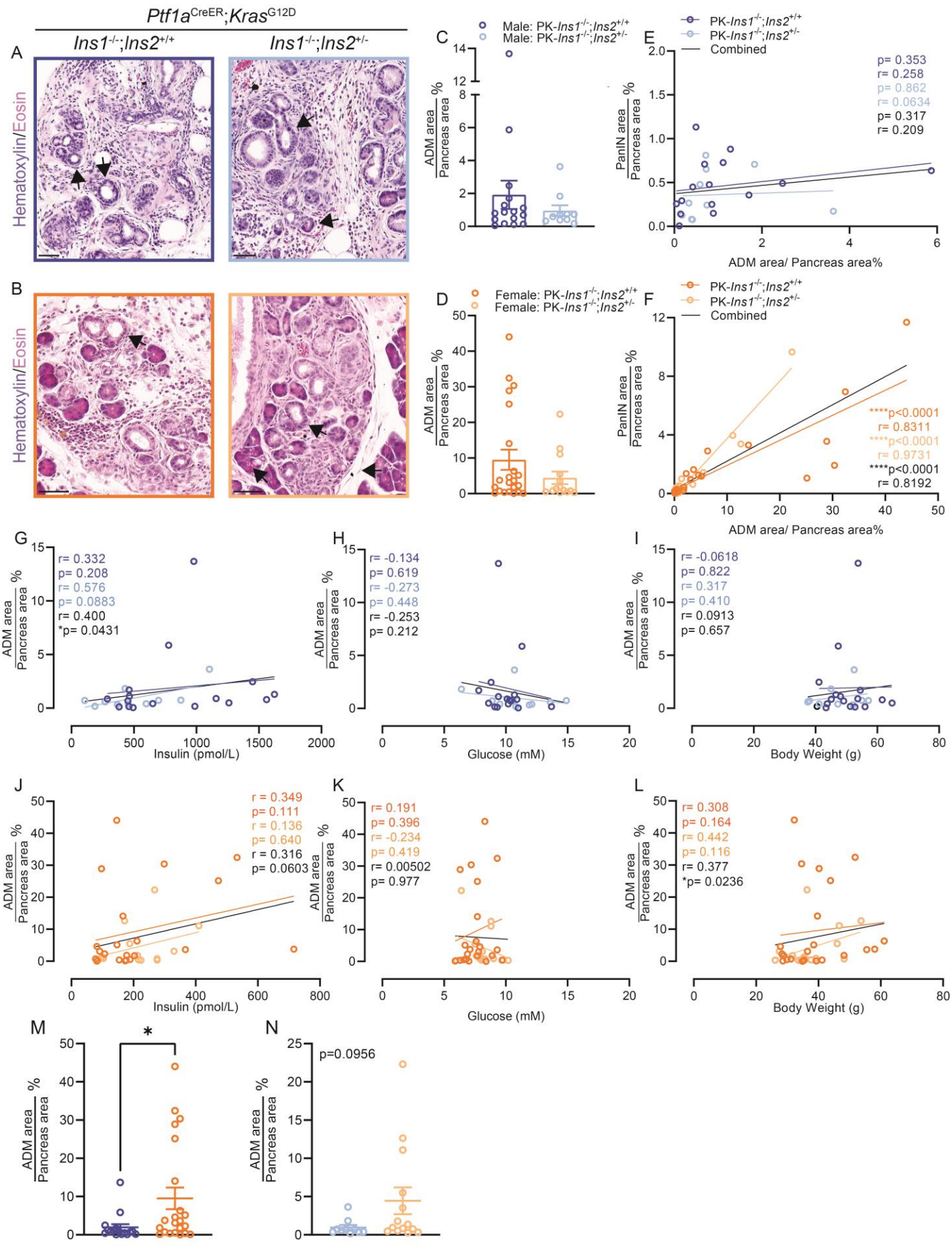
Ptf1a^CreER;Kras^G12D
Ins1^-/-;Ins2^+/+
Ins1^-/-;Ins2^+/-
A
B
Hematoxylin/Eosin
C
Male: PK-Ins1^-/-;Ins2^+/+
Male: PK-Ins1^-/-;Ins2^+/-
D
Female: PK-Ins1^-/-;Ins2^+/+
Female: PK-Ins1^-/-;Ins2^+/-
ADM area / Pancreas area %
E
PK-Ins1^-/-;Ins2^+/+
PK-Ins1^-/-;Ins2^+/-
Combined
p= 0.353
r= 0.258
p= 0.862
r= 0.0634
p= 0.317
r= 0.209
PanIN area / Pancreas area %
ADM area/ Pancreas area%
F
****p<0.0001
r= 0.8311
****p<0.0001
r= 0.9731
****p<0.0001
r= 0.8192
G
r= 0.332
p= 0.208
r= 0.576
p= 0.0883
r= 0.400
*p= 0.0431
Insulin (pmol/L)
H
r= -0.134
p= 0.619
r= -0.273
p= 0.448
r= -0.253
p= 0.212
Glucose (mM)
I
r= -0.0618
p= 0.822
r= 0.317
p= 0.410
r= 0.0913
p= 0.657
Body Weight (g)
J
r = 0.349
p= 0.111
r = 0.136
p= 0.640
r = 0.316
p= 0.0603
K
r= 0.191
p= 0.396
r= -0.234
p= 0.419
r= 0.00502
p= 0.977
L
r= 0.308
p= 0.164
r= 0.442
p= 0.116
r= 0.377
*p= 0.0236
M
*
N
p=0.0956

Figure 4.4. The effects of reduced hyperinsulinemia on acinar to ductal metaplasia.
A-B, Representative high-magnification ADM (arrowheads) images of male (**A**) and female (**B**) PK-*Ins1*$^{-/-}$;*Ins2*$^{+/+}$ and PK-*Ins1*$^{-/-}$;*Ins2*$^{+/-}$ mice. Scale bars: 0.05mm. **C-D,** Percentage of total pancreatic area occupied by ADM in male (**C**) and female (**D**) mice of each genotype (n=10-22). **E,** Correlations of composite ADM area with PanIN area (excluding tumor bearing mice) in male mice (n= 10-15). **F,** Correlations of composite ADM area with PanIN area (excluding tumor bearing mice) in female mice (n= 12-14). **G-I,** Correlations of composite ADM area with fasting insulin levels (**G**), fasting glucose (**H**), or body weight (**I**) in male mice (n= 10-16). **J-L,** Correlations of composite ADM area with fasting insulin levels (**J**), fasting glucose (**K**), or body weight (**L**) in female mice (n= 11-16). **M,** Comparison of percent of total ADM area in male and female PK-*Ins1*$^{-/-}$; *Ins2*$^{+/+}$ mice (n= 16-22). **N,** Comparison of percent of ADM area in male and female PK-*Ins1*$^{-/-}$; *Ins2*$^{+/-}$ mice (n= 10-14). Values are shown as mean ± SEM. *p<0.05, ****p<0.0001.

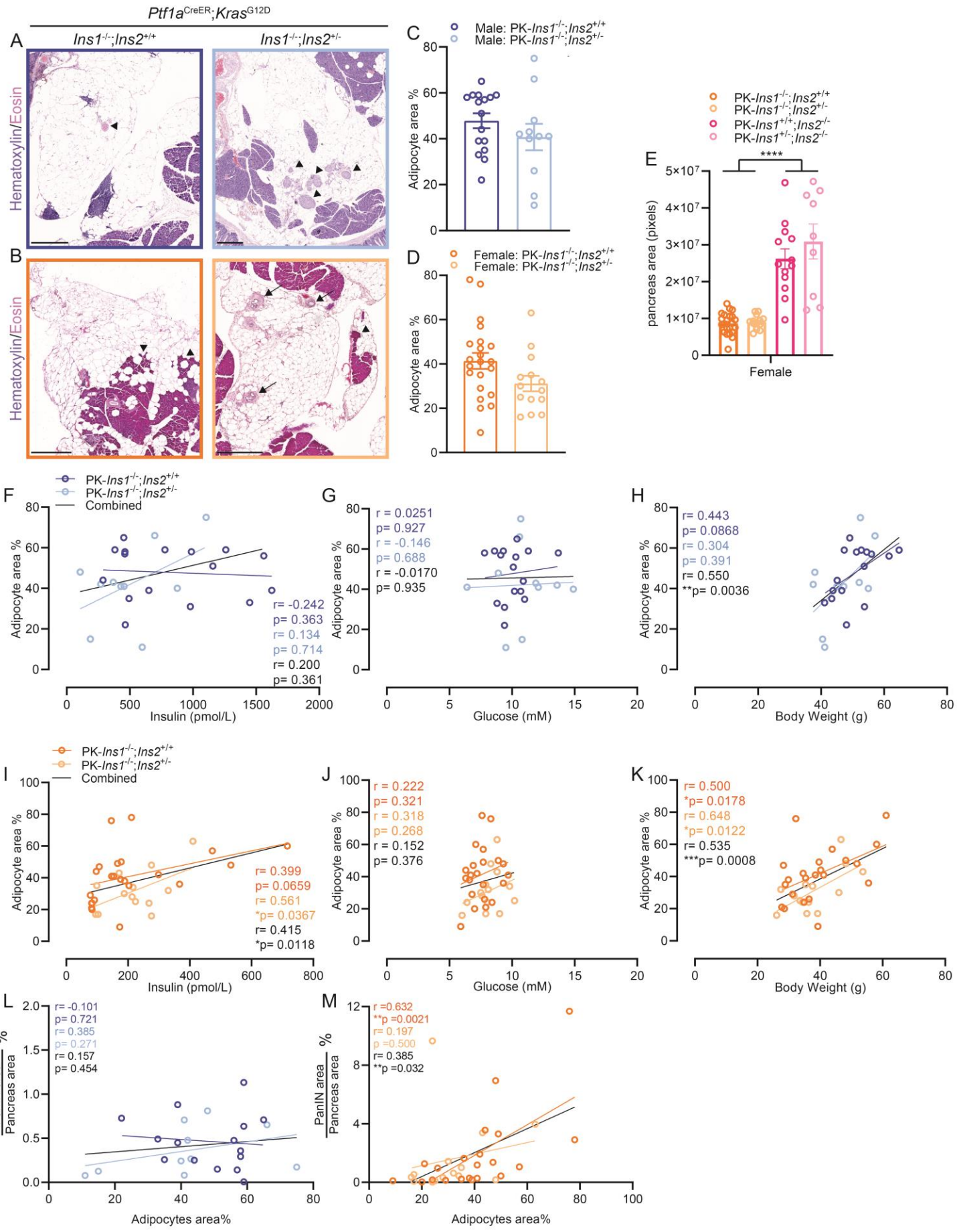
Ptf1a^CreER;Kras^G12D
A
Ins1-/-;Ins2+/+
Ins1-/-;Ins2+/-
Hematoxylin/Eosin
B
Hematoxylin/Eosin
C
Male: PK-Ins1-/-;Ins2+/+
Male: PK-Ins1-/-;Ins2+/-
Adipocyte area %
D
Female: PK-Ins1-/-;Ins2+/+
Female: PK-Ins1-/-;Ins2+/-
Adipocyte area %
E
PK-Ins1-/-;Ins2+/+
PK-Ins1-/-;Ins2+/-
PK-Ins1+/+;Ins2-/-
PK-Ins1+/-;Ins2-/-
****
pancreas area (pixels)
Female
F
PK-Ins1-/-;Ins2+/+
PK-Ins1-/-;Ins2+/-
Combined
Adipocyte area %
r= -0.242
p= 0.363
r= 0.134
p= 0.714
r= 0.200
p= 0.361
Insulin (pmol/L)
G
Adipocyte area %
r = 0.0251
p= 0.927
r = -0.146
p= 0.688
r = -0.0170
p= 0.935
Glucose (mM)
H
Adipocyte area %
r= 0.443
p= 0.0868
r= 0.304
p= 0.391
r= 0.550
**p= 0.0036
Body Weight (g)
I
PK-Ins1-/-;Ins2+/+
PK-Ins1-/-;Ins2+/-
Combined
Adipocyte area %
r= 0.399
p= 0.0659
r= 0.561
*p= 0.0367
r= 0.415
*p= 0.0118
Insulin (pmol/L)
J
Adipocyte area %
r = 0.222
p= 0.321
r = 0.318
p= 0.268
r = 0.152
p= 0.376
Glucose (mM)
K
Adipocyte area %
r= 0.500
*p= 0.0178
r= 0.648
*p= 0.0122
r= 0.535
***p= 0.0008
Body Weight (g)
L
PanIN area / Pancreas area %
r= -0.101
p= 0.721
r= 0.385
p= 0.271
r= 0.157
p= 0.454
Adipocytes area%
M
PanIN area / Pancreas area %
r =0.632
**p =0.0021
r= 0.197
p =0.500
r= 0.385
**p =0.032
Adipocytes area%

Figure 4.5. Altered pancreatic adipocyte area in *Ins1*-null mice.
A-B, Representative high-magnification image of apparent adipocyte replacement of pancreas area in male (**A**) and female (**B**) mice. Black arrows point to residual ducts. Arrowheads point to remaining islets, acinar cells, and blood vessels. Scale bars: 0.5mm. **C-D,** Percentage of total pancreatic area occupied by adipocytes in male (**C**) and female (**D**) mice of each genotype (n= 11-22). **E,** Total pancreatic parenchyma area for female mice in an *Ins1*-null background or an *Ins2*-null background. **F-K,** Correlations of adipocyte area with fasting insulin levels (**F, I**), fasting glucose levels (**G, J**), or body weight (**H, K**) for male (**F-H**) and female (**I-K**) mice. (n = 11-22). **L-M,** Correlations of adipocyte area with PanIN area in non-tumor bearing male (**L**) and female (**M**) mice (n = 10-22). Values are shown as mean ± SEM. *p<0.05, **p<0.01, ***p<0.001, ****p<0.0001.

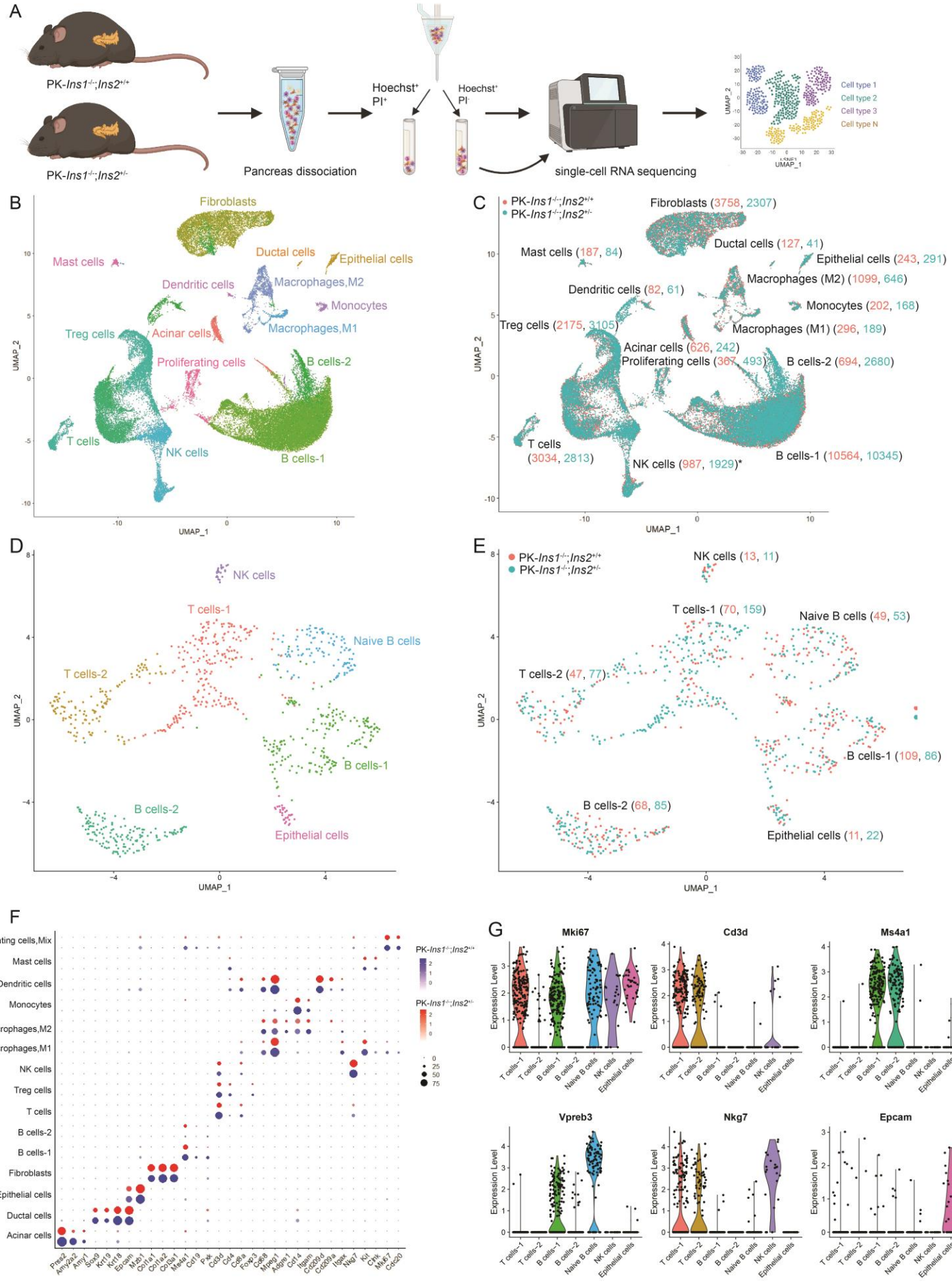
A
PK-Ins1-/-;Ins2+/+
PK-Ins1-/-;Ins2+/-
Pancreas dissociation
Hoechst+ PI+
Hoechst+ PI-
single-cell RNA sequencing
Cell type 1
Cell type 2
Cell type 3
Cell type N
B
Fibroblasts
Mast cells
Ductal cells
Epithelial cells
Dendritic cells
Macrophages,M2
Monocytes
Macrophages,M1
Treg cells
Acinar cells
Proliferating cells
B cells-2
T cells
NK cells
B cells-1
C
PK-Ins1-/-;Ins2+/+
PK-Ins1-/-;Ins2+/-
Fibroblasts (3758, 2307)
Mast cells (187, 84)
Ductal cells (127, 41)
Epithelial cells (243, 291)
Macrophages (M2) (1099, 646)
Dendritic cells (82, 61)
Monocytes (202, 168)
Treg cells (2175, 3105)
Macrophages (M1) (296, 189)
Acinar cells (626, 242)
Proliferating cells (367, 493)
B cells-2 (694, 2680)
T cells (3034, 2813)
NK cells (987, 1929)*
B cells-1 (10564, 10345)
D
NK cells
T cells-1
Naive B cells
T cells-2
B cells-1
B cells-2
Epithelial cells
E
PK-Ins1-/-;Ins2+/+
PK-Ins1-/-;Ins2+/-
NK cells (13, 11)
T cells-1 (70, 159)
Naive B cells (49, 53)
T cells-2 (47, 77)
B cells-1 (109, 86)
B cells-2 (68, 85)
Epithelial cells (11, 22)
F
Proliferating cells,Mix
Mast cells
Dendritic cells
Monocytes
Macrophages,M2
Macrophages,M1
NK cells
Treg cells
T cells
B cells-2
B cells-1
Fibroblasts
Epithelial cells
Ductal cells
Acinar cells
PK-Ins1-/-;Ins2+/+
PK-Ins1-/-;Ins2+/-
Prss2 Amy2a2 Amy1 Sox9 Krt19 Krt18 Epcam Muc1 Col1a1 Col1a2 Col3a1 Ms4a1 Cd19 Pax Cd3d Cd4 Cd8a Foxp3 Cd68 Mrc1 Adgre1 Csf1r Itgam Cd209d Cd209a Itgax Nkg7 Kit Cpa1 Mki67 Cdc20
G
Mki67
Cd3d
Ms4a1
Vpreb3
Nkg7
Epcam
Expression Level
T cells-1 T cells-2 B cells-1 B cells-2 Naive B cells NK cells Epithelial cells

Figure 4.6. Single-cell transcriptomics analysis reveals effects of hyperinsulinemia on cell type-specific gene expression.
A, Schematic describing scRNA-seq experimental design and analysis. Six PK-*Ins1*$^{-/-}$;*Ins2*$^{+/+}$ and six PK-*Ins1*$^{-/-}$;*Ins2*$^{+/-}$ mice pancreata were dissociated into single-cell suspension and the samples were sorted for hoechst^{+} and PI^{-} live cells. The live single cells were sequenced and clustered in uniform manifold approximation and projection (UMAP) space. **B,** Unsupervised clustering of cells from each genotype, represented as an UMAP plot. **C,** Numbers of cells from PK-*Ins1*$^{-/-}$;*Ins2*$^{+/+}$ and PK-*Ins1*$^{-/-}$;*Ins2*$^{+/-}$ mice for each cell type. The asterisk indicates a significant difference in the number of NK cells between the genotypes. **D,** Unsupervised sub-clustering of the proliferating cells cluster, represented as an UMAP plot. **E,** Violin plot showing the expression level of selected cell type-specific markers for identified cell types within the proliferating cells cluster. **F,** Dot plot showing selected cell type-specific markers for identifying the cell type for each cluster. The size of dots represents the fraction of cells expressing the markers. The intensity of color indicates the average expression of marker genes for each cell type. **G,** Expression level of the typical markers for identifying M1 and M2 macrophages. *$p<0.05$.

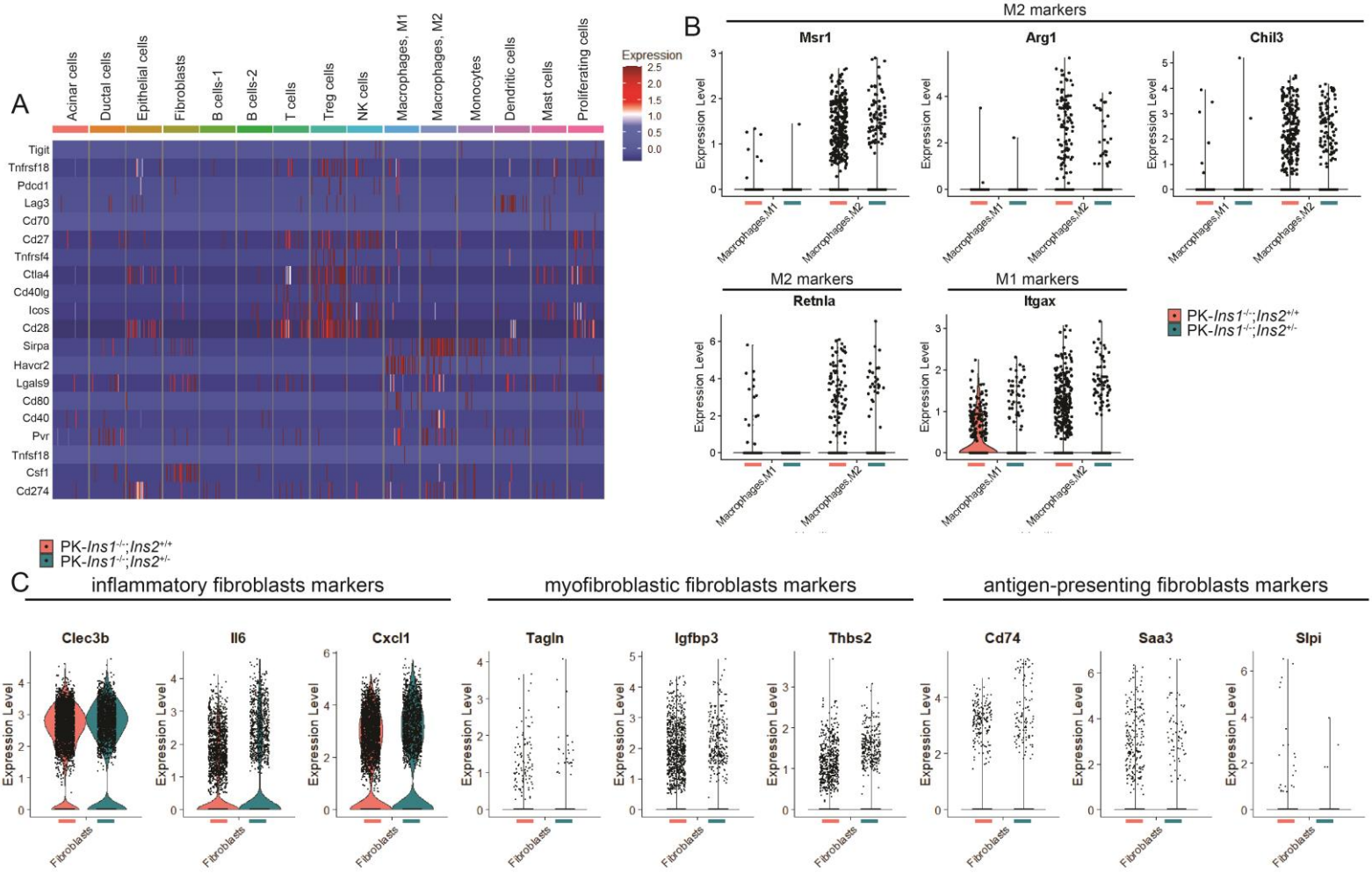

Figure 4.7. The PanIN microenvironment demonstrates evidence of immunosuppression in PK-*Ins1*$^{-/-}$;*Ins2*$^{+/+}$ and PK-*Ins1*$^{-/-}$;*Ins2*$^{+/-}$ mice.

A, Single-cell expressions of immune checkpoint ligands and receptors in each identified cell population from both genotypes. **B,** Expression of typical markers for identifying M1 and M2 macrophages for each genotype. **C,** Violin plots showing the selected markers' expression levels of inflammatory, myofibroblastic and antigen-presenting fibroblasts.

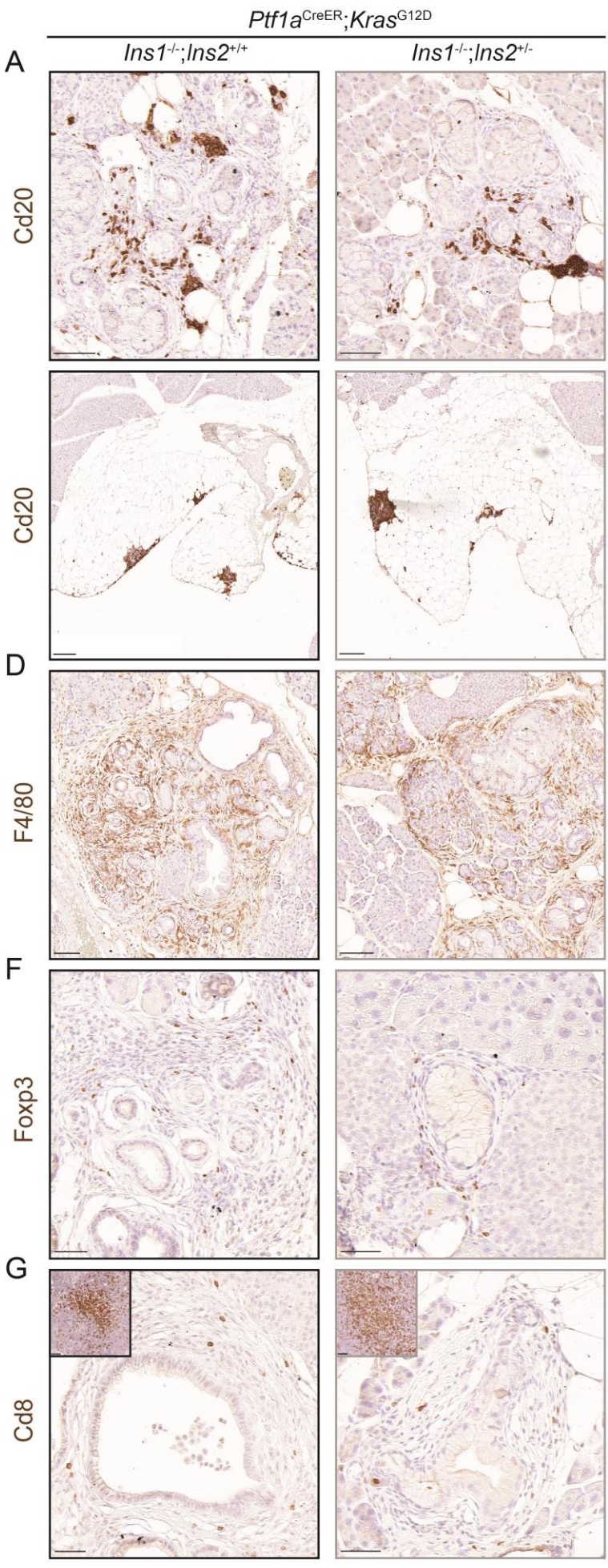
Ptf1a^CreER;Kras^G12D
Ins1-/-;Ins2+/+
Ins1-/-;Ins2+/-
A
Cd20
Cd20
D
F4/80
F
Foxp3
G
Cd8

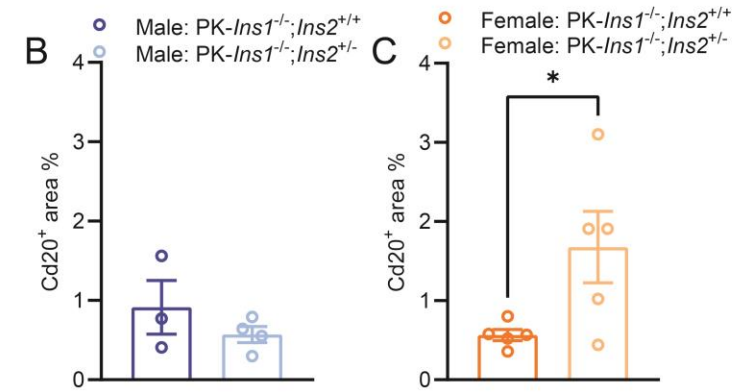
B
Male: PK-Ins1-/-;Ins2+/+
Male: PK-Ins1-/-;Ins2+/-
Cd20+ area %
0
1
2
3
4
C
Female: PK-Ins1-/-;Ins2+/+
Female: PK-Ins1-/-;Ins2+/-
*
Cd20+ area %
0
1
2
3
4

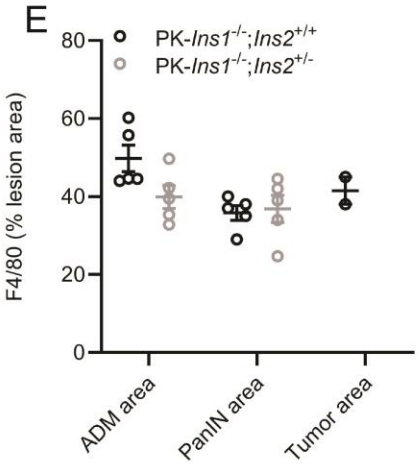
E
PK-Ins1-/-;Ins2+/+
PK-Ins1-/-;Ins2+/-
F4/80 (% lesion area)
0
20
40
60
80
ADM area
PanIN area
Tumor area

Figure 4.8. Multiple types of immune cells present around PanIN and ADM lesions of PK-*Ins1*$^{-/-}$;*Ins2*$^{+/+}$ and PK-*Ins1*$^{-/-}$;*Ins2*$^{+/-}$ mice.
A, Immunohistochemistry of Cd20 for mice pancreata from each genotype. Scale bars: 0.1mm (up) and 0.2mm (down). **B-C,** The quantification of Cd20^{+} area for male (**B**) and female (**C**) mice from each genotype. **D,** Immunohistochemistry of F4/80 for mice pancreata from each genotype. **E,** Quantification of F4/80^{+} area per lesion area for each ADM, PanIN and tumor area. No PK-*Ins1*$^{-/-}$;*Ins2*$^{+/-}$ mice developed PDAC. Scale bars: 0.1mm. **F-G,** Immunohistochemistry of Foxp3 (**F**), and Cd8 (**G**) for PK-*Ins1*$^{-/-}$;*Ins2*$^{+/+}$ and PK-*Ins1*$^{-/-}$;*Ins2*$^{+/-}$ pancreata. (Representative Cd8^{+} T cells in lymph nodes, **G** inset). Scale bars: 0.05mm. *p<0.05.

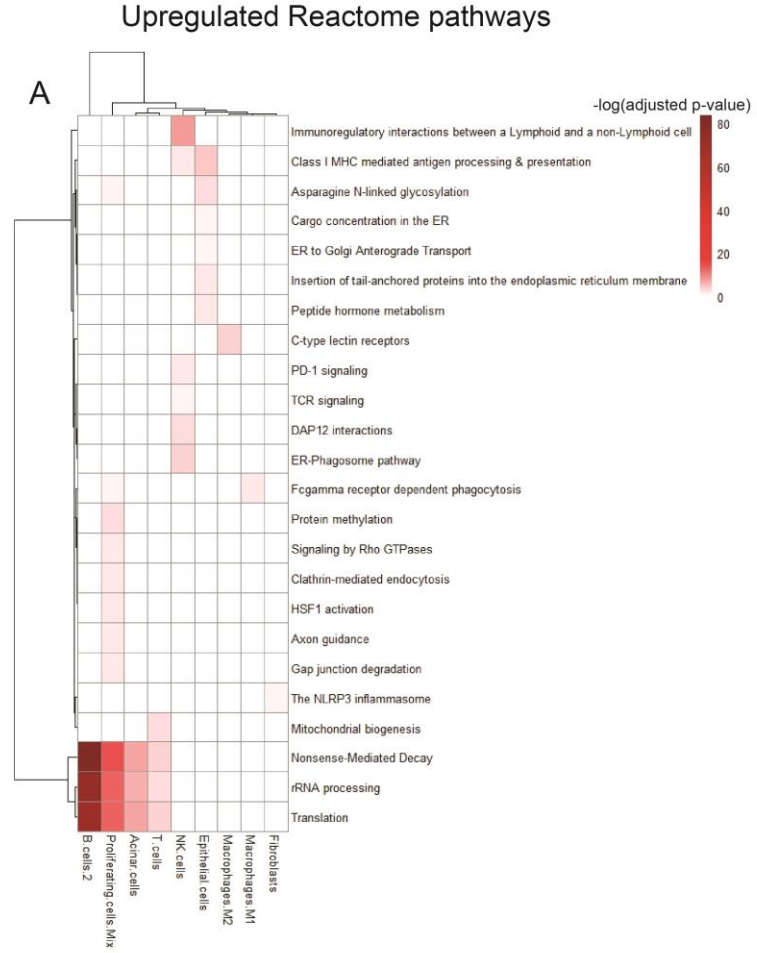
Upregulated Reactome pathways
A
-log(adjusted p-value)
80
60
40
20
0
Immunoregulatory interactions between a Lymphoid and a non-Lymphoid cell
Class I MHC mediated antigen processing & presentation
Asparagine N-linked glycosylation
Cargo concentration in the ER
ER to Golgi Anterograde Transport
Insertion of tail-anchored proteins into the endoplasmic reticulum membrane
Peptide hormone metabolism
C-type lectin receptors
PD-1 signaling
TCR signaling
DAP12 interactions
ER-Phagosome pathway
Fcgamma receptor dependent phagocytosis
Protein methylation
Signaling by Rho GTPases
Clathrin-mediated endocytosis
HSF1 activation
Axon guidance
Gap junction degradation
The NLRP3 inflammasome
Mitochondrial biogenesis
Nonsense-Mediated Decay
rRNA processing
Translation
B.cells.2
Proliferating.cells.Mix
Acinar.cells
T.cells
NK.cells
Epithelial.cells
Macrophages.M2
Macrophages.M1
Fibroblasts

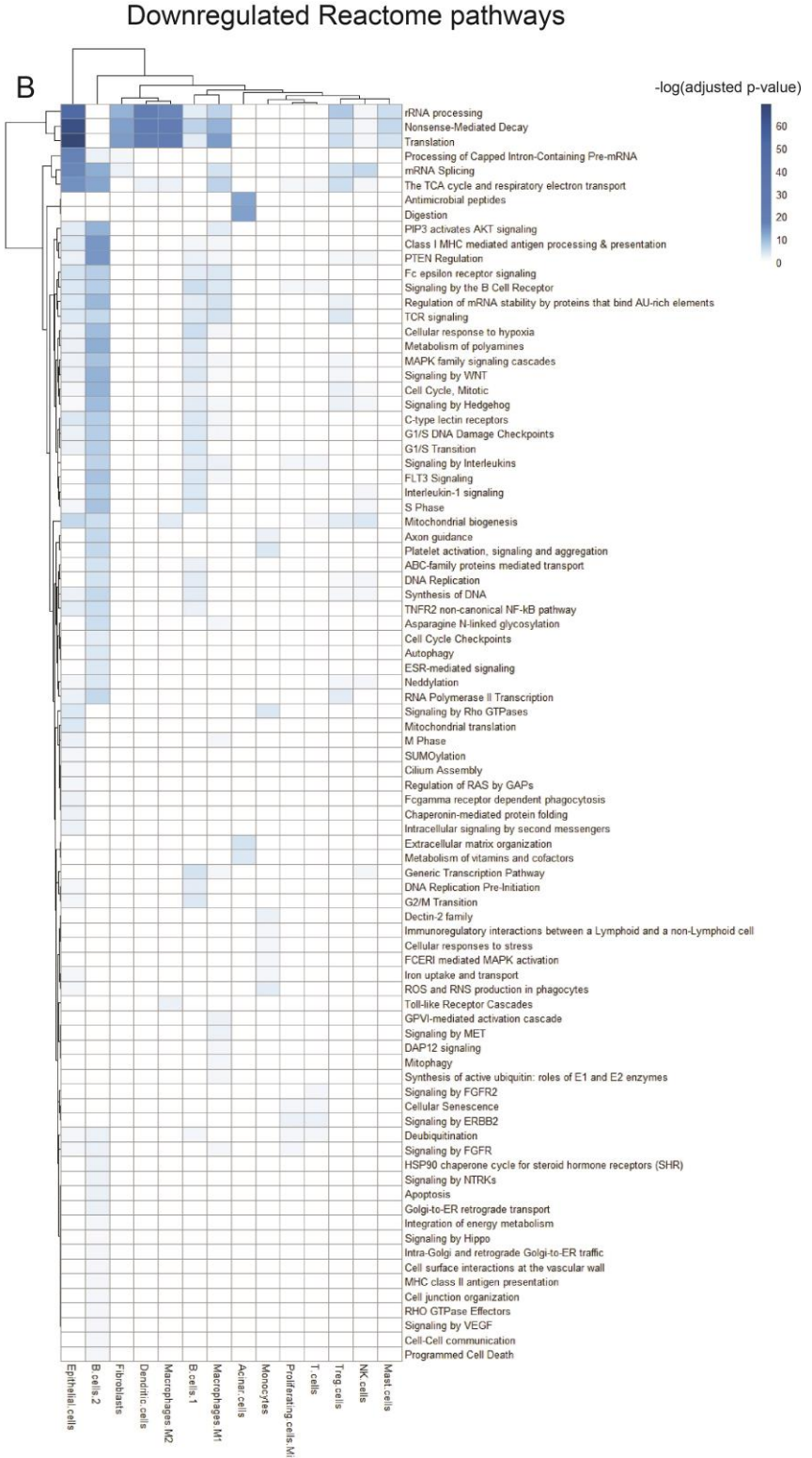
Downregulated Reactome pathways
B
-log(adjusted p-value)
60
50
40
30
20
10
0
rRNA processing
Nonsense-Mediated Decay
Translation
Processing of Capped Intron-Containing Pre-mRNA
mRNA Splicing
The TCA cycle and respiratory electron transport
Antimicrobial peptides
Digestion
PIP3 activates AKT signaling
Class I MHC mediated antigen processing & presentation
PTEN Regulation
Fc epsilon receptor signaling
Signaling by the B Cell Receptor
Regulation of mRNA stability by proteins that bind AU-rich elements
TCR signaling
Cellular response to hypoxia
Metabolism of polyamines
MAPK family signaling cascades
Signaling by WNT
Cell Cycle, Mitotic
Signaling by Hedgehog
C-type lectin receptors
G1/S DNA Damage Checkpoints
G1/S Transition
Signaling by Interleukins
FLT3 Signaling
Interleukin-1 signaling
S Phase
Mitochondrial biogenesis
Axon guidance
Platelet activation, signaling and aggregation
ABC-family proteins mediated transport
DNA Replication
Synthesis of DNA
TNFR2 non-canonical NF-kB pathway
Asparagine N-linked glycosylation
Cell Cycle Checkpoints
Autophagy
ESR-mediated signaling
Neddylation
RNA Polymerase II Transcription
Signaling by Rho GTPases
Mitochondrial translation
M Phase
SUMOylation
Cilium Assembly
Regulation of RAS by GAPs
Fcgamma receptor dependent phagocytosis
Chaperonin-mediated protein folding
Intracellular signaling by second messengers
Extracellular matrix organization
Metabolism of vitamins and cofactors
Generic Transcription Pathway
DNA Replication Pre-Initiation
G2/M Transition
Dectin-2 family
Immunoregulatory interactions between a Lymphoid and a non-Lymphoid cell
Cellular responses to stress
FCERI mediated MAPK activation
Iron uptake and transport
ROS and RNS production in phagocytes
Toll-like Receptor Cascades
GPVI-mediated activation cascade
Signaling by MET
DAP12 signaling
Mitophagy
Synthesis of active ubiquitin: roles of E1 and E2 enzymes
Signaling by FGFR2
Cellular Senescence
Signaling by ERBB2
Deubiquitination
Signaling by FGFR
HSP90 chaperone cycle for steroid hormone receptors (SHR)
Signaling by NTRKs
Apoptosis
Golgi-to-ER retrograde transport
Integration of energy metabolism
Signaling by Hippo
Intra-Golgi and retrograde Golgi-to-ER traffic
Cell surface interactions at the vascular wall
MHC class II antigen presentation
Cell junction organization
RHO GTPase Effectors
Signaling by VEGF
Cell-Cell communication
Programmed Cell Death
Epithelial.cells
B.cells.2
Fibroblasts
Dendritic.cells
Macrophages.M2
B.cells.1
Macrophages.M1
Acinar.cells
Monocytes
Proliferating.cells.Mix
T.cells
Treg.cells
NK.cells
Mast.cells

Figure 4.9. The single-cell transcriptomics analyses reveal the pathways altered by hyperinsulinemia in each cell type.
A, Heatmap showing Reactome pathways that are upregulated in PK-*Ins1*$^{-/-}$;*Ins2*$^{+/-}$ mice when compared to PK-*Ins1*$^{-/-}$;*Ins2*$^{+/+}$ mice. Color intensity indicates the negative $\log_{10}$ of adjusted p value. **B,** Heatmap of Reactome pathways that are downregulated in PK-*Ins1*$^{-/-}$;*Ins2*$^{+/-}$ mice when compared to PK-*Ins1*$^{-/-}$;*Ins2*$^{+/+}$ mice. Color intensity indicates the negative $\log_{10}$ of adjusted p value.

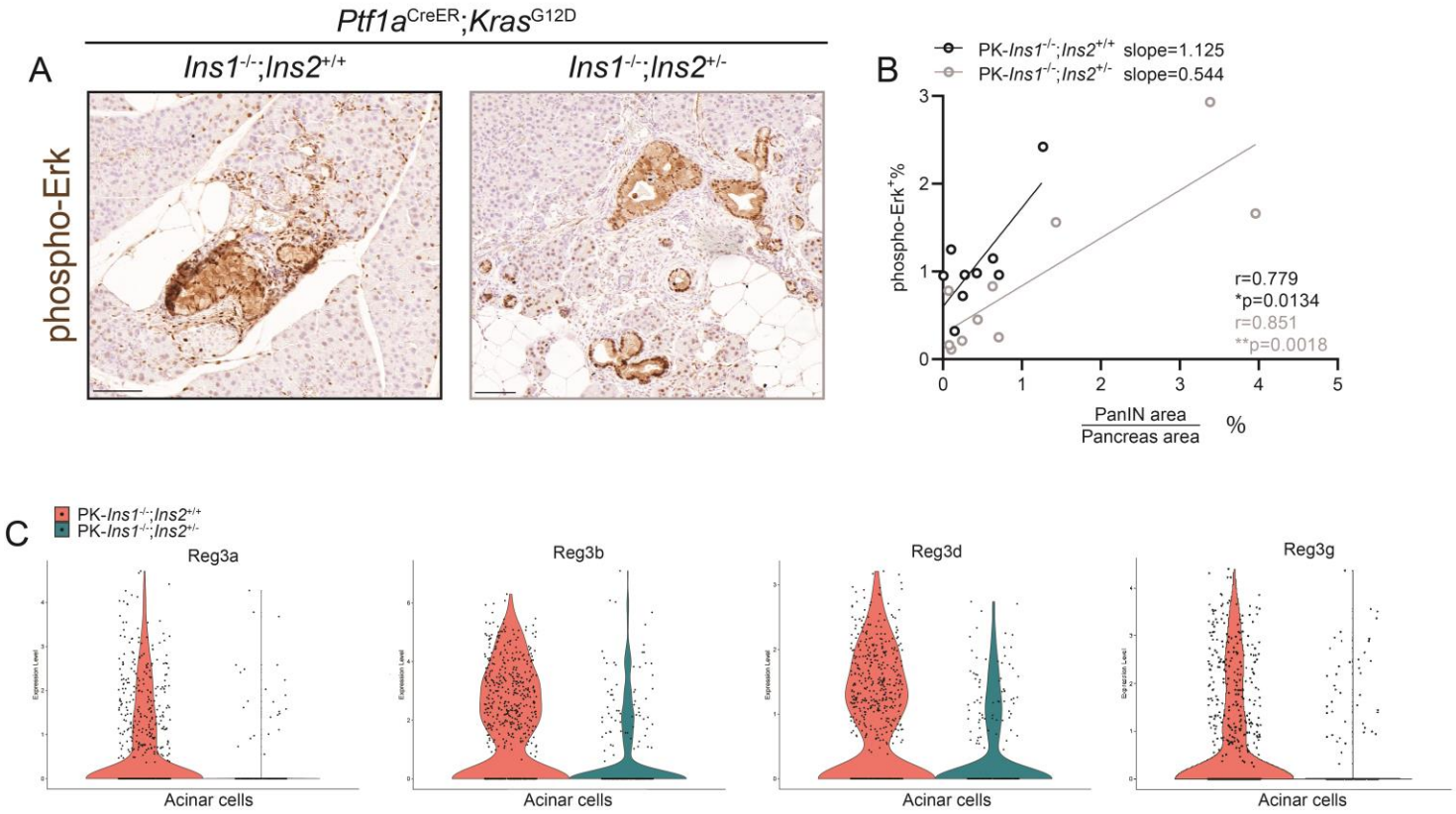

Figure 4.10. The phospho-Erk protein and *Reg* genes expression levels in PK-*Ins1*$^{-/-}$;*Ins2*$^{+/+}$ and PK-Ins1$^{-/-}$;Ins2$^{+/-}$ mice.

A, Immunohistochemistry of phospho-Erk for mice pancreata from each genotype. Scale bars: 0.1 mm. **B,** The correlation of composite PanIN area with phospho-Erk^{+} area. **C,** Expression levels of *Reg3a*, *Reg3b*, *Reg3d*, and *Reg3g* in pancreatic acinar cells from each genotype. *p<0.05, **p<0.01.

Chapter 5: Insulin receptor signaling in pancreatic acinar cells contributes to PDAC development in the context of high fat diet

5.1 Introduction

Hyperinsulinemia is a cardinal feature shared by obesity and T2D and it is proposed as one of the underlying causes for obesity and T2D associated cancer risk (63,76). Many epidemiological studies consistently demonstrate hyperinsulinemia is associated with increased PDAC risk and aggressiveness (162-164). Complementing these epidemiological associations, our *in vivo* animal experiments (Chapter 3 and Chapter 4) demonstrated that endogenous hyperinsulinemia causally contributes to PDAC development (74,235). Specifically, we found that a 50% genetic reduction of insulin production in *Ptf1a*^{CreER};*Kras*$^{LSL\text{-}G12D}$ mice resulted in a ~50% reduction in PanIN lesions compared to littermate controls (74,235). Notably, the effects of preventing hyperinsulinemia on PanIN development were independent of glycemia and observed in the absence of significant glucose intolerance (74). Qualitatively similar results were reproduced in a follow-up study using a milder reduction of insulin production (235).

Our second study used scRNA-seq to provide new information about the cellular gene expression changes associated with this protection from PDAC. We found the immune cells in the PanIN microenvironment had significant changes in their transcriptomes induced by hyperinsulinemia. Consistent with a role for insulin in the PanIN microenvironment, insulin relevant pathways like MAPK/ERK pathway were downregulated in several immune cell populations in mice with reduced insulin production (235).

While our first two studies clearly demonstrated a causal role for hyperinsulinemia in pancreatic cancer development, it is still unclear whether the protective effects of reducing insulin production in mice fed high-fat diet were direct on the tumor precursor cells or whether

they were mediated indirectly by local immune cells, local fibroblasts, or even via distant effects on adiposity (112,120-122,249). Indeed, pancreatic cancer has a characteristic intense desmoplastic reaction and high immune cell infiltration that assists tumor cell growth and survival. Theoretically, hyperinsulinemia could indirectly promote PanIN development through regulating the fibrogenic process and immune cell infiltration in the PanIN microenvironment (235). Alternatively, hyperinsulinemia may have direct oncogenic effects on the acinar cells that develop into PanIN in our pre-clinical animal models. *In vitro* studies on the PANC-1 pancreatic cancer cell line demonstrate that insulin stimulates their proliferation, suggesting that insulin can directly affect tumor cells (244). Nevertheless, it remains unclear whether hyperinsulinemia directly accelerates PanIN growth through insulin receptor signaling and its downstream signaling cascades in acinar cells *in vivo*. In fact, to date, no studies in any cancer type have examined the consequences of genetic ablation of insulin receptors.

Mutations in both the MAPK/ERK and PI3K/AKT/mTOR pathways can induce PDAC. As mentioned above, KRAS mutations are detected in ~90% of PDAC and most PDAC mouse models are designed based on the expression of the *Kras*^{G12D} oncogene (41). *PIK3CA* mutations, which is the gene encoding the catalytic p110α subunit of PI3K, can also be detected in 3-5% of PDAC patients (221-223). Additionally, when a constitutively activated PI3K was expressed in pancreatic cells (*Pdx-1*-Cre), PanIN lesions and tumors developed in these mice (224). Precursors lesions could be detected as early as 10 days of age and at 20-days old, PDAC was already detected in some mice (224). Interestingly, Sivaram *et al* found tumor-intrinsic PI3K/AKT/mTOR signaling limits T cell recognition and tumor cell clearance in the PDAC microenvironment. Specifically, when *Pik3ca* was silenced in *Pdx1*-Cre;*Kras*$^{LSL\text{-}G12D}$; *Trp53*$^{LSL\text{-}R172H}$ mice, it induced T cell infiltration, tumor repression, and increased the survival of the mice

(225). Additionally, strategies developed to systemically inhibit PI3K/AKT/mTOR signaling have inhibited PDAC development (224,226). In summary, there is a strong evidence from animal models that signaling cascades downstream of insulin/insulin receptor, the PI3K/AKT/mTOR and MAPK/ERK pathways, are both important for and dysregulated in PDAC. Many studies have reported that insulin receptors are upregulated in some cancers like breast, prostate, and liver cancers which suggests that INSR itself is dysregulated in cancer (149,202,205-207). Therefore, INSR may promote cancer cell proliferation and survival through activating either MAPK/ERK or PI3K/AKT/mTOR pathways. However, the specific role of insulin and INSR signaling in PDAC tumorigenesis through stimulating these two pathways is still unclear.

In this study, we addressed the hypothesis that insulin/insulin receptor contributes to high-fat diet mediated enhancement of PanIN and PDAC development through manipulating the *Insr* alleles in pancreatic acinar cells, a cellular origin of PDAC. We found a significant reduction in PanIN and tumor development in mice losing *Insr* in acinar cells compared to mice with wild-type *Insr* in acinar cells. This suggested that hyperinsulinemia can directly contribute to PanIN and PDAC development through INSR signaling and prophylactic anticancer therapy approaches targeting insulin receptor signaling may be beneficial in treating pancreatic cancer.

5.2 Results

5.2.1 A mouse model to investigate *INSR* signaling in PDAC development

To examine whether hyperinsulinemia affects PanIN and PDAC development through insulin receptor in acinar cells, we generated mouse models in which $Kras^{G12D}$ mutation and loss of *Insr* were both induced in acinar cells. By crossing $Ptf1a^{CreER}$;$Kras^{LSL\text{-}G12D}$;$Insr^{w/f}$;nTnG mice

with *Insr*$^{w/f}$ mice, we generated: 1) mice with full insulin receptor, *Ptf1a*^{CreER};*Kras*$^{LSL\text{-}G12D}$;*Insr*$^{w/w}$;nTnG (PK-*Insr*$^{w/w}$); 2) mice with insulin receptor reduced by approximately half, *Ptf1a*^{CreER};*Kras*$^{LSL\text{-}G12D}$;*Insr*$^{w/f}$;nTnG (PK-*Insr*$^{w/f}$); or 3) mice without insulin receptor, *Ptf1a*^{CreER};*Kras*$^{LSL\text{-}G12D}$;*Insr*$^{f/f}$;nTnG (PK-*Insr*$^{f/f}$) mice in acinar cells (Figure 5.1A). To examine the effects of deletion of *Insr* alone in acinar cells on mouse glucose homeostasis, we also examined *Ptf1a*^{CreER};*Insr*$^{w/w}$;nTnG or *Ptf1a*^{CreER};*Insr*$^{f/f}$;nTnG mice that do not have the *Kras*$^{LSL\text{-}G12D}$ allele (Figure 5.1B). To follow the fate of recombined cells, the nTnG Cre-dependent reporter allele was also included in our mouse models (276).

To induce sustained hyperinsulinemia, the mice were fed with HFD after weaning (3-week-old), and tamoxifen was injected at week 4 to induce expression of *Kras*^{G12D} and/or recombine the *Insr*^{flox} alleles specifically in acinar cells (Figure 5.1C). The mouse body weight and 4-hour-fasted blood glucose levels were routinely assessed every month and 4-hour-fasted insulin levels were measured every 3 months (Figure 5.1C). One group of mice was euthanized at 12 weeks old, and one group of mice was euthanized at 43.5 weeks old (10 months) to assess how insulin receptor affects PanIN initiation and progression, respectively (Figure 5.1C).

5.2.2 Effects of acinar cell-specific loss of insulin receptors on body weight and glucose metabolism

To investigate if loss of insulin receptor in *Kras*^{G12D}-expressing acinar cells influences glucose metabolism, we regularly measured mouse body weight, fasting glucose, and insulin levels for 10 months until euthanasia. In the *Ptf1a*^{CreER};*Kras*$^{LSL\text{-}G12D}$ genetic background, the loss of *Insr* allele(s) did not significantly affect body weight, fasting glucose, or fasting insulin levels for both male and female mice (Figure 5.2A-F). Moreover, there was no significant difference in

the ratio of pancreas weight to body weight and no difference in pancreas weight between PK-*Insr*$^{w/w}$, PK-*Insr*$^{w/f}$, and PK-*Insr*$^{f/f}$ mice at 12 weeks of age, which suggests that reducing insulin receptor in specifically in adult acinar cells has no effect on pancreas size (Figure 5.2G-H).

We then checked whether loss of the insulin receptor in wild-type acinar cells had any effect on body weight or glucose metabolism. There was no statistically significant difference in body weight between the male mice with and without *Insr* (Figure 5.3A). In contrast, we observed a small, but significant, reduction in body weight in female *Ptf1a*^{CreER};*Insr*$^{f/f}$;nTnG mice compared to *Ptf1a*^{CreER};*Insr*$^{w/w}$;nTnG mice (Figure 5.3B). As expected, there was no significant difference in fasting glucose or fasting insulin levels between *Ptf1a*^{CreER};*Insr*$^{w/w}$;nTnG and *Ptf1a*^{CreER};*Insr*$^{f/f}$;nTnG mice (Figure 5.3C-F), which showed that INSR in acinar cells did not contribute to maintaining glucose metabolism. Similarly, the pancreas weight to body weight ratio of *Ptf1a*^{CreER};*Insr*$^{w/w}$;nTnG and *Ptf1a*^{CreER};*Insr*$^{f/f}$;nTnG mice were not statistically different (Figure 5.3G), which suggests pancreatic size may not be affected by the loss of the *Insr* in wild-type acinar cells.

5.2.3 Recombination efficiency in *Insr* knockout mice

We euthanized the mice for histopathological analyses when they were 12-weeks-old or 10-months-old. To ensure that any changes observed in the frequency of PanINs was not due to the absence of efficient recombination, we performed anti-GFP IHC to check the recombination efficiency. Our mouse models included a nTnG lineage report allele, thus, the cells with active Cre-recombinase should turn on GFP expression, while the cells that were not recombined would retain Tomato expression (276).

As expected, the PanIN lesions were largely GFP positive (brown) in all male and female PK-*Insr*$^{w/w}$, PK-*Insr*$^{w/f}$, and PK-*Insr*$^{f/f}$ mice (Figure 5.4A-D). This is consistent with the idea that acinar cells need recombination and expression of the *Kras*$^{LSL\text{-}G12D}$ allele to develop into PanIN cells. Most of the morphologically normal acinar cells in the pancreas from all three genotypes were also GFP positive (Figure 5.4A-D), regardless of the age of analysis, this suggests these acinar cells also had the chance to recombine the *Kras*$^{LSL\text{-}G12D}$, *Insr*^{flox} loci too. As expected, the cells in spleen, intestine, and pancreatic islets and stroma were not labeled with GFP because the Cre recombinase-ER fusion gene, which is under the control of the *Ptf1a* promoter, is only expressed in adult acinar cells. A similar GFP expression pattern was detected in *Ptf1a*^{CreER};*Insr*$^{w/w}$;nTnG and *Ptf1a*^{CreER};*Insr*$^{f/f}$;nTnG male and female mice (Figure 5.5A-B). No PanIN lesions were detected in these KRAS wild-type mice, and the general pancreatic morphology was similar to controls (data not shown). This suggested that loss of *Insr* itself cannot induce the metaplastic transition in acinar cells. We did find that a small number of mice had very low GFP labeling. This low GFP labeling was independent of the genotype. Mice in PK-background with low GFP labeling developed very few PanIN lesions. This suggested that the initial recombination efficiency had been very low in these mice. For all remaining analyses, we only included samples from mice with a GFP labeling efficiency estimated to be above 20%.

5.2.4 The metaplasia formation is reduced in mice without insulin receptor

To quantify the extent of PanIN formation after Kras activation and high-fat diet treatment for 40.5 weeks in the presence and absence of *Insr*, we stained pancreata from PK-*Insr*$^{w/w}$, PK-*Insr*$^{w/f}$, and PK-*Insr*$^{f/f}$ mice with Alcian blue (Figure 5.6A-D). PanIN, especially low-grade PanIN, has high acidic mucin content, which can be marked by blue during Alcian blue

staining. However, not all PanIN lesions are Alcian blue positive, particularly high-grade PanINs. Therefore, Alcian blue staining is a better reporter for the presence of low-grade PanINs. We found PanIN lesions in PK-*Insr*$^{w/w}$, PK-*Insr*$^{w/f}$, and PK-*Insr*$^{f/f}$ that were Alcian blue-positive (Figure 5.6A&C). PK-*Insr*$^{f/f}$ male mice tended to have less pancreatic area occupied by Alcian blue lesions (1.86 ± 0.48%) than PK-*Insr*$^{w/w}$ (3.00 ± 0.49%), PK-*Insr*$^{w/f}$ (3.51 ± 0.39%) male mice (Figure 5.6B). In females, there appeared to be an *Insr*-gene-dosage-dependent decrease in Alcian blue^{+} area (Figure 5.6D), with a statistically significant difference between PK-*Insr*$^{f/f}$ and PK-*Insr*$^{w/w}$ females (1.05 ± 0.30% vs 3.68 ± 0.66%). These data suggest that insulin receptor in acinar cells affects low-grade PanIN development, especially in female mice.

When acinar cells contribute to ADM, PanIN, and PDAC formation most of the acinar cells lose the expression of acinar cell identity genes like CPA1, but gain expression of ductal cell identity genes like CK19 (43). Therefore, by performing IHC staining of CK19, we could assess whether there was a difference in ductal metaplasia between the mice with and without *Insr*. Expectedly, normal ductal cells, as well as cells in ADM, PanIN, and PDAC lesions, were labeled with CK19 in both male and female PK-*Insr*$^{w/w}$, PK-*Insr*$^{w/f}$, and PK-*Insr*$^{f/f}$ mice (Figure 5.7A&D). We quantified the CK19^{+} pancreatic area and found an *Insr* gene dosage-dependent reduction in CK19^{+} pancreatic area in male and female mice. PK-*Insr*$^{f/f}$ male mice had significantly less CK19^{+} pancreatic area compared to PK-*Insr*$^{w/w}$ male mice (9.89 ± 2.23% vs 23.00 ± 0.71%) (Figure 5.7B). For female mice, the reduction in CK19^{+} pancreatic area was significantly different between all genotypes (21.32 ± 1.67%, 14.54 ± 1.11%, and 8.59 ± 1.59% for PK-*Insr*$^{w/w}$, PK-*Insr*$^{w/f}$, and PK-*Insr*$^{f/f}$ mice, respectively) (Figure 5.7D). These data suggest that insulin receptor in Kras^{G12D}-expressing acinar cells promotes ductal metaplasia.

5.2.5 Loss of *Insr* in *Kras*^{G12D}-expressing acinar cells reduced PanIN initiation and development

Finally, we stained the pancreatic sections from PK-*Insr*$^{w/w}$, PK-*Insr*$^{w/f}$, and PK-*Insr*$^{f/f}$ mice with H&E and performed histopathological analyses for normal acini, PanIN and PDAC. Two cohorts of mice were euthanized at 12-week-old or 10-month-old for assessing INSR effects on PanIN initiation or development, respectively. As expected, at 12 weeks of age, the ADM and PanINs just started to initiate, so the pancreata were predominantly normal with some ductal lesions having histological characteristics of low-grade PanIN (Figure 5.8A&C). Quantitively, we found a ~5.3-fold reduction in the percentage of pancreas occupied by PanINs in PK-*Insr*$^{f/f}$ (0.31 ± 0.19%) male mice compared to PK-*Insr*$^{w/w}$ (1.64 ± 0.16%, $p<0.05$) male mice. PK-*Insr*$^{w/f}$ had a PanIN area of 1.17 ± 0.26% of the pancreas occupied by PanINs (Figure 5.8B). Moreover, there was a ~6.3-fold and ~3.5-fold reduction in the PanIN area in PK-*Insr*$^{f/f}$ (0.23 ± 0.039%) female mice when compared to PK-*Insr*$^{w/w}$ mice (1.46 ± 0.77%) and PK-*Insr*$^{w/f}$ (0.81 ± 0.21%) mice, respectively (Figure 5.8D). Therefore, our data suggest that INSR signaling contributes to PanIN initiation for both sexes.

For mice euthanized at 10 months old, we detected ductal lesions with histological characteristics of both low-grade and high-grade PanINs. However, as the representative pancreatic sections show, there were still large areas of normal acinar cells present in PK-*Insr*$^{f/f}$ mice compared to the other two genotypes (Figure 5.9A&E). Consistent with these observations, quantification of the acinar cell area per pancreas showed there was more acinar cell area in PK-*Insr*$^{f/f}$ (36.72 ± 15.85%) and PK-*Insr*$^{w/f}$ (20.39 ± 6.31%) male mice compared to PK-*Insr*$^{w/w}$ (2.67 ± 1.15%) male mice, but the difference was not statistically significant (Figure 5.9B). Female PK-*Insr*$^{w/w}$ (9.86 ± 4.68%) and PK-*Insr*$^{w/f}$ (26.75 ± 5.56%) mice had significantly reduced

normal acinar area compared to PK-*Insr*$^{f/f}$ (61.32 ± 7.84%) female mice (Figure 5.9F). This suggests that deletion of *Insr* in Kras^{G12D}-expressing acinar cells reduces the effects of oncogenic Kras and/or consuming a high-fat diet and promotes maintenance of the acinar cell morphology.

Different from our previous studies using mice models with reduced insulin production (74,235), we observed that more mice developed tumors in this mouse model. We found 1 out of 5 (20%) PK-*Insr*$^{w/w}$, 4 out of 10 (40%) PK-*Insr*$^{w/f}$, and 3 out of 6 (50%) PK-*Insr*$^{f/f}$ male mice developed tumors and they are marked as filled dots in Figure 5.9C. However, there were also one PK-*Insr*$^{w/w}$, one PK-*Insr*$^{w/f}$, and zero PK-*Insr*$^{f/f}$ male mice found dead before the experimental endpoint (10 months). Their pancreata were collected to find the cause of death, and we confirmed that tumors were in their pancreata; however, because the pancreata were highly decomposed, we did not include them for quantitative histopathological measurements. We found a ~2.9-fold significant reduction in the percentage of pancreas occupied by PanIN plus tumor in PK-*Insr*$^{f/f}$ (16.58 ± 5.53%) male mice compared to PK-*Insr*$^{w/w}$ (47.92 ± 4.05%) male mice and PK-*Insr*$^{w/f}$ had PanIN plus tumor area (30.54 ± 4.14%) in between (filled circles denote mice that developed PDAC) (Figure 5.9C). To ensure the observed difference in PanIN plus tumor area was not caused by tumor size, we also compared the PanIN only pancreatic area between the genotypes. We detected a significant 2.7-fold reduction in PK-*Insr*$^{f/f}$ (16.89 ± 4.73%) male mice, and a significant 1.7-fold reduction in PK-*Insr*$^{w/f}$ (26.59 ± 3.82%) male mice when compared to PK-*Insr*$^{w/w}$ (45.07 ± 4.81%) male mice (Figure 5.9D). Our data indicated that the insulin receptor is vital for PanIN development in male mice and hyperinsulinemia can directly affect PanIN development through INSR in the Kras^{G12D}-expressing acinar cells.

Similarly, we also found abundant ductal lesions with histological and molecular characteristics of PanINs in all female mice regardless of genotypes. Mice with only one or two

alleles of *Insr* had more normal acinar cells (Figure 5.9E). Quantitively, PK-*Insr*$^{f/f}$ (61.32 ± 7.84%) female mice had significantly more (2.3-fold and 6.2-fold, respectively) acinar cells when compared to PK-*Insr*$^{w/f}$ (26.75 ± 5.56%) and PK-*Insr*$^{w/w}$ (9.86 ± 4.68%) female mice (Figure 5.9F). This indicated that INSR signaling in acinar cells contributes to the ductal metaplasia observed in female mice from our mouse model.

There were 7 out of 9 (78%) PK-*Insr*$^{w/w}$, 8 out of 15 (53%) PK-*Insr*$^{w/f}$, and 2 out of 9 (22%) PK-*Insr*$^{f/f}$ female mice developed tumors and they are marked as filled triangles in the figure (Figure 5.9G). None of the female mice were found dead before the experimental endpoint (10 months). This suggests insulin receptor contributed to tumor initiation and this phenotype was stronger in female mice. When we quantified the percentage of pancreas occupied by PanINs plus tumors in female mice, we found a significant reduction (~5.3-fold) in PanIN plus tumor area in PK-*Insr*$^{f/f}$ (8.96 ± 4.28%) pancreata compared to PK-*Insr*$^{w/w}$ (47.19 ± 5.67%) pancreata and a significant reduction (~2.7-fold) when compared to PK-*Insr*$^{w/f}$ (24.45 ± 4.48%) pancreata (filled triangles donated mice developed PDAC) (Figure 5.9G). When the tumor area was removed in the female samples, we still detected a significant reduction in PanIN area in PK-*Insr*$^{f/f}$ (6.86 ± 2.69%) pancreata compared to PK-*Insr*$^{w/f}$ (19.56 ± 2.62%) and PK-*Insr*$^{w/w}$ (27.02 ± 4.66%) pancreata (3.9-fold and 2.9-fold reduction, respectively) (Figure 5.9H). Our data suggested that the loss of INSR signaling also reduces the PanIN formation in female mice. In sum, our evidence strongly suggests hyperinsulinemia promotes PanIN and PDAC development from acinar cells through its paracrine activation of INSR in Kras^{G12D}-expressing acinar cells.

5.2.6 The sex differences in histopathological parameters

In our previous study, we found there was a sex difference in PanIN and ADM development for mice in *Ins1*-null genetic background and the male mice tended to develop less PanIN and ADM lesions compared to the female mice from the same genotype (235). To check if there was also a sex difference in precursor lesions development in this study, we compared male and female mice from the same genotype for each histologic measurement. For Alcian blue^{+} area, there was no statistically significant difference between male and female mice from PK-*Insr*$^{w/w}$ and PK-*Insr*$^{f/f}$ genotypes; nevertheless, there was a significant reduction in Alcian blue^{+} area in female PK-*Insr*$^{w/f}$ compared to male PK-*Insr*$^{w/f}$ mice (Figure 5.10A-C). In contrast, there was no significant difference in CK19^{+} pancreatic area between male and female mice from all three genotypes (Figure 5.10D-F). Even though there was a trend toward higher normal acinar cell area in female mice than male mice for all three genotypes, the difference was not statistically significant (Figure 5.10G-I). In addition, we did not find a significant difference in PanIN plus tumor pancreatic area between male and female mice from all three genotypes (Figure 5.10J-L). However, we observed that in comparison to PK-*Insr*$^{w/f}$ and PK-*Insr*$^{f/f}$ male mice, PK-*Insr*$^{w/f}$ and PK-*Insr*$^{f/f}$ female mice tended to have less PanIN plus tumor area which is consistent with the observations of an increased normal acinar area in these mice (Figure 5.10K-L). Overall, female mice seem to be more sensitive to loss of *Insr* than male mice, but the sex difference was not very strong.

5.3 Discussion

The purpose of this study was to investigate the role of insulin receptor during HFD-promoted PanIN and PDAC development in the context of acinar-cell-specific expression of

Kras^{G12D}. Taken collectively with the other studies in this thesis, we have clearly shown that hyperinsulinemia acts through insulin receptors on acinar cells to enhance *Kras*^{G12D}-induced PanIN initiation and expansion from acinar cells. Our results do not preclude the possibility that insulin may also have indirect effects on PanIN development, such as modulating the immune microenvironment (235) or other locally important cell types.

Stimulation of insulin receptor signaling can activate both PI3K/AKT/mTOR and MAPK/ERK signaling cascades, both of which have mitogenic effects and the effector proteins in these two pathways are frequently mutated during tumorigenesis (178,179,194,195). Many investigators have proposed that hyperinsulinemia promotes cancer cell growth through over-activating the downstream signaling cascades of INSR (63,76,140,265). Nevertheless, there is no *in vivo* study in any cancer using specific *Insr* deletion to study its causal role in the cancer cell of origin. All cells in the body express INSR protein and require insulin signaling for key cellular functions, including nutrient uptake for storage and anabolism. While the roles of INSR in hepatocytes, myocytes, and adipocytes are well studied, the consequences of *Insr* knockout in pancreatic acinar cells is understudied. In this study, we specifically knocked out *Insr* gene from acinar cells using the *Ptf1a*$^{CreER/w}$ allele and confirmed that insulin insensitivity in acinar cells had no effects on systemic glucose homeostasis or serum insulin levels regardless of whether acinar cells expressed the *Kras*^{G12D} variant. In contrast, a previous study suggested that insulin may regulate acinar cell function (107). For instance, when the β-cells were killed by streptozotocin in rats, there was a diminishment in amylase production but when insulin was injected, the synthesis and release of amylase was restored (107,277,278). Therefore, the serum amylase levels in PK-*Insr*$^{w/w}$, PK-*Insr*$^{w/f}$, and PK-*Insr*$^{f/f}$ mice should be measured to examine if the deletion of INSR is disrupting the normal exocrine physiology. Moreover, pancreatitis can be

induced when acinar cells are overstimulated by CCK to secrete digestive enzymes which can then accelerate PanIN progression (43). Therefore, deletion of INSR in acinar cells may reduce PanIN development through reducing acinar cell workload and its associated inflammation.

Previous studies reported that HFD could accelerate PanIN and PDAC development (70-72). For example, Chang *et al* showed that at 9 months, ~80% and ~95% of the analyzed pancreatic ducts were PanINs for mice fed with chow diet and HFD, respectively (72). Previous studies suggested this HFD-accelerated PanIN development was because of increased inflammation (70). However, in this study, we showed that the loss of INSR significantly reduced the amount of PanIN lesions and increased the amount of acinar cells remaining in the pancreas. This indicated that INSR signaling may be upstream of increased inflammation.

By using anti-GFP IHC staining, we demonstrated that the remaining acinar cells present in each mouse were not solely cells that escaped tamoxifen-induced Cre recombination. This suggests that these acinar cells were unlikely to remain morphologically normal because they did not carry KRAS mutation. However, because the nTnG reporter allele is not linked to *Kras* and *Insr* genes, it was unlikely but possible for the PanINs in PK-*Insr*$^{f/f}$ and PK-*Insr*$^{w/f}$ mice arose from acinar cells retaining the *Insr* gene. It would also be interesting to perform anti-INSR staining and determine the abundance of INSR in the PanIN lesions from PK-*Insr*$^{f/f}$ and PK-*Insr*$^{w/f}$ mice.

Insulin can also bind to IGF-1 receptors and hybrid receptors, although at a lower affinity (149,202). Therefore, high insulin levels may activate and carry its downstream signaling through IGF1R signaling pathways. Future studies should be conducted to compare the levels of IGF1R and phosphorylated IGF1R between PK-*Insr*$^{w/w}$, PK-*Insr*$^{w/f}$, and PK-*Insr*$^{f/f}$ mice to see if there is a compensation of insulin signaling, especially on the PanIN cells. Ultimately, an acinar

cell-specific *Insr*/*Igf1r* double-knockout mouse could be generated to rule out any compensation between these related receptor tyrosine kinases.

High fat diet increases beta-cell mass (112), and induces basal insulin hypersecretion from β cells, resulting in sustained hyperinsulinemia. As expected, the mouse model used in this Chapter, which had four full copies of insulin genes (both *Ins1* and *Ins2*), had higher fasting insulin levels than our previous mouse models, which had only two copies of insulin genes or only one copy of insulin (1000-1500 pmol/L vs 400-800 pmol/L for males and ~500 pmol/L vs 100-200 pmol/L for females) (74,235). Consistent with the hypothesis that endogenous hyperinsulinemia contributes to pancreatic cancer development, the PK-*Insr*$^{w/w}$ mice in this study had ~50% PanIN plus tumor area while PK-*Ins1*$^{+/+}$;*Ins2*$^{-/-}$ mice had ~25% PanIN plus tumor area and PK-*Ins1*$^{-/-}$;*Ins2*$^{+/+}$ mice had ~1-4% PanIN plus tumor area (74,235). Moreover, the endpoint of mice with reduced insulin production was 57 weeks while the endpoint for mice from this study was 43.5 weeks. Also, ~70% of female PK-*Insr*$^{w/w}$ mice developed tumors while only 5-7% of female mice with reduced insulin production developed tumors (74,235). This together again supports and validates that hyperinsulinemia can promote PanIN formation.

Male mice are generally more resistant to insulin signaling than female mice (112,120-122). For instance, Mehran *et al* showed that compared to male *Ins2*$^{-/-}$ mice, female *Ins2*$^{-/-}$ mice had lower fasting insulin levels, regardless of the copy of *Ins1* alleles (112). The same sex difference was also observed for mice in *Ins1*$^{-/-}$ genetic background (120,122). However, as shown by insulin tolerance tests, male mice were more resistant to insulin than female mice (112,120-123). Consistently, in this study, we found male mice tended to develop more PanIN lesions than female mice, especially for PK-*Insr*$^{f/f}$ genotype. In contrast, we observed female mice developed more PanIN and ADM lesions than male mice in mouse model with reduced insulin production

(235). Together, the difference in PanIN development between sexes suggests female mice were more sensitive to effects of insulin and insulin signaling on PanIN development. Future studies are needed to investigate the molecular mechanism underlying how male and female mice have different sensitivity to the loss of INSR in $Kras^{G12D}$-expressing acinar cells.

Although we demonstrated that INSR signaling inhibition could significantly suppress PanIN initiation and progression in this study, we do not know the specific molecular mechanisms for this effect. We do not know if hyperinsulinemia promotes PanIN initiation and formation through the proposed PI3K/AKT/mTOR and MAPK/ERK signaling pathways or through other signaling pathways. Also, we do not know if hyperinsulinemia executes its mitogen effects more through PI3K/AKT/mTOR arm or the MAPK/ERK arm of INSR signaling. Therefore, future studies, like RNA-sequencing and phospho-proteomics, should be performed to find the signaling pathways and gene expression patterns significantly altered between the mice with and without INSR. It is also important to check if the deletion of *Insr* at the transcript level led to a deletion of INSR at the protein level. Collectively, our data strongly suggest that insulin receptor in acinar cells contributes to the PanIN and PDAC development. However, INSR on other local or distant cell types may also play a crucial role in promoting PanIN formation as our previous study demonstrated that hyperinsulinemia altered cellular pathways in immune cells in the microenvironment (235). As a result, prophylactic approaches targeting insulin receptor signaling pathways, or hyperinsulinemia itself, may be beneficial in treating and preventing pancreatic cancer.

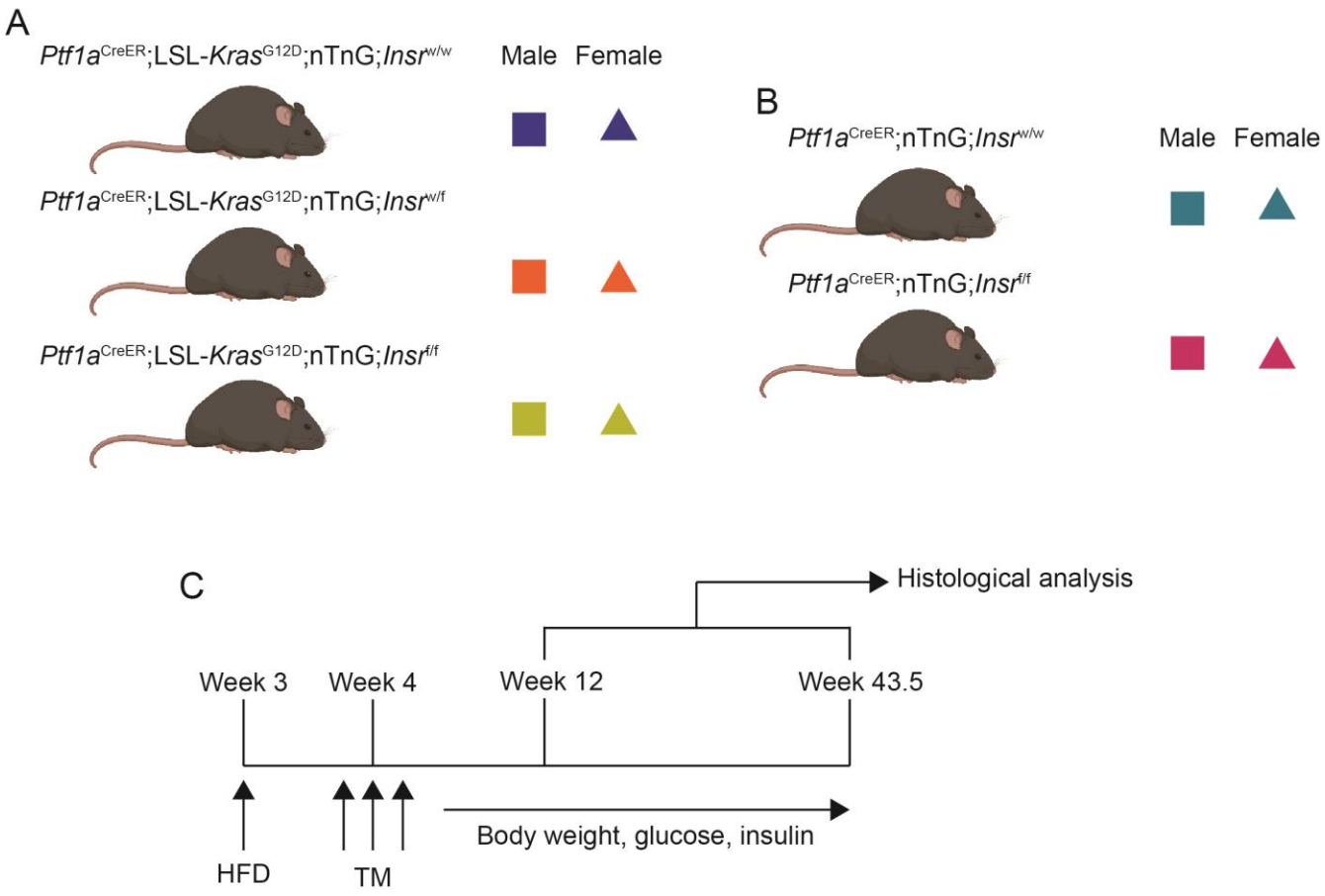

Figure 5.1. Mouse models used to test the role of insulin receptors in pancreatic cancer. **A,** Schematic describing a mouse model designed to test the role of insulin receptor signaling on HFD-accelerated PDAC initiation. On the background of the *Ptf1a*^{CreER}-induced *Kras*^{G12D} pancreatic cancer model (PK), we generated mice having two wild-type alleles of *Insr* (*Insr*$^{w/w}$), one floxed allele of *Insr* (*Insr*$^{w/f}$), or two floxed alleles of *Insr* (*Insr*$^{f/f}$). **B,** Schematic describing a mouse model designed to test the role of insulin receptor signaling on pancreatic acinar cells. On the background of *Ptf1a*^{CreER} mice, we generated mice having two wild-type alleles of *Insr* (*Insr*$^{w/w}$) or two floxed alleles of *Insr* (*Insr*$^{f/f}$). **C,** Three-week-old mice were weaned to an HFD, and at 4-weeks-old, they were injected with TM for 3 consecutive days. Physiological measures were routinely followed for 10 months, a cohort of mice was euthanized at 12 weeks of age and the other cohort mice were euthanized at 10 months of age for histopathological analyses.

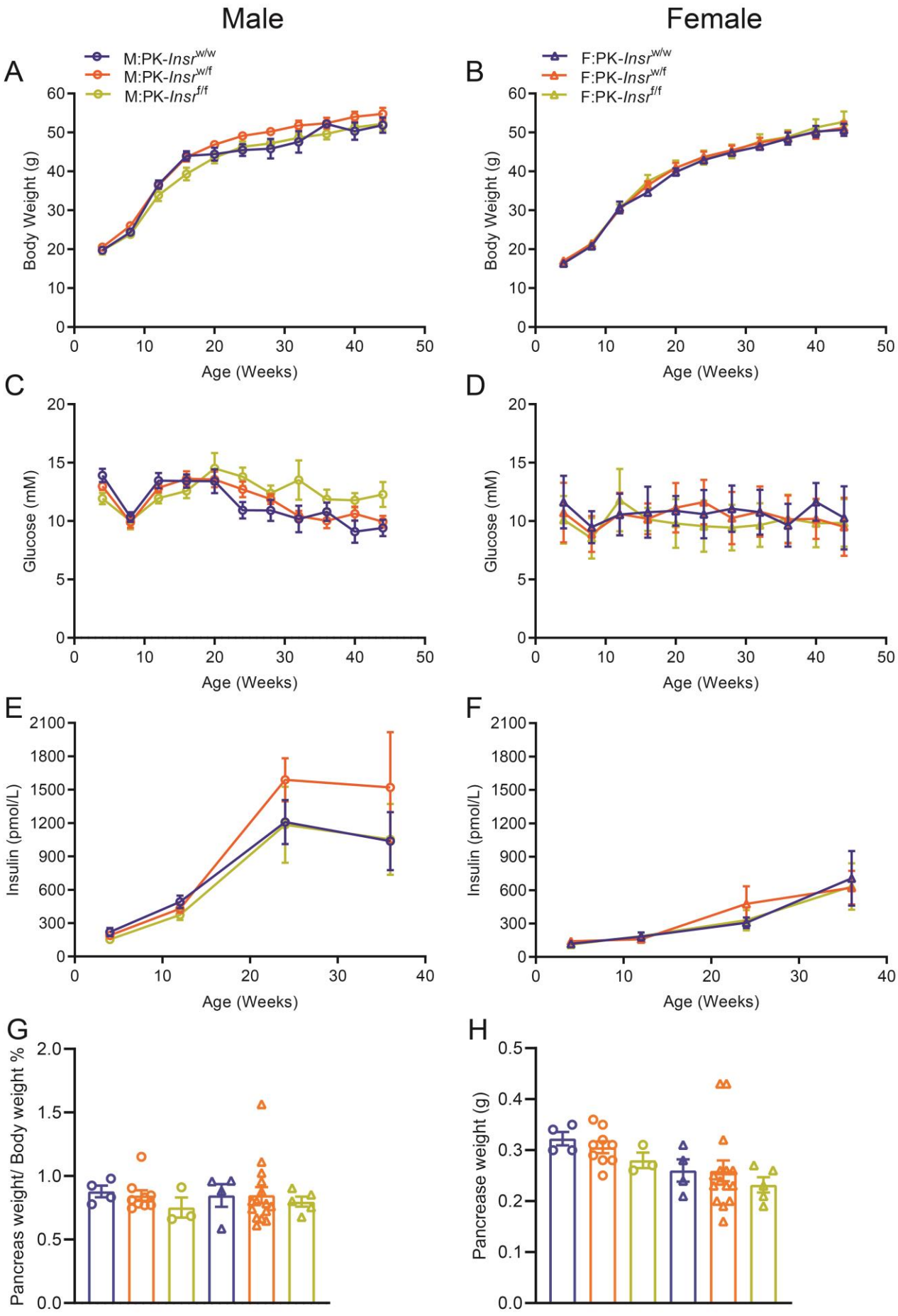
Male
Female
A
M:PK-Insr w/w
M:PK-Insr w/f
M:PK-Insr f/f
Body Weight (g)
Age (Weeks)
B
F:PK-Insr w/w
F:PK-Insr w/f
F:PK-Insr f/f
Body Weight (g)
Age (Weeks)
C
Glucose (mM)
Age (Weeks)
D
Glucose (mM)
Age (Weeks)
E
Insulin (pmol/L)
Age (Weeks)
F
Insulin (pmol/L)
Age (Weeks)
G
Pancreas weight/ Body weight %
H
Pancrease weight (g)

Figure 5.2. Loss of *Insr* in pancreatic acinar cells does not affect glucose homeostasis in *Ptf1a*^{CreER}-induced *Kras*^{G12D} pancreatic cancer model.
A-B, Body weight in PK-*Insr*$^{w/w}$, PK-*Insr*$^{w/f}$, and PK-*Insr*$^{f/f}$ male (**A**) and female (**B**) mice measured over 1 year (n= 13-33). **C-D,** Fasting blood glucose in PK-*Insr*$^{w/w}$, PK-*Insr*$^{w/f}$, and PK-*Insr*$^{f/f}$ male (**C**) and female (**D**) mice measured over 1 year (n= 13-33). **E-F,** Fasting insulin in PK-*Insr*$^{w/w}$, PK-*Insr*$^{w/f}$, and PK-*Insr*$^{f/f}$ male (**E**) and female (**F**) mice measured over 1 year (n= 3-33). **G,** The ratio of pancreas weight to mouse body weight for male and female mice from each genotype (n= 3-15). **H,** Pancreas weight for male and female mice from each genotype (n= 3-15). Values are shown as mean ± SEM.

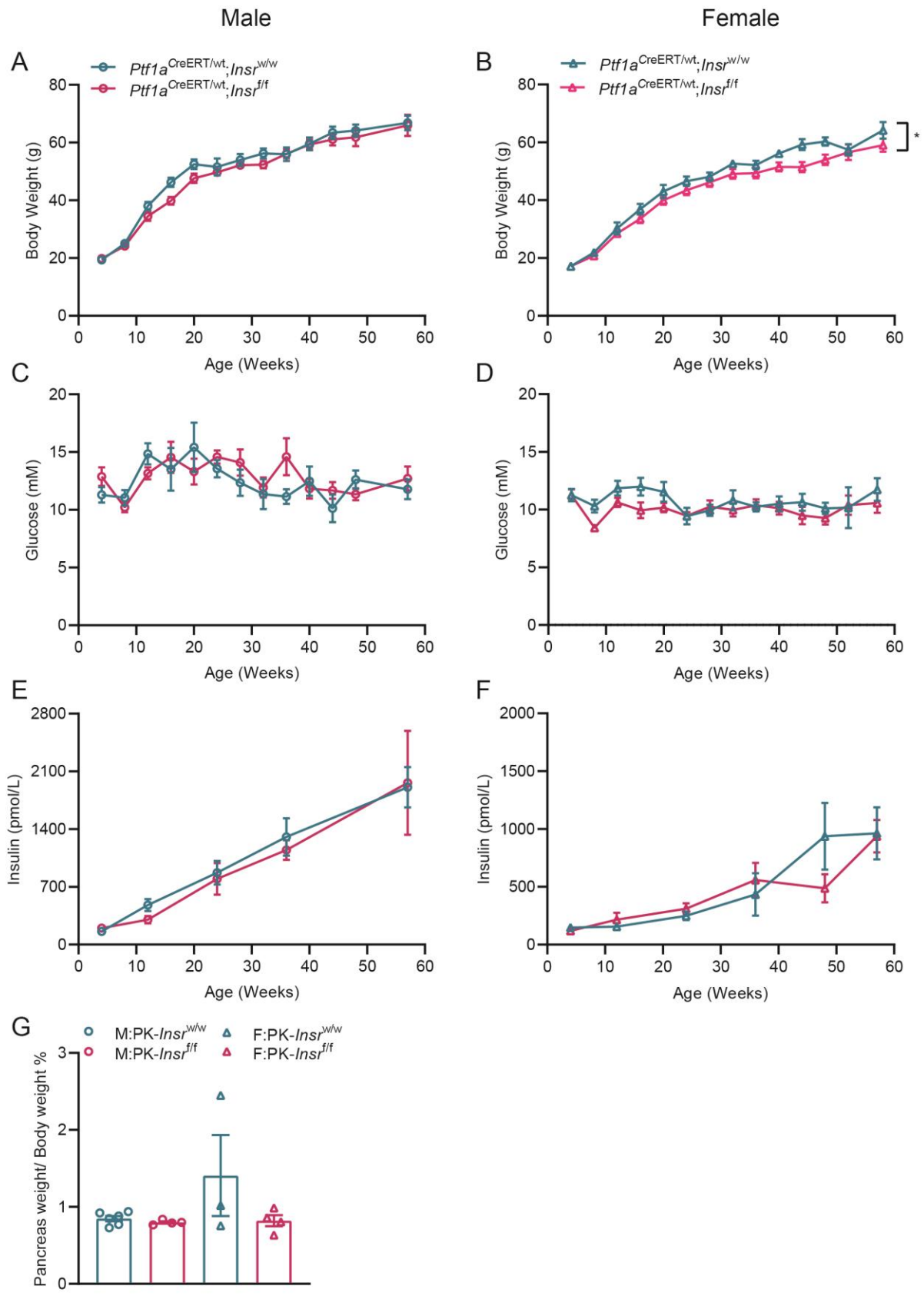
Male
Female
A
B
C
D
E
F
G
Ptf1a^CreERT/wt;Insr^w/w
Ptf1a^CreERT/wt;Insr^f/f
Body Weight (g)
Glucose (mM)
Insulin (pmol/L)
Age (Weeks)
*
M:PK-Insr^w/w
M:PK-Insr^f/f
F:PK-Insr^w/w
F:PK-Insr^f/f
Pancreas weight/ Body weight %

Figure 5.3. Loss of *Insr* in pancreatic acinar cells does not affect glucose homeostasis. **A-B,** Body weight in *Ptf1a*^{CreER}-*Insr*$^{w/w}$ and *Ptf1a*^{CreER}-*Insr*$^{f/f}$ male (**A**) and female (**B**) mice measured over 1 year (n= 11-17). **C-D,** Fasting blood glucose in *Ptf1a*^{CreER}-*Insr*$^{w/w}$ and *Ptf1a*^{CreER}-*Insr*$^{f/f}$ male (**C**) and female (**D**) mice measured over 1 year (n= 11-17). **E-F,** Fasting insulin in *Ptf1a*^{CreER}-*Insr*$^{w/w}$ and *Ptf1a*^{CreER}-*Insr*$^{f/f}$ male (**E**) and female (**F**) mice measured over 1 year (n= 10-17). **G,** The ratio of pancreas weight to mouse body weight for male and female *Ptf1a*^{CreER}-*Insr*$^{w/w}$ and *Ptf1a*^{CreER}-*Insr*$^{f/f}$ mice (n= 3-6). Values are shown as mean ± SEM. *p<0.05.

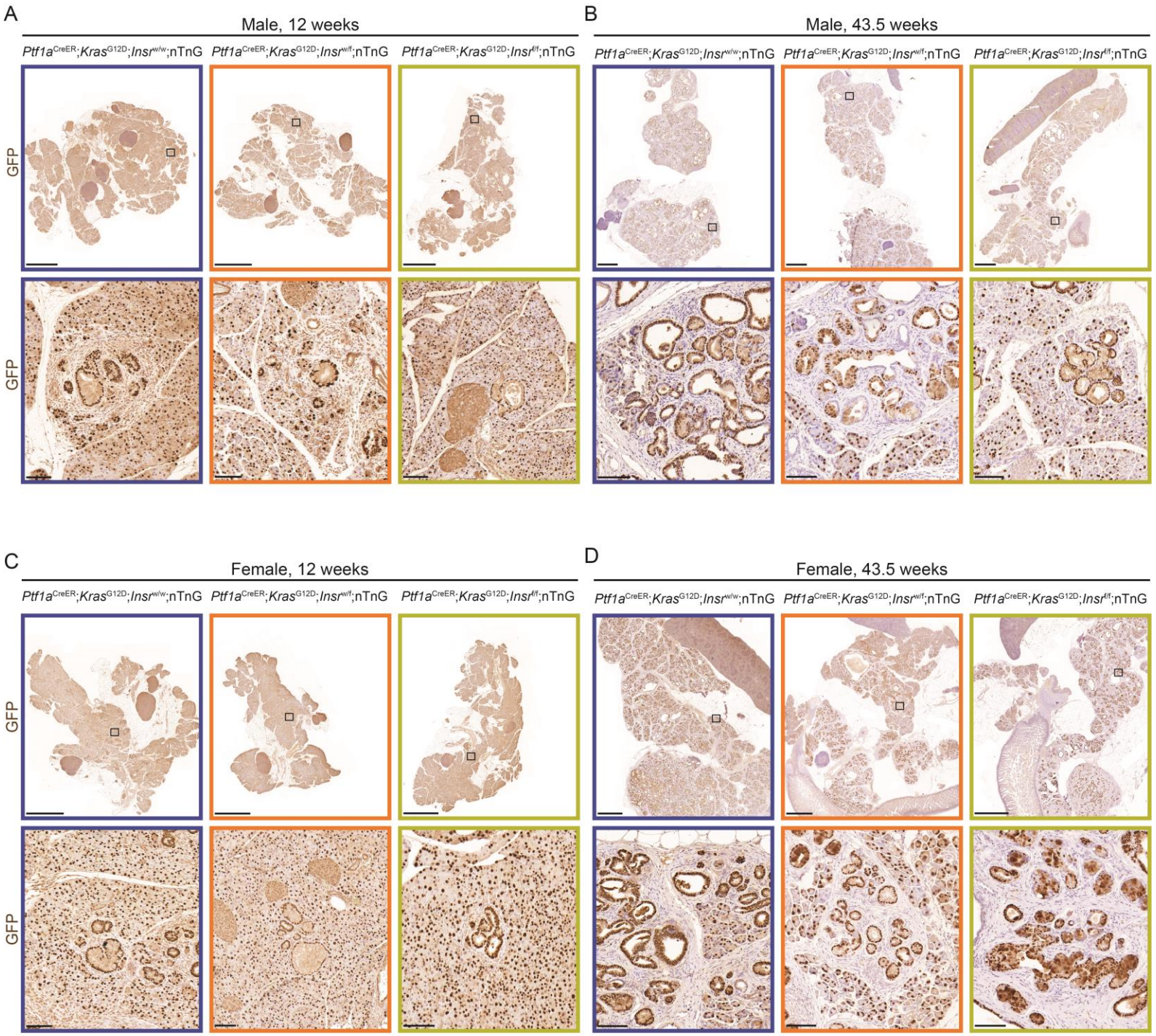

Figure 5.4. The *Ptf1a*^{CreER} allele specifically and efficiently labeled acinar cells and acinar cell-derived PanINs.

A-B, Immunohistochemical staining for nTnG lineage marker on 12-week-old (**A**) and 43.5-week-old (**B**) male PK-*Insr*$^{w/w}$, PK-*Insr*$^{w/f}$, and PK-*Insr*$^{f/f}$ pancreatic sections. **C-D,** Immunohistochemical staining for GFP lineage marker on 12-weeks-old (**C**) and 43.5-weeks-old (**D**) female PK-*Insr*$^{w/w}$, PK-*Insr*$^{w/f}$, and PK-*Insr*$^{f/f}$ pancreatic sections Scale bars: 2 mm (top) and 0.1mm (bottom).

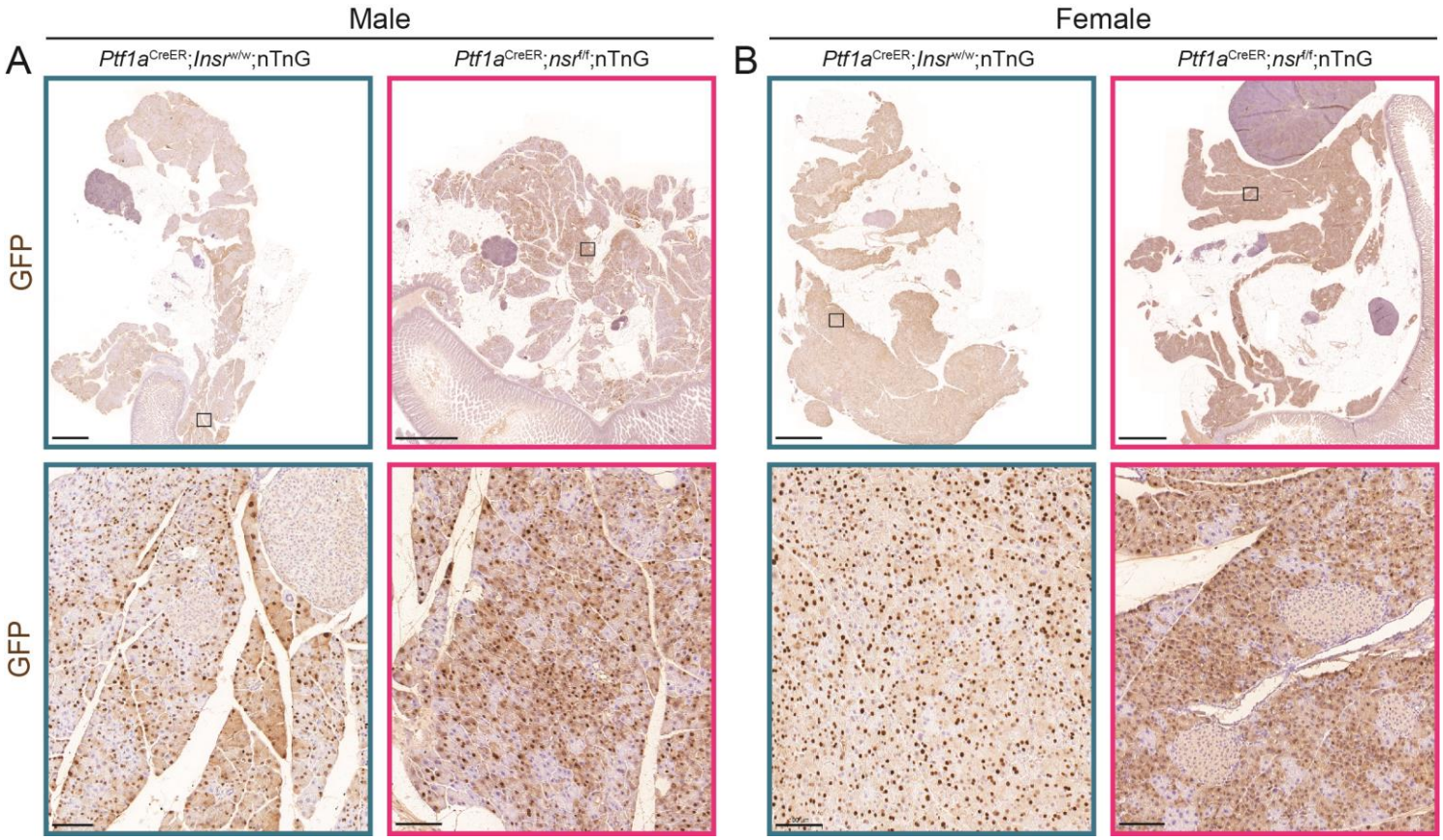

Figure 5.5. *Ptf1a*^{CreER} allele specifically and efficiently labeled acinar cells.
A-B, Immunohistochemical staining for nTnG lineage marker on male (**A**) and female (**B**) *Ptf1a*^{CreER}-*Insr*$^{w/w}$ and *Ptf1a*^{CreER}-*Insr*$^{f/f}$ pancreatic sections. Scale bars: 2 mm (top) and 0.1mm (bottom).

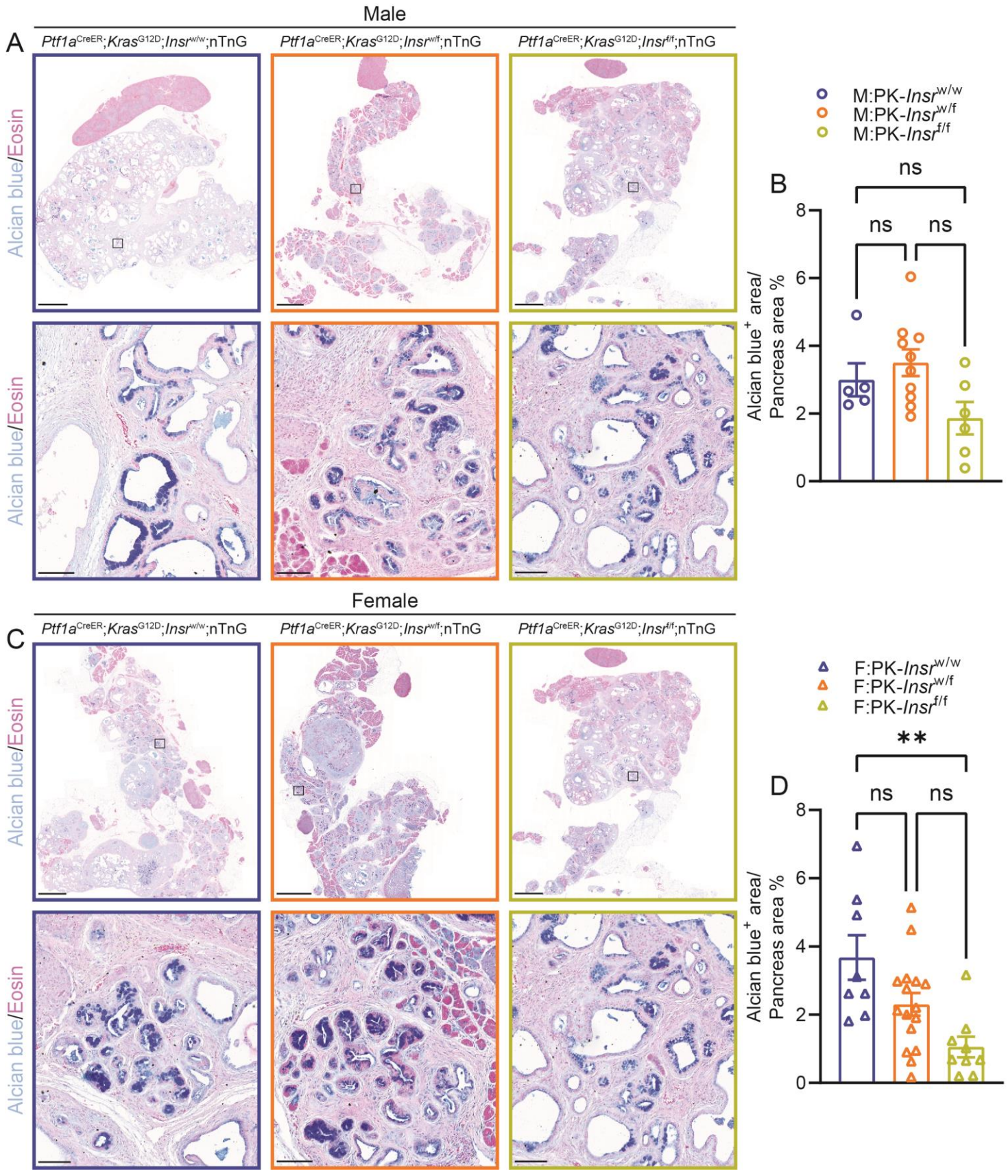
Male
A
Ptf1a^CreER;Kras^G12D;Insr^w/w;nTnG
Ptf1a^CreER;Kras^G12D;Insr^w/f;nTnG
Ptf1a^CreER;Kras^G12D;Insr^f/f;nTnG
Alcian blue/Eosin
Alcian blue/Eosin
M:PK-Insr^w/w
M:PK-Insr^w/f
M:PK-Insr^f/f
B
ns
ns
ns
Alcian blue+ area/ Pancreas area %
0
2
4
6
8
Female
C
Ptf1a^CreER;Kras^G12D;Insr^w/w;nTnG
Ptf1a^CreER;Kras^G12D;Insr^w/f;nTnG
Ptf1a^CreER;Kras^G12D;Insr^f/f;nTnG
Alcian blue/Eosin
Alcian blue/Eosin
F:PK-Insr^w/w
F:PK-Insr^w/f
F:PK-Insr^f/f
D
**
ns
ns
Alcian blue+ area/ Pancreas area %
0
2
4
6
8

Figure 5.6. The inhibition of insulin receptor signaling in acinar cells reduced low-grade PanIN lesions in female mice.
A, Representative whole section (top) and high-magnification (bottom) images of pancreatic slides from PK-*Insr*$^{w/w}$, PK-*Insr*$^{w/f}$, and PK-*Insr*$^{f/f}$ male mice stained with Alcian blue. **B,** Quantification of Alcian blue positive area in male mice from each genotype (n= 5-10). **C,** Representative whole section (top) and high-magnification (bottom) images of pancreatic slides from PK-*Insr*$^{w/w}$, PK-*Insr*$^{w/f}$, and PK-*Insr*$^{f/f}$ female mice stained with Alcian blue. **D,** Quantification of Alcian blue positive area in female mice from each genotype (n= 8-16). Scale bars: 2 mm (top) and 0.1mm (bottom). Values are shown as mean ± SEM. **p<0.01.

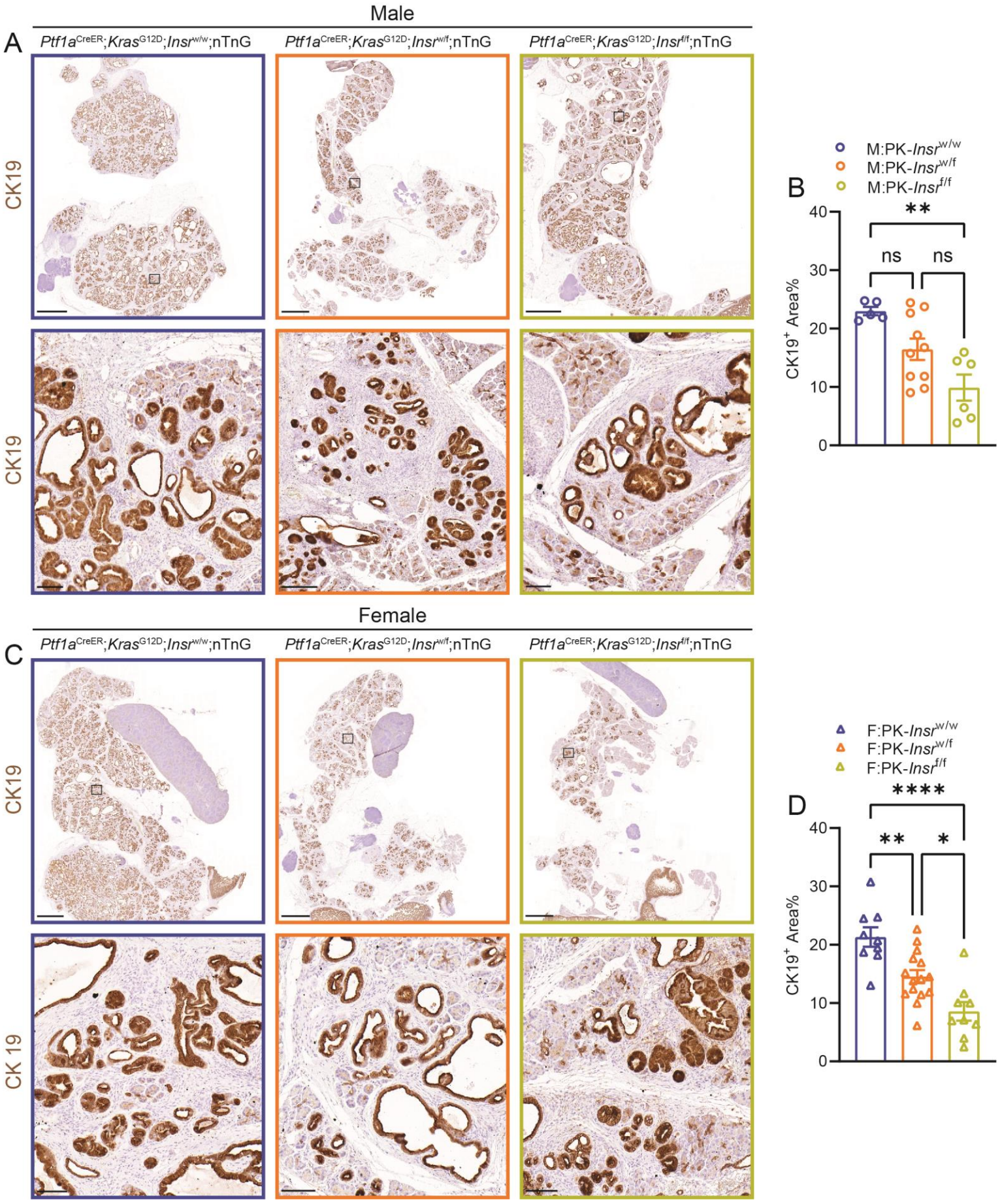
Male
A
Ptf1a^CreER;Kras^G12D;Insr^w/w;nTnG
Ptf1a^CreER;Kras^G12D;Insr^w/f;nTnG
Ptf1a^CreER;Kras^G12D;Insr^f/f;nTnG
CK19
CK19
B
M:PK-Insr^w/w
M:PK-Insr^w/f
M:PK-Insr^f/f
**
ns
ns
CK19+ Area%
0
10
20
30
40
Female
C
Ptf1a^CreER;Kras^G12D;Insr^w/w;nTnG
Ptf1a^CreER;Kras^G12D;Insr^w/f;nTnG
Ptf1a^CreER;Kras^G12D;Insr^f/f;nTnG
CK19
CK 19
D
F:PK-Insr^w/w
F:PK-Insr^w/f
F:PK-Insr^f/f
****
**
*
CK19+ Area%
0
10
20
30
40

Figure 5.7. Loss of *Insr* in acinar cells reduced metaplasia formation.
A, Representative whole section (top) and high-magnification (bottom) images of immunohistochemical staining of CK19 for PK-*Insr*$^{w/w}$, PK-*Insr*$^{w/f}$, and PK-*Insr*$^{f/f}$ male mice. **B,** Quantification of CK19 positive area in male mice from each genotype (n= 5-10). **C,** Representative whole section (top) and high-magnification (bottom) images of immunohistochemical staining of CK19 for PK-*Insr*$^{w/w}$, PK-*Insr*$^{w/f}$, and PK-*Insr*$^{f/f}$ female mice. **D,** Quantification of the of CK19 positive area in female mice from each genotype (n= 9-15). Scale bars: 2 mm (top) and 0.1mm (bottom). Values are shown as mean ± SEM. *p<0.05, **p<0.01, ***p<0.001, ****p<0.0001.

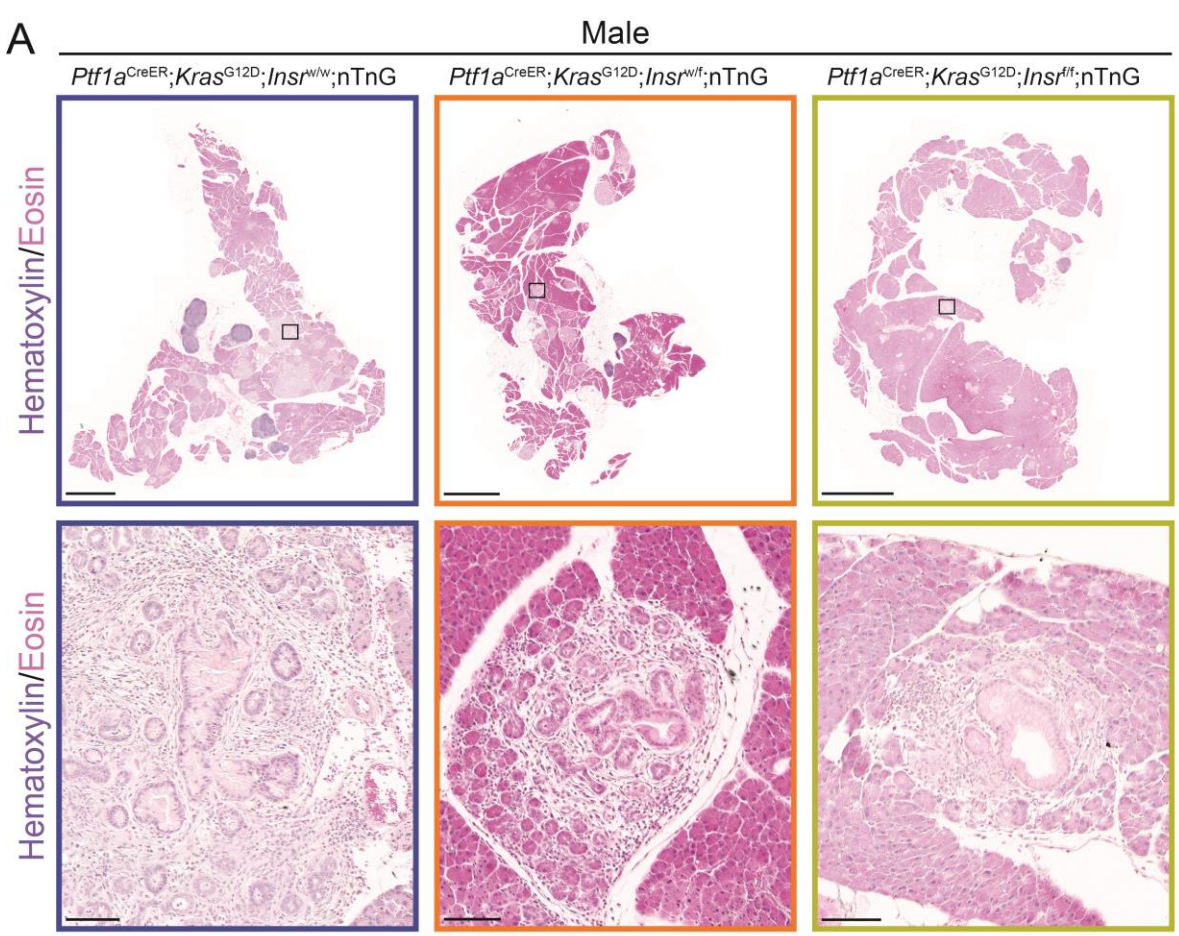
A
Male
Ptf1a^CreER;Kras^G12D;Insr^w/w;nTnG
Ptf1a^CreER;Kras^G12D;Insr^w/f;nTnG
Ptf1a^CreER;Kras^G12D;Insr^f/f;nTnG
Hematoxylin/Eosin
Hematoxylin/Eosin

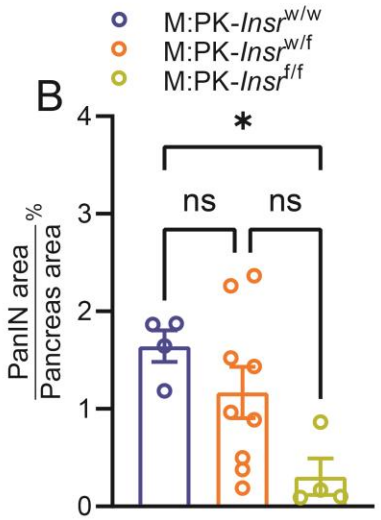
B
M:PK-Insr^w/w
M:PK-Insr^w/f
M:PK-Insr^f/f
*
ns
ns
PanIN area / Pancreas area %
0
1
2
3
4

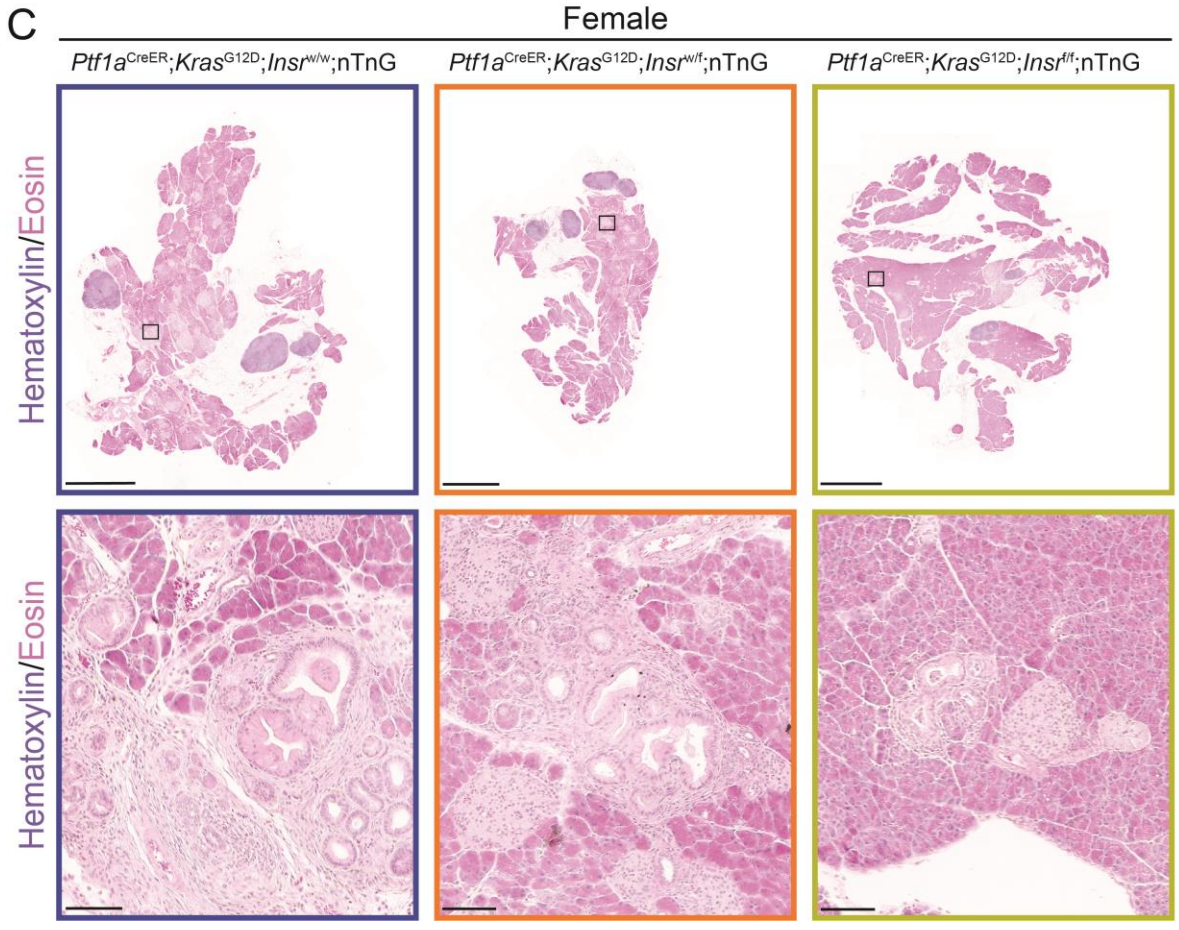
C
Female
Ptf1a^CreER;Kras^G12D;Insr^w/w;nTnG
Ptf1a^CreER;Kras^G12D;Insr^w/f;nTnG
Ptf1a^CreER;Kras^G12D;Insr^f/f;nTnG
Hematoxylin/Eosin
Hematoxylin/Eosin

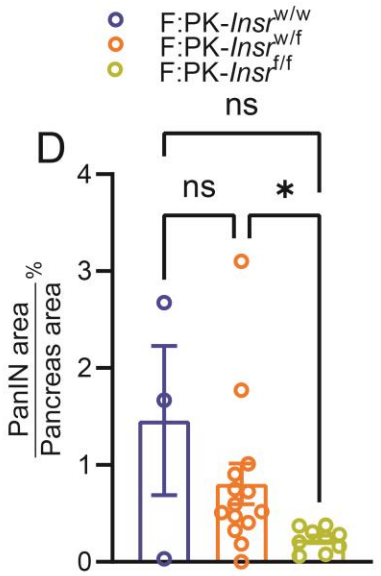
F:PK-Insr^w/w
F:PK-Insr^w/f
F:PK-Insr^f/f
D
ns
ns
*
PanIN area / Pancreas area %
0
1
2
3
4

Figure 5.8. Loss of *Insr* in acinar cells reduced PanIN lesions initiation.
A, Representative whole section (top) and high-magnification (bottom) images of pancreatic slides from PK-*Insr*$^{w/w}$, PK-*Insr*$^{w/f}$, and PK-*Insr*$^{f/f}$ male mice stained with H&E. **B,** Quantification of PanIN area in male mice from each genotype (n= 4-9). **C,** Representative whole section (top) and high-magnification (bottom) images of pancreatic slides from PK-*Insr*$^{w/w}$, PK-*Insr*$^{w/f}$, and PK-*Insr*$^{f/f}$ female mice stained with H&E. **D,** Quantification of PanIN area in female mice from each genotype (n= 3-14). Scale bars: 2 mm (top) and 0.1mm (bottom). Values are shown as mean ± SEM. *$p<0.05$

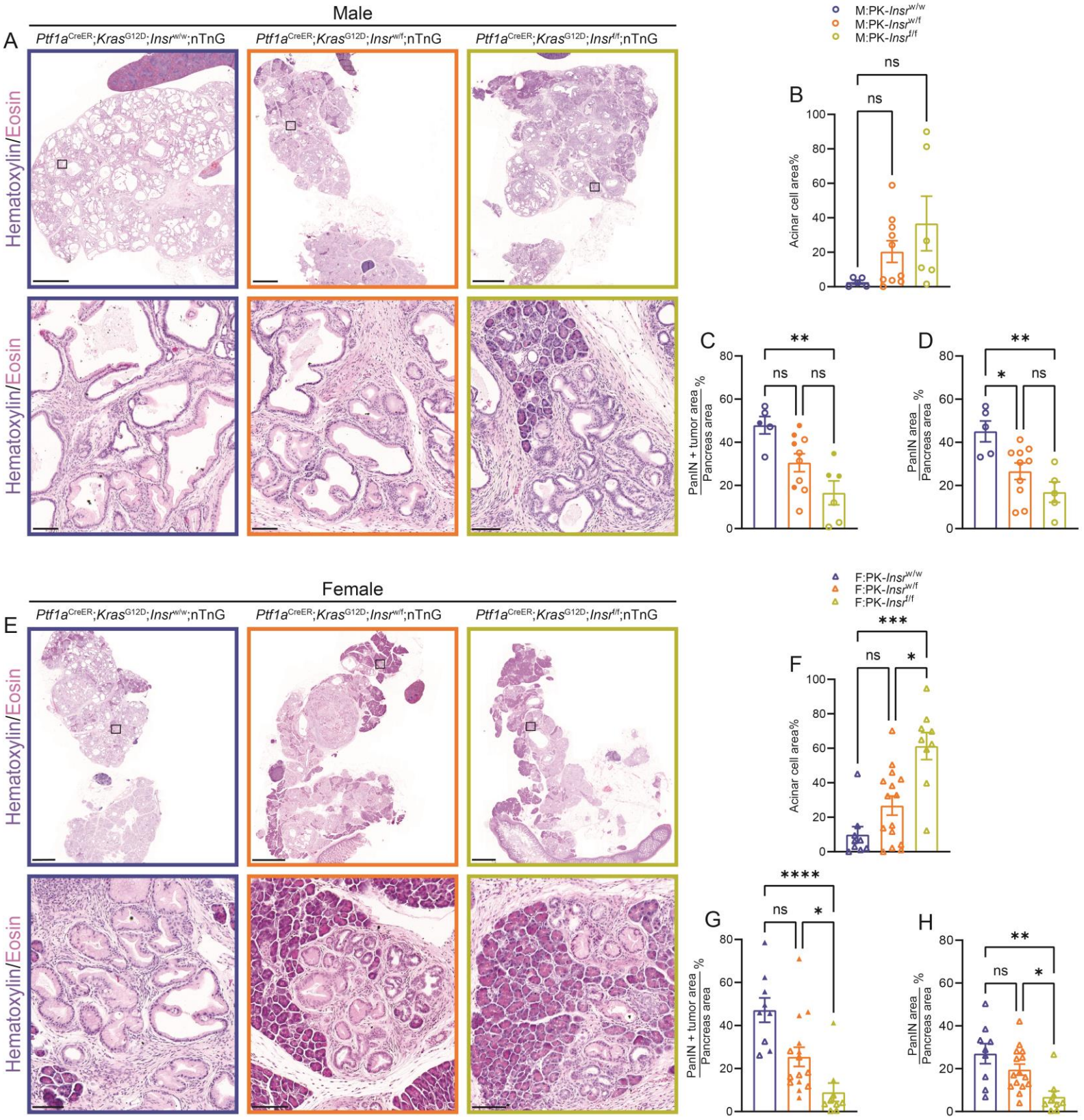

Figure 5.9. Loss of *Insr* in acinar cells reduced PanIN lesions formation.
A, Representative whole section (top) and high-magnification (bottom) images of pancreatic slides from PK-*Insr*$^{w/w}$, PK-*Insr*$^{w/f}$, and PK-*Insr*$^{f/f}$ male mice (10 months) stained with H&E. **B-D,** Quantification of acinar cell area (**B**), PanIN plus tumor area (**C**), and only PanIN area (**D**) in male mice (10 months) from each genotype (n= 5-10). Filled dots denote mice that developed

tumors in **C**. **E,** Representative whole section (top) and high-magnification (bottom) images of pancreatic slides from PK-*Insr*$^{w/w}$, PK-*Insr*$^{w/f}$, and PK-*Insr*$^{f/f}$ female mice (10 months) stained with H&E. **F-H,** Quantification of acinar cell area (**F**), PanIN plus tumor area (**G**), and only PanIN area (**H**) in female mice (10 months) from each genotype (n= 8-16). Filled triangles denote mice that developed tumors in **G**. Scale bars: 2 mm (top) and 0.1mm (bottom). Values are shown as mean ± SEM. *p<0.05, **p<0.01, ***p<0.001, ****p<0.0001.

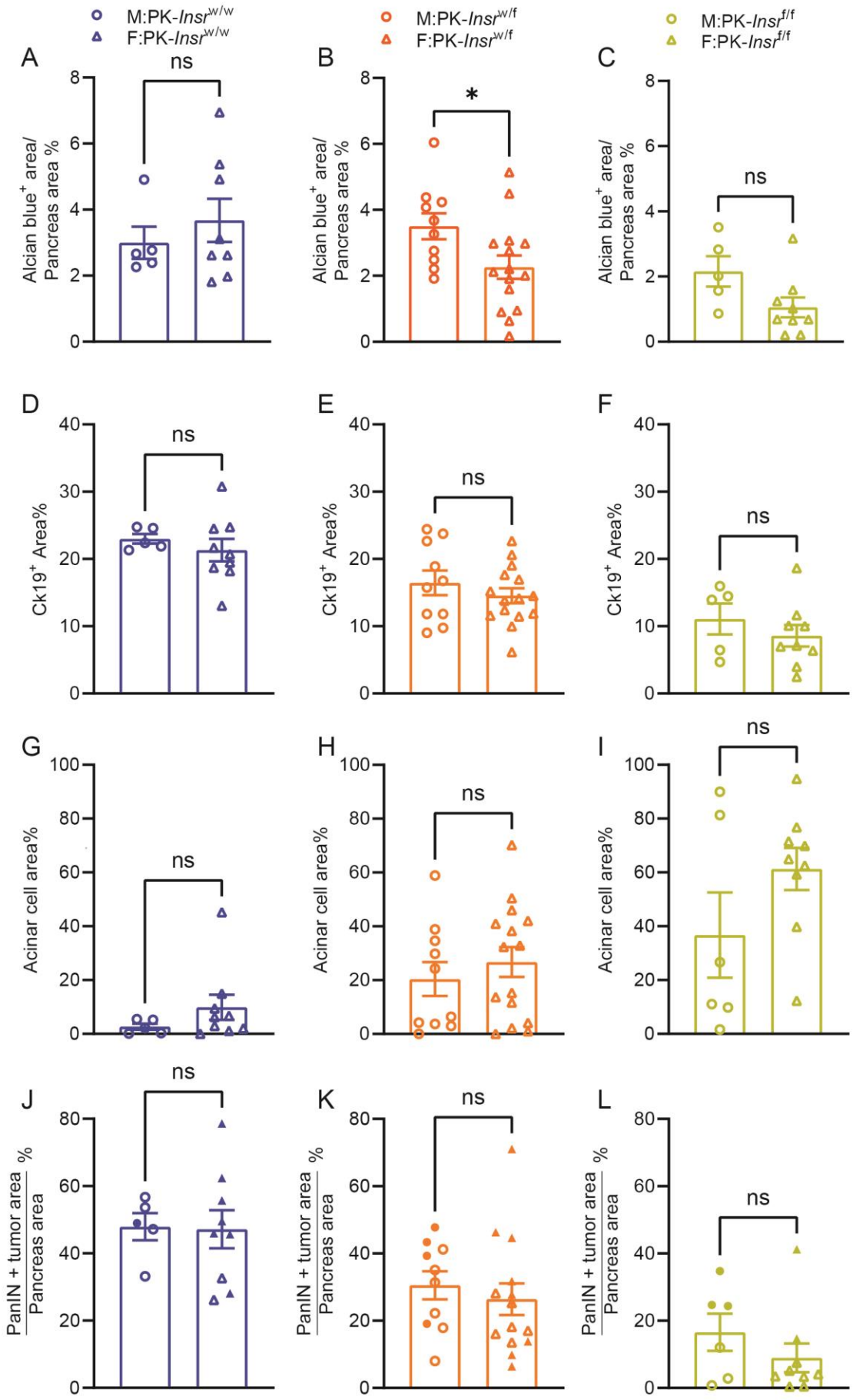
M:PK-Insr w/w
F:PK-Insr w/w
M:PK-Insr w/f
F:PK-Insr w/f
M:PK-Insr f/f
F:PK-Insr f/f
A
B
C
D
E
F
G
H
I
J
K
L
ns
*
Alcian blue+ area/ Pancreas area %
Ck19+ Area%
Acinar cell area%
PanIN + tumor area / Pancreas area %

Figure 5.10. The comparison in multiple histopathological measurements between male and female mice.

A-C, Comparison of Alcian blue^{+} area between male and female PK-*Insr*$^{w/w}$ (**A**), PK-*Insr*$^{w/f}$ (**B**), or PK-*Insr*$^{f/f}$ (**C**) mice (n= 5-15). **D-F,** The comparison of CK19^{+} area between male and female PK-*Insr*$^{w/w}$ (**D**), PK-*Insr*$^{w/f}$ (**E**), or PK-*Insr*$^{f/f}$ (**F**) mice (n= 5-15). **G-I,** Comparison of acinar cell area between male and female PK-*Insr*$^{w/w}$ (**G**), PK-*Insr*$^{w/f}$ (**H**), or PK-*Insr*$^{f/f}$ (**I**) mice (n= 5-15). **J-L,** Comparison of pancreatic area occupied by PanIN plus tumor between male and female PK-*Insr*$^{w/w}$ (**G**), PK-*Insr*$^{w/f}$ (**H**), or PK-*Insr*$^{f/f}$ (**I**) mice (n= 5-15). Filled dots and triangles denote mice that developed tumors. Values are shown as mean ± SEM. *$p<0.05$.

Chapter 6: Discussion and conclusion

6.1 Summary and overall discussion

This doctoral dissertation was to understand whether and how hyperinsulinemia and insulin/insulin receptor contributes to pancreatic cancer initiation and development. By manipulating the *Ins1* and *Ins2* gene alleles, we found mice with reduced insulin production had reduced PanIN lesions and fibrogenesis. Via scRNA-seq, we found that hyperinsulinemia might indirectly affect PanIN development through modulating the immune cells in the PanIN microenvironment and the PI3K/AKT/mTOR and MAPK/ERK signaling pathways were downregulated in mice with reduced insulin production. We also found hyperinsulinemia can promote PanIN formation directly through insulin receptor in acinar cells using a mouse model with *Insr* deleted in $Kras^{G12D}$ expressing acinar cells. These are the first *in vivo* studies to directly demonstrate that limiting the increases in circulating insulin induced by high-fat diet via genetic means or reducing the signaling through the INSR can reduce precursor lesion development in any type of cancers. Therefore, our work suggests that strategies that lowering insulin levels (like lifestyle changes) and targeting insulin receptor signaling pathways (like PI3K inhibitors) may be useful in preventing and treating pancreatic cancer in some contexts.

Hyperinsulinemia has been proposed as one of the potential factors connecting T2D and obesity to increased cancer risk; however, there are very limited studies investigating insulin-cancer relationship. Because diet and obesity-induced hyperinsulinemia is usually accompanied by other metabolic disorders like hyperglycemia, dyslipidemia, and altered adipokines, the LeRoith group developed a mouse model, which was called MKR mice, developed hyperinsulinemia without hyperglycemia or dyslipidemia (279). The hyperinsulinemia was induced by muscle insulin resistance which was caused by overexpressing a dominant-negative

IGF1R specifically in skeletal muscle (280). They found MKR mice had more severe progression of breast cancer, melanoma, and oesophageal adenocarcinoma, as well as increased lung metastases (216,280-284). They also showed that pharmacological blockade of PI3K or IR/IGF-IR signaling by a small-molecule tyrosine kinase inhibitor can cause a reduction in breast cancer growth in MKR mice (280,285,286). Using the MKR mouse model, other investigators showed that hyperinsulinemia was associated with an acceleration of the development of various types of cancers (216,280-284); however, there was no direct knockout experiment to show that knocking out insulin gene could reduce cancer development. Moreover, they did not show the relationship between hyperinsulinemia and pancreatic cancer, which is one of the cancers with the strongest association to hyperinsulinemia (60). My study showed that irrespective of the insulin gene used to reduce circulating insulin in mice, the mice with lower fasting insulin levels had lower PanIN lesions (74,235). The fasting insulin level at endpoint significantly correlated with the PanIN plus tumor area in the pancreas for female mice (Figure 3.3A&Figure 4.3H). Also, compared to female mice with two alleles of both *Ins1* and *Ins2*, there was about a 2-fold reduction in PanIN plus tumor area in female mice with only one or two alleles of *Ins1*. This suggests that solely knocking out two copies of the insulin gene in mice fed a high-fat diet was sufficient to reduce PanIN development. Together with the MKR mouse model studies, our studies using multiple mouse models strongly suggest that hyperinsulinemia, in the absence of hyperglycemia, contributes to cancer development.

Several studies have demonstrated that HFD can predispose mice expressing the *Kras*^{G12D} mutation in the pancreas to accelerate PanIN and PDAC development (70-72,287). In some of these studies, investigators showed that it was increased inflammation and desmoplasia that linked obesity to PanIN promotion. For instance, Incio *et al* showed that pancreatic stellate cells

secreted IL1β that recruited tumor-associated neutrophils, and the inactivation of pancreatic stellate cells by inhibiting angiotensin II type-1 receptor and IL1β inhibition by antibody neutralization could prevent obesity-promoted tumor growth (70). Moreover, Khasawneh *et al* showed that blocking of TNFα signaling could reduce HFD-mediated enhancement of PanIN formation (287). These findings support the proposed idea that increased inflammation underlies the risk of developing PDAC in obese individuals (63). However, in all these studies using HFD to induce obesity, the mice not only had increased inflammation, but also developed hyperinsulinemia, hyperglycemia, hyperlipidemia, and elevated IGF-1. Because complex metabolic and inflammatory cytokine alterations are induced by HFD, it is difficult to rule out whether other tumor-promoting factors (like hyperinsulinemia) also play a role in accelerating PDAC in these studies. By only deleting the insulin genes, we showed that PanIN lesions were reduced in mice with reduced insulin production which suggested that HFD-induced hyperinsulinemia is also one of the factors mediating HFD-promoted PanIN development. Moreover, through scRNA-seq, we showed that the immune cell composition (like increased NK cell number) and immune cells transcriptomes in the ductal metaplasia and PanIN microenvironment were significantly altered between mice with and without hyperinsulinemia. Therefore, it is also possible that hyperinsulinemia is upstream of the inflammation examined in the studies of Incio and Khasawneh *et al*.

Hyperglycemia is another factor that is proposed to connect obesity and T2D to cancer risk (63). However, based on our results, PanIN lesions were decreased in mice with reduced hyperinsulinemia regardless of the fasting glucose levels and this indicates that glucose does not affect pancreatic cancer progression. Therefore, our studies suggest it is hyperinsulinemia but not hyperglycemia that contributes to pancreatic cancer. Future studies aimed at assessing the effect

of glucose levels on PanIN lesions can be conducted to directly test the role of hyperglycemia on PDAC.

In addition to HFD, investigators also used leptin-deficient *ob/ob* mice model to investigate the mechanism of obesity-driven pancreatic tumorigenesis (73). Nevertheless, *ob/ob* mice lack leptin and leptin may play an important role during tumorigenesis as well (76). Meanwhile, individuals with obesity usually have elevated leptin levels compared with normal-weight individuals. Therefore, it will be interesting to check if β cells also express CCK in HFD-induced obesity and to investigate if leptin itself can affect pancreatic tumorigenesis. In sum, as shown by various studies, the mechanism of HFD- (or obesity-) promoted pancreatic cancer progression is complex and no sole molecular factor is independently and completely responsible for the acceleration.

For all of the mouse models developed and characterized in my studies, we observed sex differences in glucose metabolism. For example, as previously reported, male mice could not survive with only one copy of *Ins1* gene but female mice could (53,74). Male mice also tended to develop fewer PanIN lesions than female mice in insulin gene knockout experiments, while males tended to develop more PanIN lesions than females when the *Insr* is knocked out of acinar cells in an *insulin* gene wild-type background. This phenotype is consistent with the well-known sex differences that are observed in almost all animal models. Specifically, males are more likely to become insulin resistant, and more likely to develop obesity and T2D (112,120-122,288,289). Clinical and experimental studies have suggested that endogenous estrogens protect females from insulin resistance (288). Studies showed that sex hormones were responsible for the differences in insulin sensitivity. For example, estrogen replacement in ovariectomized wild-type mice can improve insulin sensitivity (290,291). Androgens also have sex-dependent actions as

androgen deficiency in men causes insulin resistance, while androgen excess in women causes insulin resistance (289,292,293). Therefore, future studies exploring the specific molecular differences between male and female mice from our mouse models would be of value to understanding how sex hormones and biological sex-determinant factors contribute to PDAC development. Also, future studies should analyze and report results from male and female mice separately when exploring the insulin or glucose metabolism' effects on pancreatic cancer initiation and development.

6.2 Limitations

Although my studies showed insulin and local insulin signaling can contribute to pancreatic cancer initiation through various mouse models, there are some limitations of these studies. For example, except for my *Insr* knockout mouse model, a lineage reporter allele for the mouse models used in the first two studies was not included. As a result, I could not assess whether the recombination efficiency at the KRAS allele was similar between the genotypes, which could subsequently affect the amount of PanIN lesions. Our studies also have limited insight into how hyperinsulinemia and INSR signaling affect mice survival and metastasis. Future studies could perform survival analysis (like Kaplan–Meier curve) to investigate if there is a difference in survival rate, tumor number, tumor size, or metastasis when insulin/insulin receptor signaling is manipulated.

Because all of our animal models were fed with a high-fat diet throughout the study, we do not know if inhibition of hyperinsulinemia or INSR signaling can also reduce PanIN formation without HFD-induced obesity. If time and funding are allowed, it would be interesting to generate another cohort of mice from each genotype fed CD or HFD. By comparing the mice

from different genotypes and diet groups, we could assess whether hyperinsulinemia and INSR signaling could completely diminish the HFD-accelerated PanIN formation. For instance, we can check that in the HFD group, if the mice with reduced insulin production have a similar amount of PanIN lesions as the mice in the CD group.

For the mice with *Ins1*-null genetic background, we observed only about 1-4% of their pancreata was occupied by PanIN lesions and we also observed ~50% of their pancreata was replaced by adipocytes. We don't know when this adipocytes replacement occurred, and it is possible that it happens early enough that *Kras*^{G12D} expressing acinar cells are replaced by fat before they have a chance to transform into PanIN cells. If lineage reporter allele was incorporated, we could test whether lineage-labeled Kras^{G12D}-expressing acinar cells are selectively eliminated in this mouse model, potentially suggesting that KRAS^{G12D} affects the survival of acinar cells in high fat diet, low insulin conditions. In addition, the source of the adipocytes is also unknown, and incorporating the lineage label could help delineate whether adipocytes were arising from *Kras*^{G12D} expressing acinar cells. As we suggested above, the adipocyte replacement was possibly caused by the combined effects of loss of the *Ins1* gene, HFD, and *Kras*^{G12D} mutation. Future studies to measure the fat area in CD- and HFD-fed *Ins1* null mice with and without KRAS mutations may extend our understanding of this phenotype.

Lastly, our studies could not examine how acinar cells and PanIN cells' transcriptomes were altered by hyperinsulinemia and INSR signaling. We performed single-cell RNA-sequencing on PK-*Ins1*$^{-/-}$;*Ins2*$^{+/+}$ and PK-*Ins1*$^{-/-}$;*Ins2*$^{+/-}$ mice and performed single nucleus RNA-sequencing on PK-*Insr*$^{w/w}$, PK-*Insr*$^{w/f}$, and PK-*Insr*$^{f/f}$ mice. However, despite our diligent attempts to optimize the protocol for these experiments, we could not isolate a large number of high-quality, healthy, single acinar cells. Acinar cells are full of digestive enzymes and RNAse and the majority of the

acinar cells are lysed during the dissociation process. As a result, we could not investigate the specific molecular mechanisms of how hyperinsulinemia and INSR signaling regulate acinar cells or PanIN cells themselves.

6.3 Future directions

For my thesis investigations, we only studied the effects of hyperinsulinemia and insulin receptor in an acinar-cell-derived PDAC mouse model. However, many previous studies have shown the importance of cells of origin in PDAC (10,43). For instance, Lee *et al* showed that acinar-cell-derived PDAC and ductal-cell-derived PDAC have different precursor lesion initiation, disease progression, and tumor phenotype (10). Thus, future experiments should investigate whether inhibition of hyperinsulinemia and INSR signaling can also reduce PanIN progression in a *Sox9Cre*;*Kras*^{G12D} mouse model, which expresses *Kras*^{G12D} in ductal cells. Future studies should also investigate if hyperinsulinemia and INSR signaling can affect other types of PDAC precursor lesion development, like IPMN and MCN, using mouse models described in (9,294).

Furthermore, investigators have also proposed metabolic subtypes of PDAC based on their transcriptomes. For instance, Moffitt *et al*. identified 2 PDAC subtypes: classical and basal-like subtypes and Bailey *et al*. identified four subtypes: squamous, pancreatic progenitor, immunogenic, and aberrantly differentiated endocrine exocrine (295,296). Karasinska *et al*. also stratified PDAC into four metabolic subgroups based on expression of glycolytic and cholesterogenic genes: quiescent, glycolytic, cholesterogenic, and mixed (297). These tumor subtypes were associated with different patient survival rate and sensitivity to chemotherapies.

Therefore, it will be interesting to examine whether hyperinsulinemia and INSR signaling have similar effects on these tumor subtypes.

Lastly, the findings from this study should be tested and validated in clinical studies. Some patients that are diagnosed with PDAC also have diabetes, but oncologists generally do not manage their glucose homeostasis, as PDAC is more life-threatening. Therefore, we are collaborating with Dr. Daniel Renouf's group to see if managing the PDAC patients' diabetes can improve their PDAC treatment outcome. We are also generating patient-derived organoids to see if insulin and INSR signaling influences their growth to examine how these factors affect PDAC tumorigenesis after the epithelium is already transformed.

During my doctoral studies, I investigated whether hyperinsulinemia and INSR signaling affect pancreatic cancer development. My data showed that endogenous hyperinsulinemia contributed to pancreatic cancer development through indirectly regulating the immune cells and fibroblasts in the PanIN microenvironment, as well as through directly INSR signaling in the acinar cells. This thesis contributes to the body evidence that demonstrates hyperinsulinemia is a factor linking obesity and T2D to excess PDAC risk and my studies provide useful mouse models and scRNA-seq dataset for future studies. PDAC is one of the most lethal cancers with a 5-year survival rate of less than 10% and there is less funding available in the PDAC field. Hopefully, continued research in the PDAC field will ultimately lead to better interventions for this lethal cancer and better diagnostic tools to detect it at an early stage.

References

1. Canadian Cancer Statistics Advisory Committee in collaboration with the Canadian Cancer Society SCatPHAoC. Canadian Cancer Statistics. 2021;

2. Rahib L, Smith BD, Aizenberg R, Rosenzweig AB, Fleshman JM, Matrisian LM. Projecting cancer incidence and deaths to 2030: the unexpected burden of thyroid, liver, and pancreas cancers in the United States. Cancer Res 2014; 74:2913-2921

3. Kleeff J, Korc M, Apte M, La Vecchia C, Johnson CD, Biankin AV, Neale RE, Tempero M, Tuveson DA, Hruban RH, Neoptolemos JP. Pancreatic cancer. Nat Rev Dis Primers 2016; 2:16022

4. Bardeesy N, DePinho RA. Pancreatic cancer biology and genetics. Nat Rev Cancer 2002; 2:897-909

5. Walter F. Boron ELB. Medical Physiology. 3rd edition ed: Elsevier Canada.

6. Luchini C, Capelli P, Scarpa A. Pancreatic Ductal Adenocarcinoma and Its Variants. Surg Pathol Clin 2016; 9:547-560

7. Basturk O, Hong SM, Wood LD, Adsay NV, Albores-Saavedra J, Biankin AV, Brosens LA, Fukushima N, Goggins M, Hruban RH, Kato Y, Klimstra DS, Kloppel G, Krasinskas A, Longnecker DS, Matthaei H, Offerhaus GJ, Shimizu M, Takaori K, Terris B, Yachida S, Esposito I, Furukawa T, Baltimore Consensus M. A Revised Classification System and Recommendations From the Baltimore Consensus Meeting for Neoplastic Precursor Lesions in the Pancreas. Am J Surg Pathol 2015; 39:1730-1741

8. Collisson EA, Bailey P, Chang DK, Biankin AV. Molecular subtypes of pancreatic cancer. Nat Rev Gastroenterol Hepatol 2019; 16:207-220

9. Kopp JL, Dubois CL, Schaeffer DF, Samani A, Taghizadeh F, Cowan RW, Rhim AD, Stiles BL, Valasek M, Sander M. Loss of Pten and Activation of Kras Synergistically Induce Formation of Intraductal Papillary Mucinous Neoplasia From Pancreatic Ductal Cells in Mice. Gastroenterology 2018; 154:1509-1523 e1505

10. Lee AYL, Dubois CL, Sarai K, Zarei S, Schaeffer DF, Sander M, Kopp JL. Cell of origin affects tumour development and phenotype in pancreatic ductal adenocarcinoma. Gut 2019; 68:487-498

11. Pantsar T. The current understanding of KRAS protein structure and dynamics. Comput Struct Biotechnol J 2020; 18:189-198

12. Vatansever S, Erman B, Gumus ZH. Oncogenic G12D mutation alters local conformations and dynamics of K-Ras. Sci Rep 2019; 9:11730

13. Ji B, Tsou L, Wang H, Gaiser S, Chang DZ, Daniluk J, Bi Y, Grote T, Longnecker DS, Logsdon CD. Ras activity levels control the development of pancreatic diseases. Gastroenterology 2009; 137:1072-1082, 1082 e1071-1076

14. Cannon A, Thompson C, Hall BR, Jain M, Kumar S, Batra SK. Desmoplasia in pancreatic ductal adenocarcinoma: insight into pathological function and therapeutic potential. Genes Cancer 2018; 9:78-86

15. Thomas D, Radhakrishnan P. Tumor-stromal crosstalk in pancreatic cancer and tissue fibrosis. Mol Cancer 2019; 18:14

16. Ozdemir BC, Pentcheva-Hoang T, Carstens JL, Zheng X, Wu CC, Simpson TR, Laklai H, Sugimoto H, Kahlert C, Novitskiy SV, De Jesus-Acosta A, Sharma P, Heidari P, Mahmood U, Chin L, Moses HL, Weaver VM, Maitra A, Allison JP, LeBleu VS, Kalluri

R. Depletion of carcinoma-associated fibroblasts and fibrosis induces immunosuppression and accelerates pancreas cancer with reduced survival. Cancer Cell 2014; 25:719-734

17. Haqq J, Howells LM, Garcea G, Metcalfe MS, Steward WP, Dennison AR. Pancreatic stellate cells and pancreas cancer: current perspectives and future strategies. Eur J Cancer 2014; 50:2570-2582

18. Helms E, Onate MK, Sherman MH. Fibroblast Heterogeneity in the Pancreatic Tumor Microenvironment. Cancer Discov 2020; 10:648-656

19. Vonlaufen A, Joshi S, Qu C, Phillips PA, Xu Z, Parker NR, Toi CS, Pirola RC, Wilson JS, Goldstein D, Apte MV. Pancreatic stellate cells: partners in crime with pancreatic cancer cells. Cancer Res 2008; 68:2085-2093

20. Rhim AD, Oberstein PE, Thomas DH, Mirek ET, Palermo CF, Sastra SA, Dekleva EN, Saunders T, Becerra CP, Tattersall IW, Westphalen CB, Kitajewski J, Fernandez-Barrena MG, Fernandez-Zapico ME, Iacobuzio-Donahue C, Olive KP, Stanger BZ. Stromal elements act to restrain, rather than support, pancreatic ductal adenocarcinoma. Cancer Cell 2014; 25:735-747

21. Lee JJ, Perera RM, Wang H, Wu DC, Liu XS, Han S, Fitamant J, Jones PD, Ghanta KS, Kawano S, Nagle JM, Deshpande V, Boucher Y, Kato T, Chen JK, Willmann JK, Bardeesy N, Beachy PA. Stromal response to Hedgehog signaling restrains pancreatic cancer progression. Proc Natl Acad Sci U S A 2014; 111:E3091-3100

22. Karamitopoulou E. Tumour microenvironment of pancreatic cancer: immune landscape is dictated by molecular and histopathological features. Br J Cancer 2019; 121:5-14

23. Huber M, Brehm CU, Gress TM, Buchholz M, Alashkar Alhamwe B, von Strandmann EP, Slater EP, Bartsch JW, Bauer C, Lauth M. The Immune Microenvironment in Pancreatic Cancer. Int J Mol Sci 2020; 21

24. Nywening TM, Belt BA, Cullinan DR, Panni RZ, Han BJ, Sanford DE, Jacobs RC, Ye J, Patel AA, Gillanders WE, Fields RC, DeNardo DG, Hawkins WG, Goedegebuure P, Linehan DC. Targeting both tumour-associated CXCR2(+) neutrophils and CCR2(+) macrophages disrupts myeloid recruitment and improves chemotherapeutic responses in pancreatic ductal adenocarcinoma. Gut 2018; 67:1112-1123

25. Liou GY, Doppler H, Necela B, Edenfield B, Zhang L, Dawson DW, Storz P. Mutant KRAS-induced expression of ICAM-1 in pancreatic acinar cells causes attraction of macrophages to expedite the formation of precancerous lesions. Cancer Discov 2015; 5:52-63

26. Griesmann H, Drexel C, Milosevic N, Sipos B, Rosendahl J, Gress TM, Michl P. Pharmacological macrophage inhibition decreases metastasis formation in a genetic model of pancreatic cancer. Gut 2017; 66:1278-1285

27. Nielsen SR, Quaranta V, Linford A, Emeagi P, Rainer C, Santos A, Ireland L, Sakai T, Sakai K, Kim YS, Engle D, Campbell F, Palmer D, Ko JH, Tuveson DA, Hirsch E, Mielgo A, Schmid MC. Macrophage-secreted granulin supports pancreatic cancer metastasis by inducing liver fibrosis. Nat Cell Biol 2016; 18:549-560

28. Davis M, Conlon K, Bohac GC, Barcenas J, Leslie W, Watkins L, Lamzabi I, Deng Y, Li Y, Plate JM. Effect of pemetrexed on innate immune killer cells and adaptive immune T cells in subjects with adenocarcinoma of the pancreas. J Immunother 2012; 35:629-640

29. Lim SA, Kim J, Jeon S, Shin MH, Kwon J, Kim TJ, Im K, Han Y, Kwon W, Kim SW, Yee C, Kim SJ, Jang JY, Lee KM. Defective Localization With Impaired Tumor Cytotoxicity Contributes to the Immune Escape of NK Cells in Pancreatic Cancer Patients. Front Immunol 2019; 10:496
30. Piro G, Simionato F, Carbone C, Frizziero M, Malleo G, Zanini S, Casolino R, Santoro R, Mina MM, Zecchetto C, Merz V, Scarpa A, Bassi C, Tortora G, Melisi D. A circulating TH2 cytokines profile predicts survival in patients with resectable pancreatic adenocarcinoma. Oncoimmunology 2017; 6:e1322242
31. Balli D, Rech AJ, Stanger BZ, Vonderheide RH. Immune Cytolytic Activity Stratifies Molecular Subsets of Human Pancreatic Cancer. Clin Cancer Res 2017; 23:3129-3138
32. Carstens JL, Correa de Sampaio P, Yang D, Barua S, Wang H, Rao A, Allison JP, LeBleu VS, Kalluri R. Spatial computation of intratumoral T cells correlates with survival of patients with pancreatic cancer. Nat Commun 2017; 8:15095
33. Liyanage UK, Moore TT, Joo HG, Tanaka Y, Herrmann V, Doherty G, Drebin JA, Strasberg SM, Eberlein TJ, Goedegebuure PS, Linehan DC. Prevalence of regulatory T cells is increased in peripheral blood and tumor microenvironment of patients with pancreas or breast adenocarcinoma. J Immunol 2002; 169:2756-2761
34. Jang JE, Hajdu CH, Liot C, Miller G, Dustin ML, Bar-Sagi D. Crosstalk between Regulatory T Cells and Tumor-Associated Dendritic Cells Negates Anti-tumor Immunity in Pancreatic Cancer. Cell Rep 2017; 20:558-571
35. Zhang Y, Lazarus J, Steele NG, Yan W, Lee HJ, Nwosu ZC, Halbrook CJ, Menjivar RE, Kemp SB, Sirihorachai VR, Velez-Delgado A, Donahue K, Carpenter ES, Brown KL, Irizarry-Negron V, Nevison AC, Vinta A, Anderson MA, Crawford HC, Lyssiotis CA, Frankel TL, Bednar F, Pasca di Magliano M. Regulatory T-cell Depletion Alters the Tumor Microenvironment and Accelerates Pancreatic Carcinogenesis. Cancer Discov 2020; 10:422-439
36. Coussens LM, Werb Z. Inflammation and cancer. Nature 2002; 420:860-867
37. Singh N, Baby D, Rajguru JP, Patil PB, Thakkannavar SS, Pujari VB. Inflammation and cancer. Ann Afr Med 2019; 18:121-126
38. Greten FR, Grivennikov SI. Inflammation and Cancer: Triggers, Mechanisms, and Consequences. Immunity 2019; 51:27-41
39. Hausmann S, Kong B, Michalski C, Erkan M, Friess H. The role of inflammation in pancreatic cancer. Adv Exp Med Biol 2014; 816:129-151
40. Shadhu K, Xi C. Inflammation and pancreatic cancer: An updated review. Saudi J Gastroenterol 2019; 25:3-13
41. Herreros-Villanueva M, Hijona E, Cosme A, Bujanda L. Mouse models of pancreatic cancer. World J Gastroenterol 2012; 18:1286-1294
42. Hingorani SR, Petricoin EF, Maitra A, Rajapakse V, King C, Jacobetz MA, Ross S, Conrads TP, Veenstra TD, Hitt BA, Kawaguchi Y, Johann D, Liotta LA, Crawford HC, Putt ME, Jacks T, Wright CV, Hruban RH, Lowy AM, Tuveson DA. Preinvasive and invasive ductal pancreatic cancer and its early detection in the mouse. Cancer Cell 2003; 4:437-450
43. Kopp JL, von Figura G, Mayes E, Liu FF, Dubois CL, Morris JPt, Pan FC, Akiyama H, Wright CV, Jensen K, Hebrok M, Sander M. Identification of Sox9-dependent acinar-to-

ductal reprogramming as the principal mechanism for initiation of pancreatic ductal adenocarcinoma. Cancer Cell 2012; 22:737-750
44. Feil S, Valtcheva N, Feil R. Inducible Cre mice. Methods Mol Biol 2009; 530:343-363
45. Hingorani SR, Wang L, Multani AS, Combs C, Deramaudt TB, Hruban RH, Rustgi AK, Chang S, Tuveson DA. Trp53R172H and KrasG12D cooperate to promote chromosomal instability and widely metastatic pancreatic ductal adenocarcinoma in mice. Cancer Cell 2005; 7:469-483
46. Yadav D, Lowenfels AB. The epidemiology of pancreatitis and pancreatic cancer. Gastroenterology 2013; 144:1252-1261
47. Ilic M, Ilic I. Epidemiology of pancreatic cancer. World J Gastroenterol 2016; 22:9694-9705
48. Raimondi S, Lowenfels AB, Morselli-Labate AM, Maisonneuve P, Pezzilli R. Pancreatic cancer in chronic pancreatitis; aetiology, incidence, and early detection. Best Pract Res Clin Gastroenterol 2010; 24:349-358
49. Bosetti C, Lucenteforte E, Silverman DT, Petersen G, Bracci PM, Ji BT, Negri E, Li D, Risch HA, Olson SH, Gallinger S, Miller AB, Bueno-de-Mesquita HB, Talamini R, Polesel J, Ghadirian P, Baghurst PA, Zatonski W, Fontham E, Bamlet WR, Holly EA, Bertuccio P, Gao YT, Hassan M, Yu H, Kurtz RC, Cotterchio M, Su J, Maisonneuve P, Duell EJ, Boffetta P, La Vecchia C. Cigarette smoking and pancreatic cancer: an analysis from the International Pancreatic Cancer Case-Control Consortium (Panc4). Ann Oncol 2012; 23:1880-1888
50. Genkinger JM, Spiegelman D, Anderson KE, Bernstein L, van den Brandt PA, Calle EE, English DR, Folsom AR, Freudenheim JL, Fuchs CS, Giles GG, Giovannucci E, Horn-Ross PL, Larsson SC, Leitzmann M, Mannisto S, Marshall JR, Miller AB, Patel AV, Rohan TE, Stolzenberg-Solomon RZ, Verhage BA, Virtamo J, Willcox BJ, Wolk A, Ziegler RG, Smith-Warner SA. A pooled analysis of 14 cohort studies of anthropometric factors and pancreatic cancer risk. Int J Cancer 2011; 129:1708-1717
51. Michaud DS, Giovannucci E, Willett WC, Colditz GA, Stampfer MJ, Fuchs CS. Physical activity, obesity, height, and the risk of pancreatic cancer. JAMA 2001; 286:921-929
52. Li D. Diabetes and pancreatic cancer. Mol Carcinog 2012; 51:64-74
53. Johnson JD. On the causal relationships between hyperinsulinaemia, insulin resistance, obesity and dysglycaemia in type 2 diabetes. Diabetologia 2021; 64:2138-2146
54. Hart PA, Bellin MD, Andersen DK, Bradley D, Cruz-Monserrate Z, Forsmark CE, Goodarzi MO, Habtezion A, Korc M, Kudva YC, Pandol SJ, Yadav D, Chari ST, Consortium for the Study of Chronic Pancreatitis D, Pancreatic C. Type 3c (pancreatogenic) diabetes mellitus secondary to chronic pancreatitis and pancreatic cancer. Lancet Gastroenterol Hepatol 2016; 1:226-237
55. Saeedi P, Petersohn I, Salpea P, Malanda B, Karuranga S, Unwin N, Colagiuri S, Guariguata L, Motala AA, Ogurtsova K, Shaw JE, Bright D, Williams R, Committee IDFDA. Global and regional diabetes prevalence estimates for 2019 and projections for 2030 and 2045: Results from the International Diabetes Federation Diabetes Atlas, 9(th) edition. Diabetes Res Clin Pract 2019; 157:107843
56. Organization WH. Diabetes. 2021; https://www.who.int/news-room/fact-sheets/detail/diabetes. Accessed Dec 6, 2021.

57. CANADA D. What is diabetes? 2021; https://www.diabetes.ca/about-diabetes/what-is-diabetes. Accessed Dec 6, 2021.
58. DeFronzo RA, Ferrannini E, Groop L, Henry RR, Herman WH, Holst JJ, Hu FB, Kahn CR, Raz I, Shulman GI, Simonson DC, Testa MA, Weiss R. Type 2 diabetes mellitus. Nat Rev Dis Primers 2015; 1:15019
59. Yaribeygi H, Farrokhi FR, Butler AE, Sahebkar A. Insulin resistance: Review of the underlying molecular mechanisms. J Cell Physiol 2019; 234:8152-8161
60. Pearson-Stuttard J, Papadimitriou N, Markozannes G, Cividini S, Kakourou A, Gill D, Rizos EC, Monori G, Ward HA, Kyrgiou M, Gunter MJ, Tsilidis KK. Type 2 Diabetes and Cancer: An Umbrella Review of Observational and Mendelian Randomization Studies. Cancer Epidemiol Biomarkers Prev 2021; 30:1218-1228
61. Suh S, Kim KW. Diabetes and Cancer: Cancer Should Be Screened in Routine Diabetes Assessment. Diabetes Metab J 2019; 43:733-743
62. Vigneri P, Frasca F, Sciacca L, Pandini G, Vigneri R. Diabetes and cancer. Endocr Relat Cancer 2009; 16:1103-1123
63. Gallagher EJ, LeRoith D. Obesity and Diabetes: The Increased Risk of Cancer and Cancer-Related Mortality. Physiol Rev 2015; 95:727-748
64. Campbell PT, Newton CC, Patel AV, Jacobs EJ, Gapstur SM. Diabetes and cause-specific mortality in a prospective cohort of one million U.S. adults. Diabetes Care 2012; 35:1835-1844
65. Organization WH. Obesity and overweight. 2021; https://www.who.int/news-room/fact-sheets/detail/obesity-and-overweight. Accessed Dec 6, 2021.
66. Calle EE, Rodriguez C, Walker-Thurmond K, Thun MJ. Overweight, obesity, and mortality from cancer in a prospectively studied cohort of U.S. adults. N Engl J Med 2003; 348:1625-1638
67. Adams TD, Stroup AM, Gress RE, Adams KF, Calle EE, Smith SC, Halverson RC, Simper SC, Hopkins PN, Hunt SC. Cancer incidence and mortality after gastric bypass surgery. Obesity (Silver Spring) 2009; 17:796-802
68. Christou NV, Lieberman M, Sampalis F, Sampalis JS. Bariatric surgery reduces cancer risk in morbidly obese patients. Surg Obes Relat Dis 2008; 4:691-695
69. Parker ED, Folsom AR. Intentional weight loss and incidence of obesity-related cancers: the Iowa Women's Health Study. Int J Obes Relat Metab Disord 2003; 27:1447-1452
70. Incio J, Liu H, Suboj P, Chin SM, Chen IX, Pinter M, Ng MR, Nia HT, Grahovac J, Kao S, Babykutty S, Huang Y, Jung K, Rahbari NN, Han X, Chauhan VP, Martin JD, Kahn J, Huang P, Desphande V, Michaelson J, Michelakos TP, Ferrone CR, Soares R, Boucher Y, Fukumura D, Jain RK. Obesity-Induced Inflammation and Desmoplasia Promote Pancreatic Cancer Progression and Resistance to Chemotherapy. Cancer Discov 2016; 6:852-869
71. Dawson DW, Hertzer K, Moro A, Donald G, Chang HH, Go VL, Pandol SJ, Lugea A, Gukovskaya AS, Li G, Hines OJ, Rozengurt E, Eibl G. High-fat, high-calorie diet promotes early pancreatic neoplasia in the conditional KrasG12D mouse model. Cancer Prev Res (Phila) 2013; 6:1064-1073
72. Chang HH, Moro A, Takakura K, Su HY, Mo A, Nakanishi M, Waldron RT, French SW, Dawson DW, Hines OJ, Li G, Go VLW, Sinnett-Smith J, Pandol SJ, Lugea A, Gukovskaya AS, Duff MO, Rosenberg DW, Rozengurt E, Eibl G. Incidence of pancreatic

cancer is dramatically increased by a high fat, high calorie diet in KrasG12D mice. PLoS One 2017; 12:e0184455

73. Chung KM, Singh J, Lawres L, Dorans KJ, Garcia C, Burkhardt DB, Robbins R, Bhutkar A, Cardone R, Zhao X, Babic A, Vayrynen SA, Dias Costa A, Nowak JA, Chang DT, Dunne RF, Hezel AF, Koong AC, Wilhelm JJ, Bellin MD, Nylander V, Gloyn AL, McCarthy MI, Kibbey RG, Krishnaswamy S, Wolpin BM, Jacks T, Fuchs CS, Muzumdar MD. Endocrine-Exocrine Signaling Drives Obesity-Associated Pancreatic Ductal Adenocarcinoma. Cell 2020; 181:832-847 e818

74. Zhang AMY, Magrill J, de Winter TJJ, Hu X, Skovso S, Schaeffer DF, Kopp JL, Johnson JD. Endogenous Hyperinsulinemia Contributes to Pancreatic Cancer Development. Cell Metab 2019; 30:403-404

75. Pearson-Stuttard J, Zhou B, Kontis V, Bentham J, Gunter MJ, Ezzati M. Worldwide burden of cancer attributable to diabetes and high body-mass index: a comparative risk assessment. Lancet Diabetes Endocrinol 2018; 6:e6-e15

76. Gallagher EJ, LeRoith D. Hyperinsulinaemia in cancer. Nat Rev Cancer 2020; 20:629-644

77. Scully T, Ettela A, LeRoith D, Gallagher EJ. Obesity, Type 2 Diabetes, and Cancer Risk. Front Oncol 2020; 10:615375

78. Liberti MV, Locasale JW. The Warburg Effect: How Does it Benefit Cancer Cells? Trends Biochem Sci 2016; 41:211-218

79. Vander Heiden MG, Cantley LC, Thompson CB. Understanding the Warburg effect: the metabolic requirements of cell proliferation. Science 2009; 324:1029-1033

80. Arcidiacono B, Iiritano S, Nocera A, Possidente K, Nevolo MT, Ventura V, Foti D, Chiefari E, Brunetti A. Insulin resistance and cancer risk: an overview of the pathogenetic mechanisms. Exp Diabetes Res 2012; 2012:789174

81. Shafie SM, Grantham FH. Role of hormones in the growth and regression of human breast cancer cells (MCF-7) transplanted into athymic nude mice. J Natl Cancer Inst 1981; 67:51-56

82. Cocca C, Martin G, Rivera E, Davio C, Cricco G, Lemos B, Fitzsimons C, Gutierrez A, Levin E, Levin R, Croci M, Bergoc RM. An experimental model of diabetes and cancer in rats. Eur J Cancer 1998; 34:889-894

83. Bell RH, Jr., McCullough PJ, Pour PM. Influence of diabetes on susceptibility to experimental pancreatic cancer. Am J Surg 1988; 155:159-164

84. Alikhani N, Ferguson RD, Novosyadlyy R, Gallagher EJ, Scheinman EJ, Yakar S, LeRoith D. Mammary tumor growth and pulmonary metastasis are enhanced in a hyperlipidemic mouse model. Oncogene 2013; 32:961-967

85. Zhuang L, Lin J, Lu ML, Solomon KR, Freeman MR. Cholesterol-rich lipid rafts mediate akt-regulated survival in prostate cancer cells. Cancer Res 2002; 62:2227-2231

86. Locke AE, Kahali B, Berndt SI, Justice AE, Pers TH, Day FR, Powell C, Vedantam S, Buchkovich ML, Yang J, Croteau-Chonka DC, Esko T, Fall T, Ferreira T, Gustafsson S, Kutalik Z, Luan J, Magi R, Randall JC, Winkler TW, Wood AR, Workalemahu T, Faul JD, Smith JA, Zhao JH, Zhao W, Chen J, Fehrmann R, Hedman AK, Karjalainen J, Schmidt EM, Absher D, Amin N, Anderson D, Beekman M, Bolton JL, Bragg-Gresham JL, Buyske S, Demirkan A, Deng G, Ehret GB, Feenstra B, Feitosa MF, Fischer K, Goel A, Gong J, Jackson AU, Kanoni S, Kleber ME, Kristiansson K, Lim U, Lotay V,

Mangino M, Leach IM, Medina-Gomez C, Medland SE, Nalls MA, Palmer CD, Pasko D, Pechlivanis S, Peters MJ, Prokopenko I, Shungin D, Stancakova A, Strawbridge RJ, Sung YJ, Tanaka T, Teumer A, Trompet S, van der Laan SW, van Setten J, Van Vliet-Ostaptchouk JV, Wang Z, Yengo L, Zhang W, Isaacs A, Albrecht E, Arnlov J, Arscott GM, Attwood AP, Bandinelli S, Barrett A, Bas IN, Bellis C, Bennett AJ, Berne C, Blagieva R, Bluher M, Bohringer S, Bonnycastle LL, Bottcher Y, Boyd HA, Bruinenberg M, Caspersen IH, Chen YI, Clarke R, Daw EW, de Craen AJM, Delgado G, Dimitriou M, Doney ASF, Eklund N, Estrada K, Eury E, Folkersen L, Fraser RM, Garcia ME, Geller F, Giedraitis V, Gigante B, Go AS, Golay A, Goodall AH, Gordon SD, Gorski M, Grabe HJ, Grallert H, Grammer TB, Grassler J, Gronberg H, Groves CJ, Gusto G, Haessler J, Hall P, Haller T, Hallmans G, Hartman CA, Hassinen M, Hayward C, Heard-Costa NL, Helmer Q, Hengstenberg C, Holmen O, Hottenga JJ, James AL, Jeff JM, Johansson A, Jolley J, Juliusdottir T, Kinnunen L, Koenig W, Koskenvuo M, Kratzer W, Laitinen J, Lamina C, Leander K, Lee NR, Lichtner P, Lind L, Lindstrom J, Lo KS, Lobbens S, Lorbeer R, Lu Y, Mach F, Magnusson PKE, Mahajan A, McArdle WL, McLachlan S, Menni C, Merger S, Mihailov E, Milani L, Moayyeri A, Monda KL, Morken MA, Mulas A, Muller G, Muller-Nurasyid M, Musk AW, Nagaraja R, Nothen MM, Nolte IM, Pilz S, Rayner NW, Renstrom F, Rettig R, Ried JS, Ripke S, Robertson NR, Rose LM, Sanna S, Scharnagl H, Scholtens S, Schumacher FR, Scott WR, Seufferlein T, Shi J, Smith AV, Smolonska J, Stanton AV, Steinthorsdottir V, Stirrups K, Stringham HM, Sundstrom J, Swertz MA, Swift AJ, Syvanen AC, Tan ST, Tayo BO, Thorand B, Thorleifsson G, Tyrer JP, Uh HW, Vandenput L, Verhulst FC, Vermeulen SH, Verweij N, Vonk JM, Waite LL, Warren HR, Waterworth D, Weedon MN, Wilkens LR, Willenborg C, Wilsgaard T, Wojczynski MK, Wong A, Wright AF, Zhang Q, LifeLines Cohort S, Brennan EP, Choi M, Dastani Z, Drong AW, Eriksson P, Franco-Cereceda A, Gadin JR, Gharavi AG, Goddard ME, Handsaker RE, Huang J, Karpe F, Kathiresan S, Keildson S, Kiryluk K, Kubo M, Lee JY, Liang L, Lifton RP, Ma B, McCarroll SA, McKnight AJ, Min JL, Moffatt MF, Montgomery GW, Murabito JM, Nicholson G, Nyholt DR, Okada Y, Perry JRB, Dorajoo R, Reinmaa E, Salem RM, Sandholm N, Scott RA, Stolk L, Takahashi A, Tanaka T, van 't Hooft FM, Vinkhuyzen AAE, Westra HJ, Zheng W, Zondervan KT, Consortium AD, Group A-BW, Consortium CAD, Consortium CK, Glgc, Icbp, Investigators M, Mu TC, Consortium MI, Consortium P, ReproGen C, Consortium G, International Endogene C, Heath AC, Arveiler D, Bakker SJL, Beilby J, Bergman RN, Blangero J, Bovet P, Campbell H, Caulfield MJ, Cesana G, Chakravarti A, Chasman DI, Chines PS, Collins FS, Crawford DC, Cupples LA, Cusi D, Danesh J, de Faire U, den Ruijter HM, Dominiczak AF, Erbel R, Erdmann J, Eriksson JG, Farrall M, Felix SB, Ferrannini E, Ferrieres J, Ford I, Forouhi NG, Forrester T, Franco OH, Gansevoort RT, Gejman PV, Gieger C, Gottesman O, Gudnason V, Gyllensten U, Hall AS, Harris TB, Hattersley AT, Hicks AA, Hindorff LA, Hingorani AD, Hofman A, Homuth G, Hovingh GK, Humphries SE, Hunt SC, Hypponen E, Illig T, Jacobs KB, Jarvelin MR, Jockel KH, Johansen B, Jousilahti P, Jukema JW, Jula AM, Kaprio J, Kastelein JJP, Keinanen-Kiukaanniemi SM, Kiemeney LA, Knekt P, Kooner JS, Kooperberg C, Kovacs P, Kraja AT, Kumari M, Kuusisto J, Lakka TA, Langenberg C, Marchand LL, Lehtimaki T, Lyssenko V, Mannisto S, Marette A, Matise TC, McKenzie CA, McKnight B, Moll FL, Morris AD, Morris AP, Murray JC, Nelis M,

Ohlsson C, Oldehinkel AJ, Ong KK, Madden PAF, Pasterkamp G, Peden JF, Peters A, Postma DS, Pramstaller PP, Price JF, Qi L, Raitakari OT, Rankinen T, Rao DC, Rice TK, Ridker PM, Rioux JD, Ritchie MD, Rudan I, Salomaa V, Samani NJ, Saramies J, Sarzynski MA, Schunkert H, Schwarz PEH, Sever P, Shuldiner AR, Sinisalo J, Stolk RP, Strauch K, Tonjes A, Tregouet DA, Tremblay A, Tremoli E, Virtamo J, Vohl MC, Volker U, Waeber G, Willemsen G, Witteman JC, Zillikens MC, Adair LS, Amouyel P, Asselbergs FW, Assimes TL, Bochud M, Boehm BO, Boerwinkle E, Bornstein SR, Bottinger EP, Bouchard C, Cauchi S, Chambers JC, Chanock SJ, Cooper RS, de Bakker PIW, Dedoussis G, Ferrucci L, Franks PW, Froguel P, Groop LC, Haiman CA, Hamsten A, Hui J, Hunter DJ, Hveem K, Kaplan RC, Kivimaki M, Kuh D, Laakso M, Liu Y, Martin NG, Marz W, Melbye M, Metspalu A, Moebus S, Munroe PB, Njolstad I, Oostra BA, Palmer CNA, Pedersen NL, Perola M, Perusse L, Peters U, Power C, Quertermous T, Rauramaa R, Rivadeneira F, Saaristo TE, Saleheen D, Sattar N, Schadt EE, Schlessinger D, Slagboom PE, Snieder H, Spector TD, Thorsteinsdottir U, Stumvoll M, Tuomilehto J, Uitterlinden AG, Uusitupa M, van der Harst P, Walker M, Wallaschofski H, Wareham NJ, Watkins H, Weir DR, Wichmann HE, Wilson JF, Zanen P, Borecki IB, Deloukas P, Fox CS, Heid IM, O'Connell JR, Strachan DP, Stefansson K, van Duijn CM, Abecasis GR, Franke L, Frayling TM, McCarthy MI, Visscher PM, Scherag A, Willer CJ, Boehnke M, Mohlke KL, Lindgren CM, Beckmann JS, Barroso I, North KE, Ingelsson E, Hirschhorn JN, Loos RJF, Speliotes EK. Genetic studies of body mass index yield new insights for obesity biology. Nature 2015; 518:197-206

87. Pelton K, Freeman MR, Solomon KR. Cholesterol and prostate cancer. Curr Opin Pharmacol 2012; 12:751-759

88. Sekine Y, Koike H, Nakano T, Nakajima K, Takahashi S, Suzuki K. Remnant lipoproteins induced proliferation of human prostate cancer cell, PC-3 but not LNCaP, via low density lipoprotein receptor. Cancer Epidemiol 2009; 33:16-23

89. Llaverias G, Danilo C, Mercier I, Daumer K, Capozza F, Williams TM, Sotgia F, Lisanti MP, Frank PG. Role of cholesterol in the development and progression of breast cancer. Am J Pathol 2011; 178:402-412

90. Llaverias G, Danilo C, Wang Y, Witkiewicz AK, Daumer K, Lisanti MP, Frank PG. A Western-type diet accelerates tumor progression in an autochthonous mouse model of prostate cancer. Am J Pathol 2010; 177:3180-3191

91. Chen H, Qin S, Wang M, Zhang T, Zhang S. Association between cholesterol intake and pancreatic cancer risk: evidence from a meta-analysis. Sci Rep 2015; 5:8243

92. Gabitova-Cornell L, Surumbayeva A, Peri S, Franco-Barraza J, Restifo D, Weitz N, Ogier C, Goldman AR, Hartman TR, Francescone R, Tan Y, Nicolas E, Shah N, Handorf EA, Cai KQ, O'Reilly AM, Sloma I, Chiaverelli R, Moffitt RA, Khazak V, Fang CY, Golemis EA, Cukierman E, Astsaturov I. Cholesterol Pathway Inhibition Induces TGF-beta Signaling to Promote Basal Differentiation in Pancreatic Cancer. Cancer Cell 2020; 38:567-583 e511

93. Martinez J, Sanchez-Paya J, Palazon JM, Suazo-Barahona J, Robles-Diaz G, Perez-Mateo M. Is obesity a risk factor in acute pancreatitis? A meta-analysis. Pancreatology 2004; 4:42-48

94. Khatua B, El-Kurdi B, Singh VP. Obesity and pancreatitis. Curr Opin Gastroenterol 2017; 33:374-382

95. Mendonsa AM, Chalfant MC, Gorden LD, VanSaun MN. Modulation of the leptin receptor mediates tumor growth and migration of pancreatic cancer cells. PLoS One 2015; 10:e0126686
96. Xu Y, Tan M, Tian X, Zhang J, Zhang J, Chen J, Xu W, Sheng H. Leptin receptor mediates the proliferation and glucose metabolism of pancreatic cancer cells via AKT pathway activation. Mol Med Rep 2020; 21:945-952
97. Vansaun MN. Molecular pathways: adiponectin and leptin signaling in cancer. Clin Cancer Res 2013; 19:1926-1932
98. Huang B, Cheng X, Wang D, Peng M, Xue Z, Da Y, Zhang N, Yao Z, Li M, Xu A, Zhang R. Adiponectin promotes pancreatic cancer progression by inhibiting apoptosis via the activation of AMPK/Sirt1/PGC-1alpha signaling. Oncotarget 2014; 5:4732-4745
99. Jiang J, Fan Y, Zhang W, Shen Y, Liu T, Yao M, Gu J, Tu H, Gan Y. Adiponectin Suppresses Human Pancreatic Cancer Growth through Attenuating the beta-Catenin Signaling Pathway. Int J Biol Sci 2019; 15:253-264
100. Steppan CM, Bailey ST, Bhat S, Brown EJ, Banerjee RR, Wright CM, Patel HR, Ahima RS, Lazar MA. The hormone resistin links obesity to diabetes. Nature 2001; 409:307-312
101. Kim HJ, Lee YS, Won EH, Chang IH, Kim TH, Park ES, Kim MK, Kim W, Myung SC. Expression of resistin in the prostate and its stimulatory effect on prostate cancer cell proliferation. BJU Int 2011; 108:E77-83
102. Zhang M, Yan L, Wang GJ, Jin R. Resistin effects on pancreatic cancer progression and chemoresistance are mediated through its receptors CAP1 and TLR4. J Cell Physiol 2019; 234:9457-9466
103. Fu Z, Gilbert ER, Liu D. Regulation of insulin synthesis and secretion and pancreatic Beta-cell dysfunction in diabetes. Curr Diabetes Rev 2013; 9:25-53
104. Venkatanarayan A, Raulji P, Norton W, Chakravarti D, Coarfa C, Su X, Sandur SK, Ramirez MS, Lee J, Kingsley CV, Sananikone EF, Rajapakshe K, Naff K, Parker-Thornburg J, Bankson JA, Tsai KY, Gunaratne PH, Flores ER. IAPP-driven metabolic reprogramming induces regression of p53-deficient tumours in vivo. Nature 2015; 517:626-630
105. Haeusler RA, McGraw TE, Accili D. Biochemical and cellular properties of insulin receptor signalling. Nat Rev Mol Cell Biol 2018; 19:31-44
106. Rask-Madsen C, Kahn CR. Tissue-specific insulin signaling, metabolic syndrome, and cardiovascular disease. Arterioscler Thromb Vasc Biol 2012; 32:2052-2059
107. Henderson JR, Daniel PM, Fraser PA. The pancreas as a single organ: the influence of the endocrine upon the exocrine part of the gland. Gut 1981; 22:158-167
108. Leroux L, Desbois P, Lamotte L, Duvillie B, Cordonnier N, Jackerott M, Jami J, Bucchini D, Joshi RL. Compensatory responses in mice carrying a null mutation for Ins1 or Ins2. Diabetes 2001; 50 Suppl 1:S150-153
109. Duvillie B, Cordonnier N, Deltour L, Dandoy-Dron F, Itier JM, Monthioux E, Jami J, Joshi RL, Bucchini D. Phenotypic alterations in insulin-deficient mutant mice. Proc Natl Acad Sci U S A 1997; 94:5137-5140
110. Szabat M, Page MM, Panzhinskiy E, Skovso S, Mojibian M, Fernandez-Tajes J, Bruin JE, Bround MJ, Lee JT, Xu EE, Taghizadeh F, O'Dwyer S, van de Bunt M, Moon KM, Sinha S, Han J, Fan Y, Lynn FC, Trucco M, Borchers CH, Foster LJ, Nislow C, Kieffer

TJ, Johnson JD. Reduced Insulin Production Relieves Endoplasmic Reticulum Stress and Induces beta Cell Proliferation. Cell Metab 2016; 23:179-193
111. Wentworth BM, Schaefer IM, Villa-Komaroff L, Chirgwin JM. Characterization of the two nonallelic genes encoding mouse preproinsulin. J Mol Evol 1986; 23:305-312
112. Mehran AE, Templeman NM, Brigidi GS, Lim GE, Chu KY, Hu X, Botezelli JD, Asadi A, Hoffman BG, Kieffer TJ, Bamji SX, Clee SM, Johnson JD. Hyperinsulinemia drives diet-induced obesity independently of brain insulin production. Cell Metab 2012; 16:723-737
113. Soares MB, Schon E, Henderson A, Karathanasis SK, Cate R, Zeitlin S, Chirgwin J, Efstratiadis A. RNA-mediated gene duplication: the rat preproinsulin I gene is a functional retroposon. Mol Cell Biol 1985; 5:2090-2103
114. Deltour L, Leduque P, Blume N, Madsen O, Dubois P, Jami J, Bucchini D. Differential expression of the two nonallelic proinsulin genes in the developing mouse embryo. Proc Natl Acad Sci U S A 1993; 90:527-531
115. Deltour L, Montagutelli X, Guenet JL, Jami J, Paldi A. Tissue- and developmental stage-specific imprinting of the mouse proinsulin gene, Ins2. Dev Biol 1995; 168:686-688
116. Hay CW, Docherty K. Comparative analysis of insulin gene promoters: implications for diabetes research. Diabetes 2006; 55:3201-3213
117. Meur G, Qian Q, da Silva Xavier G, Pullen TJ, Tsuboi T, McKinnon C, Fletcher L, Tavare JM, Hughes S, Johnson P, Rutter GA. Nucleo-cytosolic shuttling of FoxO1 directly regulates mouse Ins2 but not Ins1 gene expression in pancreatic beta cells (MIN6). J Biol Chem 2011; 286:13647-13656
118. McAuley KA, Williams SM, Mann JI, Walker RJ, Lewis-Barned NJ, Temple LA, Duncan AW. Diagnosing insulin resistance in the general population. Diabetes Care 2001; 24:460-464
119. Zhang AMY, Wellberg EA, Kopp JL, Johnson JD. Hyperinsulinemia in Obesity, Inflammation, and Cancer. Diabetes Metab J 2021; 45:285-311
120. Templeman NM, Mehran AE, Johnson JD. Hyper-Variability in Circulating Insulin, High Fat Feeding Outcomes, and Effects of Reducing Ins2 Dosage in Male Ins1-Null Mice in a Specific Pathogen-Free Facility. PLoS One 2016; 11:e0153280
121. Templeman NM, Flibotte S, Chik JHL, Sinha S, Lim GE, Foster LJ, Nislow C, Johnson JD. Reduced Circulating Insulin Enhances Insulin Sensitivity in Old Mice and Extends Lifespan. Cell Rep 2017; 20:451-463
122. Templeman NM, Clee SM, Johnson JD. Suppression of hyperinsulinaemia in growing female mice provides long-term protection against obesity. Diabetologia 2015; 58:2392-2402
123. Søs Skovsø EP, Jelena Kolic, Haoning Howard Cen, Derek A. Dionne, Xiao-Qing Dai, Rohit B. Sharma, Lynda Elghazi, Cara E. Ellis, Katharine Faulkner, Stephanie A.M. Marcil, Peter Overby, Nilou Noursadeghi, Daria Hutchinson, Xiaoke Hu, Hong Li, Honey Modi, Jennifer S. Wildi, J. Diego Botezelli, Hye Lim Noh, Sujin Suk, Brian Gablaski, Austin Bautista, Ryekjang Kim, Cras-Méneur, Stephane Flibotte, Sunita Sinha, Dan S. Luciani, Corey Nislow, Elizabeth J. Rideout, Eric N. Cytrynbaum, Jason Kim, Ernesto Bernal-Mizrachi, Laura C. Alonso, Patrick E. MacDonald, James D. Johnson. Beta-cell specific Insr deletion promotes glucose-stimulated insulin hypersecretion and improves glucose tolerance prior to global insulin resistance. BioRxiv 2021;

124. Cen HH, Hussein B, Botezelli JD, Wang S, Zhang JA, Noursadeghi N, Jessen N, Rodrigues B, Timmons JA, Johnson JD. Human and mouse muscle transcriptomic analyses identify insulin receptor mRNA downregulation in hyperinsulinemia-associated insulin resistance. FASEB J 2022; 36:e22088

125. Ma J, Giovannucci E, Pollak M, Leavitt A, Tao Y, Gaziano JM, Stampfer MJ. A prospective study of plasma C-peptide and colorectal cancer risk in men. J Natl Cancer Inst 2004; 96:546-553

126. Jenab M, Riboli E, Cleveland RJ, Norat T, Rinaldi S, Nieters A, Biessy C, Tjonneland A, Olsen A, Overvad K, Gronbaek H, Clavel-Chapelon F, Boutron-Ruault MC, Linseisen J, Boeing H, Pischon T, Trichopoulos D, Oikonomou E, Trichopoulou A, Panico S, Vineis P, Berrino F, Tumino R, Masala G, Peters PH, van Gils CH, Bueno-de-Mesquita HB, Ocke MC, Lund E, Mendez MA, Tormo MJ, Barricarte A, Martinez-Garcia C, Dorronsoro M, Quiros JR, Hallmans G, Palmqvist R, Berglund G, Manjer J, Key T, Allen NE, Bingham S, Khaw KT, Cust A, Kaaks R. Serum C-peptide, IGFBP-1 and IGFBP-2 and risk of colon and rectal cancers in the European Prospective Investigation into Cancer and Nutrition. Int J Cancer 2007; 121:368-376

127. Hvidtfeldt UA, Gunter MJ, Lange T, Chlebowski RT, Lane D, Farhat GN, Freiberg MS, Keiding N, Lee JS, Prentice R, Tjonneland A, Vitolins MZ, Wassertheil-Smoller S, Strickler HD, Rod NH. Quantifying mediating effects of endogenous estrogen and insulin in the relation between obesity, alcohol consumption, and breast cancer. Cancer Epidemiol Biomarkers Prev 2012; 21:1203-1212

128. Dossus L, Lukanova A, Rinaldi S, Allen N, Cust AE, Becker S, Tjonneland A, Hansen L, Overvad K, Chabbert-Buffet N, Mesrine S, Clavel-Chapelon F, Teucher B, Chang-Claude J, Boeing H, Drogan D, Trichopoulou A, Benetou V, Bamia C, Palli D, Agnoli C, Galasso R, Tumino R, Sacerdote C, Bueno-de-Mesquita HB, van Duijnhoven FJ, Peeters PH, Onland-Moret NC, Redondo ML, Travier N, Sanchez MJ, Altzibar JM, Chirlaque MD, Barricarte A, Lundin E, Khaw KT, Wareham N, Fedirko V, Romieu I, Romaguera D, Norat T, Riboli E, Kaaks R. Hormonal, metabolic, and inflammatory profiles and endometrial cancer risk within the EPIC cohort--a factor analysis. Am J Epidemiol 2013; 177:787-799

129. Loftfield E, Freedman ND, Lai GY, Weinstein SJ, McGlynn KA, Taylor PR, Mannisto S, Albanes D, Stolzenberg-Solomon RZ. Higher Glucose and Insulin Levels Are Associated with Risk of Liver Cancer and Chronic Liver Disease Mortality among Men without a History of Diabetes. Cancer Prev Res (Phila) 2016; 9:866-874

130. Michaud DS, Wolpin B, Giovannucci E, Liu S, Cochrane B, Manson JE, Pollak MN, Ma J, Fuchs CS. Prediagnostic plasma C-peptide and pancreatic cancer risk in men and women. Cancer Epidemiol Biomarkers Prev 2007; 16:2101-2109

131. Hidaka A, Sasazuki S, Goto A, Sawada N, Shimazu T, Yamaji T, Iwasaki M, Inoue M, Noda M, Tajiri H, Tsugane S, Group JS. Plasma insulin, C-peptide and blood glucose and the risk of gastric cancer: the Japan Public Health Center-based prospective study. Int J Cancer 2015; 136:1402-1410

132. Otokozawa S, Tanaka R, Akasaka H, Ito E, Asakura S, Ohnishi H, Saito S, Miura T, Saito T, Mori M. Associations of Serum Isoflavone, Adiponectin and Insulin Levels with Risk for Epithelial Ovarian Cancer: Results of a Case-control Study. Asian Pac J Cancer Prev 2015; 16:4987-4991

133. Pierce BL, Kraft P, Zhang C. Mendelian randomization studies of cancer risk: a literature review. Curr Epidemiol Rep 2018; 5:184-196
134. Gunter MJ, Xie X, Xue X, Kabat GC, Rohan TE, Wassertheil-Smoller S, Ho GY, Wylie-Rosett J, Greco T, Yu H, Beasley J, Strickler HD. Breast cancer risk in metabolically healthy but overweight postmenopausal women. Cancer Res 2015; 75:270-274
135. Walraven I, van 't Riet E, Stehouwer CD, Polak BC, Moll AC, Dekker JM, Nijpels G. Fasting proinsulin levels are significantly associated with 20 year cancer mortality rates. The Hoorn Study. Diabetologia 2013; 56:1148-1154
136. Balkau B, Kahn HS, Courbon D, Eschwege E, Ducimetiere P, Paris Prospective S. Hyperinsulinemia predicts fatal liver cancer but is inversely associated with fatal cancer at some other sites: the Paris Prospective Study. Diabetes Care 2001; 24:843-849
137. Irwin ML, Duggan C, Wang CY, Smith AW, McTiernan A, Baumgartner RN, Baumgartner KB, Bernstein L, Ballard-Barbash R. Fasting C-peptide levels and death resulting from all causes and breast cancer: the health, eating, activity, and lifestyle study. J Clin Oncol 2011; 29:47-53
138. Colangelo LA, Gapstur SM, Gann PH, Dyer AR, Liu K. Colorectal cancer mortality and factors related to the insulin resistance syndrome. Cancer Epidemiol Biomarkers Prev 2002; 11:385-391
139. Tsujimoto T, Kajio H, Sugiyama T. Association between hyperinsulinemia and increased risk of cancer death in nonobese and obese people: A population-based observational study. Int J Cancer 2017; 141:102-111
140. Godsland IF. Insulin resistance and hyperinsulinaemia in the development and progression of cancer. Clin Sci (Lond) 2009; 118:315-332
141. Draznin B, Miles P, Kruszynska Y, Olefsky J, Friedman J, Golovchenko I, Stjernholm R, Wall K, Reitman M, Accili D, Cooksey R, McClain D, Goalstone M. Effects of insulin on prenylation as a mechanism of potentially detrimental influence of hyperinsulinemia. Endocrinology 2000; 141:1310-1316
142. Wu Y, Yakar S, Zhao L, Hennighausen L, LeRoith D. Circulating insulin-like growth factor-I levels regulate colon cancer growth and metastasis. Cancer Res 2002; 62:1030-1035
143. Bhalla V, Joshi K, Vohra H, Singh G, Ganguly NK. Effect of growth factors on proliferation of normal, borderline, and malignant breast epithelial cells. Exp Mol Pathol 2000; 68:124-132
144. Hadsell DL, Murphy KL, Bonnette SG, Reece N, Laucirica R, Rosen JM. Cooperative interaction between mutant p53 and des(1-3)IGF-I accelerates mammary tumorigenesis. Oncogene 2000; 19:889-898
145. Leung KC, Doyle N, Ballesteros M, Waters MJ, Ho KK. Insulin regulation of human hepatic growth hormone receptors: divergent effects on biosynthesis and surface translocation. J Clin Endocrinol Metab 2000; 85:4712-4720
146. Roberts CT, Jr., Brown AL, Graham DE, Seelig S, Berry S, Gabbay KH, Rechler MM. Growth hormone regulates the abundance of insulin-like growth factor I RNA in adult rat liver. J Biol Chem 1986; 261:10025-10028
147. Clemmons DR, Underwood LE. Nutritional regulation of IGF-I and IGF binding proteins. Annu Rev Nutr 1991; 11:393-412

148. Straus DS. Nutritional regulation of hormones and growth factors that control mammalian growth. FASEB J 1994; 8:6-12
149. Belfiore A, Malaguarnera R, Vella V, Lawrence MC, Sciacca L, Frasca F, Morrione A, Vigneri R. Insulin Receptor Isoforms in Physiology and Disease: An Updated View. Endocr Rev 2017; 38:379-431
150. Othman EM, Leyh A, Stopper H. Insulin mediated DNA damage in mammalian colon cells and human lymphocytes in vitro. Mutat Res 2013; 745-746:34-39
151. Othman EM, Kreissl MC, Kaiser FR, Arias-Loza PA, Stopper H. Insulin-mediated oxidative stress and DNA damage in LLC-PK1 pig kidney cell line, female rat primary kidney cells, and male ZDF rat kidneys in vivo. Endocrinology 2013; 154:1434-1443
152. Storz P. KRas, ROS and the initiation of pancreatic cancer. Small GTPases 2017; 8:38-42
153. Zhang L, Li J, Zong L, Chen X, Chen K, Jiang Z, Nan L, Li X, Li W, Shan T, Ma Q, Ma Z. Reactive Oxygen Species and Targeted Therapy for Pancreatic Cancer. Oxid Med Cell Longev 2016; 2016:1616781
154. Chvanov M, Petersen OH, Tepikin A. Free radicals and the pancreatic acinar cells: role in physiology and pathology. Philos Trans R Soc Lond B Biol Sci 2005; 360:2273-2284
155. Pedersen DJ, Guilherme A, Danai LV, Heyda L, Matevossian A, Cohen J, Nicoloro SM, Straubhaar J, Noh HL, Jung D, Kim JK, Czech MP. A major role of insulin in promoting obesity-associated adipose tissue inflammation. Mol Metab 2015; 4:507-518
156. Krogh-Madsen R, Plomgaard P, Keller P, Keller C, Pedersen BK. Insulin stimulates interleukin-6 and tumor necrosis factor-alpha gene expression in human subcutaneous adipose tissue. Am J Physiol Endocrinol Metab 2004; 286:E234-238
157. Soop M, Duxbury H, Agwunobi AO, Gibson JM, Hopkins SJ, Childs C, Cooper RG, Maycock P, Little RA, Carlson GL. Euglycemic hyperinsulinemia augments the cytokine and endocrine responses to endotoxin in humans. Am J Physiol Endocrinol Metab 2002; 282:E1276-1285
158. Westerbacka J, Corner A, Kannisto K, Kolak M, Makkonen J, Korsheninnikova E, Nyman T, Hamsten A, Fisher RM, Yki-Jarvinen H. Acute in vivo effects of insulin on gene expression in adipose tissue in insulin-resistant and insulin-sensitive subjects. Diabetologia 2006; 49:132-140
159. Tsai S, Clemente-Casares X, Zhou AC, Lei H, Ahn JJ, Chan YT, Choi O, Luck H, Woo M, Dunn SE, Engleman EG, Watts TH, Winer S, Winer DA. Insulin Receptor-Mediated Stimulation Boosts T Cell Immunity during Inflammation and Infection. Cell Metab 2018; 28:922-934 e924
160. Han JM, Patterson SJ, Speck M, Ehses JA, Levings MK. Insulin inhibits IL-10-mediated regulatory T cell function: implications for obesity. J Immunol 2014; 192:623-629
161. Fischer HJ, Sie C, Schumann E, Witte AK, Dressel R, van den Brandt J, Reichardt HM. The Insulin Receptor Plays a Critical Role in T Cell Function and Adaptive Immunity. J Immunol 2017; 198:1910-1920
162. Stolzenberg-Solomon RZ, Graubard BI, Chari S, Limburg P, Taylor PR, Virtamo J, Albanes D. Insulin, glucose, insulin resistance, and pancreatic cancer in male smokers. JAMA 2005; 294:2872-2878
163. Pisani P. Hyper-insulinaemia and cancer, meta-analyses of epidemiological studies. Arch Physiol Biochem 2008; 114:63-70

164. Perseghin G, Calori G, Lattuada G, Ragogna F, Dugnani E, Garancini MP, Crosignani P, Villa M, Bosi E, Ruotolo G, Piemonti L. Insulin resistance/hyperinsulinemia and cancer mortality: the Cremona study at the 15th year of follow-up. Acta Diabetol 2012; 49:421-428
165. Bodmer M, Becker C, Meier C, Jick SS, Meier CR. Use of antidiabetic agents and the risk of pancreatic cancer: a case-control analysis. Am J Gastroenterol 2012; 107:620-626
166. Li D, Yeung SC, Hassan MM, Konopleva M, Abbruzzese JL. Antidiabetic therapies affect risk of pancreatic cancer. Gastroenterology 2009; 137:482-488
167. Tokarz VL, MacDonald PE, Klip A. The cell biology of systemic insulin function. J Cell Biol 2018; 217:2273-2289
168. Wang M, Li J, Lim GE, Johnson JD. Is dynamic autocrine insulin signaling possible? A mathematical model predicts picomolar concentrations of extracellular monomeric insulin within human pancreatic islets. PLoS One 2013; 8:e64860
169. Song SH, Kjems L, Ritzel R, McIntyre SM, Johnson ML, Veldhuis JD, Butler PC. Pulsatile insulin secretion by human pancreatic islets. J Clin Endocrinol Metab 2002; 87:213-221
170. Maclean N, Ogilvie RF. Quantitative estimation of the pancreatic islet tissue in diabetic subjects. Diabetes 1955; 4:367-376
171. Wright JJ, Saunders DC, Dai C, Poffenberger G, Cairns B, Serreze DV, Harlan DM, Bottino R, Brissova M, Powers AC. Decreased pancreatic acinar cell number in type 1 diabetes. Diabetologia 2020; 63:1418-1423
172. Dombrowski F, Mathieu C, Evert M. Hepatocellular neoplasms induced by low-number pancreatic islet transplants in autoimmune diabetic BB/Pfd rats. Cancer Res 2006; 66:1833-1843
173. Evert M, Sun J, Pichler S, Slavova N, Schneider-Stock R, Dombrowski F. Insulin receptor, insulin receptor substrate-1, Raf-1, and Mek-1 during hormonal hepatocarcinogenesis by intrahepatic pancreatic islet transplantation in diabetic rats. Cancer Res 2004; 64:8093-8100
174. Castellano E, Downward J. RAS Interaction with PI3K: More Than Just Another Effector Pathway. Genes Cancer 2011; 2:261-274
175. Lee JW, Soung YH, Kim SY, Lee HW, Park WS, Nam SW, Kim SH, Lee JY, Yoo NJ, Lee SH. PIK3CA gene is frequently mutated in breast carcinomas and hepatocellular carcinomas. Oncogene 2005; 24:1477-1480
176. Xiang L, Jiang W, Li J, Shen X, Yang W, Yang G, Wu X, Yang H. PIK3CA mutation analysis in Chinese patients with surgically resected cervical cancer. Sci Rep 2015; 5:14035
177. Levine DA, Bogomolniy F, Yee CJ, Lash A, Barakat RR, Borgen PI, Boyd J. Frequent mutation of the PIK3CA gene in ovarian and breast cancers. Clin Cancer Res 2005; 11:2875-2878
178. Yang J, Nie J, Ma X, Wei Y, Peng Y, Wei X. Targeting PI3K in cancer: mechanisms and advances in clinical trials. Mol Cancer 2019; 18:26
179. Samuels Y, Wang Z, Bardelli A, Silliman N, Ptak J, Szabo S, Yan H, Gazdar A, Powell SM, Riggins GJ, Willson JK, Markowitz S, Kinzler KW, Vogelstein B, Velculescu VE. High frequency of mutations of the PIK3CA gene in human cancers. Science 2004; 304:554

180. Shen S, Liu H, Wang Y, Wang J, Ni X, Ai Z, Pan H, Liu H, Shao Y. Long non-coding RNA CRNDE promotes gallbladder carcinoma carcinogenesis and as a scaffold of DMBT1 and C-IAP1 complexes to activating PI3K-AKT pathway. Oncotarget 2016; 7:72833-72844
181. Liu XX, Xiong HP, Huang JS, Qi K, Xu JJ. Highly expressed long non-coding RNA CRNDE promotes cell proliferation through PI3K/AKT signalling in non-small cell lung carcinoma. Clin Exp Pharmacol Physiol 2017; 44:895-902
182. Ellis BC, Graham LD, Molloy PL. CRNDE, a long non-coding RNA responsive to insulin/IGF signaling, regulates genes involved in central metabolism. Biochim Biophys Acta 2014; 1843:372-386
183. Du DX, Lian DB, Amin BH, Yan W. Long non-coding RNA CRNDE is a novel tumor promoter by modulating PI3K/AKT signal pathways in human gastric cancer. Eur Rev Med Pharmacol Sci 2017; 21:5392-5398
184. Yang HY, Huang CP, Cao MM, Wang YF, Liu Y. Long non-coding RNA CRNDE may be associated with poor prognosis by promoting proliferation and inhibiting apoptosis of cervical cancer cells through targeting PI3K/AKT. Neoplasma 2018; 65:872-880
185. Tang Q, Zheng X, Zhang J. Long non-coding RNA CRNDE promotes heptaocellular carcinoma cell proliferation by regulating PI3K/Akt /beta-catenin signaling. Biomed Pharmacother 2018; 103:1187-1193
186. Wang Y, Kong D. LncRNA GAS5 Represses Osteosarcoma Cells Growth and Metastasis via Sponging MiR-203a. Cell Physiol Biochem 2018; 45:844-855
187. Li S, Zhou J, Wang Z, Wang P, Gao X, Wang Y. Long noncoding RNA GAS5 suppresses triple negative breast cancer progression through inhibition of proliferation and invasion by competitively binding miR-196a-5p. Biomed Pharmacother 2018; 104:451-457
188. Yuan S, Wu Y, Wang Y, Chen J, Chu L. An Oncolytic Adenovirus Expressing SNORD44 and GAS5 Exhibits Antitumor Effect in Colorectal Cancer Cells. Hum Gene Ther 2017; 28:690-700
189. Li J, Yen C, Liaw D, Podsypanina K, Bose S, Wang SI, Puc J, Miliaresis C, Rodgers L, McCombie R, Bigner SH, Giovanella BC, Ittmann M, Tycko B, Hibshoosh H, Wigler MH, Parsons R. PTEN, a putative protein tyrosine phosphatase gene mutated in human brain, breast, and prostate cancer. Science 1997; 275:1943-1947
190. Liaw D, Marsh DJ, Li J, Dahia PL, Wang SI, Zheng Z, Bose S, Call KM, Tsou HC, Peacocke M, Eng C, Parsons R. Germline mutations of the PTEN gene in Cowden disease, an inherited breast and thyroid cancer syndrome. Nat Genet 1997; 16:64-67
191. Chen CY, Chen J, He L, Stiles BL. PTEN: Tumor Suppressor and Metabolic Regulator. Front Endocrinol (Lausanne) 2018; 9:338
192. Manning BD, Cantley LC. AKT/PKB signaling: navigating downstream. Cell 2007; 129:1261-1274
193. Cheng X, Xia W, Yang JY, Hsu JL, Lang JY, Chou CK, Du Y, Sun HL, Wyszomierski SL, Mills GB, Muller WJ, Yu D, Hung MC. Activation of murine double minute 2 by Akt in mammary epithelium delays mammary involution and accelerates mammary tumorigenesis. Cancer Res 2010; 70:7684-7689
194. McCubrey JA, Steelman LS, Chappell WH, Abrams SL, Wong EW, Chang F, Lehmann B, Terrian DM, Milella M, Tafuri A, Stivala F, Libra M, Basecke J, Evangelisti C,

Martelli AM, Franklin RA. Roles of the Raf/MEK/ERK pathway in cell growth, malignant transformation and drug resistance. Biochim Biophys Acta 2007; 1773:1263-1284

195. Guo YJ, Pan WW, Liu SB, Shen ZF, Xu Y, Hu LL. ERK/MAPK signalling pathway and tumorigenesis. Exp Ther Med 2020; 19:1997-2007

196. Garnett MJ, Marais R. Guilty as charged: B-RAF is a human oncogene. Cancer Cell 2004; 6:313-319

197. Witkiewicz AK, McMillan EA, Balaji U, Baek G, Lin WC, Mansour J, Mollaee M, Wagner KU, Koduru P, Yopp A, Choti MA, Yeo CJ, McCue P, White MA, Knudsen ES. Whole-exome sequencing of pancreatic cancer defines genetic diversity and therapeutic targets. Nat Commun 2015; 6:6744

198. Mebratu Y, Tesfaigzi Y. How ERK1/2 activation controls cell proliferation and cell death: Is subcellular localization the answer? Cell Cycle 2009; 8:1168-1175

199. Brunet A, Roux D, Lenormand P, Dowd S, Keyse S, Pouyssegur J. Nuclear translocation of p42/p44 mitogen-activated protein kinase is required for growth factor-induced gene expression and cell cycle entry. EMBO J 1999; 18:664-674

200. Huang C, Jacobson K, Schaller MD. MAP kinases and cell migration. J Cell Sci 2004; 117:4619-4628

201. Chakraborti S, Mandal M, Das S, Mandal A, Chakraborti T. Regulation of matrix metalloproteinases: an overview. Mol Cell Biochem 2003; 253:269-285

202. Belfiore A, Frasca F, Pandini G, Sciacca L, Vigneri R. Insulin receptor isoforms and insulin receptor/insulin-like growth factor receptor hybrids in physiology and disease. Endocr Rev 2009; 30:586-623

203. Frasca F, Pandini G, Scalia P, Sciacca L, Mineo R, Costantino A, Goldfine ID, Belfiore A, Vigneri R. Insulin receptor isoform A, a newly recognized, high-affinity insulin-like growth factor II receptor in fetal and cancer cells. Mol Cell Biol 1999; 19:3278-3288

204. Pandini G, Frasca F, Mineo R, Sciacca L, Vigneri R, Belfiore A. Insulin/insulin-like growth factor I hybrid receptors have different biological characteristics depending on the insulin receptor isoform involved. J Biol Chem 2002; 277:39684-39695

205. Aljada A, Saleh AM, Al-Aqeel SM, Shamsa HB, Al-Bawab A, Al Dubayee M, Ahmed AA. Quantification of insulin receptor mRNA splice variants as a diagnostic tumor marker in breast cancer. Cancer Biomark 2015; 15:653-661

206. Harrington SC, Weroha SJ, Reynolds C, Suman VJ, Lingle WL, Haluska P. Quantifying insulin receptor isoform expression in FFPE breast tumors. Growth Horm IGF Res 2012; 22:108-115

207. Law JH, Habibi G, Hu K, Masoudi H, Wang MY, Stratford AL, Park E, Gee JM, Finlay P, Jones HE, Nicholson RI, Carboni J, Gottardis M, Pollak M, Dunn SE. Phosphorylated insulin-like growth factor-i/insulin receptor is present in all breast cancer subtypes and is related to poor survival. Cancer Res 2008; 68:10238-10246

208. Forest A, Amatulli M, Ludwig DL, Damoci CB, Wang Y, Burns CA, Donoho GP, Zanella N, Fiebig HH, Prewett MC, Surguladze D, DeLigio JT, Houghton PJ, Smith MA, Novosiadly R. Intrinsic Resistance to Cixutumumab Is Conferred by Distinct Isoforms of the Insulin Receptor. Mol Cancer Res 2015; 13:1615-1626

209. Webster NJ, Resnik JL, Reichart DB, Strauss B, Haas M, Seely BL. Repression of the insulin receptor promoter by the tumor suppressor gene product p53: a possible mechanism for receptor overexpression in breast cancer. Cancer Res 1996; 56:2781-2788
210. Jiang W, Jin Z, Zhou F, Cui J, Wang L, Wang L. High co-expression of Sp1 and HER-2 is correlated with poor prognosis of gastric cancer patients. Surg Oncol 2015; 24:220-225
211. Wang J, Kang M, Qin YT, Wei ZX, Xiao JJ, Wang RS. Sp1 is over-expressed in nasopharyngeal cancer and is a poor prognostic indicator for patients receiving radiotherapy. Int J Clin Exp Pathol 2015; 8:6936-6943
212. Sumter TF, Xian L, Huso T, Koo M, Chang YT, Almasri TN, Chia L, Inglis C, Reid D, Resar LM. The High Mobility Group A1 (HMGA1) Transcriptome in Cancer and Development. Curr Mol Med 2016; 16:353-393
213. Foti D, Iuliano R, Chiefari E, Brunetti A. A nucleoprotein complex containing Sp1, C/EBP beta, and HMGI-Y controls human insulin receptor gene transcription. Mol Cell Biol 2003; 23:2720-2732
214. Yang WM, Jeong HJ, Park SY, Lee W. Saturated fatty acid-induced miR-195 impairs insulin signaling and glycogen metabolism in HepG2 cells. FEBS Lett 2014; 588:3939-3946
215. Trajkovski M, Hausser J, Soutschek J, Bhat B, Akin A, Zavolan M, Heim MH, Stoffel M. MicroRNAs 103 and 107 regulate insulin sensitivity. Nature 2011; 474:649-653
216. Ferguson RD, Novosyadlyy R, Fierz Y, Alikhani N, Sun H, Yakar S, Leroith D. Hyperinsulinemia enhances c-Myc-mediated mammary tumor development and advances metastatic progression to the lung in a mouse model of type 2 diabetes. Breast Cancer Res 2012; 14:R8
217. Mulligan AM, O'Malley FP, Ennis M, Fantus IG, Goodwin PJ. Insulin receptor is an independent predictor of a favorable outcome in early stage breast cancer. Breast Cancer Res Treat 2007; 106:39-47
218. Besic V, Shi H, Stubbs RS, Hayes MT. Aberrant liver insulin receptor isoform a expression normalises with remission of type 2 diabetes after gastric bypass surgery. PLoS One 2015; 10:e0119270
219. Kaminska D, Hamalainen M, Cederberg H, Kakela P, Venesmaa S, Miettinen P, Ilves I, Herzig KH, Kolehmainen M, Karhunen L, Kuusisto J, Gylling H, Laakso M, Pihlajamaki J. Adipose tissue INSR splicing in humans associates with fasting insulin level and is regulated by weight loss. Diabetologia 2014; 57:347-351
220. Bruce JIE, Sanchez-Alvarez R, Sans MD, Sugden SA, Qi N, James AD, Williams JA. Insulin protects acinar cells during pancreatitis by preserving glycolytic ATP supply to calcium pumps. Nat Commun 2021; 12:4386
221. Heestand GM, Kurzrock R. Molecular landscape of pancreatic cancer: implications for current clinical trials. Oncotarget 2015; 6:4553-4561
222. Janku F, Wheler JJ, Naing A, Falchook GS, Hong DS, Stepanek VM, Fu S, Piha-Paul SA, Lee JJ, Luthra R, Tsimberidou AM, Kurzrock R. PIK3CA mutation H1047R is associated with response to PI3K/AKT/mTOR signaling pathway inhibitors in early-phase clinical trials. Cancer Res 2013; 73:276-284
223. Schonleben F, Qiu W, Remotti HE, Hohenberger W, Su GH. PIK3CA, KRAS, and BRAF mutations in intraductal papillary mucinous neoplasm/carcinoma (IPMN/C) of the pancreas. Langenbecks Arch Surg 2008; 393:289-296

224. Payne SN, Maher ME, Tran NH, Van De Hey DR, Foley TM, Yueh AE, Leystra AA, Pasch CA, Jeffrey JJ, Clipson L, Matkowskyj KA, Deming DA. PIK3CA mutations can initiate pancreatic tumorigenesis and are targetable with PI3K inhibitors. Oncogenesis 2015; 4:e169

225. Sivaram N, McLaughlin PA, Han HV, Petrenko O, Jiang YP, Ballou LM, Pham K, Liu C, van der Velden AW, Lin RZ. Tumor-intrinsic PIK3CA represses tumor immunogenecity in a model of pancreatic cancer. J Clin Invest 2019; 129:3264-3276

226. Hopkins BD, Pauli C, Du X, Wang DG, Li X, Wu D, Amadiume SC, Goncalves MD, Hodakoski C, Lundquist MR, Bareja R, Ma Y, Harris EM, Sboner A, Beltran H, Rubin MA, Mukherjee S, Cantley LC. Suppression of insulin feedback enhances the efficacy of PI3K inhibitors. Nature 2018; 560:499-503

227. Nasir Ud Din MZ, Jamshid Abdul-Ghafar, Zubair Ahmad Pancreatic mucinous cystic neoplasms: a clinicopathological study of 11 cases and detailed review of literature. Surg Exp Pathol 2020;

228. Verocq C, Racu ML, Bafort D, Butorano G, Perez-Casanova Garcia L, Navez J, Witterwulghe M, Sheahan K, Swan N, Closset J, Van Laethem JL, Maris C, D'Haene N. Pancreatic medullary carcinoma developed on a pancreatic intraductal papillary mucinous neoplasm with loss of MSH2 and MSH6 expression: a case report. Diagn Pathol 2021; 16:117

229. Pan FC, Bankaitis ED, Boyer D, Xu X, Van de Casteele M, Magnuson MA, Heimberg H, Wright CV. Spatiotemporal patterns of multipotentiality in Ptf1a-expressing cells during pancreas organogenesis and injury-induced facultative restoration. Development 2013; 140:751-764

230. Tuveson DA, Shaw AT, Willis NA, Silver DP, Jackson EL, Chang S, Mercer KL, Grochow R, Hock H, Crowley D, Hingorani SR, Zaks T, King C, Jacobetz MA, Wang L, Bronson RT, Orkin SH, DePinho RA, Jacks T. Endogenous oncogenic K-ras(G12D) stimulates proliferation and widespread neoplastic and developmental defects. Cancer Cell 2004; 5:375-387

231. Prigge JR, Wiley JA, Talago EA, Young EM, Johns LL, Kundert JA, Sonsteng KM, Halford WP, Capecchi MR, Schmidt EE. Nuclear double-fluorescent reporter for in vivo and ex vivo analyses of biological transitions in mouse nuclei. Mamm Genome 2013;

232. Bruning JC, Michael MD, Winnay JN, Hayashi T, Horsch D, Accili D, Goodyear LJ, Kahn CR. A muscle-specific insulin receptor knockout exhibits features of the metabolic syndrome of NIDDM without altering glucose tolerance. Mol Cell 1998; 2:559-569

233. Søs Skovsø EP, Jelena Kolic, Haoning Howard Cen, Derek A. Dionne, Xiao-Qing Dai, Rohit B. Sharma, Lynda Elghazi, Cara E. Ellis, Katharine Faulkner, Stephanie A.M. Marcil, Peter Overby, Nilou Noursadeghi, Daria Hutchinson, Xiaoke Hu, Hong Li, Honey Modi, Jennifer S. Wildi, J. Diego Botezelli, Hye Lim Noh, Sujin Suk, Brian Gablaski, Austin Bautista, Ryekjang Kim, Cras-Méneur, Stephane Flibotte, Sunita Sinha, Dan S. Luciani, Corey Nislow, Elizabeth J. Rideout, Eric N. Cytrynbaum, Jason K. Kim, Ernesto Bernal-Mizrachi, Laura C. Alonso, Patrick E. MacDonald, James D. Johnson. Beta-cell specific Insr deletion promotes insulin hypersecretion and improves glucose tolerance prior to global insulin resistance. biRxiv 2021;

234. Lee AYL, Dubois CL, Sarai K, Zarei S, Schaeffer DF, Sander M, Kopp JL. Cell of origin affects tumour development and phenotype in pancreatic ductal adenocarcinoma. Gut 2018;
235. Anni M.Y. Zhang TJJdW, Su Wang, Stephane Flibotte, Yiwei Bernie Zhao, Xiaoke Hu, Hong Li, David F. Schaeffer, James D. Johnson, Janel L. Kopp. Effects of hyperinsulinemia on pancreatic cancer development and the immune microenvironment revealed through single-cell transcriptomics. bioRxiv 2021;
236. Butler A, Hoffman P, Smibert P, Papalexi E, Satija R. Integrating single-cell transcriptomic data across different conditions, technologies, and species. Nat Biotechnol 2018; 36:411-420
237. Stuart T, Butler A, Hoffman P, Hafemeister C, Papalexi E, Mauck WM, 3rd, Hao Y, Stoeckius M, Smibert P, Satija R. Comprehensive Integration of Single-Cell Data. Cell 2019; 177:1888-1902 e1821
238. Elyada E, Bolisetty M, Laise P, Flynn WF, Courtois ET, Burkhart RA, Teinor JA, Belleau P, Biffi G, Lucito MS, Sivajothi S, Armstrong TD, Engle DD, Yu KH, Hao Y, Wolfgang CL, Park Y, Preall J, Jaffee EM, Califano A, Robson P, Tuveson DA. Cross-Species Single-Cell Analysis of Pancreatic Ductal Adenocarcinoma Reveals Antigen-Presenting Cancer-Associated Fibroblasts. Cancer Discov 2019; 9:1102-1123
239. Steele NG, Carpenter ES, Kemp SB, Sirihorachai V, The S, Delrosario L, Lazarus J, Amir ED, Gunchick V, Espinoza C, Bell S, Harris L, Lima F, Irizarry-Negron V, Paglia D, Macchia J, Chu AKY, Schofield H, Wamsteker EJ, Kwon R, Schulman A, Prabhu A, Law R, Sondhi A, Yu J, Patel A, Donahue K, Nathan H, Cho C, Anderson MA, Sahai V, Lyssiotis CA, Zou W, Allen BL, Rao A, Crawford HC, Bednar F, Frankel TL, Pasca di Magliano M. Multimodal Mapping of the Tumor and Peripheral Blood Immune Landscape in Human Pancreatic Cancer. Nat Cancer 2020; 1:1097-1112
240. Hosein AN, Huang H, Wang Z, Parmar K, Du W, Huang J, Maitra A, Olson E, Verma U, Brekken RA. Cellular heterogeneity during mouse pancreatic ductal adenocarcinoma progression at single-cell resolution. JCI Insight 2019; 5
241. Kuleshov MV, Jones MR, Rouillard AD, Fernandez NF, Duan Q, Wang Z, Koplev S, Jenkins SL, Jagodnik KM, Lachmann A, McDermott MG, Monteiro CD, Gundersen GW, Ma'ayan A. Enrichr: a comprehensive gene set enrichment analysis web server 2016 update. Nucleic Acids Res 2016; 44:W90-97
242. Reimand J, Isserlin R, Voisin V, Kucera M, Tannus-Lopes C, Rostamianfar A, Wadi L, Meyer M, Wong J, Xu C, Merico D, Bader GD. Pathway enrichment analysis and visualization of omics data using g:Profiler, GSEA, Cytoscape and EnrichmentMap. Nat Protoc 2019; 14:482-517
243. Dugnani E, Balzano G, Pasquale V, Scavini M, Aleotti F, Liberati D, Di Terlizzi G, Gandolfi A, Petrella G, Reni M, Doglioni C, Bosi E, Falconi M, Piemonti L. Insulin resistance is associated with the aggressiveness of pancreatic ductal carcinoma. Acta Diabetol 2016; 53:945-956
244. Ding XZ, Fehsenfeld DM, Murphy LO, Permert J, Adrian TE. Physiological concentrations of insulin augment pancreatic cancer cell proliferation and glucose utilization by activating MAP kinase, PI3 kinase and enhancing GLUT-1 expression. Pancreas 2000; 21:310-320

245. Chan MT, Lim GE, Skovso S, Yang YH, Albrecht T, Alejandro EU, Hoesli CA, Piret JM, Warnock GL, Johnson JD. Effects of insulin on human pancreatic cancer progression modeled in vitro. BMC Cancer 2014; 14:814
246. Sousa CM, Biancur DE, Wang X, Halbrook CJ, Sherman MH, Zhang L, Kremer D, Hwang RF, Witkiewicz AK, Ying H, Asara JM, Evans RM, Cantley LC, Lyssiotis CA, Kimmelman AC. Pancreatic stellate cells support tumour metabolism through autophagic alanine secretion. Nature 2016; 536:479-483
247. Yang J, Waldron RT, Su HY, Moro A, Chang HH, Eibl G, Ferreri K, Kandeel FR, Lugea A, Li L, Pandol SJ. Insulin promotes proliferation and fibrosing responses in activated pancreatic stellate cells. Am J Physiol Gastrointest Liver Physiol 2016; 311:G675-G687
248. Apte MV, Park S, Phillips PA, Santucci N, Goldstein D, Kumar RK, Ramm GA, Buchler M, Friess H, McCarroll JA, Keogh G, Merrett N, Pirola R, Wilson JS. Desmoplastic reaction in pancreatic cancer: role of pancreatic stellate cells. Pancreas 2004; 29:179-187
249. Templeman NM, Skovso S, Page MM, Lim GE, Johnson JD. A causal role for hyperinsulinemia in obesity. J Endocrinol 2017; 232:R173-R183
250. Seifert GJ, Sander KC, Richter S, Wittel UA. Murine genotype impacts pancreatitis severity and systemic inflammation: An experimental study. Ann Med Surg (Lond) 2017; 24:8-14
251. Chen Z, Downing S, Tzanakakis ES. Four Decades After the Discovery of Regenerating Islet-Derived (Reg) Proteins: Current Understanding and Challenges. Front Cell Dev Biol 2019; 7:235
252. Mukherjee S, Vaishnava S, Hooper LV. Multi-layered regulation of intestinal antimicrobial defense. Cell Mol Life Sci 2008; 65:3019-3027
253. Zhang MY, Wang J, Guo J. Role of Regenerating Islet-Derived Protein 3A in Gastrointestinal Cancer. Front Oncol 2019; 9:1449
254. Yin G, Du J, Cao H, Liu X, Xu Q, Xiang M. Reg3g Promotes Pancreatic Carcinogenesis in a Murine Model of Chronic Pancreatitis. Dig Dis Sci 2015; 60:3656-3668
255. Li Q, Wang H, Zogopoulos G, Shao Q, Dong K, Lv F, Nwilati K, Gui XY, Cuggia A, Liu JL, Gao ZH. Reg proteins promote acinar-to-ductal metaplasia and act as novel diagnostic and prognostic markers in pancreatic ductal adenocarcinoma. Oncotarget 2016; 7:77838-77853
256. Ramkissoon R, Gardner TB. Pancreatic steatosis: an update. Curr Opin Gastroenterol 2019; 35:440-447
257. Gukovskaya AS, Gukovsky I. Which way to die: the regulation of acinar cell death in pancreatitis by mitochondria, calcium, and reactive oxygen species. Gastroenterology 2011; 140:1876-1880
258. Teper Y, Eibl G. Pancreatic Macrophages: Critical Players in Obesity-Promoted Pancreatic Cancer. Cancers (Basel) 2020; 12
259. Zaytouni T, Tsai PY, Hitchcock DS, DuBois CD, Freinkman E, Lin L, Morales-Oyarvide V, Lenehan PJ, Wolpin BM, Mino-Kenudson M, Torres EM, Stylopoulos N, Clish CB, Kalaany NY. Critical role for arginase 2 in obesity-associated pancreatic cancer. Nat Commun 2017; 8:242
260. Chang JH, Jiang Y, Pillarisetty VG. Role of immune cells in pancreatic cancer from bench to clinical application: An updated review. Medicine (Baltimore) 2016; 95:e5541

261. Clark CE, Hingorani SR, Mick R, Combs C, Tuveson DA, Vonderheide RH. Dynamics of the immune reaction to pancreatic cancer from inception to invasion. Cancer Res 2007; 67:9518-9527
262. Wachsmann MB, Pop LM, Vitetta ES. Pancreatic ductal adenocarcinoma: a review of immunologic aspects. J Investig Med 2012; 60:643-663
263. Zhang Y, Yan W, Mathew E, Bednar F, Wan S, Collins MA, Evans RA, Welling TH, Vonderheide RH, di Magliano MP. CD4+ T lymphocyte ablation prevents pancreatic carcinogenesis in mice. Cancer Immunol Res 2014; 2:423-435
264. Covarrubias AJ, Aksoylar HI, Horng T. Control of macrophage metabolism and activation by mTOR and Akt signaling. Semin Immunol 2015; 27:286-296
265. Anni M.Y. Zhang EAW, Janel L. Kopp, James D. Johnson. Hyperinsulinemia in obesity, inflammation, and cancer. Diabetes & Metabolism Journal In press;
266. Lee KE, Spata M, Bayne LJ, Buza EL, Durham AC, Allman D, Vonderheide RH, Simon MC. Hif1a Deletion Reveals Pro-Neoplastic Function of B Cells in Pancreatic Neoplasia. Cancer Discov 2016; 6:256-269
267. Spear S, Candido JB, McDermott JR, Ghirelli C, Maniati E, Beers SA, Balkwill FR, Kocher HM, Capasso M. Discrepancies in the Tumor Microenvironment of Spontaneous and Orthotopic Murine Models of Pancreatic Cancer Uncover a New Immunostimulatory Phenotype for B Cells. Front Immunol 2019; 10:542
268. Pylayeva-Gupta Y, Das S, Handler JS, Hajdu CH, Coffre M, Koralov SB, Bar-Sagi D. IL35-Producing B Cells Promote the Development of Pancreatic Neoplasia. Cancer Discov 2016; 6:247-255
269. Gunderson AJ, Kaneda MM, Tsujikawa T, Nguyen AV, Affara NI, Ruffell B, Gorjestani S, Liudahl SM, Truitt M, Olson P, Kim G, Hanahan D, Tempero MA, Sheppard B, Irving B, Chang BY, Varner JA, Coussens LM. Bruton Tyrosine Kinase-Dependent Immune Cell Cross-talk Drives Pancreas Cancer. Cancer Discov 2016; 6:270-285
270. Strobel O, Dor Y, Alsina J, Stirman A, Lauwers G, Trainor A, Castillo CF, Warshaw AL, Thayer SP. In vivo lineage tracing defines the role of acinar-to-ductal transdifferentiation in inflammatory ductal metaplasia. Gastroenterology 2007; 133:1999-2009
271. Basu R, Dalla Man C, Campioni M, Basu A, Klee G, Toffolo G, Cobelli C, Rizza RA. Effects of age and sex on postprandial glucose metabolism: differences in glucose turnover, insulin secretion, insulin action, and hepatic insulin extraction. Diabetes 2006; 55:2001-2014
272. Marchese E, Rodeghier C, Monson RS, McCracken B, Shi T, Schrock W, Martellotto J, Oberholzer J, Danielson KK. Enumerating beta-Cells in Whole Human Islets: Sex Differences and Associations With Clinical Outcomes After Islet Transplantation. Diabetes Care 2015; 38:e176-177
273. Mauvais-Jarvis F. Sex differences in metabolic homeostasis, diabetes, and obesity. Biol Sex Differ 2015; 6:14
274. Gale EA, Gillespie KM. Diabetes and gender. Diabetologia 2001; 44:3-15
275. Horie I, Abiru N, Eto M, Sako A, Akeshima J, Nakao T, Nakashima Y, Niri T, Ito A, Nozaki A, Haraguchi A, Akazawa S, Mori Y, Ando T, Kawakami A. Sex differences in insulin and glucagon responses for glucose homeostasis in young healthy Japanese adults. J Diabetes Investig 2018; 9:1283-1287

276. Muzumdar MD, Tasic B, Miyamichi K, Li L, Luo L. A global double-fluorescent Cre reporter mouse. Genesis 2007; 45:593-605
277. Soling HD, Unger KO. The role of insulin in the regulation of -amylase synthesis in the rat pancreas. Eur J Clin Invest 1972; 2:199-212
278. Frier BM, Saunders JH, Wormsley KG, Bouchier IA. Exocrine pancreatic function in juvenile-onset diabetes mellitus. Gut 1976; 17:685-691
279. Fernandez AM, Kim JK, Yakar S, Dupont J, Hernandez-Sanchez C, Castle AL, Filmore J, Shulman GI, Le Roith D. Functional inactivation of the IGF-I and insulin receptors in skeletal muscle causes type 2 diabetes. Genes Dev 2001; 15:1926-1934
280. Novosyadlyy R, Lann DE, Vijayakumar A, Rowzee A, Lazzarino DA, Fierz Y, Carboni JM, Gottardis MM, Pennisi PA, Molinolo AA, Kurshan N, Mejia W, Santopietro S, Yakar S, Wood TL, LeRoith D. Insulin-mediated acceleration of breast cancer development and progression in a nonobese model of type 2 diabetes. Cancer Res 2010; 70:741-751
281. Ferguson RD, Gallagher EJ, Cohen D, Tobin-Hess A, Alikhani N, Novosyadlyy R, Haddad N, Yakar S, LeRoith D. Hyperinsulinemia promotes metastasis to the lung in a mouse model of Her2-mediated breast cancer. Endocr Relat Cancer 2013; 20:391-401
282. Shlomai G, Zelenko Z, Antoniou IM, Stasinopoulos M, Tobin-Hess A, Vitek MP, LeRoith D, Gallagher EJ. OP449 inhibits breast cancer growth without adverse metabolic effects. Endocr Relat Cancer 2017; 24:519-529
283. Arcidiacono D, Dedja A, Giacometti C, Fassan M, Nucci D, Francia S, Fabris F, Zaramella A, Gallagher EJ, Cassaro M, Rugge M, LeRoith D, Alberti A, Realdon S. Hyperinsulinemia Promotes Esophageal Cancer Development in a Surgically-Induced Duodeno-Esophageal Reflux Murine Model. Int J Mol Sci 2018; 19
284. Zelenko Z, Gallagher EJ, Antoniou IM, Sachdev D, Nayak A, Yee D, LeRoith D. EMT reversal in human cancer cells after IR knockdown in hyperinsulinemic mice. Endocr Relat Cancer 2016; 23:747-758
285. Fierz Y, Novosyadlyy R, Vijayakumar A, Yakar S, LeRoith D. Mammalian target of rapamycin inhibition abrogates insulin-mediated mammary tumor progression in type 2 diabetes. Endocr Relat Cancer 2010; 17:941-951
286. Gallagher EJ, Fierz Y, Vijayakumar A, Haddad N, Yakar S, LeRoith D. Inhibiting PI3K reduces mammary tumor growth and induces hyperglycemia in a mouse model of insulin resistance and hyperinsulinemia. Oncogene 2012; 31:3213-3222
287. Khasawneh J, Schulz MD, Walch A, Rozman J, Hrabe de Angelis M, Klingenspor M, Buck A, Schwaiger M, Saur D, Schmid RM, Kloppel G, Sipos B, Greten FR, Arkan MC. Inflammation and mitochondrial fatty acid beta-oxidation link obesity to early tumor promotion. Proc Natl Acad Sci U S A 2009; 106:3354-3359
288. Tramunt B, Smati S, Grandgeorge N, Lenfant F, Arnal JF, Montagner A, Gourdy P. Sex differences in metabolic regulation and diabetes susceptibility. Diabetologia 2020; 63:453-461
289. Varlamov O, Bethea CL, Roberts CT, Jr. Sex-specific differences in lipid and glucose metabolism. Front Endocrinol (Lausanne) 2014; 5:241
290. Camporez JP, Jornayvaz FR, Lee HY, Kanda S, Guigni BA, Kahn M, Samuel VT, Carvalho CR, Petersen KF, Jurczak MJ, Shulman GI. Cellular mechanism by which

estradiol protects female ovariectomized mice from high-fat diet-induced hepatic and muscle insulin resistance. Endocrinology 2013; 154:1021-1028
291. Macotela Y, Boucher J, Tran TT, Kahn CR. Sex and depot differences in adipocyte insulin sensitivity and glucose metabolism. Diabetes 2009; 58:803-812
292. Corbould A. Effects of androgens on insulin action in women: is androgen excess a component of female metabolic syndrome? Diabetes Metab Res Rev 2008; 24:520-532
293. Ding EL, Song Y, Malik VS, Liu S. Sex differences of endogenous sex hormones and risk of type 2 diabetes: a systematic review and meta-analysis. JAMA 2006; 295:1288-1299
294. Izeradjene K, Combs C, Best M, Gopinathan A, Wagner A, Grady WM, Deng CX, Hruban RH, Adsay NV, Tuveson DA, Hingorani SR. Kras(G12D) and Smad4/Dpc4 haploinsufficiency cooperate to induce mucinous cystic neoplasms and invasive adenocarcinoma of the pancreas. Cancer Cell 2007; 11:229-243
295. Moffitt RA, Marayati R, Flate EL, Volmar KE, Loeza SG, Hoadley KA, Rashid NU, Williams LA, Eaton SC, Chung AH, Smyla JK, Anderson JM, Kim HJ, Bentrem DJ, Talamonti MS, Iacobuzio-Donahue CA, Hollingsworth MA, Yeh JJ. Virtual microdissection identifies distinct tumor- and stroma-specific subtypes of pancreatic ductal adenocarcinoma. Nat Genet 2015; 47:1168-1178
296. Bailey P, Chang DK, Nones K, Johns AL, Patch AM, Gingras MC, Miller DK, Christ AN, Bruxner TJ, Quinn MC, Nourse C, Murtaugh LC, Harliwong I, Idrisoglu S, Manning S, Nourbakhsh E, Wani S, Fink L, Holmes O, Chin V, Anderson MJ, Kazakoff S, Leonard C, Newell F, Waddell N, Wood S, Xu Q, Wilson PJ, Cloonan N, Kassahn KS, Taylor D, Quek K, Robertson A, Pantano L, Mincarelli L, Sanchez LN, Evers L, Wu J, Pinese M, Cowley MJ, Jones MD, Colvin EK, Nagrial AM, Humphrey ES, Chantrill LA, Mawson A, Humphris J, Chou A, Pajic M, Scarlett CJ, Pinho AV, Giry-Laterriere M, Rooman I, Samra JS, Kench JG, Lovell JA, Merrett ND, Toon CW, Epari K, Nguyen NQ, Barbour A, Zeps N, Moran-Jones K, Jamieson NB, Graham JS, Duthie F, Oien K, Hair J, Grutzmann R, Maitra A, Iacobuzio-Donahue CA, Wolfgang CL, Morgan RA, Lawlor RT, Corbo V, Bassi C, Rusev B, Capelli P, Salvia R, Tortora G, Mukhopadhyay D, Petersen GM, Australian Pancreatic Cancer Genome I, Munzy DM, Fisher WE, Karim SA, Eshleman JR, Hruban RH, Pilarsky C, Morton JP, Sansom OJ, Scarpa A, Musgrove EA, Bailey UM, Hofmann O, Sutherland RL, Wheeler DA, Gill AJ, Gibbs RA, Pearson JV, Waddell N, Biankin AV, Grimmond SM. Genomic analyses identify molecular subtypes of pancreatic cancer. Nature 2016; 531:47-52
297. Karasinska JM, Topham JT, Kalloger SE, Jang GH, Denroche RE, Culibrk L, Williamson LM, Wong HL, Lee MKC, O'Kane GM, Moore RA, Mungall AJ, Moore MJ, Warren C, Metcalfe A, Notta F, Knox JJ, Gallinger S, Laskin J, Marra MA, Jones SJM, Renouf DJ, Schaeffer DF. Altered Gene Expression along the Glycolysis-Cholesterol Synthesis Axis Is Associated with Outcome in Pancreatic Cancer. Clin Cancer Res 2020; 26:135-146